Histone deacetylase inhibitors for the epigenetic therapy of proximal spinal muscular atrophy

Inaugural-Dissertation
zur
Erlangung des Doktorgrades
der Mathematisch-Naturwissenschaftlichen Fakultät
der Universität zu Köln

vorgelegt von
Lutz Garbes
aus Köln

Köln

2010

The Doctoral Thesis "Histone deacetylase inhibitors for the epigenetic therapy of proximal spinal muscular atrophy" was performed at the Institute of Human Genetics, Institute of Genetics and Centre for Molecular Medicine Cologne (CMMC) of the University of Cologne from November 2006 to 2010.

Für meine Eltern

Acknowledgements

Table of contents

List of abbreviations

A	adenine
ACN	Acetonitrol
amu	atomic mass unit
approx.	approximately
APS	ammonium persulfate
bp	base pair
BODIPY	boron-dipyrromethene
BSA	bovine serum albumin
C	cytosine
cAMP	cyclic-AMP
CD	cluster of differentiation
cDNA	complementary DNA
ChIP	Chromatin Immunoprecipitation
CK	creatine kinase
cM	centimorgan
cm	centimeter
CNS	central nervous system
dA	2′,5-dideoxyadenosin
DEPC	diethylpyrocarbonate
D-MEM	Dulbecco's modified Eagle medium
DMSO	dimethylsulfoxide
DNA	deoxyribonucleic acid
dNTP	deoxynucleotriphosphate
EC_{50}	half maximal effective concentration
EDTA	ethylenediaminetetraacetic acid
EGTA	ethylene glycol tetraacetic acid
e.g.	exempli gratia
EMG	electromyography
ESE	exonic splicing enhancer
ESS	exonic splicing silencer
et al.	et alii
FCS	fetal calf serum
FDA	Food & Drug Administration
FITC	fluorescein isothiocyanate
FL	full length
G	guanine
g	gravitational force
h	hours
HAT	histone acetyltransferase
HDAC	histone deacetylase
HMT	histone methyltransferase
HPLC	High-performance liquid chromatography
IBMX	3-isobutyl-1-methyl-xanthine
ISS	intronic splicing silencer
kb	kilobases
kDa	kilodalton
l	liter
IC_{50}	half maximal inhibitory concentration
M	molar
m	milli-
Mb	megabases

MDa	megadalton		SAHA	suberoylanilide hydroxamide acid
min	minutes		s.c.	subcutaneous
MIM	Mendelian inheritance in Men		SD	standard deviation
ml	milliliter		SDS	sodium dodecyl sulfate
mm	millimeter		SEM	standard error of the mean
mM	millimolar		siRNA	small interfering RNA
mRNA	messenger RNA		SNP	single nucleotide poly-morphism
MS	Mass spectrometry		SMA	autosomal recessive spinal muscular atrophy
NCV	nerve conduction velocity		SMN	survival motor neuron
n.d.	not determined		SSO	sulfo-N-succinimidyl ester
ng	nanogram		T	thymidine
nm	nanometer		TEA	Triethylamine
nM	nanomolar		TEMED	N,N,N',N'-tetramethylethy-lenediamine
nmol	nanomol		UV	ultraviolet
n.s.	not significant		VPA	valproic acid
OA	Oleic acid		μ	micro-
PND	postnatal day		μg	microgram
P	probability		μl	microliter
PAA	polyacrylamide		μM	micromolar
PAGE	PAA gel electrophoresis		μm	micrometer
PBS	phosphate-buffered saline			
PCR	polymerase chain reaction			
pH	power of hydrogen			
PKA	cAMP-dependent protein kinase A			
RNA	ribonucleic acid			
RNAi	RNA interference			
rpm	revolutions per minute			
RT	reverse transcription			

1. Introduction

A wide spectrum of diseases primarily affecting the motor neurons has been described in humanes. Among these, the spinal muscular atrophies represent a large group. Common to all of them is the progressive loss of lower motor neurons in the spinal cord, leading to a preferential denervation of the voluntary muscles. Hence, main symptoms are muscle weakness and atrophy, which can be present either proximally or distally as well symmetrically or asymmetrically. Moreover, the individual mode of inheritance ranges from sporadic cases to X-linked as well as recessive or dominant forms. The most common spinal muscular atrophy is *autosomal proximal spinal muscular atrophy*, which will therefore simply be termed *SMA* in the following. Other well-described spinal muscular atrophies include X-linked SMA (*XL-SMA*), spinal and bulbar muscular atrophy (*Kennedy´s disease*) and spinal muscular atrophy with respiratory distress (*SMARD*).

1.1   Autosomal recessive proximal spinal muscular atrophy (SMA)

In the Western European population, SMA is the second most frequent autosomal recessive disorder in humans after cystic fibrosis. Nowadays, it is the leading genetic cause of early infant death. The incidence of SMA is 1 in 10,000 to 1 in 6,000 live births in Western Europe (Emery 1991; Pearn 1978). In Germany. the carrier frequency has been estimated to be between 1:25 to 1:35 (Anhuf et al. 2003; Emery 1991; Feldkotter et al. 2002; Pearn 1978). SMA is caused by the progressive degeneration of α-motor neurons in the anterior horns of the spinal cord. This leads to a steadily increasing hypotonia and weakness of the voluntary muscles, ultimately resulting in their atrophy. Typically, muscle weakness occurs first in the voluntary muscles of proximal limbs. While the atrophy is more pronounced in the lower extremities, hands and feet are usually spared in the early stages of SMA (Markowitz et al. 2004). Further symptoms include a weak cough and cry, difficulties to suck and swallow, bladder weakness, tremor of the hands, areflexia and an increased susceptibility to respiratory tract infections (Rudnik-Schoneborn et al. 1994). In contrast, facial and oculomotor nerves are typically unaffected and also cognitive skills are not impaired.

1.1.1   Clinical diagnosis

The classical main diagnostic tool for SMA diagnosis is recording of electric pulses controlling voluntary muscle movement by electromyography (EMG). These pulses originate in the motor cortex and are transmitted by the motor neurons to the respective muscles. EMG technique allows determining of both transmission current and velocity. In SMA patients, EMG demonstrates spontaneous muscle activity with fibrillations and fasciculations of single muscle fibers as well as an increased mean duration and amplitude of action potentials. Nerve conduction velocity (NCV) is normal or mildly reduced, while the number

of motor units decreases during disease progression (Swoboda et al. 2005; Zerres and Davies 1999).

The progess made in molecular diagnostics dramatically improved SMA diagnosis. 15 years ago the SMA determining gene, termed *survival of motor neuron 1* (*SMN1*), was identified on chromosome 5q (Lefebvre et al. 1995). Its identification allowed confirmation of clinical SMA diagnosis by screening the *SMN1* gene for specific mutations, deletions or gene conversions. This eventually led to the modification of the originally forwarded diagnostic criteria from the International SMA Consortium in 1992 (Munsat and Davies 1992) by Zerres and Davies (Zerres and Davies 1999).

In order to distinguish SMA from other motor neuron diseases, exclusion criteria such as CNS dysfunction or arthrogryposis have been defined (Munsat and Davies 1992). Furthermore, serum levels of creatine kinase (CK) can be used to rule out SMA in unclear cases. CK levels are a common clinical marker for muscle membrane permeability. Typical serum levels are around 140 to 170 $^U/_l$, but can moderately be elevated by a variety of neuromuscular disorders, after external injury or even after excessive physical activity. However, highly increased CK levels (>10 fold) are a feature of conditions that cause severe muscle damage like myocardial infarction or Duchenne Muscular Dystrophy (*DMD*). In contrast to that, few mildly-affected SMA patients exhibit modestly increased serum levels (Rudnik-Schoneborn et al. 1998). In very rare cases, SMA was found to be accompanied by arthrogryposis, CNS dysfunction, increased CK levels or congenital heart defects. However, the question remains open whether these "SMA plus" cases are coincidental or indeed associated (Guillot et al. 2008; Rudnik-Schöneborn et al. 1996; Rudnik-Schoneborn et al. 2008).

In the past, clinical diagnosis has further been corroborated by histological inspection of a muscle biopsy. Muscles contain two types of fibers: Reddish type I fibers using triglycerides as storage fuel and white type II fibers, which generate energy from glycogen. While type I fibers are suited for endurance, type II fibers are effective for short bursts of muscle contraction. In contrast to healthy individuals, SMA patients exhibit groups of both atrophic type I and II fibers as well as hypertrophic type I fibers. Typically, muscle spindles are not affected (Lunn and Wang 2008) and myopathic features such as necrosis and lipid accumulation are absent with the exclusion of long-standing SMA patients (Munsat and Davies 1992).

A summary of the most commonly used inclusion and exclusion critera for SMA is given in Table 1. Based on these guidelines, a diagnostic algorithm has been proposed which combines all the above described diagnostic criteria (Lunn and Wang 2008).

System		Criteria
Muscle	**Inclusion**	weakness of trunk and limbs
		symmetrical weakness
	Exclusion	weakness of facial, oculomotor muscles or diapraghm
Neurological	**Inclusion**	fasciculation of tongue and tremor of hands
	Exclusion	sensory disturbances
		CNS dysfunction
Molecular level	**Inclusion**	homozygous absence of *SMN1*
		intragenic *SMN1* mutation
Electro-physiology	**Inclusion**	abnormal spontaneous activity by EMG
		increased mean duration and amplitude of action potentials
	Exclusion	NCV lower 70% than in healthy subjects
		abnormal sensory nerve action potentials
Histology	**Inclusion**	groups of atrophic fibers of both types
Others	Exclusion	higher than 10-fold increased CK levels

Table 1   **Inclusion and exclusion criteria for the diagnosis of SMA (Zerres and Davies 1999).**

1.1.2 Classification of proximal SMA

The phenotype of proximal SMA is highly variable. It ranges from the prenatal appearance of symptoms to first manifestations occuring during adulthood in the mildest forms. The severest form of SMA was first described more than 100 years ago by the Austrian neurologist Guido Werdnig (Werdnig 1891), whereas milder forms were reported for the first time in the 1950´s (Kugelberg and Welander 1956). Nowadays, SMA is classified into four types (type I-IV) based on the age of onset and disease severity (Munsat and Davies 1992; Zerres and Rudnik-Schoneborn 1995).

1.1.2.1 SMA type I (*Werdnig-Hoffmann disease*), MIM #25330

Werdnig-Hoffmann disease is the most common form of SMA and accounts for about 50% of SMA cases (Markowitz et al. 2004). It is the most severe form and is often referred to as SMA type I or acute SMA. Onset of the disease is typically before the age of six months - in very rare cases already in the third trimester of pregnancy - and death occurs within the first two years of life (Cobben et al. 2008; Fidzianska and Rafalowska 2002; Markowitz et al. 2004). Mean survival has been estimated to be approx. seven months (Rudnik-Schoneborn et al. 2009). SMA type I children suffer from generalized muscle weakness, hypotonia and are never able to sit unassisted ("*floppy infants*"). Furthermore, patients exhibit symmetrical paralysis and cannot control head movement. Bulbar denervation results in characteristic fasciculation of the tongue thus leading to problems with sucking and swallowing. Due to a spared diaphragm and weakened intercostals muscles, the chest is typically deformed and bell-shaped. In severe cases, also arthrogryposis multiplex congenita may occur (Falsaperla

et al. 2001; Guillot et al. 2008). Furthermore, it has been reported that in some cases SMA type I patients also suffer from congenital heart defects (Finsterer and Stollberger 1999; Rudnik-Schoneborn et al. 2008) or necrosis of fingers and toes (Araujo Ade et al. 2009; Rudnik-Schoneborn et al. 2010).

1.1.2.2 SMA type II, MIM #253550

SMA type II is an intermediate SMA type and often called chronic SMA. Disease onset of SMA type II is between the 6th and 18th month of life. Affected children are able to sit indepently, but never learn to walk and require assistance to stand. Life expectancy is reduced, but more than 70% of patients reach an age of 20 years or older (Russman et al. 1996; Zerres et al. 1997). Frequent symptoms are tremors of the hands, paraparesis and problems with tracheal secretions as well as coughing due to weak intercostal muscles (Iannaccone 1998). Often surgical intervention is needed to correct developing scoliosis (Bertini et al. 2005). The most frequent cause of death of SMA type II patients is respiratory insufficieny during adolescence.

1.1.2.3 SMA type III (*Kugelberg-Welander disease*), MIM #253400

SMA type III was described for the first time in 1956 (Kugelberg and Welander 1956). Characteristic for this juvenile form of SMA, which is often confused with limb girdle muscular dystrophy, is the appearance of disease manifestations after the 18th month of life. Depending on the actual age of onset, SMA type III is divided into two subtypes. If first symptoms occur before the age of three years the disease is classified as type IIIa, whereas in SMA type IIIb the diseases occurs after an age of three years (Zerres and Rudnik-Schoneborn 1995). Symptoms of SMA type III include a waddling gait and overall thin appearance as well as scoliosis (Iannaccone 1998). However, the overall clinical picture of SMA type III is very heterogenous. Some individuals may need wheelchair assistance, while others may be able to walk throughout their life.

1.1.2.4 SMA type IV (*adult SMA*), MIM #271150

SMA type IV is the mildest form of SMA. Typically, first disease manifestations occur after the third decade of life (Wirth 2002). Symptoms are typically very mild and patients have a normal life expectancy. However, only a very low percentage of these patients are linked to mutations in the *SMN1* gene, while for the majority an underlying molecular cause is still unknown.

1.2   The molecular basis of SMA

In order to identify the critical SMA locus, researches started linkage analysis. In 1990 finally, three independent groups mapped SMA to a 10 cM region on the long arm of chromosome 5 (5q11.2-13.3) (Brzustowicz et al. 1990; Gilliam et al. 1990; Melki et al. 1990).

Progress in the development of highly polymorphic markers allowed narrowing down the SMA locus to an interval less than 750 kb between the markers A31 and 95/23-CA (DiDonato et al. 1994; Melki et al. 1993; Melki et al. 1994; Soares et al. 1993; Wirth et al. 1995; Wirth et al. 1994). Subsequent studies identified an inverted duplication of a 500 kb element within this region, of which each of the duplicates can be present in zero to four copies (Lefebvre et al. 1995; Wirth et al. 2006a). This complex genomic organization severely hampered the construction of a uniform physical map of the region surrounding the SMA determining gene (Melki et al. 1994; Roy et al. 1995a; Roy et al. 1995b; Thompson et al. 1993). However, in 95% of healthy controls, a newly identified 20 kb gene was present in both the centromeric and telomeric 500 kb copy, whereas the telomeric one was either lacking or interrupted in the vast majority of patients. This suggested that the identified telomoric gene copy is indeed the SMA determing gene. Since SMA is characterized by the degeneration of motor neurons, the gene was termed *survival motor neuron* (*SMN*) (Lefebvre et al. 1995). Besides *SMN*, another four genes have been shown to be included in the duplicated 500 kb segment: *BIRC1* (*baculoviral IAP repeat-containing protein 1*) which is also known as *NAIP* (*neuronal apoptosis inhibitory protein*), *SERF1* (*small EDRK-rich factor 1*), also termed *H4F5*, *GTF2H2* (*general transcription factor IIH*) or *p44*, and *OCLN* (*occludin*) (Lefebvre et al. 1995; Schmutz et al. 2004). Proximally, this highly polymorphic region is flanked by *RAD17*, whereas the distally adjacent gene is *BDP1* (Figure 1) (Deimling von et al. 1999; Kelter et al. 2000)
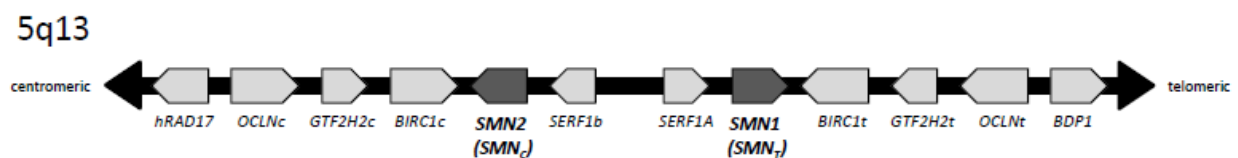
Figure 1 **Schematic overview of the "SMA region" on chromosome 5q13. Arrow heads indicated reading direction. (*SMN_c* = centromeric *SMN*, *SMN_t* = telomeric *SMN*)**

1.2.1 *SMN1* and *SMN2*

Within the SMA region, two copies of *SMN* have been identified each spanning 28 kb on genomic level (Chen et al. 1998). Both genes consist of nine exons (1, 2a, 2b, 3-8) with an open reading frame of 882 bp (294 codons) encoding for a 38 kDa protein (Lefebvre et al. 1995). The 1.5 kb *SMN* transcript is expressed in all somatic tissues, in which the expression is ~50- to 100-fold higher in the spinal cord compared to other tissues (Coovert et al. 1997; Lefebvre et al. 1997). The telomeric *SMN* copy, termed *SMN1*, has been identified as the SMA determining gene (Lefebvre et al. 1995). Over 96% of SMA patients have homozygous deletions or gene conversion from *SMN1* into *SMN2* (Lefebvre et al. 1995; Wirth 2000). The latter case is predominantly found in type II or III patients who have multiple *SMN2* copies (Wirth et al. 1997). Besides homozygous deletion of *SMN1* in approx. 4% of SMA patients intragenic *SMN1* mutations are observed, which interfere with normal gene function or lead

to *Nonsense-mediated-mRNA-decay* (NMD). These patients are typically compound heterozygous, with a deletion of one *SMN1* allele and a mutation in the other allele (Brichta et al. 2008; Lefebvre et al. 1995; Sun et al. 2005; Wirth 2000).

All SMA patients retain at least one copy of *SMN2*. Although *SMN2* produces 90% truncated protein due to alternative splicing (presented in detail in 1.2.2), the remaining 10% full-length protein substantially influence the SMA phenotype: The more *SMN2* copies are present, the less severe is the phenotype. Most of SMA type I patients have two *SMN2* copies, whereas e.g the majority of SMA type II cases possess three copies (Lefebvre et al. 1995; Wirth 2000).

Recently, a positive modifier of the SMA phenotype has been identified within *SMN2*. At position +25 in exon 7, a single base substitution (c.859G>C) was identified, leading to a less severe SMA phenotype than expected from the *SMN2* copy number (Prior et al. 2009; Vezain et al. 2010). However, the SMA phenotype is also influenced by other genes. For example in very rare cases, high expression levels of *PLS3* have been found to fully protect women from developing SMA (Oprea et al. 2008).

The finding that deletion of *SMN1* causes SMA, whereas *SMN2* only modifies the actual phenotype, was of particular interest since both genes are almost identical except for 5 nucleotide exchanges in the 3´-end of *SMN2* (Burglen et al. 1996; Lefebvre et al. 1995):

- **Intron 6**   nt position 27092   G>A

- **Exon 7**   nt position 27141   c.840C>T, codon 280 (TTC>TTT, Phe>Phe)

- **Intron 7**   nt position 27289   A>G
                 nt position 27404   A>G

- **Exon 8**   nt position 27869   G>A (untranslated region)

Nowadays, several other gene variants have been described, but these occur in both *SMN1* and *SMN2* (Brahe et al. 1996; Hahnen and Wirth 1996; Monani et al. 1999).

Phylogenetic analysis showed that the SMN protein is highly conserved from yeast to man (Miguel-Aliaga et al. 1999; Paushkin et al. 2000; Schrank et al. 1997). The gene duplication event occurred for the first time in primates roughly five million years ago. However, also in man´s closest relative *Pan troglodytes*, only two to seven copies of *SMN1* are present whereas the *SMN2* gene is unique to humans (Rochette et al. 2001)

1.2.2   *SMN* splicing

Although *SMN1* and *SMN2* differ by 5 nucleotides, both genes encode for the identical protein since these nucleotide exchanges are either intronic, in 3´-UTR or translationally silent (Burglen et al. 1996; Lefebvre et al. 1995). However, on mRNA level both *SMN* genes exhibit clear differences. *SMN1* produces almost exclusively full-length transcripts, whereas

90% of *SMN2* transcripts are alternatively spliced and lack exon 7 (*SMN2Δ7*). Merely 10% of *SMN2* pre-mRNAs are correctly spliced and are processed to full-length transcripts (*FL-SMN2*) (Gennarelli et al. 1995; Lefebvre et al. 1995; Lorson et al. 1999). The lack of *SMN* exon 7 dramatically influences SMN protein production, since it encodes the C-terminal 16 aa and contains the first stop codon of full-length *SMN* transcripts (position +49 to +51). If exon 7 is included in the mature mRNA, it is translated into full-length SMN protein consisting of 294 aa. However, if exon 7 is skipped, an alternative stop codon at position 13 of exon 8 is used, resulting in a truncated 282 aa protein (Figure 2) (Gennarelli et al. 1995; Lorson et al. 1998). Recently, it has been shown that this altered C-terminus creates a degron, which leads to a more rapid degradation of the Δ7-protein compared to the full-length protein (Burnett et al. 2009; Cho and Dreyfuss 2010; Lorson and Androphy 2000). Furthermore, the truncated protein also exhibits a reduced oligomerization capacity (Lorson et al. 1998). From both *SMN* genes, also three other transcripts are produced, namely *SMNΔ5* lacking exon 5, *SMNΔ3* deficient of exon 3 as well as *SMNΔ5Δ7* in which both exons 5 and 7 are skipped (Chang et al. 2001; Gennarelli et al. 1995; Singh 2007; Sossi et al. 2001).

Self-evidently, research has focused on why *SMN2* exon 7 is spliced in a different way than *SMN1* exon 7. *SMN* exon 7 is a relatively short exon, spanning only 54 nucleotides. It is characterized by a weak 3` splice site due to a suboptimal polypyrimidine tract, making it prone to alternative splicing (Lim and Hertel 2001). Nowadays, two different hypotheses have been proposed to explain the differences in exon 7 splicing. Fundamental to both is the C to T transition in *SMN2* at position +6 of exon 7. On the one hand, researchers argue that this particular nucleotide exchange destroys an exonic splicing enhancer (ESE) located at the beginning of exon 7 (Lorson and Androphy 2000; Lorson et al. 1999). This heptameric motif is typically recognized by the splice factor SF2/ASF, which favors exon inclusion. In the case of *SMN2*, SF2/ASF is not able to bind this ESE thus exon 7 is skipped (Figure 2) (Cartegni et al. 2006; Cartegni and Krainer 2002). A concurring hypothesis suggests that the C to T transition leads to a formation of a novel exonic splicing silencer (ESS), which in turn recruits the splice factor hnRNP A1 leading to exon 7 skipping (Kashima and Manley 2003; Kashima et al. 2007a; Singh et al. 2004). Furthermore, it has been shown that Sam68 also binds to the putative ESS and interacts with hnRNP A1 to cooperatively promote exon 7 skipping (Pedrotti et al. 2010). However, both hypotheses can also be combined in such a way that the C to T transition destroys an ESE and creates an ESS instead (Figure 2).

In addition to SF2/ASF, hnRNP A1 and Sam68, a plethora of additional other factors is involved in the splicing of *SMN2*-pre-mRNA . Among these, the SR-like splice factor hTRA2-β1 (SFRS10, Serine/Arginine rich splice factor 10) has an exceptional role since its overexpression reverses the *SMN2* splicing to 80% full-length *FL-SMN2* (Hofmann et al. 2000). hTRA2-β1 binds to GA-rich second ESE in the central region of *SMN* exon 7 and acts as an platform for the binding of other splice factors, such as SRp30, hnRNP-G or TDP-43. All three of them have been demonstrated to favour SMN exon 7 inclusion by direct binding to

hTRA2-β1 (Figure 2) (Bose et al. 2008; Helmken and Wirth 2000; Hofmann and Wirth 2002; Young et al. 2002).

Adjacent to *SMN* exon 7, several regulatory elements have been identified (Figure 2). Among these, two positively acting intronic elements termed I7-1 and I7-2 have been identified in intron 7. It has clearly been demonstrated that I7-1 acts as an intronic splicing enhancer (ISE), which favors exon 7 inclusion (Gladman and Chandler 2009). In addition, several potent negatively acting elements have been detected, such as element 1 (E1) in intron 6 which is bound by PTB and FUSE (Baughan et al. 2009; Miyajima et al. 2002). Moreover, in intron 7 the stem-loop forming element 2 (E2) (Miyaso et al. 2003) as well as ISS-N1, which is recognized by hnRNP-A1, have both been identified to promote exon 7 skipping (Kashima et al. 2007b; Singh et al. 2006).
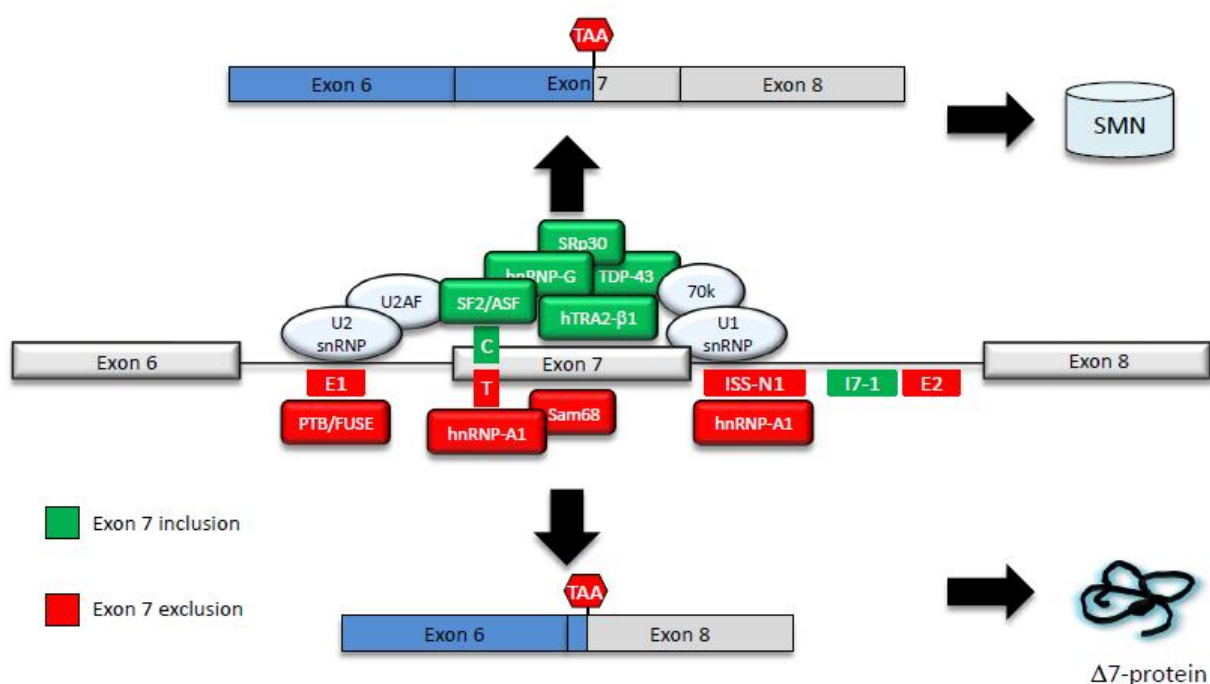
Figure 2   **Proposed molecular mechanism for *SMN* exon 7 inclusion and exclusion. In the case of *SMN1* depicted in the upper part, SF2/ASF binds to the ESE at the beginning of exon 7. SF2/ASF interacts via U2AF with the U2 snRNP to facilitate the removal of intron 6. Additional splice factors such as hTRA2-β1 or hnRNP-G act positively on exon 7 inclusion. In the case of *SMN2* depicted in the lower part binding of hnRNP-A1 and Sam68 abolishs binding of SF2/ASF (potentially also of the U2 snRNP) thereby promoting exon 7 exclusion. Several *cis*-acting elements like E1, ISSN1 or I7-1 individually act on exon 7 inclusion or exclusion. (Modified from (Lorson et al. 2010))**

Furthermore, a positive acting element within *SMN2* in exon 7 has recently been identified in several SMA patients, showing a much milder phenotype than expected from the *SMN2* copy number. Downstream of the putative ESE/ESS at position +25 a single base

substitution (c.859G>C) was located, which creates another putative SF2/ASF binding motif (Prior et al. 2009; Vezain et al. 2010).

Although *SMN2* splicing is quite complex, several therapeutic approaches have been undertaken which either directly or indirectly target *SMN2* splicing. Though, these will be presented in 1.6.

1.3   The SMN protein

The human SMN protein is expressed in virtually all tissues, with highest levels present in the CNS and liver (Carvalho et al. 1999; Young et al. 2001; Young et al. 2000). Since SMN abundance markedly declines after birth, it is thought that elevated SMN levels may play an important role throughout prenatal development (Burlet et al. 1998). Similarly to that, also the rodent *Smn* is present at the highest levels before birth, but its abundance decreases soon thereafter by *Smn* promoter hypoacetylation (Battaglia et al. 1997; Jablonka et al. 2000; Kernochan et al. 2005; Liu et al. 2010).

SMN has a molecular weight of 38 kDa and consists of 294 aa (Lefebvre et al. 1995). Like the majority of cytoplasmatic proteins, SMN is degraded via the ubiquitin-proteasome-system (UPS) (Burnett et al. 2009; Chang et al. 2004). Very recently, the ubiquitin-ligase UCHL1 has been identified to transfer activated ubiquitin onto SMN, thus regulating its degradation (Hsu et al. 2010). Within the SMN protein, several functional domains have been identified during the last years. N-terminally, Exon 2b and the beginning of exon three encode for RNA-binding-domain (RBD) (Bertrandy et al. 1999), whereas the major part of exon 3 is spanned by a Tudor-domain facilitating Sm protein binding during U snRNP biogenesis (Selenko et al. 2001). In exons 4 and 5 a proline-rich stretch was identified, mediating interaction with Profilins (Bowerman et al. 2009; Bowerman et al. 2007; Giesemann et al. 1999). Furthermore, it has been shown that the YG-box, encoded by exon 6 in conjunction with exon 2b, is required for SMN self-oligomerization (Lorson et al. 1998).

Inside the cell, SMN is present in both the cytoplasm and the nucleus. While in the cytoplasm it is diffusely distributed, distinct SMN foci are observed inside the nucleus. These foci are most often found in close proximity or even overlapping with coiled bodies (also known as Cajal bodies). Based on these observations, the nuclear SMN foci were termed *Gemini of coiled bodies* or gems (Burlet et al. 1998; Coovert et al. 1997; Liu and Dreyfuss 1996; Liu et al. 1997). In addition to the 38 kDa SMN protein, another shortened isoform has been identified which is selectively expressed in the axons of developing motor neurons (aSMN). This isoform includes exons 1 to 3 and a retained part of intron 3 (Setola et al. 2007).

1.3.1 The SMN complex

SMN is the major constituent of a large multi-subunit protein complex weighing approx. 1 MDa, termed the SMN complex. The further core components Gemins2 to -8 are stably associated with the SMN complex and present in a stoichiometric manner (Carissimi et al. 2006a; Carissimi et al. 2006b; Pellizzoni et al. 2001a; Pellizzoni et al. 2002). In addition, several transient interaction partners have been identified, which are mainly involved in snRNP-biogenesis. However, it is believed that SMN and Gemin2 represent the ancestral core of the SMN complex to which the other Gemins were added blockwise during evolution (Kroiss et al. 2008). From a structural point of view, SMN functions as modular backbone of the SMN complex since its ability to self-oligomerize allows binding of a multitude of partners (Figure 3) (Pellizzoni 2007). Furthermore, it has been shown that complexation markedly increases SMN protein half-life from approx. 4.3 hrs to around 15 hrs (Burnett et al. 2009).

Figure 3   **Schematic overview of the SMN complex. Stable binding partners are Gemin2, -3, -5, -7 and -8 whereas Gemin4 and -6 are associated via other Gemins (taken from (Pellizzoni 2007)).**

1.3.2 Functions of SMN

Since SMN is involved in a vast number of cellular processes, these were subdivided into ubiquitous housekeeping ones and functions which are specific to either neurons or muscles.

1.3.2.1 Housekeeping functions

- *Biogenesis of snRNPs*

Small nuclear ribonucleoproteins (snRNP) are of vital importance for the splice process in every cell since they identify and subsequently remove the introns from pre-mRNAs. snRNPs are constituented of a major proteinous part and a small nuclear RNA (snRNA) of 100 to 300 bp transcribed by RNA-Polymerases II. It has been shown that the SMN complex facilitates

addition of the Sm proteins D1, D2, E, F, G and D3, B (Smith antigen) onto the respective snRNA and catalyzes Sm ring closing (Lorson et al. 1998; Meister and Fischer 2002; Pellizzoni et al. 1999). While the SMN complex directly recruits the respective snRNA, the Sm proteins are handed over by the assembly chaperone pICln (Chari et al. 2008). Following assembly, the SMN-snRNP-complex shuttles into the nucleus and is typically stored in gems until further usage. Once the snRNP is released, the SMN complex is translocated out of the nucleus and enters another round of snRNP assembly (Chari et al. 2009).

However, several point mutations in *SMN1* have been shown to impair binding of SMN to the Sm proteins, thus leading to generalized splicing defects (Gabanella et al. 2007; Lorson et al. 1998; Pellizzoni 2007; Sun et al. 2005; Zhang et al. 2008).

- *Stress response*

Exposure of a cell to stress factors such as heat or UV irradiation triggers wide-spread alterations in expression as well as distribution of cellular constituents. Studies showed that specific stress-induced genes e.g. the heat-shock-proteins (HSPs), which mostly fullfil chaperoning functions, are actively expressed upon stress stimulus while most other genes are silenced (Buchan and Parker 2009). The key factor in this process is the phosphorylation of eukaryotic initiation factor 2α (eIF2α), leading to reduced global translation (Underhill et al. 2005). More than 50% of total mRNA transcripts are actively recruited into stress granules (SG) to protect them from degradation or denaturation (Buchan and Parker 2009). Stress granules are formed by shuttling of the RNA binding proteins TIA-1(T-cell internal antigen-1) and TIA-R (TIA1-related protein) from the nucleus into the cytoplasm where these proteins self-aggregate (Kedersha et al. 1999). However, it has been shown that SMN interacts with TIA-1/R as well as Rpp20, which accumulate in stress granules (Hua and Zhou 2004a, b). Nevertheless, since SMN accumulation precedes that of TIA-1/R, it has been suggested that SMN serves as a facilitator of SG formation (Hua and Zhou 2004b).

- *Regulation of transcription*

Transcription is opposingly regulated by the so-called co-activator and co-respressor complexes, which consist and recruit enzymes involved in chromatin remodelling or translational initiaton (Rosenfeld et al. 2006). Several years ago, it was shown that SMN interacts via its YG-box with mSin3A (Zou et al. 2004), which interacts with the corepressors SMRT and N-CoR (Nagy et al. 1997). Since both, SMN and mSin3A, are involved in formation of a >40 MDa complex, it has been suggested that SMN may also be involved in the regulation of transcriptional repression (Zou et al. 2004). Further evidence came from the observations that SMN associates with RNA polymerase II (Pellizzoni et al. 2001b) and dp103, a putative RNA helicase (Campbell et al. 2000).

- *Regulation of translation*

Based on the finding that SMN is transporting mRNA along axons (1.3.2.2), it has been suggested that SMN may also be involved in translational regulation. Furter evidence pointing into this direction came from the observation that the C-terminal YG-box of SMN interacts with FMRP (Fragile X Mental Retardation Protein) (Piazzon et al. 2008). FMRP is involved in nuclear export and transport of yet unknown target mRNAs and is often detected near polysomes (Bardoni et al. 2001). However, debate is still ongoing whether the SMN complex is involved in the assembly of FRMP-containing mRNPs or whether SMN alone is transiently interacting with mRNPs during their transport.

1.3.2.2 Neuron-specific functions

- *Axonal mRNA transport*

It has been observed that neurons of SMA-like mice exhibit reduced levels of *β-Actin* mRNA at the axonal growth cones, which suggested that SMN is involved in mRNA transport along axons. This is in line with the finding that SMN interacts with hnRNP-R (heterogenus nuclear ribonucleoportein-R), which controls β-actin localization (Rossoll et al. 2003). Furthermore, it has been demonstrated that SMN complexes traffic along neuronal processes to the growth cones of motor neurons (Zhang et al. 2006) and that SMN, Gemin2 and Gemin3 associate with *β-Actin* mRNA in the cytoplasm of neuronal cells (Todd et al. 2010). Based on these findings, it was suggested that SMN or the SMN complex is actively involved in the transport of axonal mRNAs such as β-Actin. However, it has been shown that also other cytoskeletal mRNAs like tubulin, peripherin and vimentin are transported along axons, but it has not yet been reported whether SMN is involved in their transport (Willis et al. 2007).

- *Neurite outgrowth*

Several *in vitro* as well as *in vivo* studies in zebrafish and mice showed that SMN depletion strongly reduces neurite outgrowth, a process depending on actin remodelling (Bowerman et al. 2009; Fan and Simard 2002; McWhorter et al. 2003; Oprea et al. 2008). Since knockdown of *SMN* alters the G-/F-actin ratio, it has been proposed that SMN may be involved in microfilament metabolism (van Bergeijk et al. 2007). In line with this, the protective SMA modifier PLS3 is an actin-bundling protein presumably restoring disturbed G-/F-actin ratios in SMA patients (Oprea et al. 2008). Furthermore, SMN depletion alters Profillin II expression, thus impairing the RhoA/ROCK actin remodelling pathway (Bowerman et al. 2007).

- *Neuromuscular junction formation*

Neuromuscular junctions (NMJ) are the connecting pieces between the axon terminal of a motor neuron and the respective muscle. Histological inspection of SMA-like mice revealed that the maturation of NMJs was severely reduced and AChR (Acetylcholine Receptor)

clusters did not form proper pretzel-like structures. Moreover, pre-terminal sprouting was also descreased (Kariya et al. 2008). Electrophysiologic examinations showed that reduced SMN levels in mice indeed lead to lower evoked endplate currents (EPC) due to reduced neurotransmitter release (Kong et al. 2009). Furthermore, even in *Drosophila* SMN depletion severely impaired NMJ structure and function (Chang et al. 2008).

1.3.2.3 Muscle-specific functions

Although in SMA the motor neurons are primarily affected, also muscle-specific functions of SMN have been identified. It has been shown that *Smn* knockdown in mouse C2C12 myoblasts results in defective myoblast fusion and malformed myotubes, most likely due to Z-disc deficiency (Shafey et al. 2005; Walker et al. 2008). In addition, it has been proven that the *Smn* complex colocalizes with the Z-disc marker α-Actinin in both skeletal and cardiac myofibrils and that SMN is a direct target of the muscle-specific protease Calpain-3 (Walker et al. 2008).

Although the underlying cause is not known, recent findings suggest that *Smn* may also have a cardiac-specific role, since SMA-like mice exhibit bradycardia and develop dilated cardiomyopathy (Bevan et al. 2010; Shababi et al. 2010b). However, whether this is a primary effect of reduced *Smn* levels or a secondary one due to neuronal deficits remains to be determined.

1.4   Animal models of SMA

A number of animal models has been generated within the last ten years to model the SMA phenotype and to allow detailed examination of the pathophysiology and *in vivo* drug testing. However, humans are the only species known carrying the *SMN2* gene. Complete loss of *SMN/Smn* leads to lethality in all organisms.

1.4.1   Non-vertebrate SMA models

- *Schizosaccharomyces pombe*

Using a bioinformatic approach, an orthologue of *SMN* termed *smn1+* was identified in the split yeast *S.pombe*. It has been demonstrated that *smn1+* is essential for viability in *S.pombe* and that missense mutations mimicking SMA type I lead to Smn1p mislocalization and decreased cell viability. Furthermore, it has been shown that Smn1p interacts with human SMN and Sm proteins, thus implying a highly conserved function (Owen et al. 2000; Paushkin et al. 2000).

- *Caenorhabditis elegans*

More than 10 years ago, the nematode ortholgue of *SMN* termed *smn-1/CeSMN* was identified. While both disruption and overexpression result in reduced progeny as well as locomotive defects, transient knockdown causes sterility by embryonic lethality (Miguel-

Aliaga et al. 1999). Smn-1 is expressed in various tissues, including the nervous system and body wall muscles. The hypomorphic *smn-1* mutation (*smn-1(ok355)*) reduces lifespan and impairs locomotion and pharyngeal pumping. Interestingly, neuronal but not muscle-directed expression of *smn-1* rescues the *smn-1(ok355)* phenotype (Briese et al. 2009). Moreover, the nematode`s orthologue of *Gemin2*, termed *SMI-1*, interacts with *smn-1*, suggesting the presence of a simplified SMN complex in *C.elegans* (Burt et al. 2006).

- *Drosophila melanogaster*

Within the Drosophila genome only a single, but highly conserved orthologue of SMN is present. SMN loss of function (*Smn^{73Ao}*) leads to recessive larval lethality and NMJ abnormalities such as an enlargement. However, the observed survival up to the larvae stage is depending on maternal wild-type *smn* stored in the nurse cells. Electrophysiologic examination revealed that these flies exhibit reduced exciaitory postsynaptic currents (EPSC), which is in line with the observed NMJ phenotype. Noteworthy, the expression of *Smn*`s C-terminus partially overcomes the phenotype (Chan et al. 2003). Unexpectedly, Smn-null mutations did not exhibit any detectable snRNP reduction, suggesting that larvae lethality is due to a neuron-specific phenotype. In contrast to the *Smn null* allele, flies carrying hypomorphic *Smn* mutations survive but display atrophy and flightlessness (Rajendra et al. 2007).

1.4.2 Vertebrate SMA models

- *Danio rerio*

Using Zebrafish is an elegant way to study motor neuron development *in vivo*, since the transparent embryos allow easy analysis of the phenotype (McWhorter et al. 2003; Oprea et al. 2008). Antisense morpholino knockdown of *Smn* led to motor axon specific effects like truncation and increased branching (McWhorter et al. 2003). Using ENU-induced mutants, it could be shown that, similar to flies, maternal RNAs and proteins deposited in egg allow survival of these mutants up to the larvae stage. However, analysis of these ENU-mutants revealed extremely reduced levels of the presynaptic protein SV2 in *Smn* mutants. This suggested a specific role for SMN in production and/or stability of SV2, which is important for effective vesicle release. Interestingly, motor neuron specific expression of human SMN corrected the NMJ defect, underlining the necessity of SMN for NMJ integrity (Boon et al. 2009).

Studies using Gemin2 and pICln morphants revealed a similar axonal phenotype (Winkler et al. 2005), but a reduced snRNP biogenesis could be excluded as the underlying cause (Carrel et al. 2006). However, refined experiments in which Gemin2 was knocked down exclusively in motor neurons, demonstrated that the axonal phenotype of ubiquitous Gemin2 morphants is rather a secondary than a primary effect (McWhorter et al. 2008).

- *Mus musculus*

More than 10 years ago, the first classical knock-out of the murine *Smn* gene was described. Targeted insertion of a *lacZ/Neomycin* cassette-transgene into exon 2 resulted in early embryonic lethality between E2.5 and E3.5 due to a disorganized morula leading to apoptosis (Schrank et al. 1997). However, heterozygous $Smn^{+/-}$ mice exhibited no obvious muscle atrophy, but were found to have 46% reduced Smn levels and a SMA type III like degeneration of the α-motor neurons without any visible clinical impairment (Jablonka et al. 2000). In another approach, *Smn* exon 7 was replaced by a *HPRT* cassette, leading to embryonic lethality at around E6.5 in the homozygous embryos (Hsieh-Li et al. 2000). In conclusion, none of the generated *Smn* knock-out mice allowed analysis of the SMN phenotype due to the early lethality. To overcome this pitfall, it was tried to mimic the SMA phenotype by addition of the human *SMN2* into a murine *null* $Smn^{-/-}$ background.

- *SMN2* transgenic mice

Almost simultaneously, two groups reported the successfull generation of *SMN2* transgenic mice. Remarkedly, already one or two copies of the *SMN2* transgene are sufficient to overcome the early embryonic lethality reported earlier. However, although present at a normal number at birth, motor neurons were dramatically reduced at postnatal day five and SMA animals died soon thereafter which ressembled a SMA type I. Similarly to humans, addition of more *SMN2* copies ameliorated the phenotype and eigth *SMN2* copies resulted in a rescue of the phenotype (Monani et al. 2000). In the same year, a Taiwanese group could demonstrate that integration of a BAC clone containing two human *SMN2* copies gives rise to living pups. Several different founder lines were generated on a mixed background, exhibiting either a SMA type I, II or III phenotype. One of these strains is now commercially available on a pure FVB/N background. While homozygous $Smn^{-/-};SMN2^{tg/tg}$ mice carrying four *SMN2* copies are fertile and survive for about one year (Hsieh-Li et al. 2000) their $Smn^{-/-};SMN2^{tg/wt}$ littermates exhibit a SMA type I like phenotype, are lighter than their healthy littermates and survive for approx. 10 days (Hsieh-Li et al. 2000; Riessland et al. 2010).

Several years later, the *SMN2Δ7* cDNA was introduced on a $Smn^{-/-};SMN2^{tg/tg}$ background to test whether SMNΔ7 is beneficial or detrimental. It could be shown that survival increased from 5 to 14 days, suggesting that at least SMNΔ7 in part retains some oliogomerization capacity and stabilizes the SMN complex (Le et al. 2005).

Recently, a group of novel $Smn^{-/-};SMN2^{tg/tg}$ mice carrying one to four copies of *SMN2* was generated. Animals carrying three *SMN2* copies exhibited an intermediate phenotype characterized by decreased respiratory rate and an increased apnea frequency. In line with this, NMJ defects at the diaphragm were observed thus culminating in a median survival of 15 days (Michaud et al. 2010)

As a result of the continuous identification of novel mutations in SMA patients, two additional transgenic mice strains were generated. The first one is based on three unrelated SMA patients carrying one intact *SMN2* allele and one with an A2G missense mutation. These patients exhibited a much milder phenotype than expected from their *SMN2* copy number (Parsons et al. 1998). Therefore, a $SMN2_{A2G}$ transgene was integrated into the previously described Monani *et al.* SMA-like mouse (Monani et al. 2003). Similarly to SMA patients, these animals developed a SMA type III-like phenotype with a lifespan >15 months. Though, how SMN_{A2G} ameliorates the phenotype remains elusive, since SMN_{A2G} is markedly reduced in its oligomerization capacity. One possible explanation may be that full-length SMN serves as a scaffold which promotes formation of FL-SMN:SMN_{A2G} oligomers enhancing binding to several other proteins (Monani et al. 2003). Furthermore, it could be shown in a second mouse model that introduction of an allele carrying the previously described *SMN1* mutation (SMN_{A111G}) (Sun et al. 2005), which retains capability of snRNP assembly, is also able to ameliorate the phenotype of $Smn^{-/-}$;$SMN2^{tg/tg}$ mice. Noteworthy, the SMN_{A111G} allele was not able to rescue the SMA phenotype alone and also does not complement the A2G mutation, suggesting that both mutations affect the same function (Workman et al. 2009).

Very recently, also a humanized knock-in SMA-like mouse has been reported. In this model, the C at Pos +6 of *Smn* exon 7 was replaced by a T resulting in a murine "*Smn2*". This triggered exon 7 exclusion in 60 to 80% of *Smn* transcripts depending on the respective organ. However, although SMN protein was generally reduced by 60%, the animals developed an adult onset SMA phenotype (Gladman et al. 2010).

▪ Conditional *SMN* knock-out mice

Since neither the ubiquitous *Smn* deletion nor the addition of *SMN2* transgenes allowed the investigation of tissue-specific functions of Smn, a few conditional knock-out strains were generated by emplyoing the Cre/LoxP system.

Deletion of *Smn* exon 7 in neurons by Cre-recombinase under the control of the neuron specific enolase (NSE) resulted in motor axon loss while the cell body remained unaffected. However, *Smn exon 7*[Fl/Fl]; *NSE-Cre*[+] animals exhibited tremors, atrophic muscle fibers and had a mean survival of 25 days (Frugier et al. 2000). As a complementary experiment, *Smn* exon 7 was also deleted in the skeletal muscle using HSA-Cre (α-skeletal actin promoter driven). *Smn exon 7*[Fl/Fl]; *HAS-Cre*[+] animals are characterized by muscle paralysis after three weeks leading to death at a mean age of 33 days. Furthermore, a progressive myopathy accompanied by muscular dystrophy was observed suggesting a destabilization of the sarcolemma (Cifuentes-Diaz et al. 2001). Using *Aflp-Cre*, *Smn* exon 7 was also deleted in the liver. *Smn exon 7*[Fl/Fl]; *Aflp-Cre*[+] mice presented a dramatic liver atrophy associated with liver dysfunction and iron overload leading to embryonic lethality at E18 (Vitte et al. 2004).

In addition to tissue-specific deletion of *Smn* exon 7, full-length SMN was overexpressed by using either the neuronal-specific prion promoter (PrP) or the muscle-specific HSA promoter. *Smn*$^{-/-}$;*SMN2*$^{tg/tg}$;*PRP-SMN*$^{tg/tg}$ survive for approx. 210 days whereas *Smn*$^{-/-}$;*SMN2*$^{tg/tg}$;*HSA-SMN*$^{tg/tg}$ animals exhibited no improvement in the SMA phenotype and survival. This suggested that atrophy in SMA is rather a secondary effect due to neuron degeneration than a primary one (Gavrilina et al. 2008).

1.5   SMA: Why do specifically motor neurons die?

The major characteristic of spinal muscular atrophy in humans is the specific degeneration of the α-motor neurons in the anterior horns of the spinal cord while other cell types remain spared (Iannaccone 1998). Inspection of diverse SMA-like models led to the same conclusion that the predominant factor in disease progression is the continous degeneration of the α-motor neurons (Chang et al. 2008; Frugier et al. 2000; Kariya et al. 2008; McGovern et al. 2008; McWhorter et al. 2003). However, the fundamental question remains why specifically this type of cells is affected although SMN is ubiquitously expressed? Since SMN shows a more than 50-fold higher expression in the spinal cord compared to other tissues (Coovert et al. 1997; Lefebvre et al. 1995), it might be speculated whether α-motor neurons are more vunerable to reduced SMN levels than other cells. But which specific role fulfilled (1.3.2) by SMN is the ultimate detrimental factor?

Nowadays, based on the numerous SMA-like animal models researchers have proposed two popular hypotheses which try to explain the specific loss of α-motor neurons in SMA patients (Burghes and Beattie 2009):

▪ *SMA is caused by the disruption of a neuron-specific function of SMN*

SMN has been found in growth cones and axons of neuronal cells *in vitro* (Fan and Simard 2002; Zhang et al. 2006*)*. Furthermore, knockdown of *Smn* in zebrafish led to specific motor neuron axon defects like truncation and branching (McWhorter et al. 2003). A similar result was observed in cultured motor neurons from SMA-like mice, including shortened axons, smaller growth cones and, most importantly, reduced levels of β-actin mRNA transport (Rossoll et al. 2003). In line with this, it could be demonstrated that overexpression of *PLS3*, an actin-bundling protein, is able to overcome the SMA phenotype in zebrafish (Oprea et al. 2008). The association between β-Actin and SMN is further underlined by the observation that *Smn* knockdown in PC12 cells alters expression of *profillin II*. This leads to an inappropriate activation of the RhoA/ROCK pathway causing defective neuritogenesis (Bowerman et al. 2009; Bowerman et al. 2007). In line with this, it has been proven that ROCK-inhibition prolongs survival of SMA-like mice (Bowerman et al. 2010).

Furthermore, there is evidence that SMN may also have a NMJ-specific role, since NMJ of SMA-like mice are typically immature due to an abnormal development (Kariya et al. 2008; Kong et al. 2009). Pointing into the same direction, it has been shown that intermediate SMA

mice exhibit less synaptic vesicle release, which may explained by the reduced $Ca_v2.2$ (a Ca^{2+} channel) expression observed in cultured motor neurons of SMA mice (Jablonka et al. 2007; Kong et al. 2009). However, it might be speculated whether these observations can be attributed to the interaction between SMN and β-Actin protein/mRNA transport (Bowerman et al. 2009; Oprea et al. 2008; Rossoll et al. 2003). Although not finally proven yet, it is also conceivable that lack of SMN disturbs transport of a certain additional mRNA to the growth cone, which leads to a reduced expression at the synapse thus resulting in an altered synaptic architecture.

- ▪ *SMA is caused by impaired snRNP biogenesis*

Since impaired snRNP biogenesis affects rather every cell than only motor neurons, it has been suggested that α-motor neurons are more vulnerable to subtle defects in snRNP assembly because of their high mRNA demand (Yoo et al. 2010). Interestingly, it has been shown that there is a correlation between snRNP assembly and the severity of the SMA phenotype in mice (Gabanella et al. 2007). However, introduction of the SMN_{A111G} construct, which is capable of undergoing snRNP-biogenesis, ameliorates the SMA phenotype of $Smn^{-/-}$;$SMN2^{tg/tg}$ mice, but does not rescue lethality in $Smn^{-/-}$ mice (Monani et al. 2003). In line with this, injection of assembled snRNPs into SMA zebrafish was, at least to some extent, able to restore the phenotype (Winkler et al. 2005), suggesting that reduced snRNP contributes to the SMA phenotype. Nevertheless, the question remains what are the consequences of reduced snRNP assembly? Although recent studies using exome arrays identified wide-spread splicing differences in SMA-like mice, especially in intron-rich genes (Zhang et al. 2008), it is difficult to decipher which of these changes are caused by low SMN levels and which of them are secondary due to the SMA phenotype. Although final proof is still missing, it is conceivable that reduced snRNP-biogenesis alters splicing of certain synaptic mRNA and thus leads to an altered synaptic architecture.

In conclusion, both hypotheses provide good reasons why α-motor neurons are preferentially affected in SMA. Nevertheless, a number of questions still remain open. Especially which function of SMN is directly affecting motor axons? Is it indeed the decrease in β-actin mRNA transport or does disruption of snRNP assembly alter splicing of a gene that is indispensable for proper axon and NMJ function? Consequently, further experiments are needed to answer these questions and finally explain the underlying molecular cause of SMA.

1.6 Therapeutic approaches in SMA

Although much research has been invested in the development of a therapy for SMA, no cure for SMA is available yet. Indeed, symptomatic treatments like physical exercise or respiratory drainage to remove tracheal mucus help to improve patient´s life quality, but they do not target the underlying genetic cause of SMA. Also several non-targeting strategies

have been followed over the past years, like neurotrophic agents which reduce α-motor neuron degeneration. Although the use of these agents sounds attractive, they do not target the genetic cause of SMA. This is of particular importance, since in contrast to other genetic disorders, SMA offers the unique possibility of targeting a nearly identical copy of the disease-determining gene *SMN1*. Therefore, several therapies have been developed which will be briefly introduced in the following. However, much data comes from experiments using SMA-like mice and only a very few regimens have yet been tested in humans.

1.6.1 Epigenetic therapy targeting *SMN2* expression

Although many different approaches have been undertaken to cure SMA, none of them has made it into routine clinical use yet. However, among the proposed therapies described in section 1.6 the epigenetic SMA therapy applying Histone Deactylase Inhibitors (HDACi) has proceeded farthest, since already three clinical trials with valproic acid and sodium butyrate have been performed. Furthermore, a number of second generation HDACis are currently in the pipeline undergoing extensive *in vitro* and *in vivo* testing.

In general, *epigenetics* comprise two levels of gene expression regulation which are added as a superstructure onto the DNA. On the one hand, DNA methylation has been shown to effectively silence gene expression. For example, it has been demonstrated that methylation of four CpG-islands located within the *SMN2* promoter dramatically alters the SMA phenotype by reducing *SMN2* expression (Hauke et al. 2009). On the other hand, gene expression is controlled by covalent histone modifications. Individual modifications alter the chromatin structure in a way that either promotes or restricts gene expression (Strahl and Allis 2000).

1.6.1.1 The concept of epigenetic therapy

Conceptually, epigenetic therapy using HDACi relies on the loosening of DNA packaging leading to an enhanced transcriptional activity. DNA is associated in the nucleus with proteins to form chromatin. Since the human genome consists of approx. 3.2×10^9 bases, a completely unwound DNA would be almost 1.8 m in length. Therefore, DNA has to be packed very tightly to fit into a nucleus of around 15 µM in diameter. Consequently, approx 150 bp of the 2 nm DNA double helix are wrapped around a histone octamere, resulting in the pearl necklace like 10 nm fiber (11 nm in diameter). The next level of packaging is added by the histone H1, which binds to the interspaced DNA between two histone octameres thus forming the 30 nm fiber. A further step of DNA tightening is then introduced by attaching the 30 nm fiber to the nucleic protein matrix to form an even more condensed chromatin structure (Maeshima and Eltsov 2008; McBryant et al. 2010).
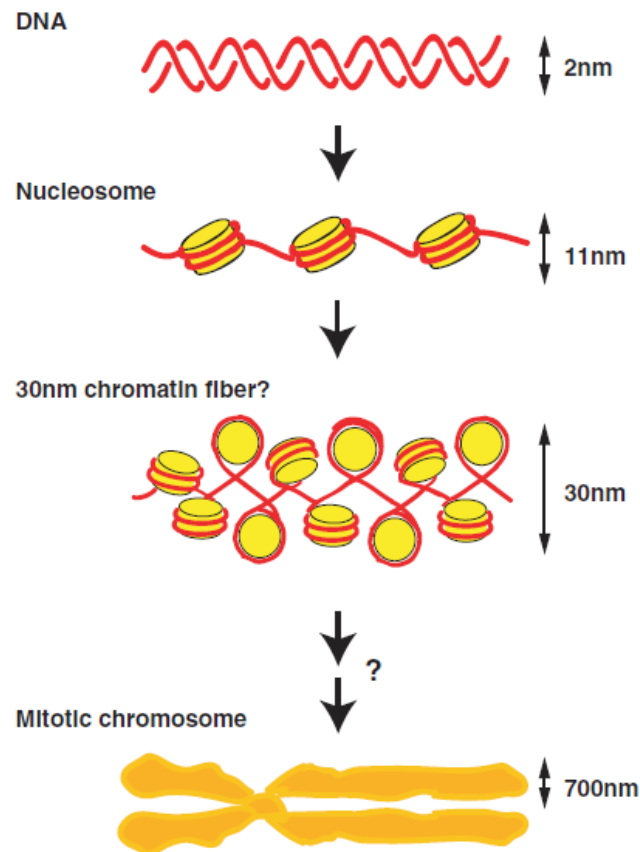
Figure 4   Packaging of eukaryotic DNA in the nucleus. The 2 nm DNA fiber is wrapped around histone octameres to form the 10 nm fiber. It is then assumed that the 10 nm fiber is further condensed to a 30 nm chromatin fiber which is finally packaged to a 0.7 µm chromatid (Maeshima and Eltsov 2008).

The basic elements of DNA packaging are the histone octameres which, together with approx. 150 bp of DNA, form the fundamental DNA packaging unit, the nucleosome. In total, five main types of histones are known for both animal and plant cells: H1, H2A, H2B, H3 and H4. Two histones of H2A, H2B, H3 and H4 each form together the histone octamere around which 1.65 superhelical turns of DNA are wrapped (Burlingame et al. 1985; McBryant et al. 2010). The nucleosome itself is stabilized by extensive dipole interactions between the arginin residues of the core structure of the histone and the negatively charged phosphate backbone of the DNA. Common to all histones is a canonical α-helical histone-fold motif of the globular core, which is responsible for the DNA interaction while the N-terminal "tail" domains (NTD) reach out of the nucleosomal structure. NTDS are 14 to 38 aa in length, enriched in lysine and arginine residues and typically without secondary structures (Luger and Richmond 1998). However, the pearl necklace like structure of nucleosomes on a DNA strand is further condensed by the linker histone H1 which binds to the interspaced DNA. Unlike the histones H2A to H4, the linker histone H1 possesses a threeparted structure with an unstructured N- (13 to 44 aa) and C-terminus (approx. 100 aa), which flank a well-folded

globular domain. Histone H1 binds asymmetrically the nucleosomal DNA entry and exit sites, thus inducing folding of the DNA to form the 30 nm fiber (McBryant et al. 2010).

The NTDs of the nucleosomal histones have gained particular interest, since a number of post-translational modifications have been identified which lead to a highly dynamic chromatin structure and thereby control expression. Based on these observations, in 2000 the "histone code" has been proposed, which tried to assign specific functions like expression or meiosis to certain NTD modifications (e.g. phosphorylation, methylation, acetylation and ubiquitinylation) (Strahl and Allis 2000). However, in the light of the identificaction and detailed characterization of numerous chromatin remodelling complexes, like SWI/SNF, ISWI, CHD and INO80, the original code has been rewritten and a final version is not yet available (Ho and Crabtree 2010).

Among the observed NTD modifications, acetylation is the best characterized one. Addition of an acetyl residue to the positively charged ε-aminogroup of a histone´s lysine neutralizes its charge. Consequently, the DNA packaging is looser and the DNA is accessible for factors involved in transcription, replication and DNA repair (Figure 5). Furthermore, it has been suggested that acetylated histones may serve as binding platforms for activators or repressors (Khan and Khan 2010). Researchers have identified two groups of enzymes which oppositionally add or remove acetyl residues from NTD of histones. The Histone Acetyl Transferases (HAT) have been shown to pass an acetyl residue from acetyl-CoA onto the terminal amino group of lysine. The counteracting entities are the Histone Deacetylases (HDAC), which remove acetyl residues from the lysine side chains thus leading to denser heterochromatic structure (Figure 5).
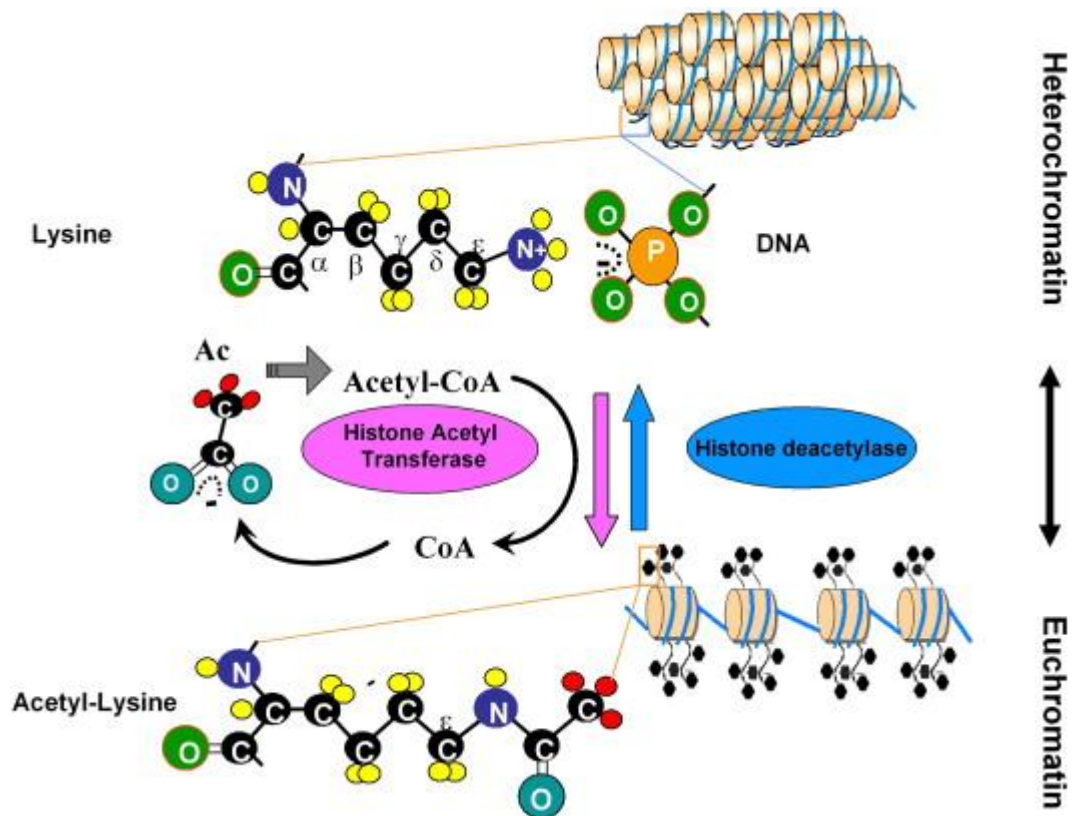
Figure 5   **Histone acetylation and deacetylation catalyzed by HAT and HDACs. The figure illustrates the molecular interaction between acetylated and deacetylated lysine residues and DNA and the resulting transition from Eu- to Heterchromatin (taken from (Khan and Khan 2010))**

Within the human genome more than 20 HATs and 11 HDACs have been identified. Based on their sequence homology, these enzymes have been classified into several sub classes which will be briefly characterized in the following.

1.6.1.2 Histone Acetyl Transferases (HAT)

In contrast to HDACs, there is no regular structure among the HATs. Common to all of them is an acetyltransferase domain which is at least in some cases only suspected. However, based on the additional domains HATs were classified into several groups (Khan and Khan 2010). Perhaps the most prominent HAT families are CBP/P300 enzymes, the GNAT family, the MYST family and finally the group of Rtt109 enzymes. Several other HAT families have been identified, but they have yet only been studied in less detail. While the CBP/P300 family is involved in rather global histone acetylation (H2B K12/15, H3 K14/18 and H4 K5/8), the enzymes of the GNAT family primarily target H3 K14 and H4 K8 (Dekker and Haisma 2009). The MYST family of HATs is mainly involved in cell cycle and growth control and has also been linked to various types of cancer, especially Tip60 (Avvakumov and Cote 2007). However, HATs have been shown to be implicated in learning (Dekker and Haisma 2009) or diseases like asthma and chronic obstructive pulmonary disease (Barnes et al. 2005). Noteworthy, the substrate specificity of HATs is not restricted to histones since also

other proteins like p53 or general transcription factors are substrates (Sterner and Berger 2000). Within the past years, also several HAT inhibitors have been identified like isothiazolones or the naturally occurring substance curcumin but none of them has yet entered everyday clinics (Balasubramanyam et al. 2004).

1.6.1.3 Histone Deacetylases (HDAC)

The 11 classical histone deacetylases are classified into three classes. Class I, which is related to yeast HDAC Rpd3, contains HDAC1-3 and 8 while class II, which is structurally similar to the yeast Hda1 histone deacetylase, includes HDAC4-7, 9 and 10. In contrast to the other groups, class IV contains only HDAC11. In addition to these classical HDACs, another group of deacetylases has been identified, the sirtuins, which are referred to as class III HDACs. However, in contrast to the classical HDACs, which are Zn^{2+}-dependent, sirtuins rely on NAD^+ as essential co-factor (Khan and Khan 2010). Notably, none of the HDACs possesses a DNA-binding domain thus target specificity must be conferred by individual binding partners (Glozak et al. 2005)

1.6.1.3.1 Class I HDACs

In contrast to class II and IV HDACs, all class I HDACs are ubiquitously expressed and are present in both cytoplasm and nucleus. The almost identical HDAC1 and 2 seem to be partly redundant, since depletion of one leads to an increase in the other (Brunmeir et al. 2009). The structure of HDAC3 is slightly different, since it lacks a second CK phosphorylation site whereas HDAC8 only possesses one PKA phosphorylation site (Yang and Seto 2008). With the exception of HDAC8 all class I HDACs are functioning as catalytic subunits of multiprotein complexes. For example, HDAC1 and 2 interact to form the catalytic subunit of the Sin3, NuRD (nucleosome remodeling deacetylase) and CoREST (corepressor of RE1-silencing transcription factor) complexes which repress transcription (Grozinger and Schreiber 2002; Yang and Seto 2008).

1.6.1.3.2 Class II HDACs

The class II HDACs are subdivided based on whether they contain one (class IIA; HDAC 4, 5, 7 and 9) or two catalytic domains (class IIB; HDAC6 and 10). All class IIA members contain three conserved 14-3-3 binding sites, myocyte enhancer factor-2 (MEF2) binding sites as well as signals for the nuclear in- and export, since they are present in both, nucleus and cytoplasm (Yang and Seto 2008). Consequently, MEF2 and 14-3-3 oppositionally regulate localization of class IIA HDACs (Nishino et al. 2008) The class IIB member HDAC6 has emerged as the major cytoplasmatic deacetylase, since *in vivo* also tubulin, Hsp90 and cortactin are HDAC6 substrates (Haggarty et al. 2003). Interestingly, HDAC6 contains a C-terminal zinc finger which is involved in several pathways like clearance of aggresomes or dendritic outgrowth (Kawaguchi et al. 2003; Kim et al. 2009). The other class IIB member HDAC10 has been found to be decreased in lung cancer patients suggesting an important

role in the maintenance of normal cells. However, although HDAC10 has been shown to deacetylate Hsp70, a fundamental understanding of its function remains elusive (Lai et al. 2010).

1.6.1.3.3 Class III HDACs (sirtuins)

Mammals contain seven sirtuins, which are characterized by their conserved NAD$^+$-dependent catalyctic domain. However, the N- and C-termini are strikingly different which goes in line with their divergent roles as regulators of physiology, calorie restriction and aging (Haigis and Guarente 2006). Since sirtuins are not inhibited by classical HDACi, they will not be discussed any further at this point.

1.6.1.3.4 Class IV HDACs

HDAC11 is a highly conserved deacetylase and the only family member of class IV HDACs. Although little is known about its function, its high conservation from *C.elegans* to man suggests a fundamental role (Yang and Seto 2008). Some *in vitro* experiments showed that HDAC11 regulates interleukin-10 expression in antigen-presenting cells (Villagra et al. 2009) as well as myelin basic protein (MBP) and proteolipid protein (PLP) levels during oliogodendrocyte maturation (Liu et al. 2009).

1.6.1.4 HDAC inhibitors

In addition to classical transcription factors, gene expression is regulated in concert by HATs and HDACs. Consequently, interference with this tightly regulated balance by inhibition of either HAT or HDACs switches transcription either on or off. In 1990, this theoretical assumption was proven by the finding that Trichostatin A, a *streptomyces* metabolite, inhibits cell cycle and differentiation by blocking HDACs (Yoshida et al. 1990). In the following, several other compounds were identified which clearly inhibited the activity of HDACs (Strahl and Allis 2000). From a mechanistic point of view, HDAC inhibition leads to an overbalance of HAT activity resulting in a boosted transcriptional rate. Since this is an unbiased approach, which virtually should affect all genes, several studies tried to elucidate the impact of HDACi treatment on global gene expression. However, depending on the type of cells and HDACi employed, values ranged between 2% and 20% of differentially expressed genes (Mariadason et al. 2000; Peart et al. 2005; Stimson and La Thangue 2009; Van Lint et al. 1996).

Initially, HDACi were intended to be used primarily in cancer therapy because excessive deacetylation was found in several cancer entities. The rationale of using HDACi was to re-express heterochromatic regulatory genes by inducing a widespread transition into the euchromatic state (Bertrand 2010; Tan et al. 2010). However, the effect of HDACi treatment is not a simple up-regulation of gene expression since several secondary effects are

triggered. Induction of regulatory genes may in turn decrease expression of other genes resulting in a rather complex expression pattern under HDACi regimen.

Depending on their chemical backbone, HDACi have been divided into several classes (Bertrand 2010):

- **Short chain fatty acids**
  - \> Phenylbutyrate (PB)
  - \> Sodium butyrate (SB)
  - \> Valproic acid (VPA)

- **Hydroxamates**
  - \> Trichostatin A (TSA)
  - \> Suberoylanilide hydroxamic acid (SAHA)
  - \> Suberic bishydroxamic acid (SBHA)
  - \> m-carboxycinnamic acid bishydroxamide (CBHA)
  - \> LBH589
  - \> NVP-LAQ824
  - \> JnJ-248645815
  - \> PCI-34051
  - \> Oxamflamtin
  - \> Scriptaid

- **Benzamides**
  - \> M344
  - \> MS-275
  - \> CI-994

- **Cyclic tetrapeptides**
  - \> Trapoxin A
  - \> Apicidin
  - \> FK228 (Depsipeptide)

Structural and mechanistic studies using TSA and SAHA suggested that HDACi block HDACs by chelating the central Zn^{2+} in the catalytic center (Bertrand 2010; Finnin et al. 1999). Based on these observations, a well-accepted pharmacophore for HDAC has been proposed comprising the Zn^{2+} binding group (ZBG; chelating the Zn^{2+}), a linker that passes through the tube-like access to the active centre and a cap group for interactions with the external surface (Figure 6).
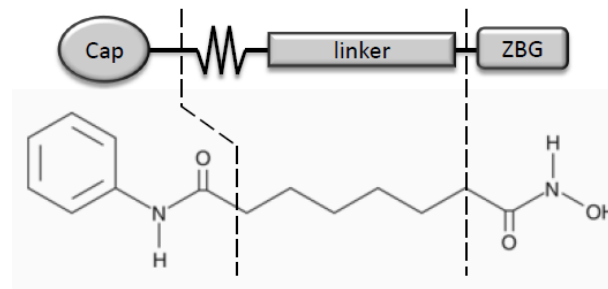
Figure 6   Diagram depicting the typical structure of HDACi consisting of Zinc-binding domain, linker and cap using the example of SAHA. Similarly to most of the second generation HDACi, zinc is chelated by the hydroxamic acid residue (modified from (Bertrand 2010))

However, depending on their chemical composition some HDACi generally inhibit HDACs (so-called panHDACi), whereas others preferentially block class I or II enzymes. Although suggested, there is no given rule yet which defines that certain residues either favor inhibition of class I or II. Nevertheless, some HDAC-specific HDACi have been developed in the past years, such as PCI-34051 which is an HDAC8-specific inhibitor (Balasubramanyam et al. 2004).

	Class I	Localization	Selected Targets
	HDAC1	Nucleus	Androgen Receptor
			p53
			MyoD
			E2F-1
			SHP
			Stat3
	HDAC2	Nucleus	Glucocorticoid Receptor
			Bcl-6
			YY-1
			Stat3
	HDAC3	Nucleus	RelA
			YY-1
			GATA-1
			SHP
			Stat3
PCI-34051	HDAC8	Nucleus	
	Class IIa		
	HDAC4	Nucleus/Cytoplasm	GATA-1
			GCMa
			HP-1
	HDAC5	Nucleus/Cytoplasm	Smad7
			GCMa
			HP-1
	HDAC7	Nucleus/Cytoplasm	Plag1/Plag2
	HDAC9	Nucleus/Cytoplasm	
	Class IIb		
Tubacin	HDAC6	Mostly Cytoplasm	α-tubulin
			Hsp90
			SHP
			Smad7
	HDAC10	Mostly Cytoplasm	
	Class IV		
	HDAC11	Nucleus/Cytoplasm	

Table 2   Inhibition profile of some HDACi and some downstream targets primarily affected by blocking of the respective HDAC. (taken from (Carew et al. 2008))

1.6.1.5 Epigenetic SMA therapy with HDACi

The rationale of using HDACi in SMA therapy is quite simple. Although *SMN1* as the major source of *FL-SMN* is lacking, *SMN2* still produces around 10% full-length transcript. Activation of *SMN2* should consequently increase the amount of *FL-SMN2*. Almost 10 years ago, it could be shown that treatment of EBV-transformed lymphoblastoid cell lines derived from SMA patients with the HDACi Sodium butyrate markedly elevated *FL-SMN2* levels (Chang et al. 2001). Within the same work, it could be demonstrated that treatment of pregnant mothers of *Smn*$^{-/-}$;*SMN2*$^{tg/tg}$ mice improves survival of the pups thus implying that HDACi are indeed a prospective group of putative SMA drugs. In the following, several additional HDACi were tested *in vitro* and *in vivo* as putative SMA drugs such as Valproic acid (1.6.1.6) (Brichta et al. 2003; Brichta et al. 2006; Swoboda et al. 2010; Swoboda et al. 2009), Phenylbutyrate (Brahe et al. 2005; Mercuri et al. 2004; Mercuri et al. 2007), TSA (Avila et al. 2007) or the second generation panHDACi SAHA (Hahnen et al. 2006; Riessland et al. 2010). In conclusion, the results were very promising although it has to be considered that highly potent panHDACi may exert several unfavorable side-effects.

1.6.1.6 VPA in SMA therapy

Valproic acid, abbreviated VPA, is a branched short-chain fatty acid. In 1963, VPA was accidently identified as a compound having anticonvulsant properties in a seizure model (Meunier et al. 1963). Since then, the therapeutic spectrum of VPA has been enlarged from epilepsy to bipolar disorder, migraine prophylaxis and even cancer. However, the mechanisms of action of VPA are poorly understood although it has been shown that VPA alters a wide variety of signalling pathways (Terbach and Williams 2009). For example, it has been shown that VPA has an inhibitory effect on a variety of ion channels, thus influencing sodium and calcium currents in hippocampal neurons (De Sarro et al. 1992; McLean and Macdonald 1986). However, it may be criticized that many of these studies used very high VPA concentrations like 400 $^{mg}/_{kg}$ bodyweight (De Sarro et al. 1992). Data from studies further investigating the effect of VPA on neurons suggested that it increases levels of the inhibitory neurotransmitter GABA, but more recent studies did not verify this observation (Lindekens et al. 2000). Furthermore, it has been shown that, similarly to the the mood-stabilizer Lithium, VPA decreases Inositol 1,4,5-triphosphate levels, thus increasing amphetamine levels (Shaltiel et al. 2007).

VPA has been widely used in epilepsy therapy for more than 30 years, therefore side-effects can be well estimated. Among the observed ones carnitine depletion is frequent. The underlying cause is that VPA, like any other fatty acid, is transferred from Co-enzyme A (CoA) onto carnitine to form Carnityl-VPA. This metabolite inhibits the carnitine transporter supplying the cell with carnitine and furthermore reduces the intracellular carnitine content by diffusing out of the cell and getting lost by renal excretion (Luch 2010).

The most important observation in terms of SMA therapy was the finding that VPA mimics the effects of TSA thus inhibits HDACs (Gottlicher et al. 2001; Phiel et al. 2001). This observation also provided a major breakthrough in the understanding of another major side effect of VPA, which is teratogenicity during pregnancy (Robert and Guibaud 1982). Since the HDACi Sodium butyrate already produced promising results, VPA was tested as a putative SMA drug *in vitro* (Brichta et al. 2003; Chang et al. 2001). It could be shown that concentrations between 0.5 and 500 µM VPA significantly elevated *SMN2* mRNA and protein levels 2- to 4-fold. Based on these promising results, a first pilot clinical trial was enrolled with 20 SMA patients and 10 SMA carriers (Brichta et al. 2006). While in seven out of 10 carriers SMN levels were elevated, the results in the VPA-treated patients were not that consistent: While in seven of the treated patients SMN blood levels were elevated, in six of them no change was detected whereas another seven SMA patients exhibited declined SMN levels under VPA regimen (Brichta et al. 2006). More recently, VPA was tested in a phase II open-label clinical trial with 42 SMA patients (2 SMA type I, 29 SMA type II and 11 SMA type III) (Swoboda et al. 2009). In conclusion, VPA was well tolerated. In some cases motor function decreased due to weight gain, but in the majority of younger SMA type II cases the mean motor score increased significantly. Unexpectedly, no change in *SMN2* expression could be detected on RNA level. However, against the background of previous findings (Brichta et al. 2006) the question may be raised whether a more differentiated analysis of individual patients would have led to a more convincing outcome. Furthermore, *SMN2* expression has not been stratified in the tested patients. Without determination of a proper basal level, it is hard to draw any final conclusion as to whether VPA affects *SMN2* levels or not. These points have to be addressed since in a study VPA treatment of SMA-like mice clearly improved motor function and motor-evoked potentials as well as decreased motor neuron degeneration (Tsai et al. 2008).

1.6.2   Further therapies targeting *SMN2*

1.6.2.1 RNA-based therapy

Since the detrimental difference between *SMN1* and *SMN2* is the splicing of exon 7, modulation of *SMN2* pre-mRNA splicing has come into focus. Based on the tremendous work which has been spent on the understanding of *SMN2* exon 7 skipping, several antisense oligonucleotides (ASO) strategies have been developed to correct *SMN2* splicing. For example *in vitro* blocking of the 3´ splice site (ss) of exon 8 with an antisense probe altered the competition of exon 7 and 8 for the joining with the 5´ss of exon 6 in such way that exon 7 was included in more than 53% (Geib and Hertel 2009; Lim and Hertel 2001). Furthermore, *in vivo* studies using *SMN2* transgenic mice demonstrated that injection of ASOs targeting the ISS in intron 7 efficiently corrects *SMN2* splicing (Hua et al. 2008).

The classical ASO approach was further extended by the creation of bifunctional RNAs binding *SMN2* exon 7. In addition to the antisense sequence, these bifunctional RNAs also contain ESE sequences or covalently bound peptides functioning as binding platforms for SF2/ASF or hTRA2-β1 to increase exon 7 inclusion (Baughan et al. 2006; Baughan et al. 2009; Marquis et al. 2007; Skordis et al. 2003). In such a way, it has been shown that addition of ESE sequences to an antisense U7 snRNAs incorporated into the U7 snRNP leads to nearly complete reinclusion of *SMN2* exon 7 (Marquis et al. 2007). As a proof of principle, a bifunctional RNA covering the negative splice regulator E1 in intron 6 was injected in SMA-like mice. Although SMN levels were more than 2-fold increased, the impact on survival was rather low (+10%) (Baughan et al. 2009). However, it could recently be demonstrated that direct infusion of an ASO targeting ISS-N1 in intron 7 via a micro-osmotic pump into the lateral cerebral ventricle in adult *SMN2* transgenic mice resulted in a robust and long lasting increase in exon 7 inclusion. Moreover, a single neonatal or embryonic dose rescued the tail and ear necrosis in SMA-like mice (Hua et al. 2010).

Furthermore, so-called trans-splicing (ts) RNAs have been developed. Conceptually, these ts-RNAs rely upon splicing between the target RNA and the therapeutic RNA providing the correct RNA sequence. Using this system to add exon 7 to the mature *SMN2* mRNA, it could be demonstrated that ts-RNAs increase *FL-SMN2* levels *in vitro* and *in vivo* (Coady and Lorson 2010; Coady et al. 2007).

1.6.2.2 Gene therapy

Another approach to treat SMA is the delivery of *SMN* into the CNS of SMA-like mice using adeno-associated vectors (AAV) to complement the lack of *Smn*. Injection of an AAV8 vector encoding human *SMN1* (AAV8-hSMN) into the CNS of newborn mice increased the survival from 15 to 50 days. Furthermore, myofiber size and NMJ architecture were substantially improved. Moreover, injection of self-complementary (sc) AAV8 vector improved efficacy of gene therapy to a median survival of more than 150 days (Passini et al. 2010). More recent results conjecture that sc-AAV9 vectors encoding for *SMN1* are the vectors of choice. Injection significantly improved motor function, NMJ architecture and the cardiac phenotype of SMA-like mice. In line with the previous results, median survival was extended from approx. 15 to more than 100 days (Bevan et al. 2010; Foust et al. 2010) or even 200 days (Valori et al. 2010).

1.6.2.3 Drug therapy

Although data from ASO or gene therapy experiments sound quite promising, it is ambiguous whether one of these approaches will become state-of-the-art therapy for SMA due to the unknown side effects. Therefore, several small molecules have been developed and identified targeting *SMN2* or the SMNΔ7 protein, respectively.

- *SMN2* promoter induction

In addition to *SMN2* splicing and stabilization of the SMNΔ7 protein, also several compounds have been identified which elevated *SMN2* expression *in vitro*. For example, it has been observed that treatment of SMA fibroblasts with β2-adrenoreceptor agonist Salbutamol rapidly increases *FL-SMN2* levels and subsequently elevates SMN protein (Angelozzi et al. 2008). Moreover, based on the identification of an interferon-response-element (IRE) in the *SMN2* promoter it could be shown that treatment with either the interferon IFN-β or IFN–γ elevates SMN levels merely 4-fold (Baron-Delage et al. 2000). Lastly, a compound screening campaign resulted in the identification of quinazolines which more than doubled *SMN2* promoter activity (Jarecki et al. 2005).

- *SMN2* splicing

Several compounds have been identified to alter *SMN2* splicing and to increase the amount of full-length SMN protein derived from *SMN2*. By screening a compound library, Aclarubicin was identified to stimulate incorporation of exon 7 in SMA fibroblasts and NSC-34 cells (Andreassi et al. 2001). Presumably via STAT5 activation the phosphatase inhibitor Na-Vanadate has been demonstrated to increase exon 7 inclusion *in vitro* (Ting et al. 2007; Zhang et al. 2001). Moreover, the cytostatic drug hydroxyurea (HU) has been tested *in vitro* and *in vivo* as a putative SMA drug. Although the exact mode of action is poorly understood, *FL-SMN2* levels were increased in B-lymphoblastoid cells from SMA patients (Grzeschik et al. 2005). However, in SMA patients treated with HU only slight improvements were observed but these may, as the authors argue, be "clinically meaningless" (Liang et al. 2008).

- SMN protein

Several aminoglycosides like Tobramycin or Geneticin have been identified to post-transcriptionally elevate SMN levels by inducing read-through of the first stop codon in exon 8 of *SMN2Δ7* (Heier and DiDonato 2009; Mattis et al. 2006; Wolstencroft et al. 2005). Read-through leads to an elongated C-terminus of the SMNΔ7 protein, thus increasing its stability (Wolstencroft et al. 2005). In subsequent studies using the aminoglycosides TC007 *in vivo*, improved motor function was recorded and survival increased significantly by 30% (Mattis et al. 2009a; Mattis et al. 2009b). Furthermore, it has been suggested that inhibition of SMN turnover by MG-132 may be beneficial for SMA patients, but this has not yet been tested *in vivo* (Chang et al. 2004).

1.6.3 *SMN2*-independent therapies

1.6.3.1 Neurotrophic agents

Riluzole, a small benzothiazol which antagonizes the effects of the neurotransmitter glutamate, was proven to be safe and effective in patients with ALS. Although Riluzole

improved median survival and NMJ architecture in SMA-like mice (Haddad et al. 2003), no such effect was detected in Riluzole-treated SMA patients. However, only 10 patients were enrolled during the clinical trial thus questioning the final conclusions (Russman et al. 2003). In another approach targeting synaptic transmission, SMA-like mice were treated with NMDA (N-Methyl-D-Aspartate) to activate the glutamatergic NMDA-receptors (NMDAR). NMDA improved NMJ maturation, induced *SMN2* expression in the spinal cord via CREB activation and reduced motor neuron apoptosis (Biondi et al. 2010). Furthermore, the role of neurotrophic factor CNTF, which is typically secreted by Schwann cells, was investigated in SMA-like mice (Simon et al. 2010). However, since systemic treatment of ALS patients with CNTF elicits severe side effects such as fever and cachexia, treating SMA patients with CNTF is not feasible (ACTS 1996).

1.6.3.2 Stem cell therapy

The underlying idea of using stem cells in SMA therapy is to either replace the degenerated α-motor neurons or to support the remaining cells by the addition of neural stem cells. Injection of spinal cord neural stem cells (NSC) in SMA-like mice improved neuromuscular function and increased life span by 40% from 13 to 18 days. Although NSC migrated into the parenchyma and generated a small proportion of motor neurons, the authors speculate that the transplanted cells rather serve as "chaperones" for host neurons and provide neuroprotective substances than replace degenerated α-motor neurons (Corti et al. 2008). The latter hypothesis was underlined by the observation that using embryonic stem cell-derived NSC, which led to a similar amelioration of the phenotype, exhibited markedly increased levels of secreted neurotrophic factors (Corti et al. 2009). Recently, it was shown that it is possible to reprogram fibroblasts by the ectopic viral overexpression of the four factors *Oct3/4*, *Sox2*, *Klf4* and *c-Myc* into induced pluripotent stem cells (iPS) (Takahashi et al. 2007). Subsequently, also SMA fibroblasts were successfully reprogrammed and *in vitro* differentiated into motor neurons expressing choline acetyltransferase (ChAT) (Dimos et al. 2008; Ebert et al. 2009). Although these data are promising, it remains elusive whether injection of (pre-differentiated) iPS-cells into a SMA patient is indeed a therapeutic option. Especially the ectoptic over-expression of several oncogenes is a risk factor which should not be underestimated.

In summary, diverse therapeutic approaches are currently ongoing or under investigation. Among these, the HDACi discussed in section 1.6.1 have an exceptional role, since they are widely used in cancer therapy. The knowledge gained from these clinical trials helps to improve and increase safety in any putative SMA clinical trial. Furthermore, some of them, like VPA, are long known drugs which already have undergone intensive clinical testing. In addition, the *in vivo* testing of the HDACi in SMA-like mice did not reveal any

severe side effects. Nevertheless, the two clinical trials with VPA (Brichta et al. 2006; Swoboda et al. 2009) underline the need for a better understanding of how and why VPA elicits its action as an HDACi in SMA patients. The deeper understanding of the cause of non-responsiveness would not only have great benefit for SMA therapy, but also improve the VPA therapy of other diseases like epilepsy or bipolar disorder. Furthermore, alternative and ideally more potent SMA drugs are still desperately needed to improve and advance future SMA therapy.

2. Study aims

Nowadays, proximal spinal muscular atrophy is the leading genetic cause of infant death. Although much research has been spent on it, there is no cure available yet. The underlying genetic factor of SMA is the functional absence of the *survival motor neuron 1* (*SMN1*) gene. While it generates nearly 100% full-length transcripts (*FL-SMN*) the majority of transcripts produced by the almost identical copy gene *SMN2* lack exon 7 due to alternative splicing. Nevertheless, *SMN2* still produces around 10% *FL-SMN*. While this is not enough to prevent disease-onset, it is sufficient to ameliorate the SMA phenotype. The more *SMN2* copies are present in a SMA patient the milder is the SMA phenotype. Based on these observations *SMN2* became naturally a major target of SMA drug therapy.

Histone deacetylase inhibitors (HDACi) have been shown in numerous studies to activate *SMN2* expression and in addition to modulate its splicing pattern which in combination boosts *FL-SMN2* levels. Among the tested HDACi the short-chain fatty acid Valproic acid (VPA) has proven its efficacy as an SMA drug *in vitro* and also *in vivo*. In a first pilot clinical trial by our group around $^1/_3$ of VPA treated SMA patients responded positively meaning that SMN levels were elevated in blood. In contrast to that in another $^1/_3$ of patients SMN amounts dropped whereas in the latter $^1/_3$ no change at all was detected.

The primary aim of the present work was to identify the underlying cause why some SMA patients react positively to VPA treatment whereas others do not. To investigate this issue fibroblast lines from SMA patients included in the first pilot clinical trial were established and their response to VPA treatment should be characterized in detail by evaluation of *SMN2* DNA, RNA and protein level. Furthermore, transcriptomes of fibroblast lines responding positively or negatively to VPA were supposed to be compared by differential μ-array analysis. Potential differentially expressed genes should be selected and their role and impact in VPA treatment should be analyzed to uncover the underlying cause of VPA none-responsiveness. The identifaction of the cause of the differential response to VPA may lead to the identification of biomarker which allows estimation of the therapeutic outcome before therapy has actually started.

Since the question remains open whether a deeper understanding of VPA treatment will lead to the identification of a switch which controls the response to VPA also another putative SMA drug should be characterized. LBH589 is a novel second generation HDACi which exhibited a promising pharmacological profile in various malignancies. Its impact and mode of action were supposed to be characterized in detail to allow decision about potential evaluation of LBH589 *in vivo* in SMA-like mice.

3. Material and Methods

3.1 Cell lines

For all primary human fibroblast cell lines used throughout this study, a genetic analysis was carried out and informed written consent was given by the respective subjects or their legal guardians. All SMA patients, who donated human material, fulfilled the diagnostic criteria for SMA (Munsat and Davies 1992) and carry homozygous absense of *SMN1* as determined by routine molecular testing. The number of *SMN2* copies was measured using DNA isolated from EDTA blood samples collected from the respective donor. Exact determination of *SMN2* copies, using either qRT-PCR or MLPA, was carried out in the diagnostic laboratory of the *Institute of Human Genetics* in Cologne (Feldkotter et al. 2002; Tomaszewicz et al. 2005). A list of all fibroblast lines used in this work is given in Table 3 on the next page.

3.2 Mouse inbred strains

Throughout this study two different SMA-like model mouse inbred strains were employed:

- **FVB.Cg-Tg(*SMN2*)2Hung *Smn1*_{tm1Hung}/J** (purchased from Jackson´s Laboratory; #005058)

  In this mouse model the *Smn* locus is disrupted by a 1.6 kb deletion targeting *Smn* exon 7 using a 115 kb large BAC-clone integrate (clone 7) containing the *SMN2* gene as well as *NAIP* and *SERF1*. Noteworthy, 2x *SMN2* copies are present per BAC integrate (Hsieh-Li et al. 2000). In the following, these mice were termed as **SMA_{Hung}** mice. These mice were originally on a mixed background, but were backcrossed by the Jackson´s Laboratory onto a pure FVB/N background.

- **FVB.Cg-Tg(*SMN2*)89Ahmb *Smn1*_{tm1Msd}/J** (kind gift from Michael Sendtner, Würzburg / Jackson´s Laboratory; # 001800). In this mouse model the *Smn* gene was disrupted by homologous recombination of the targeting vector into the *Smn* exon 2 (Schrank et al. 1997). The *SMN2* transgene, which is only present as a single copy per integrate, is located on 35.5 kb large PAC-clone BamH1 fragment (clone 215P5). These mice were originally published on a C57Bl 6J background (Monani et al. 2000), but were later on backcrossed onto a pure FVB/NJ background. In the following these mice were termed as **SMA_{Burghes}** mice.

Animals were housed in micro-isolation chambers in the mouse facility of the the *Institute of Genetics* in Cologne. All mice were humanely euthanized according to the guidelinces set forth by the *Landesamt für Natur, Umwelt und Verbraucherschutz NRW*. Mouse breedings and experiments were approved by the local animal protection committee and were performed under the reference number 9.93.2.10.31.07.292.

Fibroblast line	Phenotype	n(SMN1)	n(SMN2)	Identifier in Brichta et al.
ML16	SMA type I	---	3	---
ML17	SMA type I	---	2	---
ML86	SMA type I	---	2	---
ML95	SMA type I	---	2	---
ML111	SMA type I	---	2	---
ML108	SMA type I	---	3	---
ML5	SMA type II	---	3	---
ML62	SMA type II	---	3	P10
ML65	SMA type II	---	3	P12
ML60	SMA type II	---	3	P5
ML67	SMA type II	---	3	P8
ML71	SMA type II	---	3	P6
ML72	SMA type II	---	3	P7
ML59	SMA type II	---	3	P13
ML73	SMA type II	---	3	P14
ML79	SMA type II	---	3	---
ML89	SMA type II	---	3	---
ML94	SMA type II	---	3	---
ML96	SMA type II	---	3	---
ML104	SMA type II	---	n.d.	---
ML105	SMA type II	---	3	---
ML110	SMA type II	---	n.d.	---
ML69	SMA type III	---	4	P4
ML82	SMA type IIIa	---	3	---
ML103	SMA type IIIa	---	3	---
ML100	SMA type IIIb	---	n.d.	---
ML106	SMA type IIIb	---	4	---
ML49	Carrier	1	2	C5
ML53	Carrier	1	1	C1
ML63	Carrier	1	2	C7
ML66	Carrier	1	3	C9
ML68	Carrier	1	2	C4
ML75	Carrier	1	3	C8
ML6	healthy	2	---	---

Table 3   **Primary fibroblast lines derived from skin biopsies of SMA patients and carriers used throughout this thesis. Clinical diagnosis and number of *SMN1* and *SMN2* copies measured either by qRT-PCR or MPLA are given. In the case patients were included in the VPA pilot study by (Brichta et al. 2006) the respective identifier is given in the last column (n.d. = not determined).**

3.3   Equipment and chemicals

3.3.1 Equipment

The following equipment was used throughout daily laboratory routine.

▪	Centrifuges:	Allegra X22-R	*Beckman Coulter*
		5415 D	*Eppendorf*
		5415 R	*Eppendorf*
		Avanti J-20XPI	*Beckman Coulter*
▪	Spectrophotometer	BioPhotometer	*Eppendorf*
		NanoDrop ND-1000	*Peqlab*
▪	Cuvettes	UV-Vette	*Eppendorf*
▪	Microplate reader	Safire²	*Tecan*
▪	Luminometer	Glomax	*Promega*
▪	Thermocycler	DNAengine Tetrad 2	*MJ research*
▪	Realtime thermocycler	LightCycler 1.5	*Roche*
		ABI 7500 Taqman	*Applied Biosystems*
▪	Floating waterbath	FBC620	*FisherBrand*
▪	Electrophoresis chambers		
	○ Agarose gels	SGE-020-02	*CBS scientific*
	○ SDS-PAA gels	Mini-Protean 3 cell	*Biorad*
		Protean II xi	*Biorad*
▪	Western blot chambers	Mini-Protean 3 cell	*Biorad*
		Trans blot transfer cell	*Biorad*
▪	Autoradiography cassette	Developer cassette	*Siemens*
▪	Developer machine	Curix 60	*Agfa*
▪	Power supplies	PowerPac 1000	*Biorad*
		PowerPac HC	*Biorad*
▪	Imaging Systems	ChemiDoc XRS	*Biorad*
▪	Bacterial incubator		
	○ Shaking incubator	Innova 44	*New Brunswick scientific*
	○ Standard incubator	Kelvitron T	*Heraeus*
▪	Tissue culture hood	Hera Safe	*Heraeus*
▪	Cell incubator	Hera Cell 150	*Heraeus*
▪	Transfection apparatus	Nucleofector	*Lonza*
▪	Cell counting chamber	Neubauer chamber	*Optik Labor*
▪	Heating shaking block	HTMR-133	*HLC*
▪	Shaker	3015	*GFL*
		VS.R23	*Grant BOEKEL*

- pH meter   pH level 1   *inoLab*
- Microscopes
  - Inverted microscope   Leica DMIL   *Leica*
  - Fluorescene microscope Axioplan 2   *Zeiss*
- Tissue homogenizer   Basic Ultra Turrax   *IKA*

3.3.2 Chemicals

Whenever possible, only chemicals with the purity grade "pro analysis" were used for the experiments described in this work. All standard chemicals and organic solvents were purchased from the following companies:

- Sigma Aldrich,   Taufkirchen   *Germany*
- Roche Molecular Biochemicals, Mannheim   *Germany*
- Life sciene (formerly Invitrogen), Leek   *Netherlands*
- Merck,   Darmstadt   *Germany*
- Amersham,   Freiburg   *Germany*
- Qiagen,   Hilden   *Germany*
- AppliChem,   Darmstadt   *Germany*
- Roth,   Karlsruhe   *Germany*

For RNA isolation and analysis, only RNase-free chemicals were used.

3.3.3 Frequently used kits

The followings kits were used throughout routine lab work:

- LowCell ChIP Kit   *Diagenode*
- PowerSYBR green PCR Master Mix   *Applied Biosystems*
- BigDye Terminator V1.1 Sequencing Kit   *Applied Biosystems*
- LightCycler FastStar DNA Master SYBR green I   *Roche*
- FastStart HighFidelity PCR-System   *Roche*
- QIAshredder   *Qiagen*
- RNase-free DNase I Set   *Qiagen*
- RNeasy Mini Kit   *Qiagen*
- QuantiTect Reverse Transcription Kit   *Qiagen*
- QiaQuick PCR Purification Kit   *Qiagen*
- Qiagen MiniPrep Kit   *Qiagen*
- EndoFree Plasmid Maxi Kit   *Qiagen*
- pcDNA3.1/V5-His TOPO TA Expression kit   *Invitrogen*
- Quant-iT RiboGreen RNA assay Kit   *Invitrogen*
- Superscript VILO   *Invitrogen*
- SuperSignal West Pico ECL Substrate   *Pierce*

- BCA Protein Assay Reagent   *Pierce*
- Nucleofector Kit for primary mammalian fibroblasts   *Lonza*
- CytoTox 96 non-radioactive cytotoxicity assay   *Promega*
- Proteasome-Glo 3-Substrate Cell-Based Assay System *Promega*
- PepTag Assay for non-radioactive Detection of PKA   *Promega*
- QBT Fatty Acid Uptake Kit   *Molecular Devices*
- CatchPoint Cyclic-AMP fluorescent assay kit   *Molecular Devices*
- EpiQuik Global Histone H3 acetylation assay   *EpiGentek*

3.3.4   Reagents used for molecular biology

- ***Reagents for the work with nucleic acids***
  - Oligo d(T) primers 0.5 $^{\mu g}/_{\mu l}$ *Fermentas*
  - 100 bp DNA Ladder   *Invitrogen*
  - 1 kb DNA Ladder   *Invitrogen*
  - Agarose   *Sigma*
  - GTG low-melting agarose   *Nu Sieve*
  - TBE-buffer (10x)   *AppliChem*
  - dNTPs   *PeqLab*
  - Ethidiumbromide   *AppliChem*

- ***Reagents for the work with proteins***
  - PageRuler Plus   *Fermentas* (SM1811)
  - Non-fat dried milk powder   *AppliChem* (2710453)
  - RIPA-buffer   *Sigma*
  - Complete Mini Protease Inhibitors   *Roche*
  - Leupeptin   *Sigma*
  - Aprotinin   *Sigma*
  - Aqua plus (29:1) Acrylamide   AppliChem (50984)
  - Ammoniumpersulfat   *AppliChem*
  - SuperSignal West Pico ECL Substrate *Pierce*
  - Coomassie Brilliantblue R-250   *AppliChem*
  - Bovine serum albumin (BSA)   *Sigma*
  - Ponceau S   *Sigma*
  - Restore Western Blot Stripping Buffer *Pierce*

- ***Reagents for the work with bacteria***
  - Ampicillin   *Sigma*
  - Kanamycin   *Sigma*
  - Bacto-Trypton   *AppliChem*
  - Bacto-Yeast-Extract   *AppliChem*

3.3.5 Reagents and supplies for cell culture

- 1xPBS Dulbecco w/o Ca^{2+}, Mg^{2+}, low endotoxin   *Biochrom (L1825)*
- Trypsin-EDTA-Solution   *Sigma (T3924)*
- DharmaFECT 1 Transfection Reagent   *Dharmacon (T-2001)*
- Dimethylsulfoxide (DMSO)   *Sigma*
- Disposable Filter Unit 0.2 µm FP30/0.2 CA-S   *Whatman*
- 4',6-Diamidin-2-phenylindol (DAPI)   *Vector Labs (H-1200)*
- Thiazolyl blue tetrazolium bromide (MTT)   *Sigma*
- Amphotericin B   *Gibco*
- Dimehtylformamide (DMF)   *Sigma*
- Fetal Calf Serum,   *Biochrom AG*
- PenStrep (Penicillin Streptomycin)   *Invitrogen*
- Opti-MEM   *Invitrogen (31985)*

For individual cell culture medium formulation, contents and suppliers please see 3.5.1. For reagents which were used in specific experiments such as HDACi treatment please see Table 13.

3.3.6 Reagents for HPLC-MS/MS

- Methylene chloride   *Sigma (65463)*
- Triethylamine (TEA)   *Sigma (17924)*
- 2-chloro-1-methylpyridiniumiodide (CAS 14338-32-0)   *Sigma (198005)*
- 4-dimethylamino-benzylamindihydrochloride (CAS 34403-52-6)   *Sigma (285633)*
- Acetonitrile (ACN)   *Sigma (34998)*
- Formic acid   *AppliChem (3536)*
- HPLC-purified water   *Sigma (34877)*
- Perdeuterized valproic acid (d_{15}-VPA)(D5491)   *CDN isotopes*

3.3.7 Enzymes

The following enzymes were used throughout this study.

- Taq DNA Polymerase Recombinant   *Invitrogen (10342020)*
- RNase-free DNase I   *Qiagen (79254)*
- Exonuclease I   *NEB (M0206)*
- Shrimp alkaline phosphatase I (SAP I)   *NEB (R0569)*

3.3.8 Purchased vectors

- Myc-DDK-tagged ORF clone of Homo sapiens IGFBP5   *Origene*(RC203797)
  in pCMV 6 entry (Figure 66)

3.4 Antibodies

3.4.1 Primary antibodies

Antibody	Host species	Blocking reagent	Dilution	Incubation time	Supplier	Product number
α-SMN	mouse, monoclonal	milk	1:2,000	2 h	BD labs	S55920
α−β-actin	mouse, monoclonal	milk	1:15,000	1 h	Sigma	A1978
α−β-tubulin	rabbit, polyclonal	milk	1:2,000	1 h	Sigma	T2200
α−hTRA2−β1	rabbit, polyclonal	milk	1:2,000	2 h	produced by Epigentech	
α−SRP20	mouse, monoclonal	milk	1:200	o.n.	Abnova	H00006428-M08
α−SF2/ASF	rabbit, polyclonal	milk	1:1,000	o.n.	Abcam	ab-38017
α−Gemin2	rabbit, polyclonal	BSA	1:200	o.n.	CIND	MANSIP1a
α−Gemin3	mouse, monoclonal	BSA	1:250	o.n.	Santa Cruz	sc-57007
α−PKA$_{cat}$	rabbit, polyclonal	milk	1:200	o.n.	Abcam	ab-65067
α−ODC	mouse, monoclonal	milk	1:1,000	2 h	Abcam	ab-66067
α−Ubiquitin	mouse, monoclonal	milk	1:1,000	o.n.	Santa Cruz	sc-58448
α−p53	mouse, monoclonal	milk	1:250	o.n.	Abcam	ab-78316
α-SMN	rabbit, polyclonal	milk	1:250	o.n.	Santa Cruz	sc-15320
α-RARβ	rabbit, polyclonal	BSA	1:1,000	o.n.	Abcam	ab-53161
α-CD36	rabbit, polyclonal	BSA	1:1,000	o.n.	Santa Cruz	sc-7309
α-IGFBP5 *	rabbit, polyclonal	BSA	1:100	o.n.	Santa Cruz	sc-13093
α-SMN (FITC-labelled)	mouse, monoclonal	(used for fluorescene microscopy, see 3.8.2)			BD labs	610646
α-H3K9ac	rabbit, polyclonal	(used for ChIP, see 3.10.2.1)			Diagenode	pAb-005-044

Table 4   **List of primary antibodies used throughout this study. * whenever the α-RARβ antibody was used, the NaCl concentration in the TBS-T buffer was increased from 137mM to 500mM during antibody incubation**

Antibody	Host species	Blocking reagent	Dilution	Incubation time	Supplier	Product number
α-mouse IgG	goat	milk/BSA	1:10,000	1 h	Dianova	115-35-000
α-rabbit IgG	donkey	milk/BSA	1:5,000	1 h	GE healthcare	N934AV

Table 5   **List of secondary HRP-labeled antibodies, which were used for the detection of primary antibodies listed above (Table 4).**

3.5 Solutions and media

3.5.1 Media for eukaryotic cell culture

Media for primary human fibroblasts (for 556,4ml):

- 1xD-MEM +4500 $^{mg}/_l$ D-Glucose, +L-Glutamine,   500 ml (*Invitrogen*, #41966)
  +Pyruvate
- Fetal calf serum (FCS)   50 ml   (*Biochrom*)
- Penicilin/Streptomycin   5 ml   (*Invitrogen*)
- Amphotericin B (250 $^{µg}/_{ml}$)   1.4 ml (*Promocell*)

Media for murine embryonic fibroblasts (for 555,5ml):

- 1xD-MEM +GlutaMAX™, +4500 $^{mg}/_l$ D-Glucose,   500 ml (*Invitrogen*, #31966)
  +Pyruvate
- Fetal calf serum (FCS)   50 ml   (*Biochrom*)
- Penicilin/Streptomycin   5 ml   (*Invitrogen*)
- β-Mercaptoethanol (10mM)   555 µl (*Applichem*)

Media for stably transfected NSC-34 SMN bla cells (for 557 ml) (3.10.5):

- 1xD-MEM + 4500 $^{mg}/_l$ D-Glucose, + L-Glutamine,
  +25 mM HEPES buffer   500 ml (*Invitrogen,* #42430)
- Fetal calf serum (FCS)   50 ml   (*Biochrom*)
- Penicilin/Streptomycin   5 ml   (*Invitrogen*)
- Amphotericin B (250 $^{µg}/_{ml}$)   1.4 ml (*Promocell*)
- G-418 (500 $^{mg}/_{ml}$)   557 µl (*Gibco*)

Media for siRNA-transfection of primary human fibroblasts:

- Opti-MEM   (*Invitrogen*, #31985)

Freezing media for eukaryotic cells (for 1 ml):

- DMSO   100 µl (*Sigma*)
- Fetal calf serum (FCS)   900 µl (*Biochrom)*

3.5.2 Frequently used buffers and solutions

- *10% Ammonium persulfate solution* (10 ml)
  → 1 g APS in 10 ml dH$_2$O
- *6% Blocking solution* (100 ml)
  → 6 g fat-dry milk powder or BSA in 100 ml TBS-T
- *DEPC-H$_2$O* (1 l)
  → 1 ml Diethylpyrocarbonate in 1 l ddH$_2$O, mix o.n. then autoclave

- *100 mM dNTP-Mix* (1 ml)
    - → 12,5 μl of each dNTP, add ddH$_2$O to 1 ml
- *LB-Media* (2 l)
    - → 20 g Bacto Trypton, 10 g Bacto-Yeast Extract, 10 g NaCl, adjust pH to 7,5 then autoclave, store at 4°C
- *LB-Agar* (500 ml)
    - → 500 ml LB-Media, 7.5 g Agar, autoclave and store at 4°C
- *1 M Tris pH=6.8* (400 ml)
    - → 60 g Tris, add 300 ml dH$_2$O, adjust pH to 6,8 fill up to 400 ml
- *1.5 M Tris pH=8.8* (400 ml)
    - → 90.5 g Tris, add 300 ml dH$_2$O, adjust pH to 8.8, fill up to 400 ml
- *TE^{-4} buffer* (100 ml)
    - → 1 ml Tris pH=8.0, 20 μl 0.5 M EDTA pH=8.0, add ddH$_2$O to 100 ml

- *Bradford solution* (1 l)
    - 100 mg Coomassie Brilliant Blue G250
    - 100 ml H$_3$PO$_4$ (85%)
    - 50 ml EtOH (95%)
- *2x Laemmli buffer* (100 ml)
    - 0.757 g Tris-Base
    - 20 ml Glycerin
    - 10 mg Bromphenol blue
    - 6 g SDS
    - (Prior to use) 10 ml βMe

- *10x DNA loading buffer* (50 ml)
    - 10 ml 100 mM EDTA (pH 7.2-8.5)
    - 2.5 ml 20% SDS
    - 28.7 ml Glycerol
    - 0.05 g Bromphenol Blue
    - Add ddH$_2$O to 50 ml
- *TBS-Tween* (1 l)
    - 2.42 g Tris
    - 8 g NaCl
    - 5 ml Tween 20
    - Adjust pH to 7.56

3.5.2.1 Buffers used in combination with the Mini Protean 3 cell

- *10x Electrophoresis buffer* (1 l)
    - 30.29 g Tris-Base
    - 144.13 g Glycine
    - 10 g SDS
    - Add dH$_2$O to 1 l
- *Transfer buffer* (5 l)
    - 12.1 g Tris-Base
    - 56.3 g Glycine
    - 1 l MeOH
    - Add dH$_2$O to 5 l

3.5.2.2 Buffers used with Protean II xi cell and Trans Blot electrophoresis cell

- *5x Electrophoresis buffer* (3 l)
    - 45 g Tris-Base
    - 216 g Glycine
    - 15 g SDS
    - Add dH$_2$O to 3 l

- *Transfer buffer* (1 l)
  - 3.03 g Tris
  - 14.4 g Glycine
  - 200 ml MeOH
  - Add dH$_2$O to 1 l

Separating & stacking gel for both SDS-PAGE chambers

	12% separating gel		4% stacking gel	
	Mini Cell 5 ml	Protean II xi 25 ml	Mini Cell 2 ml	Protean II xi 5 ml
dH$_2$O	1.7 ml	8.375 ml	1.4 ml	3.05 ml
Acrylamide (29:1)	2 ml	10 ml	330 µl	650 µl
1.5 M Tris pH=8.8	1.3 ml	6.25 ml	---	---
1 M Tris pH=6.8	---	---	250 µl	1.25 ml
10% SDS	50 µl	250 µl	20 µl	50 µl
10% APS	50 µl	250 µl	20 µl	50 µl
TEMED	2 µl	10 µl	2 µl	5 µl

Table 6   **Recipes for the preparation of SDS-PAA gels. 5 ml gels were run at 50-100 V, whereas 25 ml gels were run at an amperage of 18 mA. Blots of 5 ml gels were performed at 30 V o.n. and those of 25 ml gels at 100 mA o.n. at 4°C.**

3.6   Primers and siRNAs

3.6.1 Primers

All primers used in this thesis were designed using the *Primer Select* software contained in the Lasergene package (*DNA Star Inc.*) or by hand. Primers were purchased from Metabion.

Transcript	Ensembl ID		Sequence (5´ → 3´)	ID#	Name	T$_m$
SMN FL	ENSDARG00000018494	fwd	CCA CCA CCC CAC TTA CTA TCA	1449	SMN ex5 for	63°C
		rev	GCT CTA TGC CAG CAT TTC TCC T	3054	SMN_Ex7/8_re 1	
SMN FL	ENSDARG00000018494	fwd	CCA CCA CCC CAC TTA CTA TCA	1449	SMN ex5 for	61°C
		rev	GCT CTA TGC CAG CAT TTC CAT A	1450	SMN Ex 6/8 rev	
hTRA2-β1	ENSG00000136527	fwd	CCG AAG GCA TTA TAC CCG	2836	Htra_fw1a	63°C
		rev	CTC AGC CCA AAT ACT C	2841	Htra_rev1a	
SF2/ASF	ENSG00000136450	fwd	CCG TGC GCT AGG CTT GGT G	3412	SF2/ASF fwd	63°C
		rev	CCC CCG CGG CGA TTC TTG A	3413	SF2/ASF	
SRp20	ENSG00000136450	fwd	GAA CGG GCT TTT GGC TAC TAT	3414	SRp20 fwd	61°C
		rev	TGG GCC ACG ATT TCT ACT TCT T	3415	SRp20 rev	
hnRNP A1	ENSG00000135486	fwd	GCC TGA GGA GCC ATT TTG AGC	3410	hnRNP A1 fwd	61°C
		rev	AGT GGG CAC CTG GTC TTT GAG	3411	hnRNP A1 rev	
c-Myc	ENSG00000136997	fwd	CGA CGC GGG GAG GCT ATT CTG	3607	c-Myc fwd	69°C
		rev	GTC GCG GGA GGC TGC TGG TTT	3608	c-Myc rev	

Col3A1	ENSG00000168542	fwd	CAG GGG CCC CAG GAC TTA GAG	3605	CollagenIIIafwd	68°C
		rev	GGG CCA GGA GGA CCA ATA GG	3606	CollagenIIIa rev	
RPS12	ENSG00000112306	fwd	CGC AAG CCG AAG AAG CCC AAC	3588	RPS12 fwd	61°C
		rev	GCC CCC AGC CGT CAC TTC TTC T	3589	RPS12 rev	
PKAcat$_\varepsilon$	ENSG00000072062	fwd	CCG GCG GGT GAT GCT GGT G	3774	PKA fwd	69°C
		rev	CCG ATC CGC CGT AGG TGT GA	3775	PKA rev	
Gemin2	ENSG00000092208	fwd	CCGGTAGAGCCTTGCGA TTGAC	3399	Gemin2 fwd	64°C
		rev	CCACTTGTTGCTGTTGCCATTGAA	3400	Gemin2 rev	
Gemin3	ENSG00000064703	fwd	GGAGGGACCCCATT TCACAAGA	3405	Gemin3 fwd2	65°C
		rev	CTGGCAGGCAAGGAAGAATAAAT	3406	Gemin3 rev2	

Table 7   Primers used for qRT-PCR on the LightCycler 1.5 machine (_Roche_).

Transcript	_Ensembl ID_		_Sequence (5´ → 3´)_	_ID#_	_Name_
TMTC2	ENSG00000179104	fwd	gtg ggg aag cga ggg aaa agt gaa	3798	TMTC2 fwd
		rev	gag ggc agc agc ggc aac aa	3799	TMTC2 rev
TGFα	ENSG00000163235	fwd	agt ggt gcc ggg ccc tca tct g	3800	TGFA fwd
		rev	cca cct ggc caa act cct cct ctg	3801	TGFA rev
RARβ	ENSG00000077092	fwd	cgc ccc ggc tgg att gg	3802	RARB fwd
		rev	ttt ggc acg tag gct gtt ggt ctt	3803	RARB rev
PITPNM3	ENSG00000091622	fwd	ggc cgg ccc acc aag aag ta	3804	PITPNM3 fwd
		rev	ctc cag cgc ggc cag gtg tgc	3805	PITPNM3 rev
MAB21L1	ENSG00000180660	fwd	tgg ccg gca agc aga gc	3806	MAB21L1 fwd
		rev	tgg ccc ggc agt tca agg tg	3807	MAB21L1 rev
LYPD6b	ENSG00000150556	fwd	aaa tgg gca ccc acg ctg tat gtc	3808	LYPD6bnew fwd
		rev	ggc caa tga ctc atg cag gtc tgt	3809	LYPD6bnew rev
LYPD6	ENSG00000187123	fwd	ccg agc atg aag gcc aca agg tct	3810	LYPD6 fwd
		rev	ttt cgg ggc agt ggc aag tta cag	3811	LYPD6 rev
LOC404266	ENSG00000233101	fwd	ccc ggg cgt ggc gtg gtc	3812	LOC404266 fwd
		rev	agg ggg tgg gga agg gaa tga gtc	3813	LOC404266 rev
KIAA1772	ENSG00000141449	fwd	ccc tcg gac ata cca aga ttt aga	3814	KIAA1772 fwd
		rev	tcc aag gcc gtg cga gtt a	3815	KIA1772 rev
HOXD11	ENSG00000128713	fwd	gct gtc gtt ccc cct ccc cct ctc	3816	HOXD11 fwd
		rev	ccc cca acc cgg ccc aac ttc cta	3817	HOXD11 rev
HOXD10	ENSG00000128710	fwd	caa aac cgc cga atg aaa ctc	3818	HOXD10 fwd
		rev	gaa cgc ggt gcc ccc tct c	3819	HOXD10 rev
HOXB3	ENSG00000120093	fwd	tcc cgg cac caa ctc cac cct cac	3820	HOXB3 fwd
		rev	acc gcc gcc gcc acc aca g	3821	HOXB3 rev
GALNT12	ENSG00000119514	fwd	ccg gct gct ggg ggc gtc tg	3822	GALN12 fwd
		rev	cat caa tca ccg gca cca cca ctg	3823	GALN12 rev
EPHA4	ENSG00000116106	fwd	gga agg cgt ggt cac taa atg taa	3824	EPHA4 fwd
		rev	atg ccc acc agc tga atg act	3825	EPHA4 rev
DIO2	ENSG00000211448	fwd	ggc tga ccg cat gga caa taa cg	3826	DIO2 fwd
		rev	cca gcc aat gcc gga ctt ctt	3827	DIO2 rev

C11orf87	ENSG00000185742	fwd	gcg tgg gct ccg tcc tct tct tg	3828	C11orf87 fwd
		rev	cgg cgc cct ggc act cat tg	3829	C11orf87 rev
CD36	ENSG00000135218	fwd	cag cct cat ttc cac ctt ttg	3830	CD36 fwd
		rev	cct ttc aga tta acg tcg gat tc	3831	CD36 rev
IGFBP5	ENSG00000115461	fwd	cca ccc cca acg cca tct cca	3832	IGFPB5 fwd
		rev	cac ccc caa gca acc acc gaa ata	3833	IGFBP5 rev
ANKRD1	ENSG00000148677	fwd	gca gac ctc aac gcc aaa gac ag	3834	ANKRD1 fwd
		rev	ccg cgc cat aca taa tca gga gt	3835	ANKRD1 rev
PPARγ	ENSG00000132170	fwd	cca cag gcc gag aag gag aag c	4017	PPARg fwd
		rev	cca ggg ccc gga ggt cag	4018	PPARg rev
MCT1 (SLC16A1)	ENSG00000155380	fwd	ttc ttg ggg gct tgc tac taa act	4019	MCT1 fwd
		rev	gct tgg gcc cga ttg gtc	4020	MCT1 rev
MCT2 (SLC16A7)	ENSG00000118596	fwd	agc cgg ccg gtg gtg ata g	4021	MCT2 fwd
		rev	taa ggc ggg ttg cag gtt gaa	4022	MCT2 rev
MCT3 (SLC16A8)	ENSG00000100156	fwd	cgc ccc gct tcc cca gtg c	4023	MCT3 fwd
		rev	cag agc cgg cca ggt aga aga tga	4024	MCT3 rev

Table 8　　**Primers used for qRT-PCR on the ABI 7500 Taqman machine (*Applied Biosystems*)**

Promoter		*Ensembl ID*		*Sequence (5′ → 3′)*	*ID#*	*Name*
CPT1C		ENSG00000169169	fwd	gaa ggg gcg ggg ata gaa cg	4035	cCPT1C fwd
			rev	gga gtc ctg ccc acc ccg aga t	4036	cCPT1C rev
AZGP1		ENSG00000160862	fwd	ggc ccc agg acc cag gat aa	4039	cAZGP1 fwd
			rev	gac agc agg aca ggc acc att ct	4055	cAZGP1 rev
CD36		ENSG00000135218	fwd	taa gtt tcg caa gct cag tca aga	4056	cCD36 fwd
			rev	aga ggc cag aaa aac aaa agg aac	4057	cCD36 rev
TGFα		ENSG00000163235	fwd	gcc cgc ccg ccc gta aaa tgg tc	4058	cTGFa fwd
			rev	ccg ggg gaa gca ggg tgt cg	4059	cTGFa rev
RARβ		ENSG00000077092	fwd	cag aca gaa agg cgc aca gag gaa	4060	cRARb fwd
			rev	ttg cgc cgg ctt agc ttg gaa aac	4061	cRARb rev
IGFBP5		ENSG00000115461	fwd	ggt ggc aaa gtg gga gaa aag agg	4062	cIGFBP5 fwd
			rev	cgg cgc cgc aga aca ggt aa	4063	cIGFBP5 rev
SMN	Region 1	ENSDARG00000018494	fwd	cag agt ttc ttt gtt ggg tg	3361	Husp1_fw_M
			rev	taa tcg ttt tag aga gta caa ttg	3362	Husp1_rev_M
	Region 2		fwd	ttg tac att ggc aac atc atc	3026	Husp2_fw
			rev	cac gaa agg aac ttt gag ctc ttc	3027	Husp2_rev
	Region 3		fwd	ggt ttt aaa ttc cta gta gga gct tac a	3028	Husp3_fw
			rev	ggg ttt cgg cat gtt gct t	3029	Husp3_rev
	Region 4		fwd	cac tcg tag aaa gcg tga gaa gtt a	3030	Husp4_fw
			rev	gct tct tgg gag cgg aac ag	3031	Husp4_rev

Table 9　　**Primers used for qPCR-anaylsis of ChIP experiments (3.10.2.1)**

Gene/Plasmid	Ensembl ID		Sequence (5´ → 3´)	ID#	Name
CD36	ENSG00000135218	fwd	ATG GGC TGT GAC CGG AAC TG	3921	CD36clone ex6ATG fwd
		rev	TTT TAT TGT TTT CGA TCT GCA	3922	CD36clone ex17 rev
RARβ	ENSG00000077092	fwd	ATG TTT GAC TGT ATG GAT GTT C	3925	RARßclone ex1ATG fwd
		rev	TTG CAC GAG TGG TGA CTG ACT G	3926	RARßclone ex8 rev
TGFα	ENSG00000163235	fwd	ATG GTC CCC TCG GCT GGA CAG C	3927	TGFa ex1ATG fwd
		rev	GAC CAC TGT TTC TGA GTG GC	3928	TGFa ex5/6 rev
pcDNA3.1-V5/His-Topo	---	fwd	TAA TAC GAC TCA CTA TAG GG	1840	T7 fwd
		rev	AG AAG GCA CAG TCG AGG	1282	BGH
		rev	GTT AGG GAT AGG CTT ACC TTC GAA	2951	TOPO_V5_rev

Table 10   Primers used for TOPO TA cloning (3.9.6.1) and subsequent analysis including sequencing.

Inbred strain	Gene/ transcript		Sequence (5´ → 3´)	ID#	Name	Amplicon length
SMA_Hung	Wt *Smn*	fwd	ATA ACA CCA CCA CTC TTA CTC	3370	Hung WT fw	1050 bp
		rev	GTA GCC GTG ATG CCA TTG TCA	3372	Hung WT_KO rev	
	Hung KO	fwd	AGC CTG AAG AAC GAG ATC AGC	3371	Hung KO fw	950 bp
		rev	ATA ACA CCA CCA CTC TTA CTC	3372	Hung WT_KO rev	
	transgenic 5´UTR of *SMN2*	fwd	ACT GCA ACC TCC TGG GTT CAA GTG	3373	HungSMA_mouse_tgSMN2_fw_1F	172 bp
		rev	CAG TTC GAG ACC AGC CTG ACC AAT	3374	HungSMA_mouse_tgSMN2_rev_1B	
SMA_Burghes	Wt *Smn*[a]	fwd	CCG GGA TAT TGG GAT TGT AG	2649	m_smn forw	782 bp
		rev	TTC TTT TGG CTT TTA TTC TTC TTG	2650	m_smn rev	
	Hung KO[b]	fwd	CCA GGC GAT AAG TTG GGT AAC G	2647	GNA3	600 bp
		rev	GGC CTG GAA TTC AAT ATG CTA GAC TGG	2648	GMS11	
	h*SMN2*	fwd	GTA AAC CAA AAA CCA CAC CTA AA	2713	hum SMN2 Ex2b forw	1040 bp
		rev	GGG AAA GTA GAT CGG ACA GAT	2714	hum SMN2 Ex3 rev	

Table 11   Primers used for genotyping of mice. All PCRs were performed using 0.5 µl of DNA-solution. [a] $^1/_{10}$ Vol 1 M Betain (*Sigma*) were added to the PCR mix to obtain signals. [b] $^1/_{10}$ Vol Q-Solution (*Qiagen*) were added.

3.6.2 siRNAs (small interfering RNAs)

Target Transcript	Ensembl ID	Sense Sequence	Supplier	Product number
hTRA2-β1	ENSG00000136527	r(CGA UCU GAA UCU AGG UCU A)dTdT	Qiagen	SI02653504
SRp20	ENSG00000112081	r(GGA AAU AGA AGA CAG UUU G) dTdT	Qiagen	*
CD36	ENSG00000135218	r(GAA CCU AUU GAU GGA UUA ATT)dTdT	Qiagen	SI0001330
IGFBP5	ENSG00000115461	r(GCC CAA UUG UGA CCG CAA ATT)dTdT	Qiagen	SI00012558
TGFα	ENSG00000163235	r(CGG UAA GUA UGU UUA GAA ATT)dTdT	Qiagen	SI00049427
RARβ	ENSG00000077092	r(GCC AGU UCA GUU AAU CAA AAT)dTdT	Qiagen	SI00019404
siTOX	control siRNA inducing apoptosis		Dharmacon	D-001500-01-05
AllStars Negative Control siRNA	Non-targeting siRNA		Qiagen	1027280

Table 12   siRNAs used throughout this thesis. * siRNA targeting SRp20 was a custom designed siRNA. Sequence was taken from (Bedard et al. 2007)

3.7 Software, internet programs and databases

The following software programs were used.

- Quantity One 4.5.1   (densiometric analysis)   *Biorad*
- EndNote9/X2   (reference organization)   *Thomson Research*
- SigmaPlot 9/10   (creation of graphs)   *Systat Software Inc.*
- Photoshop CS   (image editing)   *Adobe*
- Office 2003/2007   (word processing etc.)   *Microsoft*
- LightCycler Software   (qRT-PCR analysis)   *Roche*
- Sequence Detection Software   (qRT-PCR analysis)   *ABI*
- XFluor4Safire² software   (platereader)   *Tecan*
- AxioVision Rel.4.7   (fluorescence imaging)   *Zeiss*
- Lasergene Package   (Sequence analysis)   *DNAstar Inc.*

The following databases and internet programs were routinely employed.

- NCBI   http://www.ncbi.nlm.nih.gov/
- Genecards   http://www.genecards.org/
- Ensembl   http://www.ensembl.org/
- UCSC   http://genome.ucsc.edu/
- Medline   https://www.ncbi.nlm.nih.gov/pubmed
- OMIM   http://www.ncbi.nlm.nih.gov/omim
- Gene Expression Atlas database   http://www.ebi.ac.uk/gxa/
- Human promoter database   http://zlab.bu.edu/~mfrith/HPD.html
- Exon Primer   http://ihg2.helmholtz-muenchen.de/ihg/ExonPrimer.html

3.8   Cell culture procedures

All cell culture work was performed under sterile conditions to avoid any contaminations with fungi or bacteria. Sterile conditions were guaranteed by laminar flow cell culture hoods as well as sterile solutions and materials. Growing cell lines were kept in an incubator at 37°C in a humid atmosphere containing 5% CO_2. If not noted differently, cell culture media were supplemented with amphotericin B and penicillin/streptomycin.

3.8.1   Cell culture of eukaryotic cells

Fibroblast cell lines were grown as adherent monolayer cultures in D-MEM medium containing 10% FCS (3.5.1). Routinely, fibroblasts were cultured in either 25 cm^2 or 75 cm^2 flaks, and, depending on the cell division rate, fibroblasts were splitted once or twice a week into new flasks. To split fibroblasts, cells were first washed once with 1xPBS w/o Mg^{2+}, Ca^{2+} (*Biochrom*) and then trypsinised using Trypsin-EDTA (*Sigma*). After stopping the trypsinisation by addition of 1 Vol fibroblast medium, the cell suspension was evenly distributed into new flasks and media was added to a final volume of either 7 or 12 ml, respectively. For long-term storage fibroblasts were frozen in liquid nitrogen. To this aim, following trypsinisation fibroblasts were pelleted for 10 min at 500 x g and afterwards resuspended in freezing medium (3.3.5). Next, fibroblasts were frozen over night at -80°C and then transferred to -196°C. At any time these aliquots can be taken again into culture.

Murine embryonic fibroblasts (MEF) and NSC-34 cells were basically cultured using the same procedures as described above, but a different medium was used. For detailed information see 3.5.1.

3.8.1.1 Treatment of cells with different compounds

To treat cells with any compound, cells were first grown to approx. 80% confluency, trypsinised and then counted using a haemocytometer. After counting, an adequate number of cells were plated out (15 cm petri dish: $1x10^6$ cells; 10 cm petri dish: $2x10^5$ fibroblasts; 6-well plate: $1x10^5$ fibroblasts per well; 96-well plate: $1x10^4$ fibroblasts per well) and cultured for 24 h to let the cells settle and start proliferating. For every experiment, at least one petri dish served as untreated control and was incubated with the respective solvent only (Table 13). All experiments were performed at least as triplicates or three different cell lines were used to calculated data. Final results are given as mean ± SEM if not indicated different.

Assay	Compound	Supplier	Mode of action	Time of treatment	Concentration used	Solvent
SMN2 activation	*Valproic acid* (VPA)	Sigma	HDACi	16 h	5 µM - 5 mM	ddH$_2$O
	LBH589 (Panobinostat)	Novartis	HDACi	16 h - 72 h	100 nM - 1 µM	DMSO
	JnJ26481585	JnJ	HDACi	16 h - 72 h	10 nM - 5 µM	DMSO
	Sodium butyrate	Sigma	HDACi	24 h	500 $^{µg}/_{ml}$	ddH$_2$O
	Phenylbutyrate	Sigma	HDACi	4 h	2 mM	DMSO
mRNA stability	*Actinomycin D*	Sigma	RNA synthesis inhibitor	0 h - 25 h	5 $^{µg}/_{ml}$	DMSO
Protein stability	*NH$_4$Cl*	AppliChem	Lysosome inhibitor	15 h	20 mM	ddH$_2$O
	MG-132 (Z-Leu-Leu-Leu-al)	Sigma	Proteasome inhibitor	15 h	5 µM - 5 mM	DMSO
	Bortezomib (Velcade)	kind gift of Dr. Kashkar	Proteasome inhibitor	24 h	1 - 20 nM	ddH$_2$O
Fatty acid uptake	*Oligomycin*	Sigma	ATP synthase inhibitor	16 h	10 $^{µg}/_{ml}$	DMSO
	SSO (Sulfo-N-succini-midyl ester)	Santa Cruz	CD36 inhibitor	16 h	400 µM	DMSO
	Oleic acid	Sigma	fatty acid	1 mM	16 h	DMSO
	Retinoic acid	Sigma	Bioactive acid	16 h	1 µM	DMSO
cAMP ELISA	*Forskolin*	Sigma	AC activator	2 h	100 µM	DMSO
	IBMX (3-isobutyl-1-methylxanthine)	Sigma	PDE inhibitor	2 h	1 mM	DMSO
	ddA (Dideoxyadenosin)	Sigma	AC inhibitor	16 h	0,5 mM	DMSO

Table 13   **Compounds used for the treatment of primary fibroblasts (AC = Adenylyl cyclase, PDE = Phosposdiesterase). Given are concentrations and time periods typically used. Exceptions are separately mentioned in the text.**

3.8.1.2 Transient transfection of primary human fibroblasts

To study the role of any protein inside the cellular machinery, it can either be knocked-down or overexpressed. In both cases, nucleic acids have to be introduced into the cell either by lipofection, transduction or electroporation. To transfect primary human fibroblasts with either siRNAs or plasmids two different protocols were employed.

For the transfection with siRNAs, 20 µM stocks of siRNAs in ddH$_2$O were prepared, which were then diluted to a final concentration of 1 µM. 24 h prior to transfection, $2x10^5$ fibroblasts were plated out in a 6-well plate per transfection. At the day of transfection, 100 µl of the respective 1 µM siRNA solution were mixed with 100 µl Opti-MEM

(*Gibco*) and incubated for 5 min at RT. At the same time, 2 µl of the transfection reagent Dharmafect1 (*Dharmacon*) were incubated with 198 µl Opti-MEM and also incubated for 5 min at RT. Afterwards both solutions were combined and incubated for 20 min at RT to allow the formation of lipophilic complexes. Next, the culture medium was removed from the fibroblasts. Subsequently, 1.6 ml of fibroblast media w/o antibiotics were added (c_{final}[siRNA]=50 nM) to the lipophilic complexes and the solution was added onto the cells. The non-targeting AllStars Negative Control siRNA (*Qiagen*) served always as mock control, whereas the siTOX siRNA (*Dharmacon*), which induces apoptosis allowed estimations of the transfection rate. All siRNA transfections were performed as triplicates.

To transfect fibroblasts with expression plasmids, the Basic Nucleofector Kit for Primary Mammalian Fibroblasts (*Lonza*) was used according to the manufacturer's instructions. In brief, for each transfection $3x10^5$ fibroblasts from approx. 80% confluent flasks were trypsinised, pelleted and resuspended in 100 µl Nucleofector solution. 2 µg of the respective plasmid were added and transfection was carried out using the program U-20. Afterwards, 1.5 ml of pre-warmed fibroblast media were added and the cell-suspension was dispensed into a single well of a 6-well plate. Transfection with the pmaxGFP expression vector (*Lonza*) served as transfection control.

After the respective incubation time, fibroblasts were harvested for isolation of either RNA or protein (3.9.2.1.1 and 3.10.1.1.1).

3.8.1.3 Cytotoxicity and cellviability assays

To investigate the impact of HDACi treatment on the viability of fibroblasts as well as to allow estimations of toxic side effects, MTT and LDH assays were performed. Furthermore, the MTT-assay was used to assess siRNA-transfection rates (3.8.1.2).

3.8.1.3.1 MTT assay

Assessment of the number of viable fibroblasts was performed using a MTT assay. MTT (3-(4,5-Dimethylthiazol-2-yl)-2,5-diphenyltetrazoliumbromide), a yellow tetrazole salt, is reduced in active proliferating cells by the reduction equivalents NADH and NADPH to formazan (Berridge and Tan 1993). Formazan production leads to the formation of violet crystals having a distinct absorption maximum from MTT at 570 nm. Therefore, the amount of formed formazan is directly proportional to the glykolysis rate, which in turn gives a hint about the cell viability. To quantify formazan formation, some $1x10^4$ fibroblasts in 200 µl were seeded in each well of a 96-well plate as described previously (Riessland et al. 2006), and 24 h later treated with the HDACi. After the respective incubation period, medium was replaced by 225 µl fresh-medium + 25 µl MTT stock solution (50mg MTT (*Sigma*) in 10 ml 1xPBS (*Biochrom*)). Fibroblasts were again incubated for approx. 3 h at 37°C and 5% CO_2 and then lysed by adding 1 Vol 20% SDS/DMF (1:1) and subsequent shaking for 30 min and

750 rpm on a shaking incubator. Next, photometric absorption was measured on a Safire² plate reader (*Tecan*). For all measurements eight replicates were performed.

To assess siRNA transfection rates fibroblasts, transfected with AllStars Negative- (*Qiagen*) were compared to fibroblasts transfected with siTOX siRNA (*Dharmacon*) via a MTT assay as described above.

3.8.1.3.2 LDH assay

Quantifaction of cytotoxicity was performed with the CytoTox 96 non-radioactive cytotoxicity assay (*Promega*). It is based on the finding that the lactate dehydrogenase (LDH), a typically cytoplasmatic enzyme, is rapidly released in the cell culture supernatant upon necrosis. Addition of the substrate mix (containing NAD^+, lactate and INT, a tetrazole salt), leads to the reduction of lactate to pyruvate by the LDH, whereby NAD^+ is reduced to $NADH+H^+$. $NADH+H^+$ in turn reduces INT to formazan. The amount of formed formazan can be quantified by measuring absorption at 490 nm.

To assess any cytotoxic effects of HDACi-treatment, 8×10^3 fibroblasts in 200 µl were seeded into each well of a 96-well and then incubated for the respective time period with HDACi. Then, 50 µl of cell culture supernatant were transferred into a black 96-well plate and mixed with 50 µl of reconstitute substrate mix. Reactions were incubated for 30 min at RT in the absence of light and then stopped by adding 50 µl Stop-Solution. Subsequently, absorbance at 490 nm was measured on a Safire² plate reader (*Tecan*). To calculate the portion of overall released LDH, a maximal LDH release sample was prepared by lysing all cells of a well with lysis buffer. For all measurements eight replicates were performed.

3.8.2 Immunofluorescent staining of primary human fibroblasts

To stain nuclear SMN-accumulations, called gems, in primary human fibroblasts, some 1×10^5 cells were plated out onto flame-sterilized cover-slip put into a 6-well plate. After HDACi treatment, cells were washed with 1xPBS and then fixed for 10 min using ice-cold MeOH/Aceton (1:1). Next, fibroblasts were permeabilized for 15 min with 2% TX-100 in 1xPBS followed by 30 min blocking with 2% BSA in 1xPBS at gentle agitation. After addition of a mouse monoclonal FITC-labelled SMN-antibody (BD Transduction *laboratories*) for 1 h (dilution 1:1,000), fibroblasts were washed twice with 1xPBS and then mounted using the Vectashield containing DAPI (*VectorLabs*) to ensure nuclear localization of gems. For each condition, 300 nuclei were analysed on a fluorescence microscope (*Carl Zeiss*).

3.9　Molecular biology methods

3.9.1　Working with DNA

3.9.1.1 Genomic DNA isolation

To isolate genomic DNA from mouse tail-tip biopsies, tail-tips were lysed by incubation with 500 µl Tail-tip lysis buffer at 55°C for at least 3 h and 700 rpm on a shaking heating block. Hairs and other insoluble debris were pelleted by centrifugation for 15 min at 16,100 x g. The supernatant was transferred to a new 1.5 ml microcentrifuge tube and 1 Vol Isopropanol was added to precipitate nucleic acid. After centrifugation for 15 min at 16,100 x g, the nucleic acid pellet was washed once with 200 µl 70% EtOH and afterwards dried in a 37°C incubator. Finally, the pellet was resupended in 50 µl TE^{-4} containing RNase to eliminate any RNA contaminations.

> ***Tail-tip lysis buffer***
>
> - 100 mM Tris pH=8.5
> - 5 mM EDTA
> - 0.2 % (w/v) SDS
> - 200 mM NaCl
> - Added fresh → 200 $^{µg}/_{ml}$ Proteinase K (*AppliChem*)

3.9.1.2 Determination of DNA concentration

Determination of DNA concentrations was performed on a NanoDrop ND-1000 spectrophotometer (*Peqlab*) in triplicates. From the absorption measured at 260 and 280 nm, the software calculated DNA concentration as well as DNA purity. Only samples having a $^{260}/_{280}$ of approx 1.8 were regarded as pure and used for subsequent PCRs. Higher ratios would indicate RNA-contaminations, whereas lower ratios point to protein or ethanol remains.

3.9.2　Working with RNA

3.9.2.1 RNA isolation

3.9.2.1.1　RNA isolation from eukaryotic cells

Depending on the amount of RNA needed, total RNA was either extracted from a 10 cm petri dish ($2x10^5$ cells) or a 6-well plate ($1x10^5$ cells). To extract RNA, cells were lysed first with RLT-buffer and QIAshredder (*Qiagen*). Subsequently the RNeasy Mini kit (*Qiagen*) was performed according to the manufacturer´s protocol. The optional 20 min DNaseI (*Qiagen*) digestion step was always included to eliminate any DNA-contamination. Finally, RNA was eluted with ddH$_2$O.

3.9.2.1.2 RNA isolation from organ tissues

Isolation of total RNA from snap-frozen murine organ biopsies was also performed with QIAshredder and the RNeasy Mini Kit (both *Qiagen*). To ensure proper tissue breakup, samples were after thawing on ice homegenised using a Basic Ultra Turrax Homogeniser (*IKA*) prior to RNA extraction. For the isolation out of fatty organs such as brain and spinal cord, extraction steps with Qiazol (*Qiagen*) were included as given in the manufacturer´s protocol. Again DNaseI digestion was included.

3.9.2.2 Determination of RNA concentration

To circumvent any misleading RNA-concentrations leading to artificial qRT-PCR-data, RNAs were generally measured using the Quant-It RiboGreen RNA assay (*Invitrogen*) as suggested by the manufacturer. The measurement was carried out on a Safire² plate reader (*Tecan*) in 96-well format (*Greiner bio one*, #655076) and gives far more precise measurements than conventional photometric assays. The kit is based on the fluorescent dye RiboGreen, whose fluorescence is extremely enhanced when bound to nucleic acids. RiboGreen preferentially binds RNA; combination with the DNaseI digestion performed during RNA extraction (3.9.2.1) results in a RNA specific measurement. To verify that all samples are within the detection range of this assay, and to ensure RNA quality ($^{260}/_{280}$ ideally 2.0), all samples were beforehand measured using a classical spectrophotometer (*Eppendorf*).

3.9.2.3 mRNA-stability assay using Actinomycin D

Actinomycin D, a peptide antibiotic from *Streptomycus parvulus*, inhibits *de novo* RNA synthesis by intercalating with the DNA. This intercalation prevents the unwinding and opening of the DNA double helix during transcription as well as replication. Furthermore, Actinomycin D crosslinks the guanine nucleotides of the DNA, which, again, blocks DNA-dependent RNA-synthesis. To assess mRNA-stability of different transcripts, fibroblasts were treated 24 h after seeding out in a 6-well plate with 5 $^{\mu g}/_{ml}$ Actinomycin D (*Sigma*) (Table 13). After treatment for the respective time periods, RNA was isolated as describe above (3.9.2.1.1) and later on analyzed by qRT-PCR. Half-life periods ($T_{0.5}$) of different transcripts were calculated by approximated *e*-functions and are represented as means of three different experiments.

3.9.2.4 cDNA synthesis

To allow expression analysis by measuring individual mRNA abundance, RNA has first to be reversely transcribed into cDNA since RNA cannot serve as template for qRT-PCR (3.9.3.3). To this aim, cDNA was produced using the QuantiTect Reverse Transcription Kit (*Qiagen*), which also includes a DNase digestion called *gDNA wipeout*. Exclusive transcription of mRNAs was warranted using an oligo-dT Primer (*Fermentas*) binding to the mRNA-specific poly-A-tail.

In the case total coding sequences of genes should be cloned, the SuperscriptVilo Kit (*Invitrogen*) was used, since the total yield of the QuantiTect Reverse Transcription Kit (*Qiagen*) is too low for cloning but sufficient for qRT-PCR.

3.9.3 Polymerase chain reaction (PCR)

Working with DNA has greatly been boosted in 1987, when Kary Mullis published the polymerase chain reaction (PCR), which allowed rapid amplification of single-stranded DNA (Mullis et al. 1992) . This work has been honored with the Nobel Prize in chemistry in 1993. The technique is based on the finding that DNA-dependent DNA Polymerases are able to synthesize complementary copies of a single-stranded DNA, when starting from a free 3´-end. During PCR, these free 3´-ends are given by sequence specific oligo-nucleotides (primer) and are then elongated by a thermostable DNA-polymerase e.g. Taq-Polymerase from *Thermophilus aquaticus*. Numerous repetition of the 3 steps denaturing, primer binding (annealing) and elongation yields in enormous amplification of one and the same piece of DNA.

3.9.3.1 Standard PCR

Typical PCR conditions used to amplify either DNA or cDNA were as follows:

- 10 min   at   95°C   → initial denaturation
- 30 min   at   95°C   → denaturation
- 30 sec   at   XX°C   → annealing, XX°C (depending on individual primer)   35x
- XX min   at   72°C   → elongation, 1 min per kb product length
- 10 min   at   72°C   → final extension

Reactions were performed using Taq Polymerase (*Invitrogen*) and dNTPs (*PeqLab*) according to the manufacturer´s protocol. Enhancer of PCR efficiency, such as Q-Solution (*Qiagen*) or Betain (*Sigma*), were added when needed (Table 11).

3.9.3.2 Agarose gel electrophoresis/Gel-Purification of PCR-Products

Analysis of PCR products is normally done by agarose gel electrophoresis. Since the DNA backbone is negatively charged, placing DNA into an electric field leads to its migration towards the anode. To separate PCR products of different size, the electric field is put through a gel matrix out of polysaccharide agarose, which allows fast moving of small fragments but slows down big DNA molecules.

Gels were either prepared with Agarose (*Sigma*) or, if PCR products should be cloned, with Agarose/Low-Melting agarose (1:2) (*Biozym*) in 1xTBE-buffer (*AppliChem*). Routinely, PCR products were resolved on 1-2% Agarose Gels containing 1 $^{\mu g}/_{ml}$ Ethidiumbromide (*AppliChem*), which intercalates with DNA. Ethidiumbromide-DNA complexes were visualized at 254 nm using a ChemiDoc XRS imaging System (*Biorad*). Proper size of DNA fragment was

estimated by comparision with either 100bp or 1kb ladder (*Fermentas*). If PCR products should be cloned, the respective bands were cut out and purified using the Qiaquick PCR purification kit (*Qiagen*) according to the manufacturer´s instructions.

3.9.3.3 Quantitative real-time PCR (qRT-PCR)

Standard PCR, as described in 3.9.3.1, does not allow the inference of initial template amounts, since it is an endpoint determination during the plateau phase of the PCR. To draw conclusions on the template amounts, PCR product amounts have to be determined during the linear-logarithmic phase of the PCR. An easy way to do this is the addition of the fluorescent dye SYBR-green to the PCR master mix, which binds to double-stranded DNA. During each elongation step, SYBR green fluorescence is detected by an adequate detector and plotted against the cycle number. Calculations based on these data allow the deduction of the initial amount of a certain template. Typically, the quantification program is followed by a melting curve to ensure PCR product identity.

3.9.3.3.1 qRT-PCR using the LightCycler 1.5

To determine transcript levels in cells or organ tissues, total RNA was extracted and measured as described above 3.9.2. Prior to qRT-PCR, cDNA samples were diluted 1:5 with TE^{-4} and 3 µl from this dilution were used for analysis. PCR was carried out in 10 µl scale (Master Mix per sample: 4.2 µl dH$_2$O, 1.2 µl MgCl$_2$, 1 µl each primer, 0.166 µl FastStart-Mix, 0.33 µl Polymerase) with the FastStart DNA Master SYBR green I Kit (*Roche*) on a LightCycler 1.5 machine (*Roche*) in 20 µl capillaries (*Roche*). Analysis of resulting amplification curves was performed with the second derivative maximum method implemented in the LightCycler software. Primers for individual transcripts can be found in Table 7. All measurements were performed as duplicates.

3.9.3.3.2 qRT-PCR using the ABI 7500 Realtime PCR machine

Whenever more than 32 samples should be measured simultaneously (which is the maximum capacity of the LightCycler 1.5), the ABI 7500 Realtime PCR machine was used, since it allows qRT-PCR in 96-well format. To this aim, RNA extraction and cDNA-synthesis was performed analog to 3.9.3.3.1. Next, cDNAs were diluted 1:10 with TE^{-4} and 3 µl from this dilution were used per reaction. PCR was carried out in 96-well plates (*Bioplastic*) covered with an optical foil (*Bioplastic*) using the PowerSYBR green PCR Master Mix (*Applied Biosystems*) in 25 µl scale (Master Mix per sample: 12.5 µl PowerSYBR-green Mix, 8.5 µl dH$_2$O, 1 µl each primer). Analysis of raw data was performed using the Sequence Detection Software (*Applied Biosystems*). Primers for individual transcripts can be found in Table 8. All samples were at least measured as triplicates.

3.9.4 Sanger-sequencing

Sequencing of DNA was performed using the chain terminator method developed by Sanger (Sanger et al. 1977) employing the BigDye Terminator V1.1 Sequencing Kit (*Applied Biosystems*). This method is based on utilization of dNTPs combined with ddNTPs, which leads to chain termination during PCR. Each of the four didesoxynucleotides is labeled with a different fluorescent dye, which allows identification of the terminal nucleotide by capillary electrophoresis. To sequence genomic DNA, the region-of-interest was first amplified by standard PCR from 40 ng genomic DNA using the primers given in the appendix Table 18 to Table 21.

Next, PCR products were cleaned up using the EXO/SAP-reaction. Typically, sequencing reactions were set up with 5 µl 3xsequencing buffer, 1 µl Terminator Mix (*Applied Biosystems*) and 0.5-2 µl purified PCR product or 150 ng plasmid-DNA, respectively. PCR conditions were as recommended by the manufacturer using an annealing temperature of 55°C for 25 cycles. Capillary electrophoresis was carried out at the *Cologne Center for Genomics* in Cologne. Sequences were analyzed using Finch TV (*Geospiza*) and the Lasergene Package (*Lasergene*).

EXO/SAP-reaction

- ExoI (20 $^U/_{µl}$)   2 µl
- SAP (1 $^U/_{µl}$)   0.3 µl
- ddH$_2$O   1.625 µl
- PCR product   8 µl

→ 20 min at 37°C then 15 min at 72°C

3.9.5 Transcriptome-wide expression analysis using µ-arrays

To identify transcripts differentially expressed between Non- and Pos-Responders, µ-arrays (GeneChip Human Gene 1.0 ST Array, V1 April 2009, *Affymetrix*) were employed. The basic principle of expression µ-arrays is the hybridization of fluorescent-labeled sample RNA derived to a glass-chip covered with thousands of different probes (>5,000 probes/cm²). Typically, each probe is approx. 50 bp in length and hybridizes to a different transcript. To validate data, sets of probes (5-30) are often detecting one and the same transcript. After hybridization, unspecific binding is washed away and fluorescence intensity is measured by a laser scanner. After fluorescence reading, intensities were normalized to exclude any degradation effects or bad quality of extracted RNAs. Comparison of diverse samples is done by labeling with different fluorescence dyes and simultaneous hybridization.

To perform µ-arrays with fibroblast RNA, some 1x10^6 cells were plated out in 15 cm petri dishes and treated with 500 µM VPA or mock for 16h, respectively. Cells were washed with 1xPBS, trypsinized and pelleted at 500 x g for 10 min. For each sample 2 petri dishes were

pooled to get enough material. An aliquot of the cell suspension was used for protein extraction and western blot analysis (3.10.1.2) to ensure a proper treatment effect. Next, RNA was extracted as described above (3.9.2.1.1). At least 3 µg of RNA were needed with a concentration >300 $^{ng}/_{µl}$. All subsequent steps including determination of RNA purity and bioinformatical analysis were performed at the *Microarray facility* in Tübingen. In brief, using the *Bioconductor Software Package*, it was first tested whether any artifacts or defective probe spots may interfere with the subsequent analysis. Therefore a linear model of the arrays was created and both the non-normalized standard error (NUSE) as well as the relative logarithmic expression (RLE) were analysed with boxplots. Comparable boxes indicate a similar signal distribution. Furthermore, defective spots were identified by false color pictures of the arrarys and control probes were used to determine receiver-operator-characteristics (ROC). ROC is a method to analyse the dependence of the efficiency from the error rate of different parameters and varies between 0.5 and ideally 1. Since a ROC of 0.9 was determined, and also the other tests indicated no possible faults, subsequent data analysis was carried as described in the following. First steps included background correction, intensity normalization, calculation of transcript intensities from the respective probes and elimination of control probes (approx. 4,100).

After elimination of uninformative transcripts, differentially expressed transcripts were identified by three different models:

(1) Paired model   > factor: group   (Pos-Responder vs. Non-Responder)

(2) Paired model   > factor: treatment   (mock vs. VPA)

(3) Unpaired model   > combined factor: group + treatment

Based on these models, the expression profile for gene was calculated and the standard error was modeled using a Bayesian model.

3.9.6 Working with bacteria

3.9.6.1 TOPO TA cloning

One of the most common ways to study any protein-of-interest in a given context, is performing overexpression studies. Overexpression is typically done by cloning the gene into small circular double-stranded DNA-fragments of bacterial origin (plasmid), which were then transfected into the respective target cell. Most vectors contain strong expression promoters (e.g. CMV promoter) and allow the fusion with a tag (e.g. V5) to discriminate the overexpressed from the endogenous protein.

To clone our candidate genes, PCR products encompassing the respective complete coding sequence (w/o stop codon) were generated (Table 10) using the FastStart HighFidelity PCR system (*Roche*). This kit makes use of a proof-reading polymerase, which minimizes the risk

of nucleotide exchanges. Next, PCR products were cloned into the pcDNA3.1/V5-His TOPO vector (Figure 67) using the pcDNA3.1/V5-His TOPO TA Expression kit (*Invitrogen*). Since this vector does not contain an ATG initiation codon, the native initiation codon was included to express the desired protein. Contrariwise, the stop codon was excluded to fuse the protein in-frame with the V5 epitope. Cloning reactions were performed as recommended in the manufacturer´s protocol. In brief, 4 µl of fresh PCR product were combined with 1 µl salt solution and 1 µl TOPO vector and incubated for 10 min at RT. Next, 1 µl thereof was mixed with 1 aliquot of chemical competent *E.coli* TOP10 (*Invitrogen*) and incubated for 30 min on ice. Heatshock at 42°C was performed for 45 sec and after addition of 250 µl SOC medium (*Invitrogen*) bacteria were plated out (50 µl and 150 µl) on prewarmed agar plates containing 50 $^{µg}/_{ml}$ Ampicillin for selection.

Transfection of the purchased IGFBP5-coding vector in *E.coli* TOP10 was performed analogue using 30 $^{µg}/_{ml}$ Kanamycin for selection (Figure 66).

3.9.6.2 Identification of correct clones using colony PCR and sequencing

To identify positive transformants carrying the insert in the right orientation, approx. 10 clones were picked for each construct and lysed by osmotic shock in 20 µl dH$_2$O. 10 µl of lysed bacteria were then used as template for colony PCR, which was performed with one vector-specific primer (Table 10 and Figure 8) and one insert specific primer, respectively. Only if the insert was integrated in the right orientation, PCR products were obtained and these clones were then regarded as positive clones.

From each positive clone an 8 ml over-night culture was prepared and plasmids were isolated using a Qiagen MiniPrep Kit (*Qiagen*) according to the manufacturer´s protocol. The kit is based on the alkaline lysis of the bacteria followed by the binding of the plasmid DNA to a silica matrix. After several washing steps, plasmids are eluted in ddH$_2$O. From each plasmid preparation 150 ng were used for sequencing (3.9.4) to identify any possible mutations.

3.9.6.3 Maxi-Preparation of plasmids

To prepare plasmids for the transfection of eukaryotic cells, the Endo Free Plasmid Maxi Kit (*Qiagen*) was used following the manufacturer´s instructions. This kit is specially designed to eliminate any bacterial component such as lipopolysaccharide (LPS), which may interefere with subsequent transfection experiments. Typically, 250 ml of bacterial culture were used for plasmid isolation.

3.10 Proteinbiochemical and immunological methods

3.10.1 Working with proteins

3.10.1.1 Protein extraction

3.10.1.1.1 Extraction of proteins from eukaryotic cells

To isolate proteins from eukaryotic cells either after transfection or treatment with various compounds, the culture medium was aspirated and the cells were washed once with 1xPBS. All subsequent steps were performed on ice or at 4°C, since typically no protease inhibitors were used. An appropriate amount of RIPA buffer was added to the cell culture dish (10 cm petri dish: 50 µl; 6-well plate: 30 µl per well) and cells were lysed by incubation for 20 min on ice. Thereafter, cells were harvested using a cell scraper, transferred into a 1.5 ml reaction tube and incubated on ice for another 20 min to complete lysis. Next, cell debris and DNA were pelleted by centrifugation at 4°C and 16,100 x g for 20 min and the supernatant containing the protein was stored at -80°C.

3.10.1.1.2 Extraction of proteins from organ tissues

After humanely sacrification of the respective mouse, organs of interest were quickly removed and snap frozen in liquid nitrogen. To extract protein from these organs approx. 300 mg of tissue were transferred into 500 µl RIPA-buffer containing Protease Inhibitors (1 complete mini tablet per 7 ml) (*Roche*) and homogenized on ice using a Basic Ultra Turrax Homogeniser (*IKA*). Cellular debris and DNA were pelleted by centrifugation at 4°C and 16,100 x g for 20 min and the supernatant containing the protein was carefully transferred into a new 1.5 ml reaction tube and stored at -80°C.

3.10.1.1.3 Determination of protein concentration according to Bradford

The Triphenylmethan-dye Coomassie Brilliant Blue G250 unspecifically interacts with basic sidechains of amino acids, whereby its absorbance is shifted from 465 nm to 595 nm. Based on this, Bradford (Bradford 1976) developed a method to quantify the protein amount in an unknown sample. Following her protocol, 2 µl of an unknown protein sample were mixed with 500 µl Bradford solution and incubated for 15 min at RT. Afterwards absorption was measured at 595 nm using a photometer (*Eppendorf*) and protein concentrations were calculated using a BSA standard curve.

3.10.1.1.4 Determination of protein concentration using BCA

Since determination of protein concentration according to Bradford is strongly influenced by protease inhibitors, proteins were also quantified using the more robust BCA (bicinchoninic acid) method. It is based on the fact that if both protein and Cu^{2+} are present the protein reduces Cu^{2+} to Cu^+. In a next step Cu^+ forms with BCA a Cu-BCA-complex having a distinct absorption maximum at 562 nm.

To determine protein with BCA, the BCA Protein Assay Reagent (Pierce) was used according to the manufacturer´s guidelines. In brief, 1 µl of protein sample was mixed with 200 µl BCA solution, vigorously shaken for 30 sec and then incubated for 30 min at 37°C. Afterwards, absorbance was measured at 562 nm on a Safire² plate reader (*Tecan*) and protein concentrations were calculated using a BSA standard curve.

3.10.1.2 Discontinuous denaturing PAA gel electrophoresis (SDS-PAGE)

During native gel electrophoresis, the migration speed of proteins is strongly dependent on their net charge, structure and conformation, which makes identification of the correct protein sometimes quite laborious. To circumvent this stumbling block, SDS-PAGE has been developed. It is a widely used technique to separate proteins just depending on their size by employing the anionic detergent SDS. SDS unfolds proteins and applies a negative charge to these, which is directly proportional to the mass of the respective protein (typically around 1.4 g SDS per g peptide) (Laemmli 1970). Still, it has to be taken into account that some proteins, mostly glycoproteins, behave abnormal during SDS-PAGE.

The underlying principle of SDS-PAGE is that inside the stacking gel the proteins are focused in one sharp starting zone from which proteins are then separate by size inside the separating gel. Protein focusing inside the stacking gel is achieved by a discontinuous buffer system. Typically, the stacking gel is prepared using a Tris-buffer with a pH of 6.8. When current is applied the glycine – dipolar ionized at this pH - migrates after the proteins to the anode, whereas the Cl^- migrates in front of them. These 2 ions create an electric field in which all proteins are captured and are migrating depending just on their net charge. Since the net charge for all proteins is the same (1.4 g SDS per 1 g peptide) and size effects do not come into play inside the stacking gel, since its pores are too wide to hinder the proteins in their migration, proteins are concentrated in a thin starting zone. Once glycine enters the separating gel, it fully dissociates due to a pH of 8.8, the electric field collapses and glycine passes the proteins. Starting from this point onwards, proteins are separated by size since the small pores of the separating gel act as a sieve, which decreases the running speed of bigger proteins, whereas smaller protein more easily fit through it.

To prepare a SDS-PAA gel, first the 12% seperating gel was prepared according to Table 6 between 2 clean glass plates and 70% EtOH was added on top until the gel has fully polymerized. After solidification, EtOH was removed and the 4% stacking gel was poured on top of the separating gel.

Protein samples indented to be analyzed by SDS-PAGE were supplemented with 5 µl 2xLaemmli buffer and boiled for 5 min at 95°C to ensure full denaturation. Typically 7.5 µg of protein were used for analysis. Once samples were loaded onto the gel, electrophoresis was performed using the respective 1x electrophoresis buffer (3.5.2). Protein size was estimated by using the Page Ruler Plus (*Fermentas*) loaded into a separate lane.

3.10.1.3 Coomassie staining of SDS Gels

Coomassie Brilliant Blue R250 is a widely used dye to directly stain proteins inside a SDS-PAA-gel. To visualize proteins directly in a SDS-PAA gel, SDS-Page was performed as described above (3.10.1.2). Afterwards, the gel was once shortly rinsed with dH$_2$O, covered with staining solution and gently shaken for 3 h to o.n. at RT. The gel was destained with detaining solution until the desired staining intensity was reached. Pictures were taken using a ChemiDoc XRS imaging System (*Biorad*).

Staining solution (400 ml)

- 0.4 g Coomassie blue R250
- 200 ml 40% (v/v) MeOH
- Filter out insoluble remants
- Add 200 ml 20% (v/v) acetic acid in dH$_2$O

Destaining solution (1 l)

- 500 ml ddH$_2$O
- 300 ml MeOH
- 100 ml acetic acid
- Add dH$_2$O to 1 l

3.10.1.4 Transfer of proteins onto nitrocellulose membranes

After resolving proteins via SDS-PAGE, proteins were typically transferred onto nitrocellulose membranes by wet blotting to make them available for antibody detection. To this aim, membrane (Protran BA83, *Whatman*) and gel were equilibrated in the respective transfer buffer (3.5.2) and placed face-to-face between 2 filter and 2 sponge pads soaked with transfer buffer. Next, the gel sandwich was put into a transfer cell, a cooling module was added and transfer was performed over night by applying a current of 30 V. Since the current is orientated perpendicular to the gel, the charged proteins move onto the membrane where they adhere due to hydrophobic interactions, but keep the organization present in the SDS-PAA-gel. Once transferred onto the membrane, proteins are easily accessible for antibody detection.

3.10.1.5 Ponceau staining of nitrocellulose membranes

After wet blotting, protein transfer was checked by incubation of the membrane in a Ponceau S solution (*Sigma*) for 1 min. Ponceau is an azo-dye which reversibly binds to the positively charged amino-groups of proteins. Following staining the membrane was destained with TBS-T.

3.10.1.6 Immunostaining of nitrocellulose-membranes using antibodies

Immunostaining of proteins transferred onto membranes is the easiest way to specifically detect and analyze the amount of any protein-of-interest. Specificity is achieved by using primary antibodies binding an epitope exclusively present on the respective protein. Given that nitrocellulose membranes generally bind all proteins, unspecific binding of the antibodies has to be prevented by blocking the membrane either with 6% BSA (*Sigma*) or 6%

non-fat milk powder (*Applichem*) in TBS-T for at least 3 h before starting the antibody incubation. Next, membranes were incubated with a primary antibody targeting the protein-of-interest diluted in TBS-T either containing 2% BSA or milk powder (detailed information about dilution, blocking reagent and incubation time are given in Table 4.) Subsequently unspecific binding of the primary antibody was eliminated by washing the membrane three times for 10 min with TBS-T following incubation with the secondary antibody for 1 h in the same solvent as the primary antibody. The secondary antibody is directed against the host IgG of the primary antibody and typically coupled to the horseradish peroxidase (HRP) which is used as a reporter enzyme (Table 5). Again unspecific antibody binding was eliminated by washing three times for 10 min with TBS-T. To visualize bound secondary antibody the membrane was then incubated for 5 min with 8 ml of SuperSignal West Pico Chemiluminescent Substrate (Pierce). This solution contains H_2O_2, which is cleaved by the HRP and the resulting $OH^{\cdot}$ reacts with luminol by emitting light. The chemilumiscent signal was then detected by a radiographic film (*Amersham*) and later on densiometrically analyzed using a ChemiDoc XRS imaging System (*Biorad*). Typically, target-protein amounts were normalized by comparision with the housekeeping gene/protein ß-Actin. If not noted differently, all results are given as mean of three different experiment ± SEM.

3.10.2 Precipitation/Purification of proteins and chromatin

3.10.2.1 Chromatin Immunoprecipitation (ChIP)

HDACi treatment induces widespread epigenetic changes and rearrangements in treated cells. One of the best known and characterized histone modifications is the acetylation of lysine 9 of histone H3 (H3K9ac), which is a clear mark of transcriptionally active chromatin. To check whether HDACi treatment leads to a hyperacetylation of different promoters and thereby to a higher expression of target genes, the LowCell ChIP Kit (*Diagenode*) was employed following the manufacturer´s guidelines. In brief, $3x10^5$ cells were incubated with 12.5 µl 37% formaldehyde in 500 µl 1xPBS by which DNA-Protein complexes are stably cross-linked. Subsequently, cells were washed with 1xPBS, peletted at 500 x g and the pellet was resuspended in lysis buffer. Next, chromatin was sheared into 500-1,000 bp long fragments using the Bioruptor (10 min, full power, 30 sec cycles on/off) (*Diagenode*). Following steps included incubation of the sheared chromation with 2 µg of an anti-H3K9 antibody (*Diagenode*) over night, several washing steps and reverse crosslinking by boiling the sample twice for 10 min at 100°C. After cleanup of the DNA by a DNA-purification slurry contained in the kit, DNA concentrations were measured on a photometer (*Eppendorf*). Next, equal DNA amounts were used for qRT-PCR using the ABI 7500 Realtime PCR machine to quantify the amount of precipitated individual DNA pieces (Table 9). Primers for the analysis of individual promoters can be found in Table 9.

3.10.2.2 Precipitation of ubiquitinylated proteins

Ubiquitinylation is the most common post-transcriptional modification used to target proteins to proteasomal degradation. Typically, activated ubiquitin is transferred by a, presumably, target-specific E3-enzyme onto an ε-amine of a target´s protein lysine. In a next step, activated ubiquitin molecules can be added onto the bound ubiquitin e.g. onto K48, which ultimately results in poly-ubiquitin chains bound to the target protein. These chains are recognized by a certain subset of proteins, e.g. Rpn10/S5a, which are present at the regulatory subunit of the proteasome.

To precipitate ubiquitinylated proteins, agarose beads were employed covalently coupled via glutathion (GSH) to the poly-ubiqutin-binding motif of Rpn10/S5a. Precipitation was carried out as described in the following: Per sample, 1×10^6 fibroblasts were plated out in 15 cm petri dishes and incubated with HDACi for 64 h. Subsequently, cells were washed with 1xPBS, trypsinized and pelleted for 5 min at 500 x g. The cell pellet was resuspended in 500 µl 1xPBS and washed twice at 500 x g for 5 min. To lyse the cells, the pellet was resuspended in 500 µl TBS-TG and sonicated using the Bioruptor (10min, full power, 30 sec cycles on/off) (*Diagenode*). Since the Rpn10/S5a is bound via GSH to the agarose beads, the cell lysate was next pre-cleared using 50 µl GSH-Sepharose (*Sigma*) and incubated for 1 h at 4°C on a rotating wheel. The beads were pelleted and the supernatant was transferred to a new 1.5 ml microcentrifuge tube. 20 µl of Rpn10/S5a agarose (Biomol) were added and the lysate was incubated over night at 4°C on a rotating wheel. Afterwards, the beads were pelleted and washed twice with 500 µl TBS-TG for 5 min at 500 x g. To elute bound proteins, the bead-pellet was resuspended in 20 µl 2xLaemmli-buffer and boiled for 10 min at 95°C. Subsequently, SDS-PAGE and western blot were performed as described in 3.10.1.2 and 1.1.1.1. Ubiquitinylated SMN was probed with a rabbit polyclonal anti-SMN antibody (*Santa Cruz*).

TBS-TG

- TBS pH=8.5
- 5% (v/v) Glycerol
- 1% (v/v) Triton-X 100
- 1 $^{µg}/_{ml}$ Leupeptin and Aprotinin

3.10.3 Determination of enzymatic activity

3.10.3.1 Determintation of proteasomal activity

To test whether HDACi such as LBH589 have an inhibitory effect on proteasomal degradation, the catabolic rate of the three catalytic activities (Caspase-like, Trypsin-like and Chymotrypsin-like) embedded in the proteasome were measured using Proteasome-Glo 3-Substrate Cell-Based Assay System (*Promega*). The kit is based on synthetic substrates for

each of the three catalytic activities, which are conjugated to aminoluciferin. Once the proteasome substrate is degraded, aminoluciferin is liberated and available for luciferase reaction.

The assay was performed according the manufacturer´s protocol. Some 1×10^5 fibroblasts were cultured in white-wall 96-well plates (*Greiner bio one*, #655088) and treated for the respective period of time (Table 13). Medium was aspirated and substituted by 100 µl fresh pre-warmed medium. Cells were incubated for 10 min at 37°C and 5% CO_2. Next, 100 µl reconstituted Proteasome-Glo™ Cell-Based Reagent containing the individual proteasome substrate and Ultra-Glo rLuciferase (*Promega*) were added and mixed for 2 min at 700 rpm on a shaking block. This step lyses the cell while keeping the proteasome intact. Subsequently, the plate was incubated for 10 min at RT and afterwards luminescence was read on a Glomax luminometer (*Promega*). For all measurements eight replicates were performed.

3.10.3.2 Inhibition of proteasomal protein degradation by MG-132

General protein degradation under HDACi treatment was analyzed using the cell-permeable proteasome inhibitor MG-132 (*Sigma*). To this aim, fibroblasts were pre-treated for 24 h with 400 nM LBH589, and MG-132 was added at a final concentration of 5 µM for 15 h (Table 13). Within this time, proteins normally degraded by the proteasome enrich since they are not longer degraded by the proteasome. Subsequently, proteins were extracted (3.10.1.1.1) and analyzed by western blot (3.10.1.2) as described above.

3.10.3.3 Determination of PKA-activity

The cAMP-dependent protein kinase A (PKA) is an important mediator involved in the regulation of diverse cellular mechanisms. Most importantly, it has also been shown that VPA inhibits PKA activity by attenuating cellular cAMP-levels (Boeckeler et al. 2006; Chang et al. 2009). To assess PKA activity in HDACi-treated cells, the PepTag Assay for non-radioactive detection of cAMP-dependent Protein Kinase (*Promega*) was used. The underlying principle is that a synthetic PKA substrate is added to a whole cell extract, and depending on the respective PKA activity the amount of phophorylated substrate varies. Phosphorylated and unphosphorylated substrates are then separated by agarose-gel electrophoresis, since the unphosphorylated one has a positive net charge and is therefore migrating to the cathode. In contrast, the phosphorylated substrate is negatively charged and migrates to the anode. Once both substrates are separated, the respective bands are cut out, melted and quantified on a plate reader.

The determination of PKA activity was carried out as recommended by the manufacturer. 2×10^2 fibroblasts per sample were HDACi-treated for the respective time period, washed, trypsined and pelleted 5 min at 500 x g. The pellet was the resuspended in 20 µl ice-cold PKA

extraction buffer containing 0.5 mM PMSF, and sonicated using the Bioruptor (10 min, full power, 30 sec cycles on/off) (*Diagenode*). Cellular debris and DNA were removed by centrifugation for 5 min at 14,000 x g. Next, samples and controls were prepared as given in Table 14 on ice.

	Sample	Positive control	Negative control
PepTag PKA Reaction 5x Buffer	5 µl	5 µl	5 µl
PepTag A1 Peptide (0,4 $^{µg}/_{µl}$)	5 µl	5 µl	5 µl
PKA Activator 5x Solution	5 µl	5 µl	5 µl
Protein Protection Mix	1 µl	1 µl	1 µl
Recomb. PKA (2 $^{µg}/_{ml}$) *	---	5 µl	---
Sample *	9 µl	---	---
ddH$_2$O	---	4 µl	9 µl

Table 14   Composition of the sample, positive and negative control reactions for the determination of PKA activity. * sample and recombinant PKA were added after incubation for 1 min at 30°C.

Reactions were warmed up for 1 min in 30°C waterbath. Afterwards, either sample or recombinant PKA was added and reactions were incubated for 30 min at RT. Subsequently reactions were stopped by incubating for 10 min at 95°C. After cooling down 1 µl 80% glycerol was added. To separate phosphorylated and unphosphorylated PKA substrate, a 0.8% agarose gel in 50 mM Tris-HCl pH=8.0 was prepared with slots in the middle of the gel. Total reactions were loaded and both substrates were separated by applying 100 V for approx. 15 min. Respective bands were cut out and melted in 150 µl Gel Solubilization Solution (5 M Urea) at 95°C in a heating block. 120 µl of solublized gel were then mixed with 50 µl acetic acid thereby hydroylysing all agarose chains and keeping the solution liquid. Next, samples were transferred into a black 96-well plates (*Greiner bio one*, #655076) and dye intensity was measured (excitation: 568 nm / emission: 592 nm) on a Safire² plate reader (*Tecan*).

PKA extraction buffer

- 25 mM Tris-HCl (pH=7.4)
- 0.5 mM EDTA
- 0.5 mM EGTA
- 10 mM ß-Mercaptoethanol
- 1 $^{µg}/_{ml}$ Leupeptin and Aprotinin

PKA dilution buffer

- 350 mM K$_3$PO$_4$ (pH=6.8)
- 0.1 mM DTT

3.10.3.4 Determination of fatty acid uptake via BODIPY-FA

CD36 is one of major fatty-acid transporters in the human body (Abumrad et al. 1993; Coburn et al. 2000; Endemann et al. 1993). To test whether higher CD36 amounts in the Non-Responders indeed lead to a higher fatty acid uptake, the QBT Fatty Acid Uptake Kit (*Molecular Devices*) was employed. It makes use of a BODIPY-labeled oleic acid analogue, which is actively transported into the cells. BODIPY (boron-dipyrromethene), a fluorescent dye, allows monitoring fatty acid uptake, since the more fluorescent is detected inside the cells, the higher was the fatty acid uptake. The protocol was as follows: Some 1×10^5 fibroblasts were plated out in 96-well plates and 24 h later treated for 16 h either with 500 µM VPA or mock. Next, cells were deprived for 8 h with 100 $^{µl}/_{well}$ serum free medium at 37°C and 5% CO_2. Subsequently, 10 µl test compound dissolved in 1x HBSS + 0.2 g BSA were added and cells were incubated for another 30 min (Table 13). Afterwards, 100 µl 1x loading buffer were added and cells were incubated o.n. at 37°C and 5% CO_2. Medium was aspired and 200 µl 10% SDS in 1xPBS were added. Complete lysis was ensured by incubation for 10 min on a shaking block. Next, fluorescence (excitation: 485 nm; emission: 515 nm) was measured on Safire² plate reader (*Tecan*).

5x loading buffer (10 ml)

- 1 ml 10x HBSS (*Gibco*)
- 0.2 ml 1 M HEPES (*Sigma*)
- 20 mg fatty acid free BSA (*Sigma*)
- 8,8 ml ddH₂O
- 1 Vial component A (containing BODIPY-labeled oleic acid) (*Molecular Devices*)

3.10.4 Enzyme-linked immunosorbent assay (ELISA)

3.10.4.1 Quantification of intracellular cAMP-content

cAMP is an important second messenger involved in the regulation of a vast number of cellular processes (Pavan et al. 2009). To quantify basal as well as cAMP levels under VPA treatment, the CatchPoint Cyclic-AMP fluorescent assay kit was used (*Molecular Devices*). The basic principle of this kit is a competitive immunoassay using cell lysates. cAMP in the sample competes with a horseradish peroxidase-labeled cAMP conjugate for the binding sites of an anti-cAMP antibody bound to a microtiterplate. The more cAMP is present, the less cAMP-antibody conjugate is binding, thus less HRP-activity is detected.

To quantify intracellular cAMP-levels some 1×10^4 fibroblasts were plated out in a 96-well plate. The following day, cells were treated with different compounds (Table 13) for the indicated time periods. Following treatment, the media was aspirated and 50 µl 1xPBS was added to each well. Next, fibroblasts were lysed by adding 50 µl lysis reagent and gentle agitation on a shaking block for 10 min. 40 µl of cell lysate were then transferred into the

assay plate. 40 µl of reconstituted rabbit anti-cAMP antibody were added to each well the plate was gently shaken for 5 min. Subsequently, 40 µl reconstituted HRP-cAMP conjugate were added and following mixing, the assay plate was incubated for 2 h at RT. The plate contents were aspirated and the plate was washed four times with 300 µl wash buffer. 100 µl Stoplight Red substrate were added to each well and the plate was incubated for 10 min shielded from light. Finally fluorescence intensity (excitation: 530 nm; emission: 590 nm) was measured on a Safire² plate reader (*Tecan*).

To rule out any artifacts based on differential proliferation between cell lines, data was normalized to the protein amount determined by a BCA-assay (3.10.1.1.4) performed with the remaining 60 µl of protein lysate produced at the initial steps of this assay.

3.10.4.2 Quantification of global histone H3 acetylation

Change in histone acetylation is the major hallmark of HDACi-treatment. To test if HDACi are also able to induce histone hyperacetylation *in vivo* the EpiQuik Global Histone H3 acetylation assay (*EpiGentek*) was used according to the manufacturer´s guidelines to detect changes in histone H3 acetylation. In brief, mice were injected with HDACi, sacrificed by gasification and brain and spinal cord were quickly prepared. 500 mg brain tissue or the whole spinal cord, respectively, were transferred into diluted buffer GF1 and homogenized using Basic Ultra Turrax Homogeniser (*IKA*). The lysate was centrifuged for 5 min at 9,300 x g and cellular debris pellet containing chromatin was resuspended in GF2/glycerol by vortexing. After incubation for 5 min on ice nucleic debris was pelleted at 13,400 x g for 5 min at 4°C. The supernatant was transferred into a new 1.5 ml reaction tube and ¼ Vol 100% TCA was added to precipitate histones. After incubation for 30 min on ice the pellet was collected (13,400 x g for 2 min at 4°C) and washed with 1 ml acetone (13,400 x g for 2 min at 4°C). The supernatant was removed and the pellet was air dried before resuspended in 100 µl ddH$_2$O.

Protein concentration of all samples was adjusted to 400 $^{ng}/_{µl}$ with GF4 and 5 µl of the protein solution were spread into a well of the assay plate. The plate was then dried for 90 min at 37°C. 150 µl pf GF5 containing a HRP-coupled antibody directed against acetylated histone H3 were added to each well and incubated for 30 min at 37°C. After aspiration the wells were washed 4x with 150 µl with GF3. Subsequently 100 µl GF9 containing the HRP-substrate were added to each well and the plate was incubated for 10 min in the absence of light. Reactions were stopped by adding 50 µl GF10 and absorbance was read at 450 nm on a Safire² plate reader (*Tecan*). Acetylated histone H3 amounts were calculated using a standard curve provided with the kit.

3.10.5 Determination of *SMN2* promoter activity

The basic idea behind using HDACi for the therapy of SMA is to activate the *SMN2* promoter and thereby activating the production of more functional protein from *SMN2*. Therefore it is of big interest to check whether HDACi treatment indeed increases *SMN2* promoter activity. To clarify this issue, a NSC-34 reporter cell line (Jarecki et al. 2005) was used, which is stably transfected with the β-lactamase reporter gene under the control of the human *SMN2* promoter (termed *NSC-34 bla* in the following). Addition of the fluorescent dye CCF2-AM (*Invitrogen*) allows monitoring *SMN2* promoter, since the dye is cleaved by the β-lactamase in a concentration-dependent manner. The protocol was as follows: Some 8×10^5 NSC-34 bla cells were plated out in a 10 cm petri dish and treated for 64 h with different concentrations LBH589. Afterwards cells were washed twice with 1xPBS and resuspended in 2 ml culture medium w/o FCS by pipetting up and down several times. Six replicates of 100 µl cell suspension were transferred into a 96-well plate and let settle down for 3-5 h. Next 20 µl 6xCCF2-AM staining solution were added, and the plate was incubated for 1.5 h at RT in the absence of light. Next, fluorescence intensity (internalized dye: excitation: 395 nm; emission: 530 nm / dye cleaved by β-lactamase: excitation: 395 nm; emission: 460 nm) was measured on a Safire² plate reader (*Tecan*). Promoter activity was calculated as ratio ($^{460}/_{530}$) of cleaved CCF2-AM to CCF2-AM internalized by the cells.

6x CCF2-AM staining solution (Invitrogen)

- 60 µl Solution B
- 6 µl 1 mM CCF2-AM
- 12 µl 1 M Probencid (*Sigma*) in 1 M NaOH
- 1 ml Solution C

3.10.6 Mass-spectroscopic determination of intracellular VPA content

To precisely determine the intracellular VPA content HPLC-MS/MS is the method of choice, since it gives far more precise results the standard gas chromatography. After dissociation of the analyte via a HPLC-column, the separated reagents are identified by mass-spectroscopy. The underlying principle is the resolving of ionized and most often fragmented analysts in an electric field based on their charge to mass ratio (*m/z*). Ionization is typically achieved by electron-spray ionization or laser-ionization. Subsequently, ions are accelerated *in vacuo* using a static electric field, fragmented in a collision chamber and are afterwards separated based on *m/z* by a quadropol and individually detected.

Furthermore, employing HPLC-MS/MS makes it possible to distinguish VPA from its blood metabolite, 4-ene VPA, allowinging to apply the assay also for the analysis of blood samples. HPLC-MS/MS procedures were carried out by Dr. Tim Bauer on a Triplequadrupole-tandem mass spectrometer Q Trap 4000 (*Applied Biosystems*) combined with SLC-20AD Prominance

HPLC machine (*Shimadzu*) at the *Institute of Pharmacology* in Cologne. Chromatographic runs were carried out for 10 min with a flow-rate between 200 and 400 µl. All chemicals used for HPLC-MS/MS experiments were of HPLC-purity.

3.10.6.1 Derivatization of VPA/4-en VPA

For the detection of VPA and 4-ene VPA, a published protocol for the detection of VPA in human blood (Cheng et al. 2007) was adopted and some modifications were added. The underlying principle is a pre-column activation of carboxylgroups with 1-chloro-4-methylpyridinium iodide and TEA and subsequent formation of stable 4-dimethylamino-benzylamide derivates. These derivates have a much higher atomic weight (VPA: 277.3 amu, 4-ene VPA 275.2 amu) than underivatized VPA (144.3 amu) and 4-ene VPA (142.2 amu) and thereby allow easier discrimination between both compounds based on their HPLC retention time (Figure 7).

The intracellular VPA content was determined by treating $2x10^5$ fibroblasts for 16 h with 500 µM VPA in a 10 cm petri dish as described in 3.8.1.1. Subsequently, cells were washed once with 1xPBS and collected by trypsinization and centrifugation at 500 x g for 5 min. Fibroblast were lysed by osmotic shock adding 200 µl ddH$_2$O and after 5 min incubation on ice snap-frozen in liquid nitrogen. After thawing, 2 µl 3 N HCl were added to lower the pH to approx. 3. Next, proteins were precipitated by adding 300 µl methylenechloride and vigorous shaking for 30 min at 37°C in a shaking heating block. Afterwards, cell lysates were centrifuged for 1 min at 16,100 x g to separate organic and aqueous phase. 250 µl of the organic layer were transferred into the prepared 1.5 ml reaction tube containing 10 µl 2-chloro-1-methylpyridiniumiodide (10 $^{mg}/_{ml}$), 10 µl 4-dimethylamino-benzylamindihydro-chloride (10 $^{mg}/_{ml}$) and 20 µl TEA. Derivatization reactions (Figure 7) were carried out for 1 h at 900 rpm and 37°C on a shaking heating block. Subsequently, reactions were stopped by adding 200 µl acetate buffer, pH =4 and tubes were centrifuged for 1 min at 16,100 x g. 200 µl of the organic layer were transferred into a new 1.5 ml reaction tube and evaporated to dryness for 2h at 50°C and 200 rpm in a shaking heating block under a sterile hood. The remaining precipitate was reconstituted in 120 µl ACN/ddH$_2$O (1:1) containing 0.1% formic acid. Subsequent HPLC-MS/MS analysis was performed by electron-spray ionization (ESI; pos. 5500 V, neg. -4500 V) and fragmentation in multiple reaction monitoring (MRM) mode.
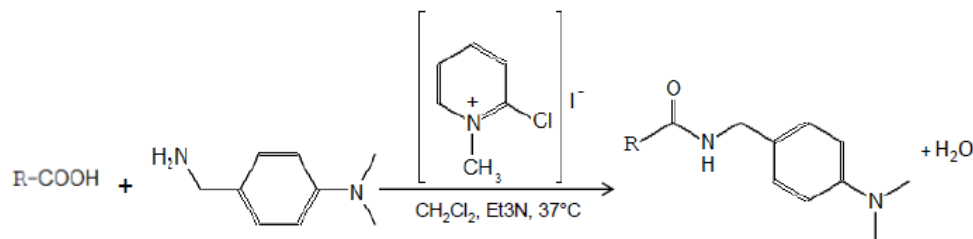
Figure 7   Reaction carried out for derivatisation of VPA, 4-ene VPA or any other organic acid. Catalyzed by 2-chloro-1-methylpyridiniumiodide and heating, 4-dimethylamino-benzyl-amindihydro-chloride is added onto the carboxylic acid residue to form an amide (adapted from (Cheng et al. 2007)

3.10.6.2 Determination of intracellular VPA content without derivatization

To determine the intracellular VPA content without the detour of derivatisation, VPA and its metabolites were directly determined without fragmentation. To this aim, 1×10^5 treated fibroblasts from a well of 6-well plate were lysed by adding 200 µl of 4 mM $HClO_4$. Proteins were pelleted by centrifugation for 1 min at 16,100 x g and 100 µl of the supernatant were used for injection into the LCMS using the single-ion-mode (SIM) without fragmentation.

To identify any putative differences in the metabolism of VPA in Non- and Pos-Responders, a shading assay was performed (Grundemann et al. 2005). To this aim, mass spectra of three pooled Non- and three pooled Pos-Responders from 0 to 400 atomic units recorded in SIM were superimposed by MS-FullView (*developed by D. Gründemann*), allocated and differences were marked in orange. To distinguish between VPA-metabolites and molecules produced in response of VPA treatment, 250 µM VPA and 250 µM d_{15}-VPA (*CDN isotopes*) were combined for treatment to give a final concentration of 500 µM VPA.

3.11 Working with mice

3.11.1 Animal breeding

All animals used throughout this thesis were housed in micro-isolation chambers in the mouse facility of the *Institute of Genetics, Cologne* under a normal dark and light rhythm (12 h). Animalbedding, cages, water and feed was regularly changed and controlled by the animal keepers. Genotyping was performed using standard PCR (3.9.3.1) and primers described in Table 11. Breedings were always set up in a 1-to-1 manner. Mice showing a very mild SMA-phenotype were generated by crossbreeding a $Smn^{-/-}$; $SMN2^{tg/tg}$ mouse (Hsieh-Li et al. 2000) with a $Smn^{+/-}$;$SMN2^{tg/tg}$ mouse (Monani et al. 2000). Obtained SMA-animals and their healthy littermates were numbered soon after birth with a water-resistant marker on the abdomen. At an age of three weeks, from all mice tail-tips were taken and numbered ear-tags were set.

3.11.2 Determination of weight progression of mice

To characterize mice showing a very mild SMA-phenotype, the weight progression was used as the main outcome measurement, since it is well-known that SMA-like mice have reduced weight compared to healthy littermates. Mice were weighed in plastic bowl placed on a standard laboratory balance. During the first 30 days of life, mice were weighed daily. Afterwards mice were weight once a week. Weighing was usually performed between 4 and 6 pm.

3.11.3 Subcutaneous injection of mice

To test whether HDACi are able to cross the blood-brain-barrier and to induce hyperacetylation in the CNS, adult $Smn^{-/-};SMN2^{tg/tg}$ (Hsieh-Li et al. 2000) mice were sub-cutaneously injected with either LBH589, JnJ26481585 or DMSO only into the neck pucker using a BD Micro-Fine + U-40 Insulin syringe (*BD Medical*). After treatment for the respective period of time, mice were killed by gasification and the organs-of-interest were removed.

3.11.4 Preparation of mouse organs

To prepare different mouse organs, the respective mouse was sacrificied by gasification on dry ice. Subsequently, the mouse was fixed on a preparation table and the body was opened by abdominal incision. Whole liver, *gastrocnemius* muscle, brain and spinal cord were removed and snap frozen in liquid nitrogen.

4. Results

Proximal spinal muscular atrophy is a common autosomal recessive disorder and the leading genetic cause of infant death in the Western European population. Although nowadays the disease phenotype is quite well known, there is no cure for SMA available yet. On molecular level, SMA is caused by functional absence of the *survival motor neuron gene 1* (*SMN1*), leading to dramatically reduced SMN protein levels (Lefebvre et al. 1995). This causes degeneration of the α-motor neurons in the anterior horns of the spinal cord resulting in progressive atrophy of the voluntary muscles and, ultimately, in lethal respiratory failure. Intensive analysis of the chromosomal regions surrounding *SMN1* revealed that *SMN1* is located in an inverted and duplicated region spanning more than 500 Kb (Lefebvre et al. 1995). Within this region, a nearly identical copy gene has been identified termed *SMN2*. Both genes encode for the same protein, but due to a silent nucleotide exchange *SMN2* splicing is dramatically altered (Lorson et al. 1999). Only approx. 10% of *SMN2* transcripts give rise to the full-length SMN protein whereas 90% of *SMN2* transcripts lack the critical exon 7, thus coding for a truncated and unstable protein (Lorson et al. 1998).

However, *SMN2* is the only origin of functional SMN protein in SMA patients. Its vital importance is further underlined by the finding that the number of *SMN2* copies inversely correlates with the SMA phenotype (Feldkotter et al. 2002; McAndrew et al. 1997; Wirth et al. 2006b). The more *SMN2* copies are present in a SMA patient, the milder is the phenotype. Therefore, quite a few therapeutic strategies have been developed within the last years which directly target *SMN2* either by gene activation, restoration the splicing pattern or gene replacement (Lorson et al. 2010).

In our laboratory, we pursued the approach to increase *SMN2* activity by means of HDAC inhibition. HDACis induce widespread chromatin hyperacetylation whereby general gene activity is increased. We identified the well-known HDACi valproic acid to markedly increase SMN protein amounts in fibroblasts derived from SMA patients (Brichta et al. 2003). Valproic acid, a short-chain fatty acid, is commonly used in the treatment of epilepsy but is also FDA-approved for the treatment of diverse types of seizures or bipolar disorder. Using VPA, a first clinical trial in SMA patients and carriers was performed and showed that VPA indeed increases blood *SMN*-mRNA levels in $^1/_3$ of treated patients (Positive Responder (Brichta et al. 2006)). However, $^1/_3$ of treated SMA patients did not show any change at all (Non-Responder) whereas the remaining $^1/_3$ of patients even showed a down-regulation of SMN (Negative Responder). More recently, a phase II open-label clinical trial with VPA has been performed in SMA type II and III patients (Swoboda et al. 2009). Although this study suggested that VPA has no positive effect on SMA disease progression, at least two critical points have to be mentioned: First, no stratification of SMA patients depending on the SMN levels has been undertaken. This is of fundamental importance since throughout the study

huge fluctuations between individual samples have been observed. Second, the clinical trial was too short to allow any final statement. Since both SMA type II and III patients are rather slow in their disease progression, a read-out time of six months is too short to detect any significant impact. This argument is further underlined by the finding that SMA-like mice treated for up to 12 months with VPA clearly exhibit an amelioration of the SMA phenotype (Tsai et al. 2008).

Based on these conflicting data, we tried to decipher the crucial factors which might help us to understand why somebody is positively responding to VPA or not. Understanding these factors would not only have great impact on SMA therapy but also on other diseases which are treated with VPA such as epilepsy. Furthermore we identified the new HDACi LBH589 as an auspicious candidate for SMA therapy and characterized its mode of action in detail.

4.1   SMA therapy with VPA: Why do we have Non- and Pos-Responders?

4.1.1   *In vitro* treatment of fibroblasts derived from SMA patients and carriers with valproic acid

To answer the question why a given SMA patient either responds positively, not or negatively to VPA treatment enough material is needed to perform all necessary experiments. Since blood samples are quite precious and available only in limited amounts a more easily accessible experimental system was required. Therefore, primary dermal fibroblast cultures were established from all nine SMA patients and six carriers included in our first clinical trial with VPA (Brichta et al. 2006). Four fibroblast lines were derived from SMA patients in which VPA increases SMN levels, whereas two fibroblast lines were derived from SMA patients showing no change in SMN expression. Additionally, further three fibroblast lines were established from SMA patients having decreased SMN levels under VPA treatment. Within the group of carriers – six in total - no change in SMN expression levels was detected under VPA treatment in blood. With this tissue system in our hands, we were able to address the question why somebody reacts to VPA treatment or not.

Since it was not known whether the response to VPA correlates among different tissues, it had first to be determined whether VPA treatment indeed triggers the same response regarding SMN levels in blood and fibroblasts. To this aim, all 15 fibroblast lines were treated for 16 h with VPA concentrations between 5 µM and 500 µM, resembling therapeutic doses routinely used in clinic (Brichta et al. 2003). Higher amounts were not used at this point since earlier publications had shown that these did not produce substantially stronger effects. All treatments were performed in triplicates from three different passages to exclude any passage-specfic effect. Protein extracts were then analyzed by semi-quantitative western blotting. β-actin was used as loading control since it has previously been shown that VPA only has minimal effects on its expression. A summary of all treated fibroblast lines is given in Table 15.

4.1.1.1 Classification of fibroblasts into Non- and Pos-Responder

To fascilitate comparison of the vast amount of western blot data derived from the VPA treatment of all 17 fibroblast lines tested, cell lines needed to be classified. Since the final goal of these experiments was to identify fibroblast lines which exhibit a similar response to VPA as the respective donor the results were sorted in two steps. The first parameter used to group VPA-treated fibroblast lines was the *in vivo* response to VPA of the individual SMA patients in the pilot clinical trial with VPA (Brichta et al. 2006): *Pos-Responder* were patients in whom VPA elevated SMN levels. *Non-Responder* included all SMA patients whi did not respond to VPA at all *in vivo* and, finally, the term *Neg-Responder* was used for patients in whom VPA declined SMN levels. Subsequently, VPA-treated fibroblast lines were discriminated by whether the response between blood and fibroblasts was concordant. Cell lines representing discrepant results were excluded from further analysis.

To determine the SMN threshold at which a cell line should be regarded as a Pos-Responder *in vitro*, the mean response of all fibroblast lines derived from SMA patients and carriers showing *in vivo* no change or reduced SMN levels under VPA treatment (ML49, ML53, ML63, ML66, ML68, ML75, ML62, ML65) was calculated. Based on this calculation (mean SMN level 114.7% +/- 5%), all cell lines exhibiting higher SMN levels than 120% under VPA treatment were defined as *Pos-Responders*. Furthermore, fibroblast lines showing reduced SMN levels upon VPA application were regarded as *Neg-Responders* whereas those exhibiting SMN amounts between 100 and 120% were classified as *Non-Responders*.

- **Carrier** fibroblasts (marked grey in Table 14)

  In line with the *in vivo* situation, VPA only slightly affected SMN levels by either increasing or decreasing SMN levels by less than 20% in four out of six carrier cell lines (ML49, ML53, ML68 and ML75). In contrast to that, VPA elevated - inconsistently to the *in vivo* data - SMN protein levels in the carrier fibroblast lines ML63 and ML66 by more than 40% at concentrations of 50 or 500 µM VPA, respectively.

- **Non-Responder** fibroblasts (marked orange in Table 14)

  Similarly to the carrier fibroblast lines ML63 and ML66, VPA dramatically altered SMN levels in both fibroblasts lines (ML62, ML65) derived from SMA patients showing no change in SMN expression under VPA treatment in *vivo*. In ML62, SMN was elevated for all three tested concentrations, whereas VPA reduced SMN in ML65 by more than 20% at every dose thus not confirming the *in vivo* data.

- **Pos-Responder** fibroblasts (marked green in Table 14)

  In total four cell lines were derived from SMA patients exhibiting augmented SMN levels under VPA treatment (ML60, ML67, ML71 and ML72). With the exception of ML71, in which a 5 to 10% decline in SMN was obtained for 5 and 50 µM, VPA

significantly increased SMN amounts in all cases. However, in ML60 the impact of VPA on SMN was rather low since its abundance was elevated only by 20% at 5 and 50 µM VPA. Noteworthy, ML67 showed the highest increase in SMN levels of all tested cell lines with > 200% at 500 µM VPA.

▪ **Neg-Responder** fibroblasts (marked red in Table 14)

In the case of the fibroblasts derived from SMA patients showing decreased SMN levels under VPA treatment (ML59, ML69, ML73 and ML82), reduced SMN levels were detected dose-dependently for ML69 and ML73. For ML82 a decline of 5 to 10% was observed for all tested concentrations. In contrast to that, ML59 showed slightly elevated SMN levels. Since these were below the Pos-Responder threshold, ML59 was regarded as a Non-Responder instead of a Neg-Responder.

Fibroblast line	Phenotype	n(SMN1)	n(SMN2)	Identifier in Brichta et al.	concentration of VPA 5 µM		50 µM		500 µM		Response in blood	Concordant data
ML49	Carrier	1	2	C5	101.7 +/- 9.7	n.s.	121.2 +/- 14.1	n.s.	98.5 +/- 8.4	n.s.	No change	yes
ML53	Carrier	1	1	C1	108.5 +/- 9.2	n.s.	110.1 +/- 8.8	n.s.	113.9 +/- 20.7	n.s.		yes
ML63	Carrier	1	2	C7	109.5 +/- 7.9	n.s.	149.1 +/- 27.2	n.s.	125.1 +/- 25.8	n.s.		No
ML66	Carrier	1	3	C9	118.2 +/- 14.4	n.s.	129.3 +/- 15.2	n.s.	147.8 +/- 21.9	n.s.		No
ML68	Carrier	1	2	C4	102.9 +/- 14.7	n.s.	101.8 +/- 10.3	n.s.	92.5 +/- 2.3	*		yes
ML75	Carrier	1	3	C8	130.6 +/- 13.7	n.s.	88.6 +/- 3.8	*	89.2 +/- 6.6	n.s.		with reservation
ML62	SMA type II	--	3	P10	139.6 +/- 4.8	**	179.6 +/- 30.9	n.s.	148.9 +/- 21.3	n.s.	No change	No
ML65	SMA type II	--	3	P12	90.9 +/- 2.6	*	80.9 +/- 7.7	n.s.	75.2 +/- 8.1	*		with reservation
ML60	SMA type II	--	3	P5	120.2 +/- 14.2	n.s.	119.0 +/- 6.9	*	109.5 +/- 10.1	n.s.	Up-regulation of SMN	with reservation
ML67	SMA type II	--	3	P8	151.6 +/- 26.8	n.s.	175.1 +/- 28.0	*	201.2 +/- 18.7	**		yes
ML71	SMA type II	--	3	P6	96.3 +/- 15.2	n.s.	83.1 +/- 16.7	n.s.	127.5 +/- 27.9	n.s.		No
ML72	SMA type II	--	3	P7	113.3 +/- 23.9	n.s.	112.3 +/- 27.2	n.s.	137.7 +/- 29.6	n.s.		yes
ML59	SMA type II	--	3	P13	120.2 +/- 14.2	n.s.	119.0 +/- 6.9	*	109.5 +/- 10.1	n.s.	Down-Regulation of SMN	yes
ML69	SMA type III	--	4	P4	85.9 +/- 15.7	n.s.	59.3 +/- 19.2	n.s.	60.7 +/- 16.6	n.s.		yes
ML73	SMA type II	--	3	P14	85.6 +/- 10.5	n.s.	67.9 +/- 1.6	***	59.2 +/- 1.6	***		yes
ML82	SMA type IIIa	--	3	---	98.9 +/- 1.9	n.s.	86.1 +/- 10.4	n.s.	93.1 +/- 10.9	n.s.		yes

Table 15 SMN protein levels in fibroblast lines after 16 h VPA treatment with the indicated concentrations. Results are given as mean of three independent experiments +/- SEM. The level of significance is given in the adjacent column (n.s. = not significant; * *P<0.05*; ** *P<0.005*; *** *P<0.001*). All treated carrier fibroblast lines are marked in light gray. For all treated patients` cell lines the highest individual change in SMN levels is marked in dark gray. In the second-to-last column the response in blood is given. Last column indicates whether response in blood and fibroblast is consistent.

In conclusion, the *in vivo* response to VPA could clearly be confirmed in nine out of 17 cases. In three further fibroblast lines (ML75, ML65 and ML60) similar tendencies as in blood were obtained but these results were not as clear as in the other fibroblast lines. Therefore,

these cell lines were regarded as confirmed but under reservation. In another four cell lines a clearly opposite response to VPA was observed as expected from the *in vivo* data (ML63, ML66, ML62 and ML71). Therefore, these cell lines were excluded from further experiments. Furthermore, cell lines derived from carriers (ML49, ML53 and ML68) were also not used for further analysis, since it was not known to what extent the present *SMN1* gene cloaks any *SMN2* activation by VPA. Thus, the following six fibroblast lines were selected for further analysis (Figure 8).

- **Pos-Responder:** ML67 and ML72
- **Non- & Neg-Responder:** ML59, ML82, ML69 and ML73

Noteworthy, both Non- and Neg-Responders were grouped together for two reasons. Firstm the actual differences in SMN levels between both groups were sometimes blurred, e.g. in the case of ML59. Second, the project´s focus was to address the question why somebody does not respond *positively* to VPA. However, it has to be kept in mind that all Neg-Responders are indeed responding to VPA, but in an opposite way. For the sake of consistency, the group of Non- and Neg-Responder will thereafter be termed *Non-Responder* in the following.

In general, a VPA concentration of 500 µM had the highest impact on SMN protein levels (six out of nine treated SMA patient cell lines). Therefore, we chose this concentration as the "standard concentration" for further experiments.
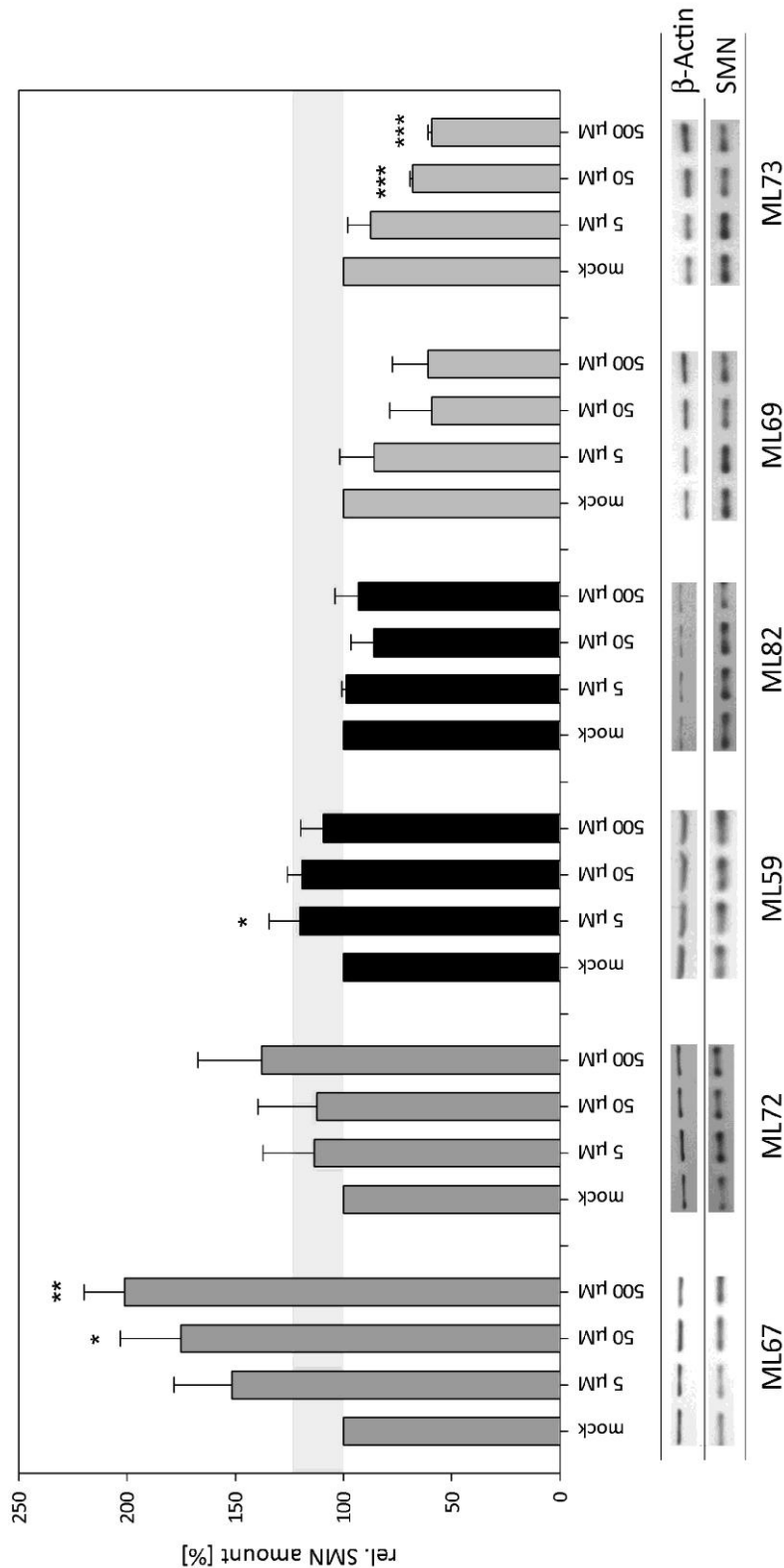
Figure 8   Response to VPA of the 5 fibroblast lines chosen for further analysis. Diagramm represents mean SMN levels of three independent experiments ± SEM. Gray area indicates interval in which fibroblasts are regarded as Non-Responder. A representative western blot using β-Actin as loading control is given for each cell line. ML67 and ML72 were Pos-Responder. ML59, ML69 and ML73 were grouped together as Non-Responder (see text). (* = $P<0.05$; ** = $P<0.005$; *** = $P<0.001$)

4.1.1.2 Generation of an unrelated control group

All cell lines characterized above had been established before the start of this work. During its accomplishment further fibroblast lines were collected from SMA patients undergoing VPA therapy. These cell lines were intended to be used as an unrelated control group, which

should serve to verify the data obtained from cell lines analyzed above (Table 15). All newly established fibroblast lines were treated in triplicate with VPA whenever they were available. To circumvent the possibility of missing some cell lines that do not react to VPA at lower concentrations but respond at higher doses, the treatment was changed in such a way that fibroblasts were treated for 16 h with 50 μM, 500 μM and 1 mM VPA.

By treating 14 further fibroblast lines with VPA two additional concordant Pos-Responders (ML94, ML95) and three additional concordant Non-Responder were identified (ML79, ML86, ML105) (Table15). In the case of the Pos-Responders ML94 and ML95, the highest increase in SMN was detected at VPA concentration of 1 mM with SMN levels of around 160 to 170%. A similar amount of SMN was also recorded at 50 μM VPA for ML94 whereas 500 μM VPA only slightly increased SMN protein. For ML95 a dose-dependent increase in SMN was found. ML79 and ML86 were both identified as concordant Non-Responder either showing no change in SMN levels or a dose-dependent decrease down to approx. 70% at 1 mM VPA for ML86. The fibroblast line ML89 was excluded from further analysis since SMN levels fluctuated between 140% at 50 μM and approx. 100% at 500 μM and 1 mM VPA, thus giving no consistent picture. ML96 showed a dose dependent increase to merely 150% SMN at 1 mM, but also had to be excluded since these data did not match *in vivo* data. Finally, the Non-Responder cell line ML105 SMN fluctuated by less than 10% at all three VPA-concentrations thereby confirming the *in vivo* data.

In total, eight further fibroblast lines were treated with VPA, but it cannot be stated yet whether these cell lines are concordant or not, since the VPA therapy of the respective SMA patients is still ongoing (Table 14). Among these cell lines, ML103 most likely is a Non-Responder since VPA treatment decreased SMN levels down to 86% at 1 mM. A similar pattern was found for ML104. In contrast to that, ML108 turned out to be a Pos-Responder since VPA significantly increased SMN levels to 144% at 1 mM VPA. In the remaining five fibroblast lines, VPA triggered neither a significant increase or decrease at all tested concentrations.

Taken together, five additional concordant fibroblast lines were identified, two of which are Pos-Responders and three are Non-Responders. For another eight fibroblast lines VPA therapy is still ongoing and therefore the classification as either concordant or discordant needs to be awaited. Nevertheless, these fibroblast lines are currently being cultivated again to verify the data presented in the following.

Fibroblast line	Phenotype	n(SMN1)	n(SMN2)	5 µM		50 µM		500 µM		1 mM		Response in blood	Concordant data
ML79	SMA type II	---	3	104.4 +/- 6.8	n.s.	101.9 +/- 10.1	n.s.	110.7 +/- 13.9	n.s.	--- +/- ---	---	Down-Regulation	yes
ML86	SMA type I	---	2	--- +/- ---	---	94.2 +/- 7.0	n.s.	93.6 +/- 8.0	n.s.	69.6 +/- 9.6	*	No change	yes
ML89	SMA type II	---	3	--- +/- ---	---	139.7 +/- 2.2	***	105.9 +/- 5.3	n.s.	111.5 +/- 13.5	n.s.	No change	no
ML94	SMA type II	---	3	--- +/- ---	---	154.4 +/- 26.2	n.s.	120.5 +/- 6.9	n.s.	160.2 +/- 14.1	*	Up-Regulation	yes
ML95	SMA type I	---	2	--- +/- ---	---	119.4 +/- 7.4	*	129.8 +/- 7.3	*	171.0 +/- 6.9	***	Up-Regulation	yes
ML96	SMA type II	---	3	--- +/- ---	---	94.9 +/- 5.9	n.s.	130.2 +/- 13.5	n.s.	145.1 +/- 23.6	n.s.	No change	no
ML100	SMA type IIIb	---	n.d.	--- +/- ---	---	107.6 +/- 3.1	n.s.	107.3 +/- 12.4	n.s.	109.9 +/- 9.1	n.s.	not determined	---
ML103	SMA type IIIa	---	3	--- +/- ---	---	96.3 +/- 8.7	n.s.	97.0 +/- 10.0	n.s.	85.7 +/- 11.0	n.s.	not determined	---
ML104	SMA type II	---	n.d.	--- +/- ---	---	93.7 +/- 1.8	*	104.5 +/- 6.4	n.s.	97.8 +/- 3.6	n.s.	not determined	---
ML105	SMA type II	---	3	--- +/- ---	---	92.8 +/- 9.6	n.s.	104.5 +/- 1.9	n.s.	99.9 +/- 0.9	n.s.	No change	yes
ML106	SMA type IIIb	---	4	--- +/- ---	---	106.8 +/- 20.5	n.s.	103.4 +/- 3.2	n.s.	126.2 +/- 22.1	n.s.	not determined	---
ML108	SMA type I	---	3	--- +/- ---	---	90.2 +/- 5.0	n.s.	112.9 +/- 15.5	n.s.	143.5 +/- 9.9	*	not determined	---
ML110	SMA type II	---	n.d.	--- +/- ---	---	114.6 +/- 8.2	n.s.	121.8 +/- 10.0	n.s.	109.1 +/- 13.0	n.s.	not determined	---
ML111	SMA type I	---	2	--- +/- ---	---	67.2 +/- 21.2	n.s.	153.1 +/- 15.2	*	135.4 +/- 22.8	n.s.	not determined	---

Table 16   SMN protein levels in fibroblast lines after 16 h VPA treatment with the indicated concentrations. Results are given as mean of three independent experiments +/- SEM and significance level in the adjacent column (n.s. = not significant; * $P<0.05$; ** $P<0.005$; *** $P<0.001$). For all treated patients cell lines the highest individual change in SMN levels is marked in dark gray. In the second-to-last column the response in blood is given; "preliminary" indicates that VPA therapy is still ongoing and no clinical data is available yet. Last column indicates whether patients' response in blood, if known, and fibroblast is consistent.

4.1.2 Search for the molecular basis of VPA Non-Responders

Based on the previously described fibroblast data the question arose why SMN is not increased in Non-Responders by VPA. Since the effect of VPA on SMN levels is mediated via HDAC inhibition, it was tested whether VPA has any effect on the acetylation status of the *SMN2* promoter in Non-Responders. To this aim, fibroblasts from three Pos-Responders and three Non-Responders were treated with 500 µM VPA for 16 h and compared via Chromatin Immunoprecipitation (ChIP) using an antibody directed against acetylated histone H3 (Roh et al. 2005). Acetylation of lysine 9 of histone H3 is a clear sign of active transcription and was therefore chosen as the pivotal parameter of *SMN2* promoter activity. Following ChIP, *SMN2* promoter acetylation was quantified by qRT-PCR at four regions known to be susceptible to HDACi-induced hyperacetylation (Kernochan et al. 2005).

VPA increased acetylation in all three Pos-Responders throughout the whole *SMN2* promoter (Figure 9). Highest increases of around 50 to 75% were detected at HuSP2, approx. 1.2kb upstream of the transcriptional start site (TSS), and HuSP4, which is located directly after the TSS. For both, HuSP1 and HuSP3, VPA increased acetylation by 25 to 50%. In contrast to that, for all three Non-Responders no general hyperacetylation was detected. In the case of HuSP1 and HuSP3 acetylation was even decreased by 25% in all three cases. Similar results were obtained for HuSP2 and HuSP4 with the exception of ML82 or ML59, respectively. Taken together, these data clearly show that VPA is not inducing histone hyperacetylation at the *SMN2* promoter in Non-Responders and therefore does not act as an HDACi.
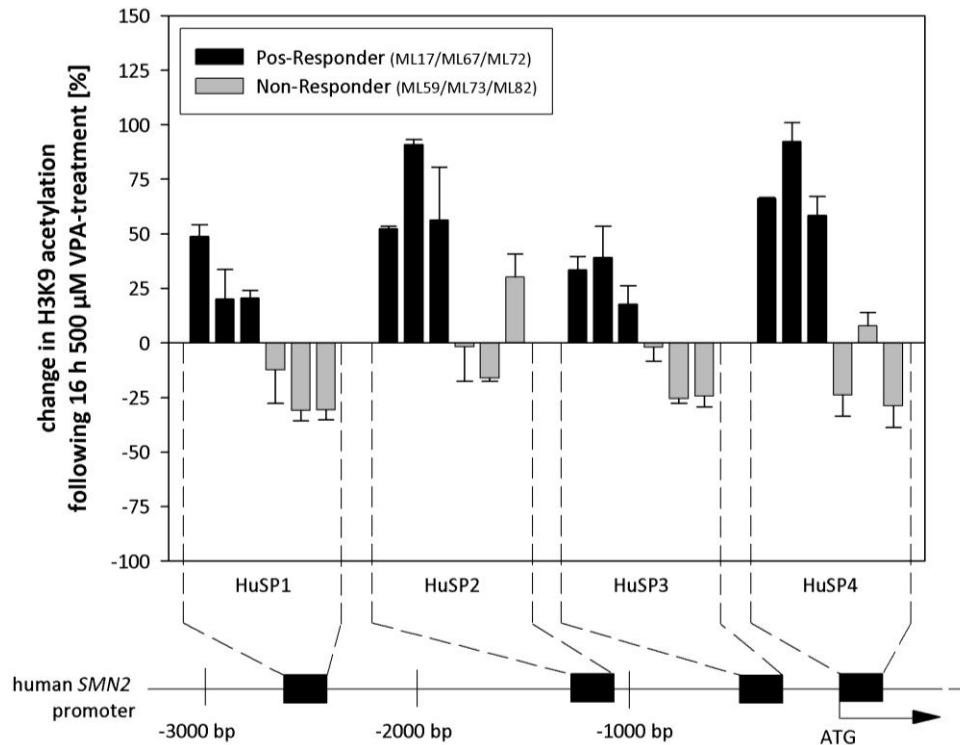
Figure 9   **Change in H3K9 acetylation after 16 h 500 µM VPA treatment in three Pos- and three Non-Responder cell lines. Location of all four analyzed regions is given in the lower part. (Pos-Responder → from left to right: ML17, ML67, ML72. Non-Responder → from left to right: ML59, ML73, ML82)**

Since ChIP analysis revealed that VPA did not induce hyperacetylation of the *SMN2* promoter in Non-Responder fibroblast lines, it was next tested whether Non-Responders are generally inert to HDACi treatment and could therefore be regarded as *General HDACi-Non-Responder*. To clarify this issue, Non-Responder fibroblast lines were treated with various HDACi. Since VPA is a branched short-chain fatty acid, different fatty acid HDACi were tested such as Sodium Butyrate, a short-chain fatty acid HDACi shown to increase SMN amounts (Chang et al. 2001). Furthermore, the aromatic fatty acid Phenylbutyrate, a derivate of Sodium Butyrate, was included. As a control HDACi having no fatty acid characteristics LBH589 was employed. Treatment conditions of all HDACi were taken from the respective publication (*VPA*: 16 h 500 µM (Brichta et al. 2003); *Sodium butyrate*: 24 h 500 $^{\mu g}/_{ml}$ (Andreassi et al. 2001); *Phenylbutyrate*: 4 h 2 mM (Andreassi et al. 2004); *LBH589* 64 h 400 nM (Garbes et al. 2009)). Following treatment, SMN levels were analyzed by semi-quantitative western blotting using a SMN and a β-Actin antibody. As shown in Figure 10, all tested HDACi increased SMN levels in the Pos-Responder ML5, thereby confirming their capacity. As expected, LBH589 had the highest impact on SMN levels. VPA and Phenylbutyrate produced similar effects and increased SMN by 50%. Sodium butyrate merely doubled SMN amounts in ML5 whereas it did not affect SMN levels in neither ML73 nor in ML59. VPA had, as expected, also no positive impact on SMN protein amounts, but

even decreased SMN in the case of ML59. There again, both Phenylbutyrate as well as LBH589 increased SMN levels comparable to ML5, thereby showing that ML73 and ML59 are not *general HDACi Non-Responder.* It rather gives the impression that the Non-Responders are inert to a small subset of HDACi, very probably those with a simple fatty acid backbone such as VPA and Sodium Butyrate.
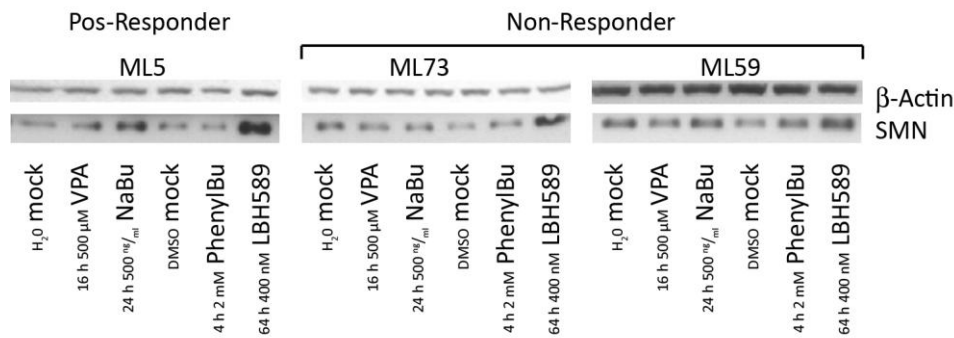
Figure 10 **Western Blots with proteins extracted from a Pos-Responder and two Non-Responder fibroblasts lines treated with various HDACi. Membranes are stained simultaneously with an anti-SMN and an anti-β-Actin antibody, which served as loading control. Individual treatment conditions are given. Solvent for VPA and Sodium butyrate (NaBu) was H$_2$O. Phenylbutyrate (PhenylBu) and LBH589 were dissolved in DMSO.**

It became clear that in Non-Responder cell lines VPA is not acting as an HDACi so that SMN protein is consequently not increased. VPA affects a variety of other cellular mechanisms of which its inhibitory effect on the cAMP-dependent Protein Kinase A (PKA) was chosen as second outcome measurement to characterize VPA treatment of Non-Responders (Boeckeler et al. 2006; Chang et al. 2009). To follow up this issue, PKA activity in VPA-treated fibroblasts was quantified *by in vitro* phosphorylation of a synthetic PKA substrate (PepTag Assay for non-radioactive Detection of cAMP-dependent Protein Kinase, *Promega*).

Following 16 h VPA treatment, a dose-dependent decrease in PKA activity was found for all three tested Pos-Responder fibroblast lines (Figure 11, Figure 60). At 50 µM VPA PKA activity was reduced by approx. 10 to 20% whereas at 500 µM and 1 mM VPA PKA activity decreased by 30 or 40%, respectively. In contrast to the Pos-Responders, PKA activity did not decrease in the Non-Responders under VPA treatment. For both ML59 and ML73 only tiny fluctuations of around 10% were detected. In the case of ML103 VPA, unexpectedly, increased PKA activity at all three assayed concentrations. Taken together these data clearly show that besides not acting as an HDACi in Non-Responders, VPA also does not act as a PKA inhibitor in these cells.
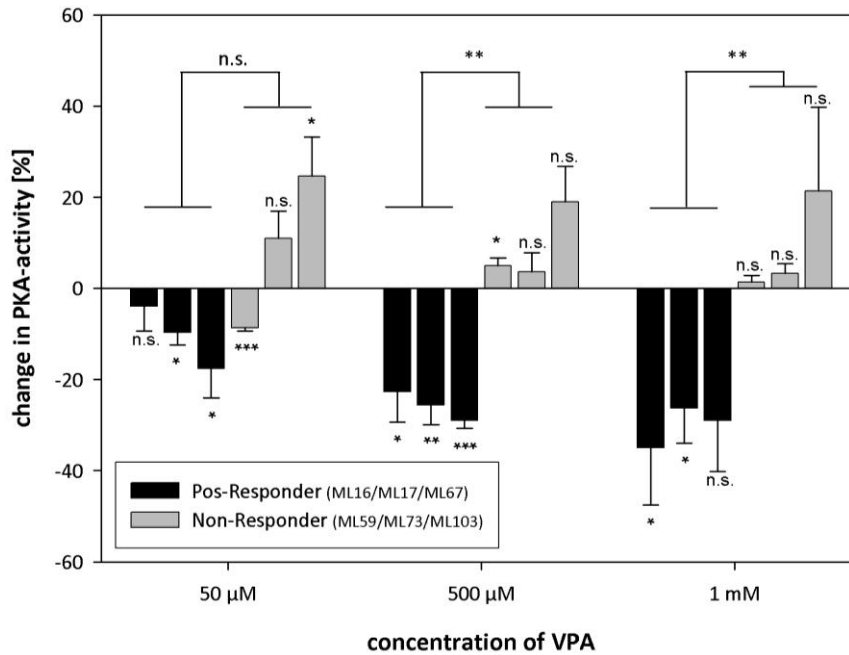
Figure 11   **Change in PKA activity compared to untreated cells. Individual significances are given at each bar, brackets indicate comparison of Pos-Responders versus Non-Responders (n.s. = not significant; * *P*<0.05; ** *P*<0.005; *** *P*<0.001). Pos-Responder → from left to right: ML16, ML17, ML67. Non-Responder → from left to right: ML59, ML73, ML103. All results are given as mean of three independent experiments.**

4.1.3 Transcriptome-wide comparison of Non- and Pos-Responders

By comparing Non-Responders and Pos-Responders, it could be shown that VPA neither triggers *SMN2* promoter hyperacetylation nor inhibits the PKA in Non-Responders. Since all fibroblasts are derived from different SMA patients, all Non-Responders should - most likely - have something in common which prevents VPA´s normal mode of action. On the other hand, this pivotal factor should not be present in Pos-Responders and therefore make up the difference why somebody reacts to VPA or not. To identify this factor, which may either be a specific gene or a group of genes, both groups should be compared by transcriptome-wide µ-array analysis.

In the previous experiments six concordant fibroblast lines were identified: two of them Pos-Responder (ML67, ML72) and four Non-Responders (ML59, ML69, ML73 and ML82). To increase the statistical power of the µ-array analysis three additional fibroblast lines were included (ML5, SMA type II, 3x *SMN2* / ML16, SMA type I, 3x *SMN2* / ML17, SMA type I, 2x *SMN2*) which previously have been shown to positively react to VPA (Brichta et al. 2003). These cell lines were not derived from SMA patients included in the pilot clinical trial with VPA (Brichta et al. 2006) but are routinely used in our laboratory for experiments with HDACi (Garbes et al. 2009; Riessland et al. 2006).

With a sufficient number of fibroblast lines available for μ-array analysis (five Pos-Responder vs. four Non-Responder), cells were plated out and 24 h later treated for 16 h either with mock or 500 μM VPA, respectively. Since the amount of RNA needed for μ-arrays is >3 μg for each sample, $1x10^6$ fibroblasts were seeded out in two separate 15 cm dishes each. In contrast to the normal procedure, cells were trypsinized, pooled, pelleted and then lysed with RLT-buffer (*Qiagen*) for RNA-extraction because a small aliquot of the cell suspension was used for protein extraction and subsequent western blot analysis. This was based on the observation that in very few cases the change in SMN levels triggered by VPA treatment was far lower than usual. To ensure that only strong samples are compared with each other, only those aliquots were used for μ-arrays in which a SMN response similar to previous data was verified by western blotting.

The collected RNA samples were then sent to the *Microarray facility* in Tübingen where all subsequent steps including the bioinformatic analysis were performed (3.9.5). For the comparison of Non- and Pos-Responders, the GeneChip Human Gene 1.0 ST Array (V1 April 2009) from *Affymetrix* was employed detecting 28,869 well-annotated genes via >760,000 probes. The probe design is based on the human genome sequence assembly from spring 2006 (UCSC Hg18, NCBI build 36) and covers more than 99% of mature mRNA (NM) sequences present in the RefSeq database (http://www.ncbi.nlm.nih.gov/refseq/). Background substraction is done by using around 17,000 background probes (GeneChip Human Gene 1.0 ST Array datasheet, *Affymetrix*).

After μ-array read-out and background substraction, both Non- and Pos-Responders were compared groupwise. Taken together four different comparisons were performed (Table 17) and the following number of transcripts were detected to be differentially expressed. A complete list of all differentially expressed transcripts is given in the Appendix, Table 22 to Table 24.

Comparison	$P≤0.05$	$P≤0.01$	$P≤0.05$ (BH corrected)
NR mock vs. NR treated	977	280	0
PR mock vs. PR treated	1987	733	58
NR mock vs. PR mock	1247	289	9
NR treated vs. PR treated	1418	293	21

Table 17 **Number of differentially expressed transcripts under different levels of significance. (NR = Non-Responder; PR = Pos-Responder; BH corrected = after Benjamini-Hochberg correction)**

False positive transcripts due to multiple testing were eliminated by Benjamini-Hochberg (BH) correction. After BH correction it became obvious that no single transcript was significantly up- or downregulated. In contrast to that, more than 50 transcripts were

differentially expressed under VPA treatment in the Pos-Responders. Most interestingly, only nine transcripts were differentially expressed between untreated Pos- and Non-Responders. These, and another 12 genes, were also found to be significantly expressed between treated Pos- and Non-Responders.

In a next step, all transcripts were eliminated which showed a less than 2-fold expression (logFC<1) since these differences may also occur randomly without a significant impact. This reduced the list to a total of 22 transcripts which are given in Figure 12.
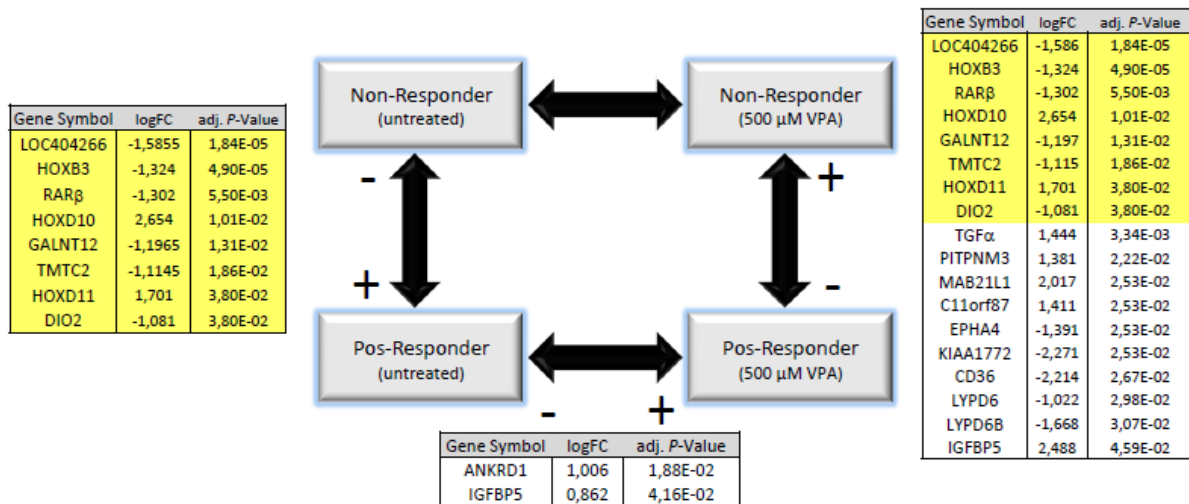

Gene Symbol	logFC	adj. P-Value
LOC404266	-1,5855	1,84E-05
HOXB3	-1,324	4,90E-05
RARβ	-1,302	5,50E-03
HOXD10	2,654	1,01E-02
GALNT12	-1,1965	1,31E-02
TMTC2	-1,1145	1,86E-02
HOXD11	1,701	3,80E-02
DIO2	-1,081	3,80E-02

Gene Symbol	logFC	adj. P-Value
LOC404266	-1,586	1,84E-05
HOXB3	-1,324	4,90E-05
RARβ	-1,302	5,50E-03
HOXD10	2,654	1,01E-02
GALNT12	-1,197	1,31E-02
TMTC2	-1,115	1,86E-02
HOXD11	1,701	3,80E-02
DIO2	-1,081	3,80E-02
TGFα	1,444	3,34E-03
PITPNM3	1,381	2,22E-02
MAB21L1	2,017	2,53E-02
C11orf87	1,411	2,53E-02
EPHA4	-1,391	2,53E-02
KIAA1772	-2,271	2,53E-02
CD36	-2,214	2,67E-02
LYPD6	-1,022	2,98E-02
LYPD6B	-1,668	3,07E-02
IGFBP5	2,488	4,59E-02

Gene Symbol	logFC	adj. P-Value
ANKRD1	1,006	1,88E-02
IGFBP5	0,862	4,16E-02

Figure 12   **Schematic overview of differentially expressed transcripts fulfilling the criteria of an adjusted *P*-Value (after BH correction) < 0.05 (5.00E-2) and logFC (log-fold change) > 1. Leading sign indicates in which group expression of the respective transcript was higher. Transcripts highlighted in yellow are differentially expressed between both treated and untreated Non- and Pos-Responder.**

Although data are corrected for multiple testing and RNAs of bad quality are excluded, µ-array analysis may lead to false positive results. Therefore, the identified 22 differentially expressed transcripts had to be verified by a second method. Therefore, aliquots of the RNAs used for µ-array analysis were reversely transcribed into cDNA and the expression in all 18 samples (five Pos-Responder + four Non-Responders, each mock and VPA-treated) were analyzed by qRT-PCR on an ABI 7500 Taqman machine. A detailed list of the qRT-PCR results and their comparison to the µ-array results is given in the appendix, Table 25 and Table 26. Taken together nine out of the 22 transcripts could be verified by qRT-PCR (*DIO2*, *GALNT12*, *RARβ*, *KIAA1772*, *LYPD6*, *MAB21L1*, *TGFα*, *CD36* and *IGFBP5*) whereas for the remaining 13 transcripts the µ-array data could not be reproduced by qRT-PCR. For example, µ-array detected a higher expression of *EPHA4* in Non-Responders, but qRT-PCR indicated for both Non- and Pos-Responders a likewise expression. Of the verified transcripts three (*DIO2*, *GALNT12*, *RARb*) were generally differentially expressed between Non- and Pos-Responders, whereas the six transcripts were only found to be unequally expressed in VPA-treated cells.

Since nine different transcripts are too many to perform subsequent experiments, a practical number of the most likely candidates had to be selected. To identify the most promising candidates, literature was mined and the transcripts rather less likely to account for a differential response to VPA were excluded from further analysis (Table 27). The following four candidates were chosen based on their described function and their connections to different pathways (Figure 13). In the following, each candidate is briefly introduced and the individual expression pattern in the assayed fibroblasts is given.

Figure 13   Schematic depiction of the detected expression pattern in Pos- and Non-Responder. CD36 = cluster of differentiation 36; RARβ = Retinoic acid receptor β; IGFBP5 = Insulin-like growth factor binding protein 5; TGF α = Transforming growth factor α

4.1.3.1 Cluster of differentiation 36 (CD36), MIM ID: 173510

- alias: thrombospondin receptor, fatty acid translocase, glycoprotein IV, scavenger receptor class B member 3
- outline: 7q11.2 / 17 exons / 471 aa > 53 kDA

CD36 was identified more than 30 years ago as the 4th major glycoprotein in platelet membranes and therefore originally termed "glycoprotein IV" (Clemetson et al. 1977). Later studies showed that CD36 is not only expressed in blood but is also present in a large variety of different tissues such as endothelium, adipocytes, skeletal muscle as well as the intestine (Febbraio et al. 2001). It is highly conserved among mammals, and orthologs have been identified down to *drosophila* (termed *emp)* (Hart and Wilcox 1993) and sponges (Muller et al. 2004). CD36 contains two transmembrane domains, a short intracellular domain but a very large extracellular domain forming a cloverleaf-like structure, which is heavily glycolysated (30-40 kDa) (Hoosdally et al. 2009; Rac et al. 2007). Within the group of vertebrates, CD36 is the defining member of class B scavenger receptor family comprising also CLA-1 and LIMP-II (Calvo et al. 1995; Calvo and Vega 1993). CD36 is virtually ubiquitously expressed and has various tissue specific-functions. One of the best characterized roles of CD36 is its function as a receptor of thrombospondin-1 (TSP1) as well as several other proteins containing thrombospondin repeats (TSR) (Silverstein et al. 1992). In this capacity, CD36 negatively controls angiogenesis, e.g. in the case of tumor growth or wound healing, by activating p59^{fyn}, p38, caspase 3-like kinase and driving the cell into apoptosis (Jimenez et al. 2000). Furthermore, CD36 functions as a scavenger/pattern recognition sensor within the innate immune system and recognizes foreign agents such as bacteria or parasites (Means et

al. 2009). Recent studies have shown that CD36 acts as a co-receptor for toll-like receptor 2 (TLR2) and is mainly responsible for the recognition of bacterial lipoproteins (Jimenez-Dalmaroni et al. 2009). Studies with mice carrying a CD36 nonsense mutation revealed that these *oblivious* mice are hypersusceptible to *Staphylococcus aureus* infections due to an insensity to MALP-2 (a bacterial lipopeptide) and lipoteichoic acid (Hoebe et al. 2005). Besides sensing foreign agents, CD36 is also involved in the recognition of endogenous specimens such as apoptotic cells (Ren et al. 1995) and oxidized lipoproteins (Endemann et al. 1993; Podrez et al. 2000; Ren et al. 2010). Especially CD36-mediated recognition of oxLDL has been intensively studied since oxLDL internalization promotes the formation of lipid-loaden macrophages and smooth muscle cells ("foam-cells") as well as atherosclerotic plaques. oxLDL binding by CD36 activates pro-inflammatory transcription factors such as NF-κB and triggers cytokine release (Febbraio et al. 2001; Kunjathoor et al. 2002). Moreover, CD36 mediates the microglial and macrophage response to β-amyloid by triggering Src kinase dependent production of inflammatory mediators thereby suggesting that CD36 takes a major position in the proinflammatory events of Alzheimer´s disease (El Khoury et al. 2003; Moore et al. 2002). Taken together, CD36 signalling is diverse but some common patterns in response to scavenger ligands are present such as activation of Src and JNK kinase as well as kinases of the MAPK family (Jimenez et al. 2000; Moore et al. 2002; Rahaman et al. 2006).

Because VPA is a short-chain fatty the most important finding in the context of this thesis is that CD36 has also been involed in the import of biologically active lipids and long-chain fatty acids (LCFA) into the cell (Abumrad et al. 1993; Coburn et al. 2000; Endemann et al. 1993). Studies using mice showed that CD36 expression is highest in tissue strongly dependent on high FA metabolism such as heart and oxidate muscles. Furthermore, it has been shown that CD36 is co-regulated with *fatty acid binding proteins* (FABP) (Poirier et al. 1996) and also increased in mice under high-fat diet (Heuckeroth et al. 1987). The exact mechanism of CD36-mediated LCFA-transport is yet unknown but its expression is regulated by the lipogenic transcription factors PPARγ, LXR and RXR. Therefore, it also has been suggested that CD36 may contribute to the pathogenesis of obesity and steatosis (Zhou et al. 2008). Furthermore, two SNPs within the CD36 promoter region, most likely reducing CD36 expression, have been associated with insulin resistance (Corpeleijn et al. 2006; Miyaoka et al. 2001). Studies in CD36 *null* rats corroborate these findings by showing that indeed their liver became insulin resistant since the muscles only utilized glucose whereby the liver was flooded with an excess of LCFAs (Goudriaan et al. 2003). Underlining the role of CD36 in metabolic syndromes it has been observed that fatty acids and insulin oppositionally regulate lysosomal degradation of CD36 by controlling its ubiquinitylation (Smith et al. 2008).

Taken together the vast number of cellular processes in which CD36 is involved, as well as function as a fatty acid transporter make it a very interesting candidate for the differential response to VPA.

The detected 5-fold higher expression of CD36 in Non-Responder compared to Pos-Responders by μ-array was verified by qRT-PCR (Figure 14). In all five tested Pos-Responder fibroblast lines CD36 expression was between 0.3 and 1.0 au. In contrast to that, expression of CD36 was between 1.5 au in the Non-Responder ML69 and 4.8 au in ML59. Although more than 3 au differences in the transcript levels of CD36 were detected within the group of Non-Responders, analysis clearly showed a significant higher expression of CD36 (P=0.0026) in this group compared to Pos-Responders.
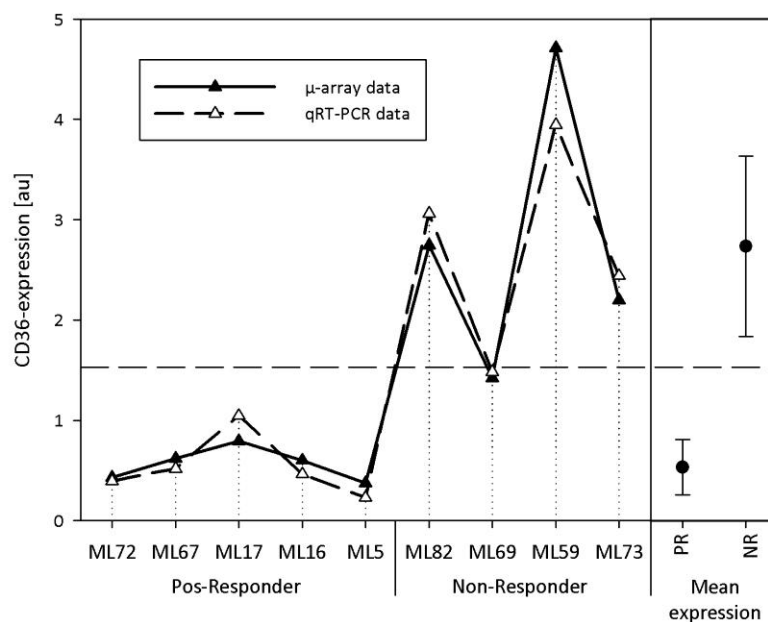
Figure 14   **Expression of CD36 in Non- and Pos-Reponders under VPA treatment determined by qRT-PCR and μ-array. On the right side mean values for both groups are given based on qRT-PCR data (PR = 0.53±0.27 au; NR = 2.73±0.89 au; P=0.0026). Dashed line represents mean expression of all nine tested fibroblast lines. (PR = Pos-Responder; NR = Non-Responder)**

4.1.3.2 Retinoic acid receptor β (RARβ), MIM ID: 180220

- alias: Nuclear receptor subfamily 1 group B member 2, hepatitis B virus activated protein 2
- outline: 3q24 / 8 exons / 455 aa > 51 kDA

Tissue homeostasis and development is regulated by a plethora of factors. Among these vitamin A and its bioactive derivates, termed retinoids, play a critical role. These non-steroid hormones are important regulators of differentiation, proliferation and apoptosis (Ross et al. 2000). Typically, the retinoic acid (RA) signal is transduced by two families of nuclear receptors each consisting of three isotypes (α, β and γ) – the retinoic acid receptors (RAR) and the retinoid X receptors (RXR), which work as RXR/RAR heterodimers (Kastner et al. 1997; Leid et al. 1992b; Mangelsdorf and Evans 1995). RARs are typically activated by all-

trans retinoic acid (RA) and its 9-cis isomer, whereas RXRs are only activated by the latter isomer. From a structural point of view, all retinoid receptors are composed of six conserved regions, of which the third one – termed C-region – harbors the DNA-binding domain (DBD) (Zechel et al. 1994a; Zechel et al. 1994b) whereas the E-region is responsible for ligand-binding (LBD) and heterodimerization (Wurtz et al. 1996). Interestingly, it has been shown that upon PKA activation a consensus site within in the LBD of RARs is phosphorylated whereby DNA binding is reduced (Rochette-Egly et al. 1995). RAR/RXR heterodimers bind to RA response elements (RARE) consisting of two direct repeats of a hexameric motif Pu(G/T)TCA (Leid et al. 1992b; Mangelsdorf and Evans 1995). Classical RAREs are found in a wide variety of promoters as in those of *HOX* genes (Dupe et al. 1997), but also in the promoters of RA-shuttle proteins CRBPI and CRAPII (Durand et al. 1992) and RARβ itself (de The et al. 1990). Typically, unliganded RAR/RXR heterodimers are bound to their respective RARE and repress transcription via recruitment of co-repressors such as N-CoR, which in turn recruit HDAC-complexes (Glass and Rosenfeld 2000). Binding of RA to the heterodimer induces conformational changes (Rastinejad et al. 2000) leading to the dissociation of the co-repressors. This triggers chromatin remodeling and allows the binding of co-activators (Depoix et al. 2001). As a last step of gene activation, retinoid receptors recruit the transcription machinery to the decondensed chromatin via the SMCC mediator complex (Dilworth and Chambon 2001). Besides activation by ligand binding, RARs are regulated by ubiquitinylation (Zhu et al. 1999) and phosphorylation, which allows cross-talk with other signalling pathways such as PKA, ERK and JNK mediated signalling (Rochette-Egly 2003).

Although much research has focused on the role of RARα and RARγ during development, there have also been some efforts to clarify the physiological role of RARβ. Similar to other RAR isotypes, several isoforms of RARβ are known (RARβ1 to RARβ4), which differ by their N-terminal A region. These different isoforms arise from alternative splicing as well as the facultative usage of two different promoters of which the second one – termed P2 - is RA-inducible (Leid et al. 1992a). RARβ$^{-/-}$ mice are viable but show symptoms like growth retardation, homeotic transformations of the cervical vertebrae and a retrolenticlar membrane due to hyperplasia of the primary vitreous body. Although the highest expression of RARβ was detected in the striatum and the interdigital mesenchyme, brain and limbs of RARβ$^{-/-}$ mice appeared normal (Ghyselinck et al. 1997). RARα/RARβ double knockouts die prenatally or soon after birth due to respiratory problems. When analyzed at fetal stages, these mice display symptoms similar to the CATCH22 syndrome (microdeletion in 22q11), which can be mimiked in chicks by ablation of the neural crest cells (NCC) (Ghyselinck et al. 1997; Mendelsohn et al. 1994). RARβ/RARγ knockout mice show major ocular defects similar to the fetal vitamin-A deficiency (VAD) syndrome (Ghyselinck et al. 1997; Lohnes et al. 1994; Mendelsohn et al. 1994). Further intensive studies using double mutants clearly reflected the roles of RAR signalling in axial rotation, brain segmentation and ontogenesis mesectodermal derived structures by controlling *HOX* gene expression (Dupe et al. 1997;

Mark et al. 1998; Mark et al. 1995). For example, it has been shown in mice that RARβ controls expression of group four *HOX* genes but is also reciprocally regulated by *Hoxb4* and *Hoxd4*, thereby controlling the segmentation of the hindbrain (Serpente et al. 2005).

Noteworthy, two additional points have to be mentioned: Typically, RARβ is not expressed or only present at very low levels in dermal fibroblasts *in vitro* but is quickly up-regulated upon RA stimulus (Redfern and Todd 1992). Furthermore, RA treatment of cells rapidly induces up-regulation of CD36 mRNA although it has not yet been worked out whether this is mediated via a RARβ/RXR heterodimer (Wuttge et al. 2001).

Similar to CD36, RARβ was confirmed by qRT-PCR to be higher expressed in Non-Responders (Figure 15). In contrast to CD36, expression of RARβ was higher in mock (12.5 au vs. 0.2 au) and VPA-treated (4.5 au vs. 0.2 au) Non-Responders. Noteworthy, at least in qRT-PCR-assay RARβ was barely expressed in all in Pos-Responders leading to considerable differences between both groups. In line with this RARβ signal intensities during μ-array analysis were only slightly over the threshold (oral communication with Dr. Walter, Tübingen). Within the group of Non-Responders, RARβ expression varied in the mock-treated cells between 7 (ML73) and 21 (ML59) au, but was still considerably highly expressed. Under VPA treatment, RARβ expression dropped to around 4.5 au in the mean. In the case of ML73, which also showed the lowest RARβ expression when mock-treated, RARβ was not longer expressed under VPA treatment.
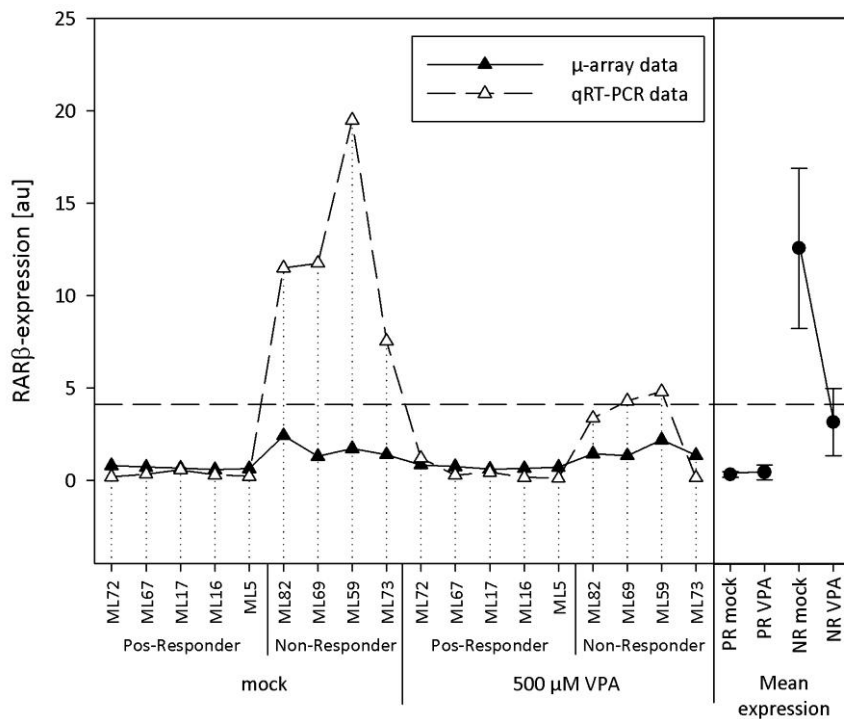
Figure 15   Expression of RARβ in Non- and Pos-Reponders under VPA treatment and mock-treated determined by qRT-PCR and μ-array. On the right side mean values for both groups are given based on qRT-PCR data (PR mock = 0.31±0.14 au; PR VPA = 0.43±0.39 au; n.s. / NR mock = 12.56±4.33 au; NR VPA = 3.15±1.81 au; *P*=0.006 /PR mock vs. NR mock; *P*<0.001 / PR VPA vs. NR VPA; *P*=0.012). Dashed line represents mean expression of all nine tested fibroblast lines. (PR = Pos-Responder; NR = Non-Responder; n.s. = not significant)

4.1.3.3 Insulin-like growth factor binding protein 5 (IGFBP5), MIM ID: 146734

- ▪ alias: IGF-binding protein 5
- ▪ outline: 2q35 / 4 exons / 272 aa > 30 kDA

During the 1970´s, the insulin-like growth factors were discovered as factors with structural homology to pro-insulin which can stimulate insulin-like effects (Rinderknecht and Humbel 1978a, b). Subsequent studies showed that in mammals a so-called IGF system is present which consists of two ligands circulating in the serum (IGF-I and IGF-II) (Daughaday and Rotwein 1989) and six classical binding proteins (IGFBP1 to IGFBP6). Downstream signal-transduction within the IGF system is elicited via the IGF type 1 receptor (IGF-1R) and controls mostly mitogenic and apoptotic effects (Gicquel and Le Bouc 2006). In contrast to that, the IGF type 2 receptor (IGF-2R/mannose-6-phosphate receptor) is not involved in signal transduction since it is devoid of a tyrosine kinase domain but rather controls extracellular IGF-II concentrations (Braulke 1999). Mice lacking IGF-2R have an increased

birth weight, heart abnormalities and usually die perinatally but can be rescued by depletion of IGF-II (Lau et al. 1994; Ludwig et al. 1996).

IGFBPs share an overall protein sequence identity of 50% and contain 16-18 conserved cysteines in the N- and C-terminus (Shimasaki and Ling 1991). Furthermore, a characteristic GCGCCXXC motif is present in the N-terminus of all IGFBPs (Oh et al. 1996; Shimasaki and Ling 1991). Generally speaking, IGFBPs compete with the IGF receptors for peptide binding by sequestering extracellulary IGFs (Baxter and Twigg 2009). Free IGFs have a half-life of approx. 10 min whereas when bound in binary 40 kDa complex with IGFBPs1-6 the half-life increases to 30 to 90 min. The half-life is even more increased to 12 h when IGFs are bound in a ternary 150 kDa complex with either IGFBP3 or IGFBP5 and ALS (acid labile subunit), suggesting that the regulation of free and bound IGF by the IGFBPs is of fundamental importance (Firth et al. 2001; Guler et al. 1989).

Nowadays, debate is ongoing whether IGFBPs should be considered as simple IGF carrier proteins since newly identified IGF low affinity binders (5 to 25 fold less than conventional IGFBPs1-6) such as IGFBP7 (Oh et al. 1996) and IGFBP8 (Kim et al. 1997) show an up to 500-fold higher affinity to insulin (Yamanaka et al. 1997). Subsequent identification of further IGFBP-related proteins such as IGFBP-rP5 (L56/HtrA) (Zumbrunn and Trueb 1996) and IGFBP-rP2 (CTGF) (Bork 1993) has led to the proposal to extend the classical IGFBP family to a superfamily consisting out of the six classical members IGFBP1-6 as well as 10 IGFBP-related proteins (Hwa et al. 1999).

The IGFBP5 gene is located on chromosome 2 only 20 kb away from the *IGFBP2* gene, suggesting that both genes developed after duplication of an ancestral IGFBP. Similar to *IGFBP4*, which is found in the vicinity of the *HOXB* genes, *IGFBP2* and *IGFBP5* map to the same chromosomal region as the *HOXD* cluster. This indicates that these genes were probably linked prior to duplication, but a common cis regulatory element has not yet been identified (Allander et al. 1994). Within the same work it has been shown that the *IGFBP5* promotor has a simple structure with conserved TATAA and CAAT sequences present upstream of the TSS (Allander et al. 1994). Subsequent studies identified an AP2 recognition side upstream of the TATA box, explaining the high expression levels in fibroblasts as well as the responsiveness to cAMP (Duan and Clemmons 1995). Throughout the human body the highest *IGFBP5* expression is found in testis, bone, trabecular meshwork, lung, uterus and placenta (Schneider et al. 2002). In adult human serum, IGFBP5 amounts are depending on the IGF-I concentration (Mohan et al. 1996), which has been verified in the brain of IGF-I transgenic mice (Ye and D'Ercole 1998). However, IGFBP5 serum levels as well as skeletal content decrease during ageing (Mohan et al. 1995; Rajaram et al. 1997).

IGFBP5 is synthesized as a 272 aa protein which is secreted after cleavage of 22 aa as a 29 kDa protein. Similarly to other IGFBPs, IGFBP5 can be cleaved by a variety of proteases thus regulating its bioavailability (Schneider et al. 2002). Most proteolytic cleavage sites are

found within the midpart, which in contrast to the higly conserved N- and C-terminus differs from the other IGFBPs. For example, in fibroblasts IGFBP5 is cleaved among others by complement C1r and C1s, resulting in a 22 kDa fragment (Busby et al. 2000). Furthermore it has been shown that all four predicted O-glykolysation sites of IGFBP5 (Thr_{103}, Thr_{104}, Thr_{111} and Thr_{152}) are indeed used making the protein less prone to proteolysis although some modifications may be tissue specific (Conover and Kiefer 1993; Standker et al. 1998). In addition, IGFBP5´s affinity to IGF-I is modulated via phosphorylation in the midpart (Coverley and Baxter 1997; Schneider et al. 2002).

IGFBP5 has been shown to bind the ECM, thereby stimulating osteoblast mitogenesis. However, although ECM-binding decreases the proteolysis of IGFBP5, it reduces its affinity to IGF-I and –II (Andress and Birnbaum 1992; Arai et al. 1994). Subsequent studies identified Arg_{207} and Arg_{214} as the most critical aa mediating ECM binding (Parker et al. 1998). Furthermore, an association has been shown between IGFBP5 and 420 kDa membrane protein which is capable to internalize IGFBP5 in osteoblasts. Although feasible it has not yet been proven whether this is an IGFBP5 receptor (Andress 1995).

In vivo studies using transgenic mice overexpressing IGFBP5 under the control of the osteocalcin promoter revealed that these animals had an up to 27% reduced total bone mineral density as well as a decreased bone mineral apposition rate most likely due to impaired osteoblastic function (Devlin et al. 2002). Ubiquitous overexpression led to increased neonatal mortality, growth reduction and retarded muscle development (Salih et al. 2004). However, ubiquitous IGFBP5 overexpression was able to rescue the lethal IGF-2R phenotype by sequestering the excess of IGF-II (Tripathi et al. 2009). Similar to the IGFBP3^{-/-} mice, IGFBP5^{-/-} mice had no obvious phenotype, suggesting that both proteins somehow compensate for each other since IGFBP3 and -5 are the only IGFBPs able to form the ternary IGF-ALS complex (Ning et al. 2006). This hypothesis was further underlined by experiments showing that IGFBP3 mRNA was increased in the jejunum of IGFBP5^{-/-} mice (Murali et al. 2007).

In contrast to CD36 and RARβ, an almost 10-fold higher expression of IGFBP5 was found in Pos-Responders compared to Non-Responders by both qRT-PCR and μ-array (Figure 16). All tested Non-Responders exhibit a likewise IGFBP5-expression of approx. 0.3 au, whereas the Pos-Responder had a mean expression of around 3.3 au. Within the group of Pos-Responders, a more than 4-fold expression difference was found between ML17, which peaked at 8 au, and ML72, ML16 and ML5 having an expression of around 2 au. However, a significant difference in expression was detected when all fibroblast lines were compared groupwise (P=0.035).
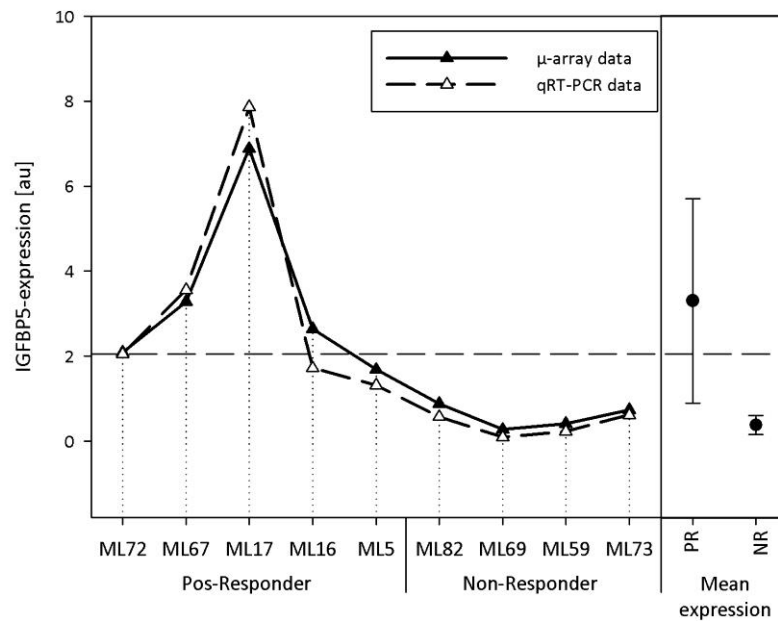
Figure 16   **Expression of IGFBP5 in Non- and Pos-Reponders under VPA treatment determined by qRT-PCR and μ-array. On the right side mean values for both groups are given based on qRT-PCR data (PR = 3.30±2.41 au; NR = 0.38±0.22 au; *P*=0.035). Dashed line represents mean expression of all nine tested fibroblast lines. (PR = Pos-Responder; NR = Non-Responder)**

4.1.3.4 Transforming growth factor α (TGFα), MIM ID: 190170

- alias: protransforming growth factor α
- outline: 2p13 / 6 exons / 160 aa > 17 kDA

TGFα is a small polypeptide growth factor which is structurally related to EGF (35% homology) and is secreted by a wide variety of neoplastic cells and during fetal development (Coffey et al. 1987; Marquardt et al. 1984). However, subsequent studies revealed that TGFα expression is not restricted to these instances but rather occurs throughout the whole organism, especially in skin keratinocytes (Coffey et al. 1987). Wound healing experiments showed that TGFα expression by wound macrophages stimulates keratinocyte proliferation and migration, thereby closing the wound. Furthermore, it has been shown that PKC activation strongly enhances TGFα expression, suggesting that TGFα is a normal physiological ligand in the skin. (Barrandon and Green 1987).

Similar to EGF, all biological activities of TGFα are elicited through the EGF receptor (ErbB1/HER1) (Todaro et al. 1980). Thus, both ligands compete for the binding and might have complementary functions (Massague 1983). However, TGFα has been shown to be far more potent than EGF in promoting angiogenesis (Schreiber et al. 1986) and inducing cell transformation *in vitro* (de Larco and Todaro 1978; Rosenthal et al. 1986; Todaro and De Larco 1978; Watanabe et al. 1987). The EGF receptor is a member of the ErbB family of

tyrosine-kinase receptors which mediate major cellular functions such as proliferation and survival (Blume-Jensen and Hunter 2001). The four members of the ErbB family are EGFR, ErbB2 (HER2), ErbB3 (HER3) and ErbB4 (HER4), of which ErbB2 is the most potent signalling molecule (Normanno et al. 2006). Nowadays, several antibodies used in cancer therapy, such as Herceptin (Trastuzumab), are on the market which directly target different members of the ErbB-family.

From the TGFα gene two different mRNAs encoding both for the same protein (1.6 and 4.5 kb in length) are generated of which the 4.5 kb mRNA is the predominant isoform. As compared to the shorter mRNA, the 3′-UTR of the 4.5 kb mRNA possesses a number of additional destabilization elements and polyadenylation signals controlling its lifetime (Qian et al. 1993). TGFα is synthesized as a 160 aa precursor transmembrane molecule which contains a 100 aa large extracellular domain, from which the mature TGFα peptide is released by cleavage with elastase-like enzymes (Lee et al. 1985). Different species of the mature TGFα have been found depending on the proteolytic cleavage and on differential N- and O-glykolysation (Bringman et al. 1987; Gentry et al. 1987). A similar domain undergoing proteolytic cleavage has been identified in the EGF precursor (Pfeffer and Ullrich 1985). Noteworthy, not only the secreted but also the membrane-bound TGFα precursors are biologically active and interact with receptors of adjacent cells (Brachmann et al. 1989).

Studies with mice tried to elucidate the different functions of TGFα in an *in vivo* context. Transgenic mice overexpressing TGFα in the mammary epithelium showed hyperplasia of the alveoli and terminal ducts. In contrast to that, males overexpressing TGFα in the reproductive organs exhibit no morphological abnormalities (Matsui et al. 1990). Subsequently, more general studies underlined the great impact of TGFα on angiogenesis and proliferation. Ubiquitous overexpression of TGFα led to the development of general epithelial hyperplasia in liver, pancreas and the gastrointestinal tract as well as tissue-specific phenotypes such as multifocal hepatocellular carcinomas (Jhappan et al. 1990; Sandgren et al. 1990). Moreover, skin-specific overexpression did not induce carcinomas of TGFα but rather induced spontaneous papillomas (presumably in conjunction with TGFβ) in regions of wounding and irritation (Vassar and Fuchs 1991). TGFα knockout mice are healthy and fertile but show a pronounced waviness of the fur and whiskers due to a misorganization of the skin and hair follicles (Mann et al. 1993). Subsequent studies showed that these mice had an increased proliferation of the prostatic buds (Abbott et al. 2003) and reduced mid- and forebrain (Blum 1998).

More than 20 years ago a polymorphism in TGFα was associated with cleft lip with or without cleft palate in humans (Ardinger et al. 1989). Interestingly, TGFα is expressed during palatogenesis in mice but TGFα^{-/-} mice do not exhibit oral clefts (Mann et al. 1993). Contrariwise, EGFR^{-/-} mice have a high incidence of cleft palate which may explain the correlation between the TGFα polymorphism and cleft lip in humans (Miettinen et al. 1999).

Subsequent meta-analysis of genome scans confirmed this association (Vieira 2006) and could furthermore show that certain TGFα haplotypes are associated with teeth agenesis (Callahan et al. 2009).

As for IGFBP5, a higher expression of TGFα was detected in VPA treated Pos-Responders compared to Non-Responders. All four Non-Responders had a quite uniform TGFα expression of around 0.3 au, whereas the Pos-Responders had an expression of around 2.8 au. Comparably high expression was detected in ML72, ML17 and ML16, whereas ML67 expressed only half of the amount, leading to a deviation between 2.4 and 1.2 au within the group of Pos-Responders. In summary, the expression differences detected by qRT-PCR were slightly less then measured by µ-array but still significant (*P*=0.001).
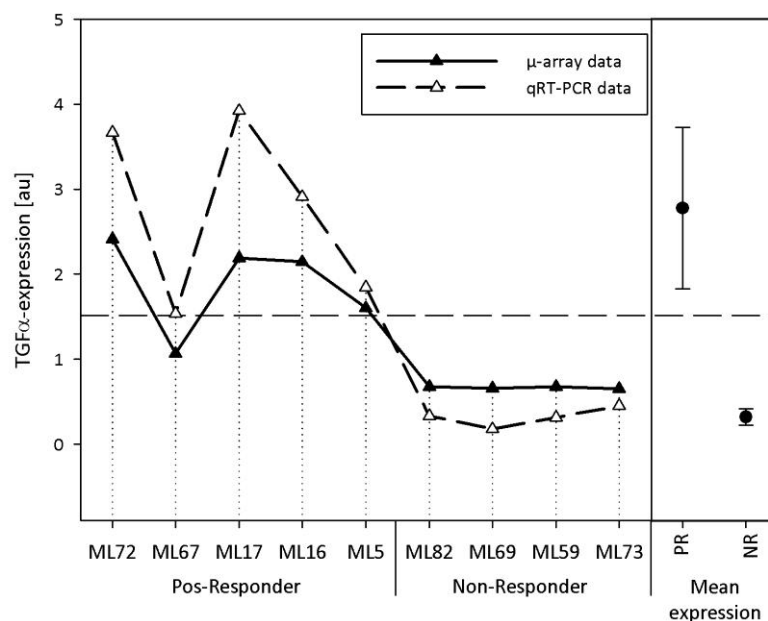
Figure 17   **Expression of TGFα in Non- and Pos-Reponders under VPA treatment determined by qRT-PCR and µ-array. On the right side mean values for both groups are given based on qRT-PCR data (PR = 2.77±0.95 au; NR = 0.32±0.02 au; *P*=0.001). Dashed line represents mean expression of all nine tested fibroblast lines. (PR = Pos-Responder; NR = Non-Responder)**

4.1.3.5 Validation of candidate genes on protein level

All previous data were based on RNA expression in fibroblasts. However, the differential response to VPA is most likely mediated on protein level e.g. by VPA-binding, transport etc. Therefore, proteins from all nine fibroblast lines were prepared and individual candidate protein amounts were quantified by quantitative western blotting.

As shown in Figure 18, levels of IGFBP5 were hard to determine. Although several antibodies were tested, no satisfying staining was achieved. Nevertheless, going in line with

the RNA data, IGFBP5 seemed to be more abundant in Pos-Responder with the highest amounts in ML16 and ML17. For all Non-Responders bands were hardly visible. RARβ could be clearly detected in all nine tested cell lines. Unexpectedly, highest amounts were found in the Pos-Responder ML17. Furthermore, ML16 and ML5 expressed modest RARβ levels under VPA treatment. The Non-Responder fibroblast lines ML59 and ML73 were found to have similarly high RARβ levels irrespective of whether VPA was added or not. Nevertheless, these data do not confirm the RNA expression levels. Similar findings were obtained for CD36. When comparing both groups with each other Pos-Responder seem to express higher amounts of CD36 than the Non-Responder and not – as expected – *vice versa*. Moreover, in ML16, ML5 and ML67 a clear increase in CD36 amounts could be detected under VPA treatment, which was not seen on RNA level. Within the group of Non-Responders, ML82, ML59 and ML69 also increased CD36 amounts under VPA treatment showed in line with the RNA data whereas no such effect was seen in ML69. However, the antibody used did not recognize glycosylated CD36, which may represent a major portion of the total CD36 content. However, taken together, these protein data do not confirm, the RNA data with the exception of IGFBP5.
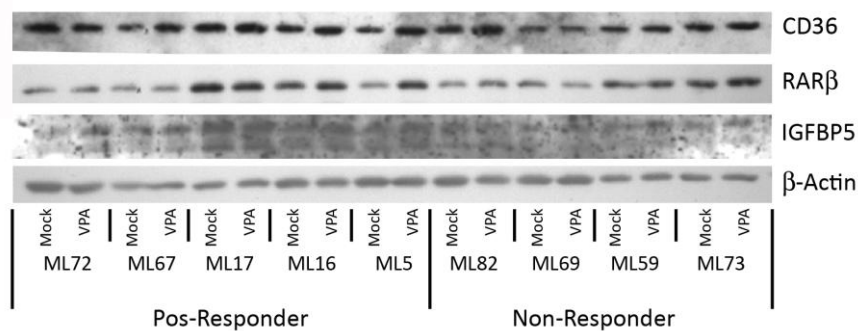
Figure 18   Western blot illustrating the individual levels of CD36, RARβ and IGFBP5. β-Actin was used as loading control. Cells were either treated with 500 μM VPA or mock for 16 h.

4.1.3.6 Confirmation of candidate genes in blood from VPA-treated SMA patients

If one of the four candidate genes will be validated as the crucial factor making the difference why a given SMA patient reacts to VPA or not, it would be of great benefit if this gene could be used as a biomarker. Possibly, its expression could be analyzed prior to VPA treatment, and depending on the result, it could be individually decided whether this patient should undergo VPA treatment. Since the most easily accessible sample from a SMA patient is blood, it was checked if the expression pattern found in fibroblasts from Non- and Pos-Responders (CD36 and RARβ ↑ in Non-Responder / IGFBP5 and TGFα ↑in Pos-Responder) is the same in the respective blood samples. Therefore, RNA from blood samples of eight SMA patients treated with VPA was reversily transcribed and analyzed by qRT-PCR. Seven of these patients had already participated in the pilot clinical trial with VPA (Brichta et al. 2006), whereas one set of blood samples was derived from a newly recruited patient

(10197/ML86). From each patient, either one or two samples were collected before treatment was started to determine basal SMN levels. Furthermore, three to five samples were collected while the patient was under VPA treatment (blood VPA level approx. 70^{mg}/$_{dl}$) in an interval of four weeks to several months. With the exception of P5/ML60 all SMA patients showed concordant results regarding the effect of VPA on SMN levels in blood and fibroblasts (Table 15).

In the case of CD36, which showed a higher expression in fibroblasts derived from Non-Responders, no correlation between the expression levels in blood and the response to VPA was found (Figure 19). Although in some cases (P2, P13, P14, 10197) differences between the individual samples were tiny, the interindividual differences within e.g. the group Pos-Responders were too large to allow any correlation. Especially patient P4 showed on the one hand extremely high CD36, but on the other hand also very big differences between individual samples.
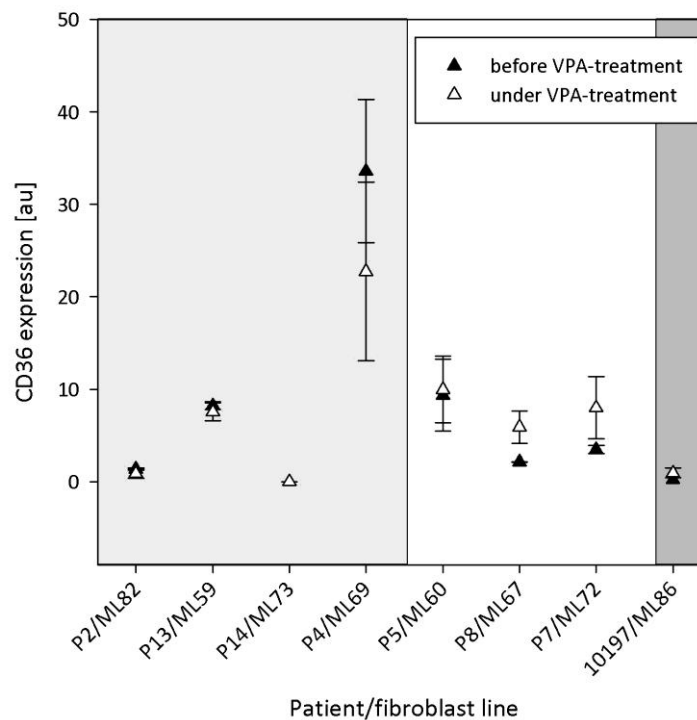
Figure 19   **Average CD36 expression measured in blood samples from SMA patients. For each patient various samples were collected before and under VPA treatment. For details see Table 28 in the appendix. Blood samples from patients showing decreased SMN levels under VPA treatment are highlighted in light gray. Those of SMA patients showing increased SMN amounts are highlighted in white. Patient 10197, highlighted in dark gray, is a Non-Responder. All samples included except P5 are derived from SMA patients showing concordant fibroblast and blood results. (Sample labeling: Identifier in Brichta et al. 2006 or patient ID / fibroblast line)**

Similar to CD36, expression of IGFBP5 did not correlate between blood and fibroblast samples (Figure 20). While IGFBP5 was up-regulated in fibroblasts of Pos-Responder, all but P4 exhibited low levels in blood. P2, P13 and P14 displayed comparably low expression levels, whereas all three patients exhibiting decreased SMN levels under VPA treatment expressed more than twice the amount of IGFBP5. Again, P4 showed exceptionally high levels. In general, within sets of samples from individual patients much higher differences were detected than in the case of CD36.

Figure 20   Average IGFBP5 expression measured in blood samples from SMA patients. Blood samples from patients showing decreased SMN levels under VPA treatment are highlighted in light gray, Pos-Responder in white and Non-Responder in dark gray (Sample labeling: Identifier in Brichta et al. 2006 or patient ID / fibroblast line).

Similar to CD36, the expression of TGFα was quite uniform for all samples (Figure 21). Although up-regulated in fibroblasts of Pos-Responders, no such tendency was observed in blood of treated SMA patients. Again samples from patient P4 produced quite confusing results which did not fit to the other samples. Most likely, a long-term infection or other unknown factors generally change the expression of the tested candidate throughout all samples investigated here.
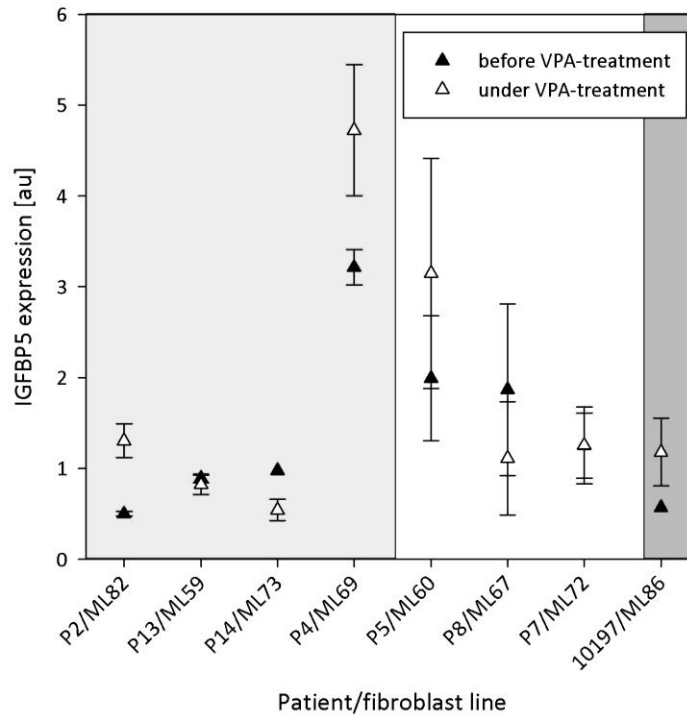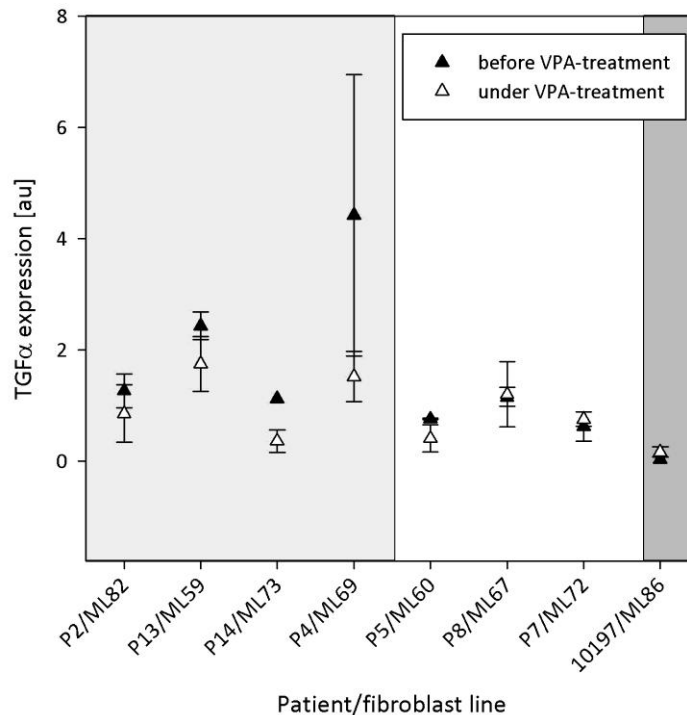
Figure 21   Averaged TGFα expression measured in blood samples from SMA-patients. Blood samples from patients showing decreased SMN levels under VPA-treatment are highlighted in light gray, Pos-Responder in white and Non-Responder in dark gray (Sample labeling: Identifier in Brichta et al. 2006 or patient ID / fibroblast line).

Furthermore, it was tried to analyze the expression of RARβ in the blood samples. However, qRT-PCR results suggested that either RARβ is not expressed in blood or its expression level is too low to allow detection by qRT-PCR. Consequently, no statement about a correlation between RARβ-expression and the phenotype could be made.

Taken together, the expression of none of the four candidate genes in blood can be used as a biomarker since at least in this tissue their expression does not correlate with the response to VPA. If potentially a correlation between a SNP and the candidate expression levels in fibroblasts was found, genotyping of this SNP could be used as a biomarker instead.

4.1.4 Analysis of differences in the expression of candidate genes

A distinct expression pattern of the four candidate genes has been demonstrated with two of them up-regulated in Pos-Responders and two of them up-regulated in Non-Responders. However, the question remained open why these genes are differentially expressed. To answer this question, as a first step the most obvious approach was undertaken and the CDS as well as the adjacent UTRs of all four candidate genes were sequenced in each patient´s fibroblast line included in the μ-array analysis. Therefore, sequencing primers were designed for all exons with the online script *Exon Primer* (http://ihg2.helmholtz-muenchen.de/ihg/ExonPrimer.html). Individual exons were amplified and subsequently sequenced. Conditions were set in such a

way that primers were located approx. 60 to 100 bp up- or downstream of the respective exon to allow also sequencing of the exon-intron-boundaries. If exons were too long for amplification or sequencing, exons were split into several pieces. After sequencing, data were analyzed and compared to the *Ensembl* reference sequence.

Sequencing of CD36 revealed no direct correlation between a SNP-type and the individual response to VPA (Appendix, Figure 61). Within all 17 exons sequenced only two SNPs located in the 5'UTR differed between the samples. In exon 1 the SNP rs1878214 was found to be heterozygously present (G/A) in three out of four Non-Responders (ML82, ML69, ML59) whereas in ML73 and all Pos-Responders the G-allele was homozygously present. This suggested that the A-allele may contribute to the higher CD36 expression levels in Non-Responders. Therefore, another set of five not yet confirmed Non-Responders was sequenced for this SNP, but a correlation between the A-allele and the response to VPA could not be verified. This discarded the hypothesis that the A-allele may be the molecular cause of the elevated CD36 expression in Non-Responders. Another SNP (rs1049654) in exon four differed among tested cell lines, but its genotype did not match with either Non- or Pos-Responders.

In the case of RARβ the previously described SNP (rs1058378) in the terminal exon 8 was shown to be G/G in ML17 and ML69 instead of the more common T-allele (Appendix, Figure 61). Another variation, which was not previously described, was identified in the coding exon 7 at position +62. In five out of nine cases the C-allele was heterozygously present, whereas it was homozygously present in ML73. Nonetheless, the C-allele does lead to an amino-acid exchange.

Sequencing of IGFBP5 revealed that with the exception of ML5 all samples were the same (Figure 62). In this case two variations in the 3'UTR encoded by exon 4 were found (rs2241194 and rs11575212). Similarly to the previous three genes, no association between a certain SNP-type and the expression levels could be drawn in the case of TGFα (Appendix, Figure 62). Although 12 variations in the highly polymorphic 3'UTR were identified to differ among the fibroblast lines, none of these could directly be connected to the higher TGFα expression levels in Pos-Responders.

Taken together, no association between a certain SNP and the response to VPA and the expression pattern, respectively, was found. However, the underlying cause of the differential expression of candidate genes must not necessarily be located in the CDS or the UTRs but rather in the promoter region. Since promoters are usually of huge dimension, sequencing is most often time-consuming. Therefore ChIP analysis of all four candidate promoters were performed to directly test if their acetylation status differs between Non- and Pos-Responders. A positive result would indicate that the detected expression differences are most likely due to different promoter activity which may caused by a promoter SNP.

Primers specific to the respective promoters were designed on either verified or very likely promoter sequences from the Human promoter database (http://zlab.bu.edu/~mfrith/HBP.html) (Materials and Methods section, Table 9). All four candidate genes were found to be significantly differentially expressed under VPA treatment. Therefore amplicons were located 500 to 1000 bp upstream of the TSS since this region is known to be typically hyperacetylated under HDACi treatment if this gene is induced by HDACi (Wang et al. 2009). To get solid data, ChIP analysis was performed with three Pos-Responders (ML17, ML67, ML72) and three Non-Responders (ML59, ML73, ML82) and mean acetylation levels were calculated for each group. All fibroblasts were seeded out 24 h before cells were treated for 16 h with VPA. ChIP analysis was performed with an antibody directed againt acetylated histone H3.

Quantifcation of the different DNA promoter fragments via qRT-PCR revealed that VPA increased mean acetylation at all six analyzed promoters in the Pos-Responders (Figure 22). In contrast to that, H3K9 acetylation was decreased in all Non-Responders under VPA treatment for all tested promoters. Furthermore, the global H3K9 acetylation levels turned out to be higher in Non-Responders, but this can be most likely attributed to the small sample size since e.g. the Pos-Responder ML69 generally showed very low acetylation levels. In conclusion, although differences between Non- and Pos-Responders were detected, no direct association between promoter acetylation levels and the expression could be drawn. For example, basal CD36 and RARβ acetylation levels were, as expected, higher in Non-Responders. On the other side also basal acetylation levels of IGFBP5 and TGFα were higher within this group although these transcripts are more abundant in Pos-Responders. Furthermore, the promoters AZGP1 (α-2-glycoprotein, zinc binding) and CPT1C (carnitine palmitoyltransferase 1C) were included in the analysis. AZGP1 was found during the μ-array analysis to be exclusively induced in Non-Responders by VPA whereas CPT1C is only increased in VPA-treated Pos-Responders. For AZGP1 no corresponding change in promoter acetylation could be detected although similarly to the other tested promoters basal acetylation levels are higher in Non-Responders. CPT1C promoter acetylation was found to be increased in VPA-treated Pos-Responders as expected.
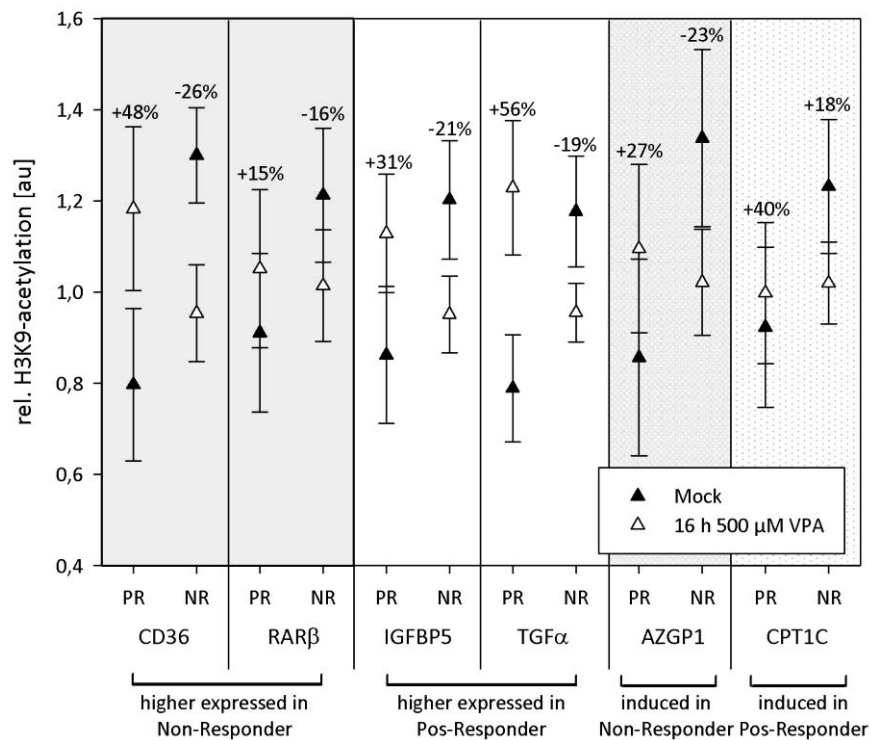
Figure 22 Mean H3K9 acetylation levels under mock and VPA treatment in three Pos-Responders and three Non-Responders at different promoters. Highlighted in light-gray are those transcripts which were found to be up-regulated in Non-Responders. The corresponding *SMN2* promoter acetylation data can be found in Figure 9. (PR = Pos-Responder; NR = Non-Responder)

Since neither sequencing nor ChIP analysis revealed any obvious reason why the candidate genes are differentially expressed between Non- and Pos-Responders, other not yet appointed mechanisms must account for the detected expression. A commonly used mechanism to post-transcriptionally regulate expression is to increase or decrease mRNA-stability. Modulation is most often done either by mRNA-binding proteins or miRNAs (Ross 1995; Wahid et al. 2010). A very easy and robust way to analyze mRNA stability is to inhibit *de novo* RNA synthesis by means of Actinomycin D. Therefore, mRNA stability should be assessed as a next step using this assay.

4.1.5 Identification of a putative candidate gene network

Transcriptome-wide comparison of Non- and Pos-Responders revealed a distinct expression pattern with IGFBP5 and TGFα being up-regulated in Pos-Responders compared to Non-Responders and CD36 and RARβ *vice versa*. Since all of these genes are to a certain extent involved in energy metabolism, the question arose whether the observed expression is coincidental or whether these genes are somehow connected.

4.1.5.1 Knockdown and overexpression studies

To identify any putative network connecting the four candidate genes two complementary sets of experiments were performed. On the one hand each candidate gene was knocked down by means of siRNA and the expression of the remaining three candidates was determined. On the other hand over-expression studies were performed to test whether the observed effects were reversed. Both sets of experiments were performed in parallel in both Non- and Pos-Responders and from each group at least two cell lines were tested to exclude any fibroblast line specific effects. A knockdown of RARβ could not be performed since none of the tested siRNAs gave reproducibly good results.

Knocking down IGFBP5 had opposite effects on CD36 in Pos- and Non-Responders (Figure 23a). While in the case of the Pos-Responders the already low expression levels further decreased, CD36 merely doubled in the Non-Responders. Similar results were obtained for RARβ: Typically barely expressed in Pos-Responders, no considerable change in the overall amount was detected when knocking down IGFBP5. Contrariwise, transcript amounts of RARβ increased by around 80% in the group of Non-Responders. In both groups TGFα was not affected by decreased IGFBP5 amounts.

In the case of CD36 depletion from the cells the high IGFBP5 levels of Pos-Responders more or less remained unaffected (Figure 23b). In contrast to that, IGFBP5 doubled within the group of Non-Responders although compared to Pos-Responders overall amounts remained infinitesimal. Similar to the knockdown of IGFBP5, reduced CD36 amounts only had minimal effects on RARβ levels in Pos-Responders. On the other hand, levels of RARβ increased by almost 100% in Non-Responders. Total amounts of TGFα remained unaffected under reduced CD36 levels although the great differences between individual Pos-Responders hamper a definite statement.

Finally, TGFα was knocked down in both groups (Figure 23c). CD36 levels increased in Non- as well as Pos-Responders while the effect in the Non-Responders was much more obvious. More drastic effects were observed when IGFBP5 levels were determined. High levels typically found in Pos-Responders were reduced by approx. 25% whereas in the Non-Responders IGFBP5 transcript amounts increased by around 30% when TGFα was knocked-down. Still it has to be taken into account that the high levels of Pos-Responders were not reached by the Non-Responders. Expression levels of RARβ were modestly increased in Non-Responders, whereas the comparably small amounts present in Pos-Responders were not considerably altered.
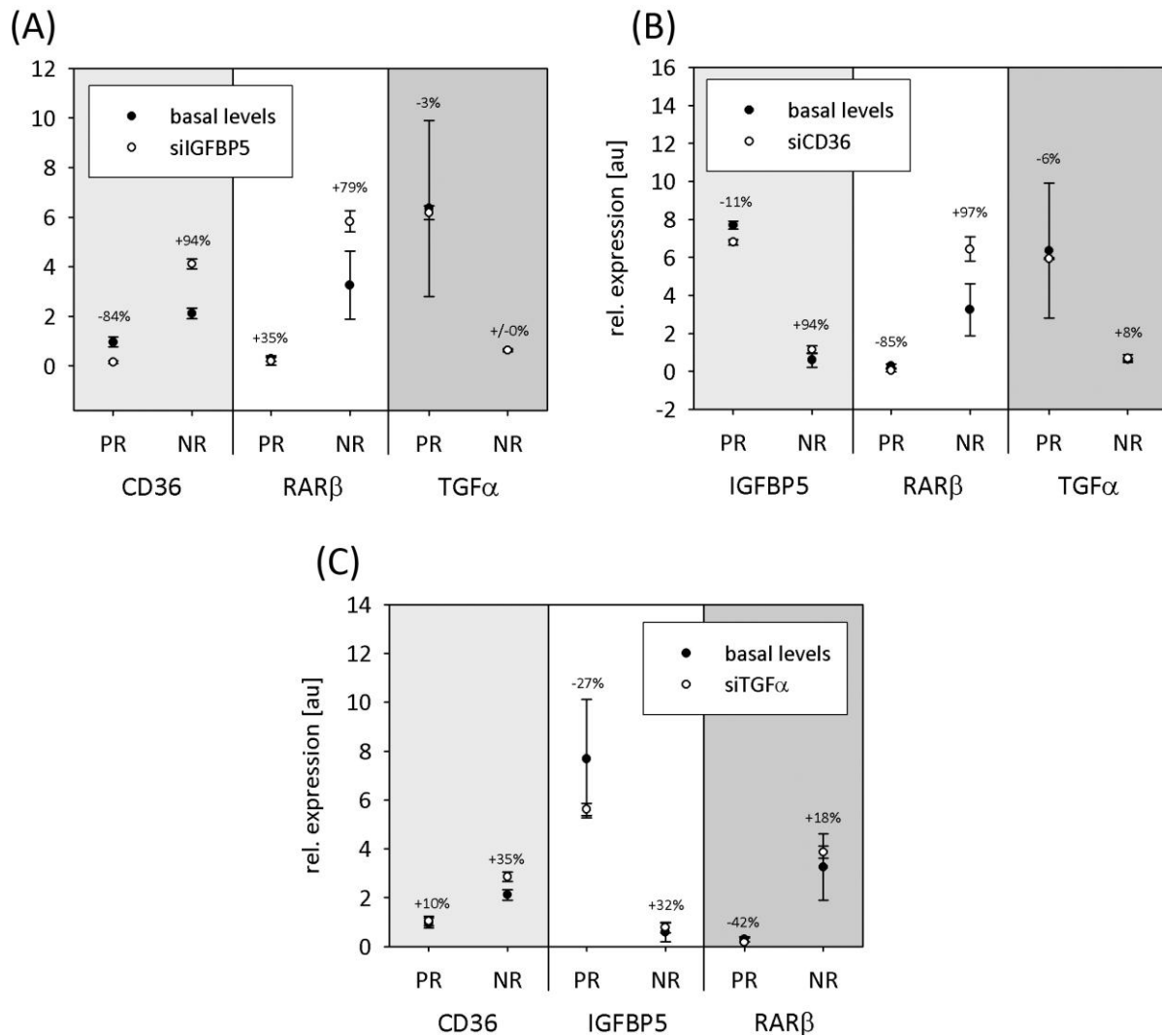
Figure 23   **Knockdown of either (A) IGFBP5, (B) CD36 or (C) TGFα in Non- and Pos-Responders`**
fibroblasts. Expression levels of the respective remaining three candidate genes are
depicted. For better comparison basal expression levels and the change in expression in %
are given for each transcript. Data are given as mean ± SMN (PR = Pos-Responder → ML16,
ML17, ML67 and ML72; NR = Non-Responder → ML59, ML73 and ML82). For RARβ
knockdown no data were available since the siRNA oligos failed to work.

In addition to the knockdown approach also overexpression studies with plasmids encoding the individual candidate genes were performed. Two Pos- (ML17 and ML72) and two Non-Responder (ML59 and ML73) were transfected and either mock or VPA treated for 16 h. By analyzing RNA amounts by qRT-PCR the following observations could be made (Figure 24).

Unfortunately, overexpression of CD36 did not prduce any consistend results. For example, IGFBP5 and TGFα levels were increase in ML72 and ML59 whereas the opposite was detected in ML17 and ML73. Similar results were obtained for RARβ, which was either increased or decreased in ML17 and ML73, respectively, whereas RARβ levels remained unchanged in the other two fibroblast lines. However, addition of VPA to

CD36-overexpressing fibroblasts dramatically changed the situation. IGFBP5 was increased by more than 100% in all tested cell lines with the highest effect in ML59. Non-Responder RARβ levels increased compared to mock treated cells and a similar effect could be observed in ML17. In summary, the greatest difference could be detected in the TGFα levels (Figure 24).

Transfection with an IGFBP5-encoding plasmid did not have any pronounced effect on either CD36 or TGFα levels. RARβ transcripts decreased by more than 50% in ML17, ML72 and ML59 while no change could be obtained in ML73. Addition of VPA to the transfected cells did not result in an effect as pronounced as in the case of CD36 overexpression. Only analysis of TGFα revealed consistent results: While in the Pos-Responder levels increased by approx. 10%, levels declined in the Non-Responders by 5 to 10% (Figure 24).

Overexpression of RARβ resulted in similar down-regulation of CD36, IGFBP5 and TGFα with the more pronounced effect in the Non-Responders. However, VPA addition reversed this effect in Pos-Responders whereas in the Non-Responders the RARβ-induced down-regulation persisted (Figure 24).

Transfection with TGFα led to a decline in CD36 and IGFBP5 amounts by 20% in Pos- and more than 50% in the Non-Responders. Interestingly, RARβ levels were elevated in ML72 whereas they decreased in ML17, ML59 and ML73, suggesting an outlier effect. However, VPA treatment changed this relatively consistent picture. Especially the Non-Responders ML59 and ML73 exhibited opposite results in their IGFBP5 and CD36 expression. Of note, RARβ expression was reversed in both Pos- and Non-Responders compared to the untreated cells (Figure 24).

Finally, expression levels of all four analyzed candidate genes in mock and VPA-treated fibroblasts transfected with GFP were determined to check whether VPA triggers the expected response. In conclusion, the detected alterations corresponded quite well with the observations made before implying that VPA treatment worked in principal (Figure 24).
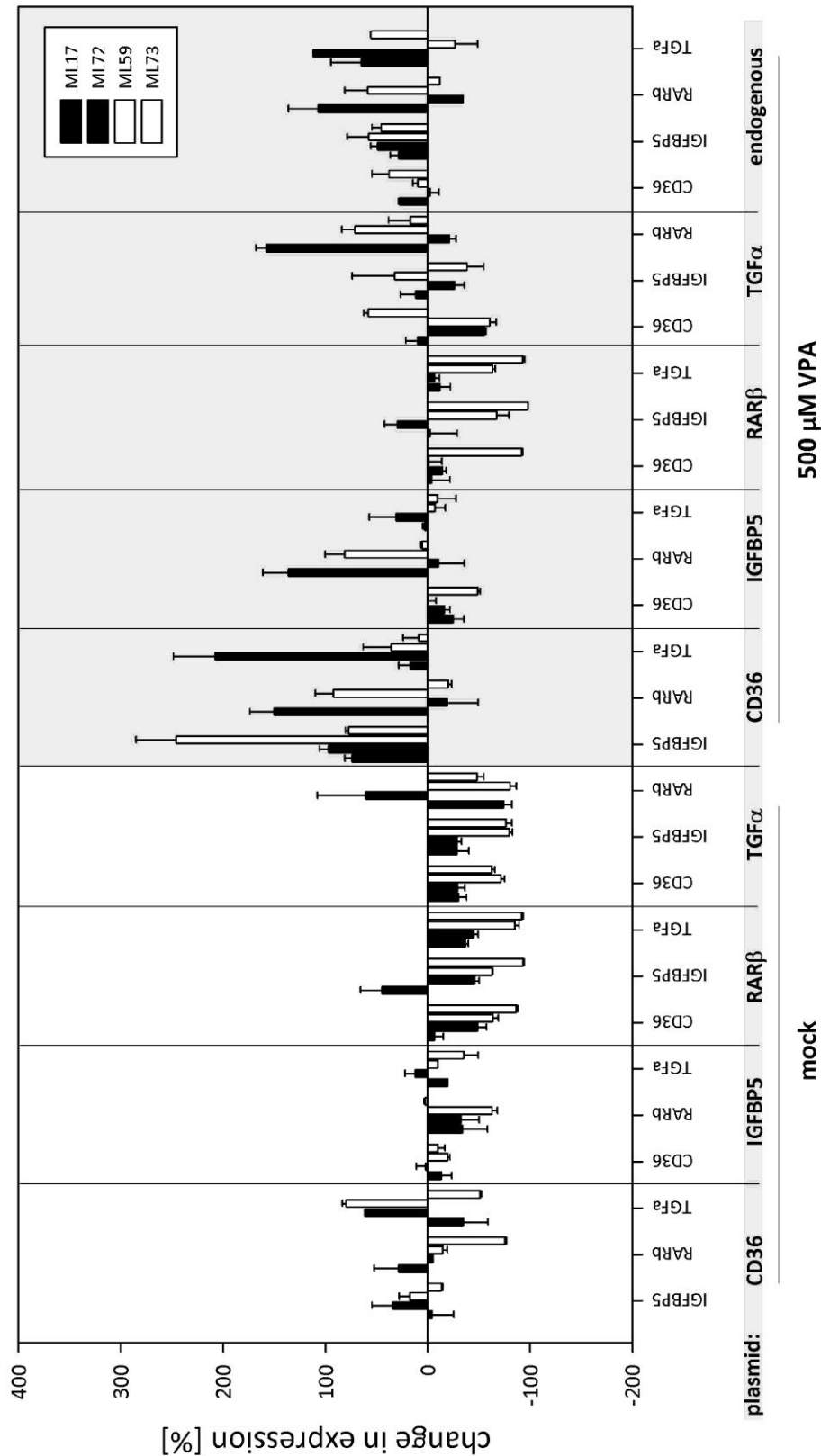
Figure 24   Overexpression studies of candidate genes in Pos- (ML17 and ML72) and Non-Responders (ML59 and ML73). Depicted are changes in expression of individual candidate gens are transfection with the indicated plasmid. Cells were either mock or VPA treated for 16 h following transfection. In the last panel alterations in expression of the endogenous candidate genes is given.

In conclusion, it has to be stated that neither the knockdown nor the overexpression studies gave a definite hint whether the expression levels of the four candidate genes are somehow linked. However, some noteworthy findings could be obtained. On the one hand

knockdown of IGFBP5 increased levels of CD36 in both Pos- and Non-Responders by more than 80%. Furthermore, knockdown of CD36 dramatically increased RARβ levels in Non-Responders by more than 90%. Although quite huge alterations in the RARβ expression of Pos-Responders could be detected in all knockdown experiments, these results have to be taken with a pinch of salt. Generally, RARβ expression is extremely low in Pos-Responders. Any subtle interference with its levels will thus immediately result high numbers while the relative change compared to Non-Responders is rather negligible.

Overexpression of RARβ transfection decreased expression of the other three candidate genes while the effect could be reversed by VPA in the Pos-Responders. Furthermore, the activating effect of VPA on candidate gene expression was boosted by CD36 overexpression. But, in general, fibroblasts from the same group exhibited often opposite results, suggesting that overexpression might not be the appropriate way to study candidate gene connections in fibroblasts.

Summarized, it may be speculated whether RARβ plays the central role in the putative candidate gene network. Since it is barely expressed in Pos-Responders while it can be robustly detected in Non-Responders, it may control and alter the expression of the other candidate genes. Anyhow, the whole system of transfecting fibroblasts is very error-prone since the transfection rates of 50-70% are rather low compared to e.g. 293 cells. Furthermore, it could be observed that individual fibroblast lines seem to be more sensitive to either electroporation or lipofection than others, which of course influences the final data.

4.1.5.2 Determination of the intracellular cAMP content

Neither overexpression nor knockdown experiments gave a definite clue, whether or how the different candidate genes are connected. However, VPA has been shown to alter the intracellular content of the second messenger cAMP (Boeckeler et al. 2006; Chang et al. 2009). Since both SMN and IGFBP5 contain cAMP-responsive elements (CRE) within their promoters (Duan and Clemmons 1995; Majumder et al. 2004) and VPA failed to inhibit PKA (cAMP-dependent protein kinase A) in Non-Responders (Figure 11), cAMP levels were determined in VPA treated fibroblasts by ELISA. Determination of the cAMP concentration in three Pos- and Non-Responders each uncovered no differences in basal levels (Figure 25). Interestingly, cAMP levels were 24% lower in VPA-treated Pos-Responders compared to Non-Responders. This fits well to the observation that PKA activity was exclusively inhibited dose-dependently in Pos-Responder. Unexpectedly, application of the adenyl cyclase (AC) inhibitor 2',5'-dideoxyadenosine (ddA) dit not result in a decline in cAMP contents but rather increased cAMP levels by 20% in both groups. In contrast to that, 100 µM Forskolin, an AC activator, produced the desired effect: In the group of Pos-Responder cAMP levels were augmented up to approx. 25 nM cAMP per µg protein whereas in Non-Responders more

than twice the amount was measured (67 nM cAMP per µg protein). Furthermore, inhibition of phosphodiesterases (PDE, catalyzing cAMP into ATP) by means of IBMX (3-isobutyl-1-methylxanthine) increased cAMP levels merely in Non-Responders. Taken together, the difference in the response to VPA, Forskolin and IBMX between Pos- and Non-Responders suggests an involvement of cAMP in the different responses to VPA. However, the underlying cause still needs to be identified.
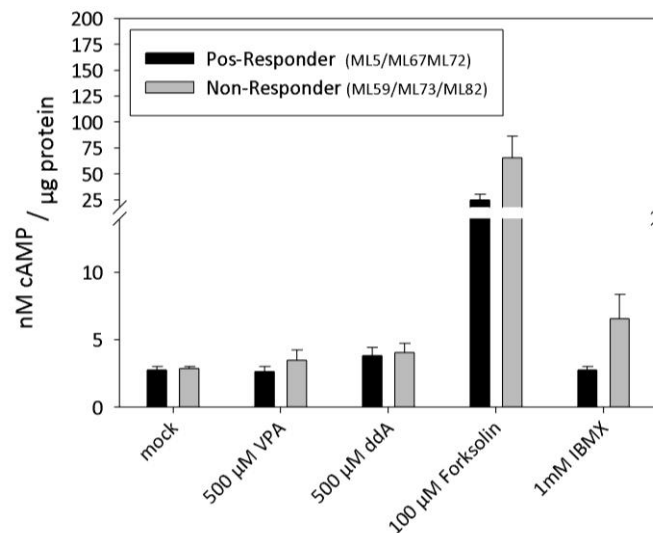
Figure 25   Determination of the intracellular cAMP content by ELISA. VPA, ddA (2',5'-dideoxyadenosine, AC inhibitor) and IBMX (3-isobutyl-1-methylxanthine, PDE inhibitor) were applied for 16 h. Forskolin (AC activator) treatment lasted for 2 h. All data are given as mean±SEM of three cell lines each measured in triplicate.

4.1.5.3 Can a Non-Responder be converted into a Pos-Responder?

Previous experiments could not fully unravel the underlying network of the four candidate genes. However, the essential issue in terms of SMA therapy is whether any of the four proteins has a direct effect on SMN and could thus be a target of a drug therapy supplemental to normal VPA regimen. To answer this question, knockdown of candidate genes combined with parallel VPA treatment was performed in both Pos- and Non-Responders.

Following CD36 knockdown in either VPA or mock-treated ML72, SMN almost completely vanished (Figure 26). In contrast to that, SMN was strongly augmented when IGFBP5 was depleted from the cells irrespective of whether VPA was added or not. Similar to that, knocking down TGFα slightly increased SMN amounts. This effect was further enhanced by the addition of VPA. The observed tendencies were the same in the Non-Responder ML82, although the effect of CD36 was not that dramatic. Most importantly, knockdown of IGFBP5 plus VPA increased SMN amounts more than 3-fold. These experiments were repeated in another set of cell lines leading to comparable results.
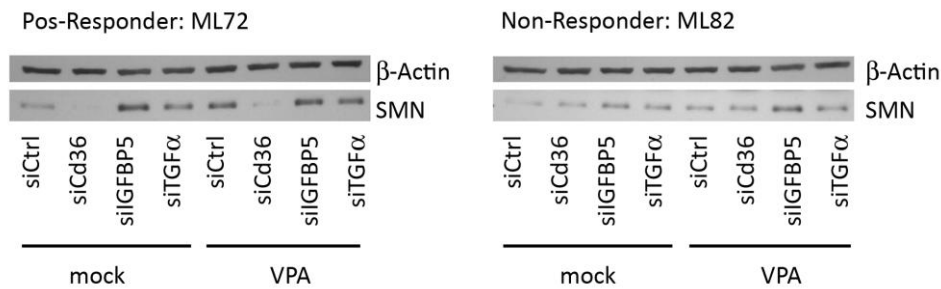
Figure 26 **Knockdown of CD36, IGFBP5 and TGFα combined w or w/o VPA treatment. β-Actin was used as loading control.**

Since knocking down CD36, IGFBP5 and TGFα altered SMN levels, it was investigated next whether SMN RNA or protein was affected. Quantification of SMN transcripts by qRT-PCR showed that these declined by 30% when CD36 was knocked down (Figure 27). This implies that CD36 depletion directly affects SMN mRNA whereby SMN protein is subsequently reduced. In contrast to that, transfection with a siRNA targeting *IGFBP5* did not notably change SMN levels, suggesting that IGFBP5 acts on SMN protein level. For TGFα no definite result was obtained. Although SMN levels increased after TGFα knockdown in Non- and Pos-Responders, mRNA levels were changed differently in opposite direction (Figure 26).

In summary, these results were rather unexpected. Knockdown of CD36 decreased SMN protein by acting on *SMN* transcript level. At least from what is known from the literature there is no direct explanation for this observation. Since it has not yet been tested, next experiments should address the question whether *SMN* expression or mRNA stability is altered in CD36-depleted cells. In contrast to CD36, knockdown of IGFBP5 notably increased SMN protein but not RNA levels. Since no direct interaction between IGFBP5 and SMN has yet been shown, it may be speculated whether IGF signalling has generally an impact on SMN protein. Further experiments are needed to test this hypothesis. However, if these indeed uncover a direct connection between IGF signalling and SMN amounts this may lead to the development of drug therapies targeting this connection.
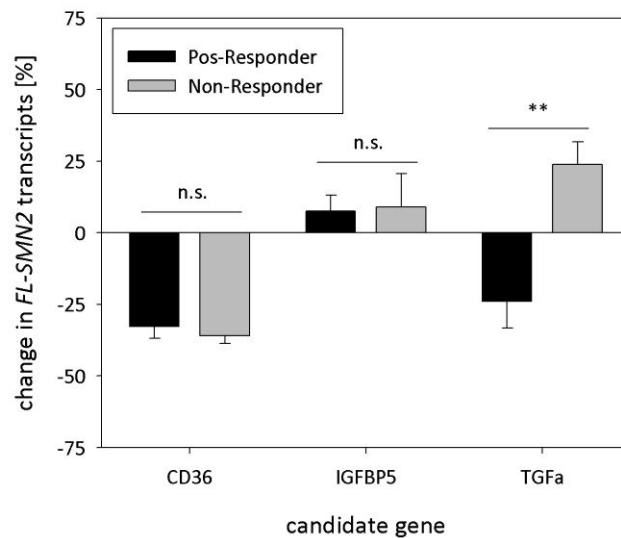
Figure 27   qRT-PCR analysis of *FL-SMN2* expression following knockdown of either CD36, IGFBP5 or TGFa. Data are given as mean of three different Pos- or Non-Responder cell lines. (* = *P*<0.05; ** = *P*<0.01; *** = *P*<0.001)

4.1.6 Analysis of CD36 as a putative VPA transporter

Comparison of fibroblasts derived from Non- and Pos-Responders by µ-array revealed a differential expression of CD36, suggesting that VPA uptake and/or metabolism might differ between both groups. Although only CD36-mediated LCFA-uptake has been reported so far (Coburn et al. 2000; Ibrahimi et al. 1996), this does not exclude the possibility that also short chain fatty acids such as VPA are likewise transported. Furthermore, CD36 is embedded into pathways encompassing PPARγ (peroxisome proliferator activator receptor γ), LXR (liver X receptor) and RXR (retinoid X receptor) (Tontonoz et al. 1998), which are triggered upon LCFA stimulus. Based on these data, constitutively high CD36 amounts in Non-Responders may alter VPA metabolism in such way that it cannot act as HDACi or PKA inhibitor.

4.1.6.1 Characterization of VPA uptake in treated fibroblasts by HPLC-MS/MS

To investigate whether VPA is indeed differentially taken up in Non- and Pos-Responders, it was initially tried to measure the VPA content in whole cells lysates from treated fibroblasts by gas chromatography at the *Institute of Pharmacology* in *Cologne*. Unfortunately the intracellular VPA concentrations were too low to be detected (data not shown).

Therefore, a HPLC-MS/MS-method originally published by Cheng et al. 2007 was adopted to quantifiy the content of VPA and its major blood metabolite 4-ene VPA (2-propyl-4-pentenoic acid) in fibroblasts. By performing the derivatization as described in 3.10.6.1 with pure VPA or 4-ene VPA in ddH$_2$O, the VPA-derivate was found to elute at 7.05

min from the HPLC column whereas the 4-ene VPA-derivate eluted at 6.67 min. Subsequent mass spectroscopic analysis was carried out, product ion mass spectra were recorded and precursor/product ion pairs (VPA 277.3/120.0; 4-ene VPA 275.2/120.0) were selected for quantification of VPA and 4-ene VPA, respectively (Appendix, Figure 70).

Based on these results, the next round of experiments was performed with lysates from VPA-treated fibroblasts. Therefore, $1x10^5$ cells were plated out in a 6-well plate 24 h prior to treatment with 500 µM VPA or mock for 16 h. Following drug incubation, fibroblasts were harvested and derivates were prepared. In parallel, 100 µl media supernatant from VPA and mock treated cells were also derivatizized to quantify elimination of VPA out of the cell culture media. Subsequently, derivates were analyzed by HPLC-MS/MS and total ion chromatograms were recorded. From these, the precursor/product ion pairs for VPA and 4-ene VPA were extracted and depicted as counts per second against HPLC retention time. Since the retention time of both compounds was determined beforehand, the respective peaks were chosen and the peak area was used to quantify VPA or 4-ene VPA amounts (Figure 28).

Analysis of exctracted ion chromatograms (XIC) for VPA of treated and untreated ML17 – a Pos-Responder – revealed that in both cases a peak at 277.3/120 and 7.05 min was detected. Noteworthy, the peak was half the size in untreated cells, therefore most likely corresponding to an intracellular constituent part having the same *m/z* spectrum and HPLC-retention time as VPA (Figure 28A). A similar result was obtained for 4-ene VPA. Again, a peak half the size was detected in the untreated cells. Taken together, these peaks originating from the cellular background determine the lower limit of detection. Since they match those peaks of VPA and 4-ene VPA and are present irrespective of whether VPA is added or not, fainter signals indeed coming from e.g. VPA will always be cloaked by them. In contrast to that, within the cell-free culture medium a clear signal for VPA was detected in medium containing 500 µM VPA whereas no such readout was detected in medium without VPA. 4-ene VPA was found to be absent in both media (Figure 28B).
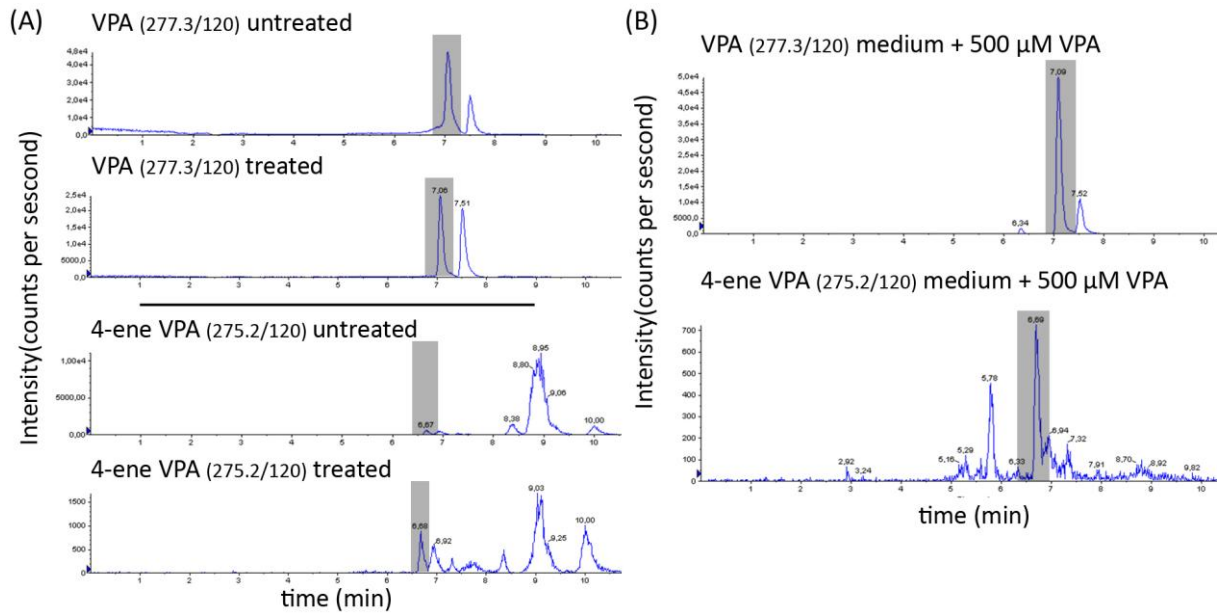
Figure 28   **Extracted ion chromatograms (XIC) for both VPA (277.3/120) and 4-ene VPA (275.2/120).**
Peaks corresponding to VPA or 4-ene VPA based on their HPLC retention time are marked in
light gray. (A) XIC for VPA- and mock-treated ML17, a Pos-Responder. (B) XIC for the cell
culture medium of treated ML17.

Although in the extracts of untreated cells similar signals were detected as in VPA-treated fibroblasts, the difference still allowed discrimination of treated and untreated cells. Therefore, the Non-Responder ML59 as well as the Pos-Responder ML17 were treated for 30, 60 and 120 min with 500 µM VPA and after the respective time period cell lysates and medium supernatants were derivatized and analyzed by HPLC-MS/MS to get an impression of the VPA uptake kinetics (Figure 29).
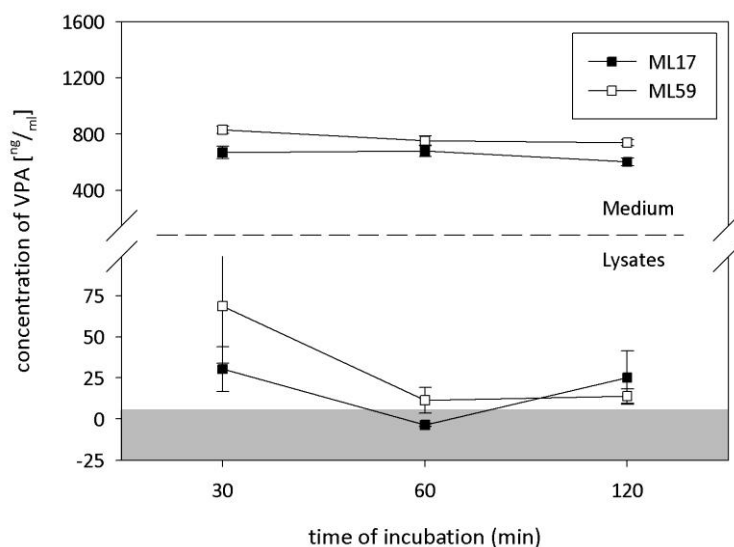
Figure 29   **Quantification of VPA in fibroblasts treated for the indicated time periods as well as the VPA content in the supernatant. VPA concentration was calculated using a VPA standard curve either prepared in fibroblast media or fibroblast lysate. The gray area indicates the lower limit of detection.**

Analysis of XIC for VPA clearly showed that in both ML17 and ML59 VPA was not considerably eliminated from the cell culture medium throughout a time period of 120 min. VPA concentration remained at around 800 $^{ng}/_{ml}$, which – when all dilution factors are eliminated – indeed matched the employed 500 µM VPA. This observation suggested that only minimal VPA uptake has taken place. This was further underlined by the finding that within the lysates of both fibroblast lines only 25 to 60 $^{ng}/_{ml}$ VPA were detected after 30 min of incubation. For longer time periods even lower VPA concentrations were detected, which were only barely above the detection limit (Figure 29) thereby giving no trustable data. In case of 4-ene VPA all samples were below the lower limit of detection (data not shown).

Since further experiments led to similar results it was doubtful whether derivatization of VPA is indeed the most effective method of quantifying the intracellular VPA content. The basic hindrance seemed to be the intracellular constituent parts such as any other short-chain fatty acid giving a very high lower level of detection. Therefore, this assay was not employed in further experiments.

4.1.6.2 Analysis of CD36-mediated VPA import

So far the question whether higher CD36 amounts present in Non-Responders indeed have any impact on VPA uptake could not be answered. Therefore, it was asked if CD36 also functions as a VPA importer. To follow up this issue, HEK293 cells were transfected with a vector encoding for CD36 (Figure 67) and a stable cell line was established by three weeks selection using G-418 in the *Institute of Pharmacology* in *Cologne*. Using this cell line an

uptake assay with 10 µM VPA was performed. Cells were plated out 24 h prior to treatment, washed once and then incubated for 1 min with 10 µM VPA in pre-warmed 1xPBS. Subsequently, cells were lysed using 4 mM $HClO_4$ and analyzed by HPLC-MS/MS. Based on the previous experiments, the VPA derivatization method was not applied and VPA was directly measured without derivatization and fragmentation in single-ion mode (SIM). Using pure VPA dissolved in 4 mM $HClO_4$, retention time and the respective ion were determined. Once the method was established, VPA contents were measured in the stably CD36 overexpressing HEK293T cells treated for 10 min with 10 µM VPA. Furthermore, a HEK293 cell line stably overexpressing SLC16A3 was included into the analysis. SLC16A3 (MCT4) was chosen since it is (besides SLC16A1 and SLC16A7) one of the major transporters of butyrate, another short-chain fatty acid HDACi (Morris and Felmlee 2008).

Quantification of the intracellular VPA amounts after 1 min of incubation revealed that overexpression of neither CD36 nor SLC16A3 led to an increased influx of VPA into the cells (Figure 30). Detected VPA signals in all samples were equal or close to the standard sample of 0 $^{ng}/_{ml}$ VPA. The experiment was repeated with 1 mM VPA to exclude any concentration-dependent effects, but the results were unchanged. Taken together, these results suggest that VPA either diffuses into the cell or is transported by a yet unknown protein. In any case, CD36 can be excluded as a VPA importer.
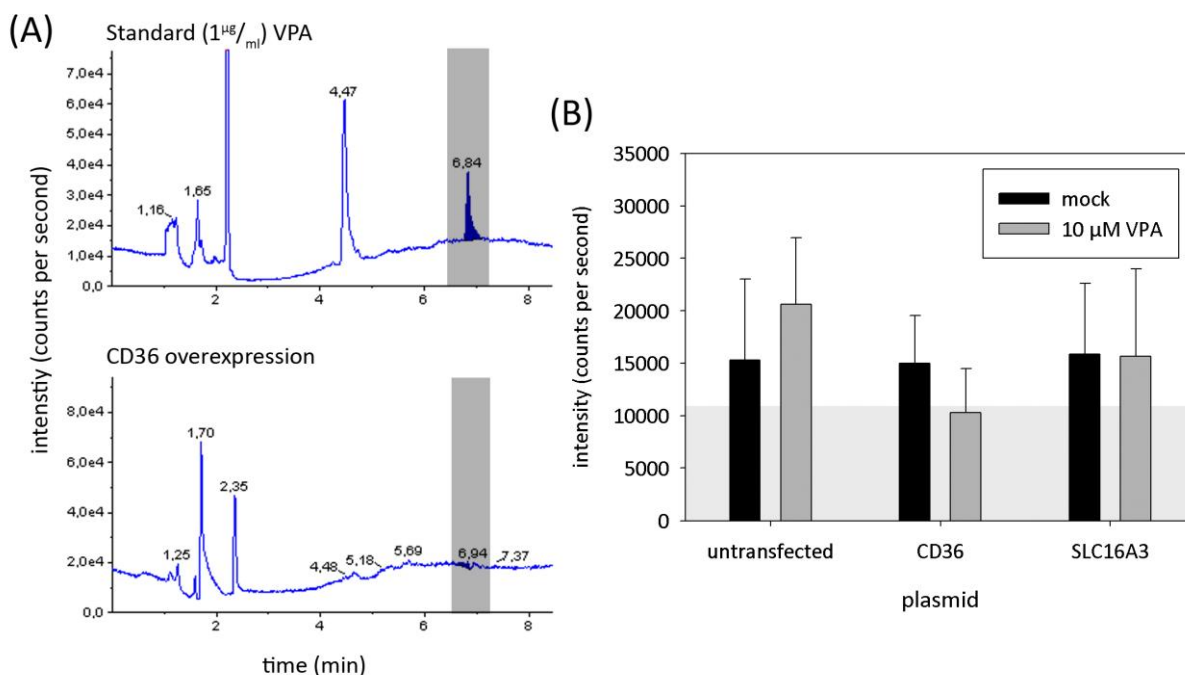
Figure 30 **(A) XIC for VPA without derivatization. A respresentative picture from a standard dilution is given illustrating the VPA peak (marked in light gray). Furthermore, a respresentative XIC for VPA-treated HEK239 cells overexpressing CD36 is given. (B) Intensity counts for HEK293 either mock or CD36 or SLC16A3 transfected, treated with VPA or mock. Gray area represents the lower limit of detection given by 0 $^{ng}/_{ml}$ VPA in 4 mM $HClO_4$. All data are given as mean ± SD.**

4.1.6.3 Comparison of VPA metabolism in Pos- and Non-Responders

Neither the derivatization experiments nor the VPA-uptake experiment with HEK293 cells provided a definitive clue to whether or how VPA uptake and metabolism differ between Non- and Pos-Responders. To clarify this issue, a HPLC-MS/MS shading assay was performed as described previously (Grundemann et al. 2005). The underlying principle is the comparison of data sets of different samples in a given mass range to identify discrepancies. Therefore, from three Pos- and three Non-Responder fibroblast lines some $1x10^5$ cells were plated out in a 6-well plate. 24 h later cells were treated with 500 µM VPA and 500 µM $_{d15}$-VPA for 16 h. Subsequently, cells were lysed with 4 mM $HClO_4$ and equal amounts were pooled groupwise based on their protein content. The pooled samples were then analyzed by HPLC-MS/MS and total ion chromatograms (TIC) were recorded up to 400 amu. To visualize differences between samples (*m/z*, retention time, intensity) the TICs were compared graphically by MS-FullView (*Gründemann*). First, ion intensities were converted into grayscales (high intensities white / low intensities black) to create 2D images with *m/z* and time axis. Next, one sample was converted into red and the other one in blue and both 2D images were superimposed. Then an algorithm highlighted compounds only present in

one sample in orange, whereas compounds present in equal amounts remained in gray (Grundemann et al. 2005). Deuterized and non-deuterized VPA were both used to allow discrimination between substances which are produced upon VPA treatment and direct VPA derivates. In the latter case two adjacent peaks should be detected since VPA and $_{d15}$-VPA differ slightly in their atomic weight whereas for endogenous substances only a single peak should be detected.

As depicted in Figure 31A, both signals for VPA and $_{d15}$-VPA could easily be identified at 6.92 min and 144.2 amu or 159.4 amu, respectively, in medium plus VPA/$_{d15}$-VPA compared to medium without. However, when matching media from both treated Pos- and Non-Responders, no apparent difference could be detected, suggesting that elimination of VPA out of the cell culture medium is the same.

Comparison of pooled lysates of Non- and Pos-Responders did not lead to the identification of a differentially produced VPA metabolite. For none of the known VPA metabolites (e.g. 4-ene VPA, 3-oxo-VPA, 2-hydroxy-VPA) a differential peak corresponding to their atomic mass could be recorded (Figure 31B). The only signal clearly differing between both samples was detected at 192.2 amu / 4.28 min. However, it could be excluded as a VPA metabolite for two reasons: First, the atomic mass did not match any of the known metabolites. Furthermore, only one signal was recorded whereas a VPA metabolite should give two signals since both VPA and $_{d15}$-VPA were combined. Moreover, lysates of VPA/$_{d15}$-VPA treated Non- and Pos-Responders were compared with untreated ones. Unfortunately, again no obvious differences could be identified, suggesting that either all VPA metabolites are present at undectable levels or that all VPA is present in higher weight (>400 amu) derivates.
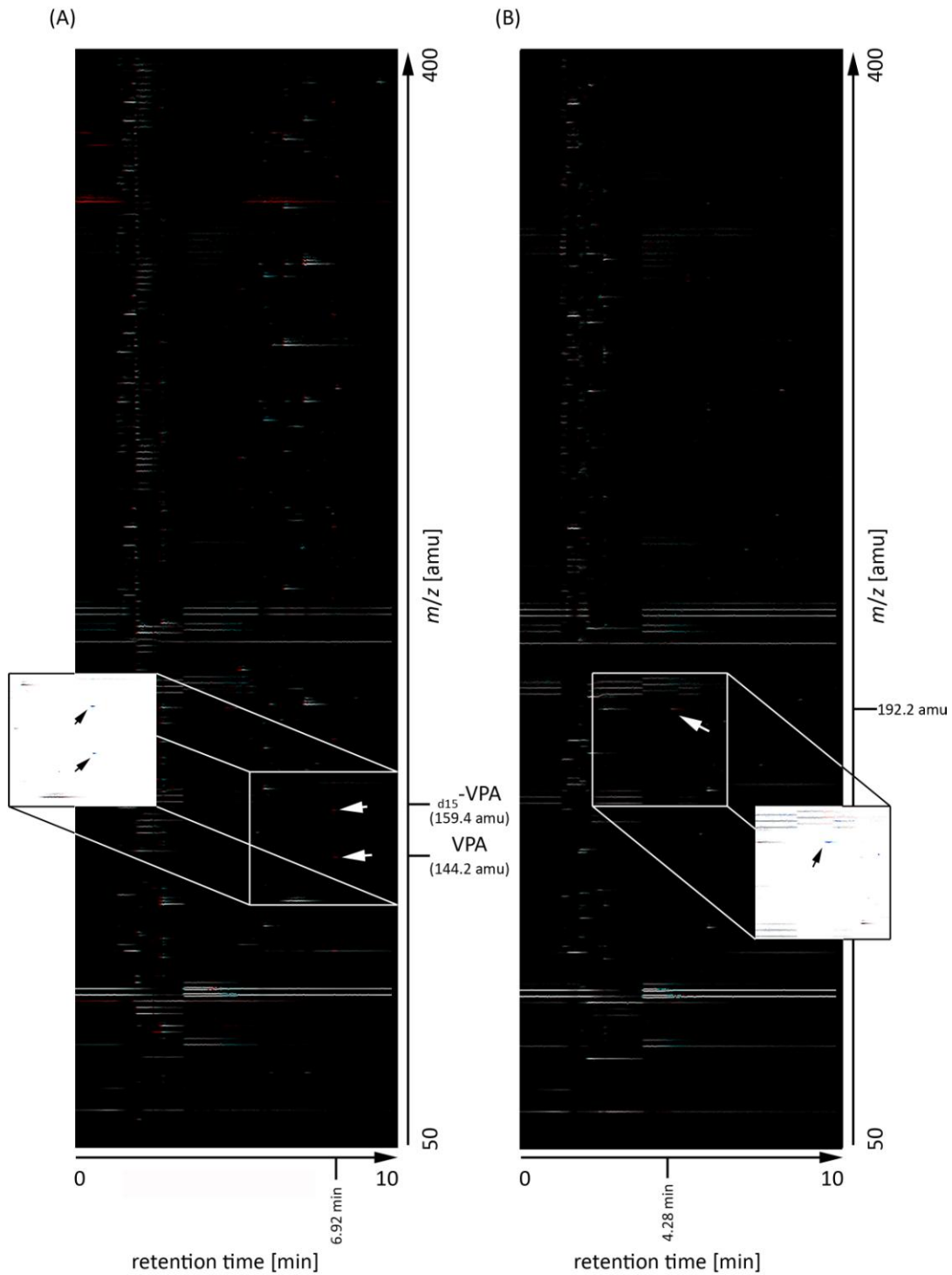
Figure 31   **Comparison of Non- and Pos-Responders by differential shading. (A) Comparison of media plus VPA/$_{d15}$-VPA versus media without. Signals of VPA and $_{d15}$-VPA are indicated by white arrows. (B) Comparison of lysates from Non- and Pos-Responders. The only difference detected at 192.2 amu /4.28 min is indicated with a white arrow. Excerpts give inverted sections of region of interest to highlight detected differences which appear in dark blue and are marked with black arrows.**

4.1.6.4 Analysis of general fatty acid transport in Non- and Pos-Responders

CD36 has been shown to facilitate LCFA import into cells (Coburn et al. 2001; Ibrahimi et al. 1996). To investigate whether there are any differences between Non- and Pos-Responders regarding their fatty acid uptake, the internalization of a BODIPY-labelled dodecanoic acid analogue (*Molecular Devices*) was monitored after 6 h of starvation. It could be demonstrated that basal LCFA uptake did not significantly differ between both groups, but was slightly higher in the Non-Responders (Figure 32A). Furthermore, addition of 500 µM VPA enlarged this difference even more, leading to a significant lower LCFA uptake in Pos-Responders. Interestingly, a similar effect was detected when 1 µM retinoic acid (RA) was added. Combination of both VPA and RA led to a synergistic effect. RA was used in these experiments for two reasons: First, it has been shown that RA increases CD36 expression (Wuttge et al. 2001). Second, the RA receptor RARβ was found to be exclusively expressed in Non-Responders, which suggested a different response to RA regimen.

Some further samples were treated with VPA, RA or both combined with 400 µM SSO, a CD36-specific inhibitor (Coort et al. 2002) to test whether the observed elevated fatty acid uptake was due to a CD36 up-regulation. Surprisingly, addition of SSO led to a higher amount of fluorescent labeled fatty acids present in the cytoplasm in all three treatment combinations. Since this was verified in another round of experiments (Figure 32B), it may be speculated whether CD36 is rather functioning as a fatty acid exporter than an importer in fibroblasts. At least this would explain the tremendous BODIPY-FA amounts after SSO addition since inhibition of CD36 - which may act as an FA exporter – would theoretically lead to a BODIPY-FA accumulation.
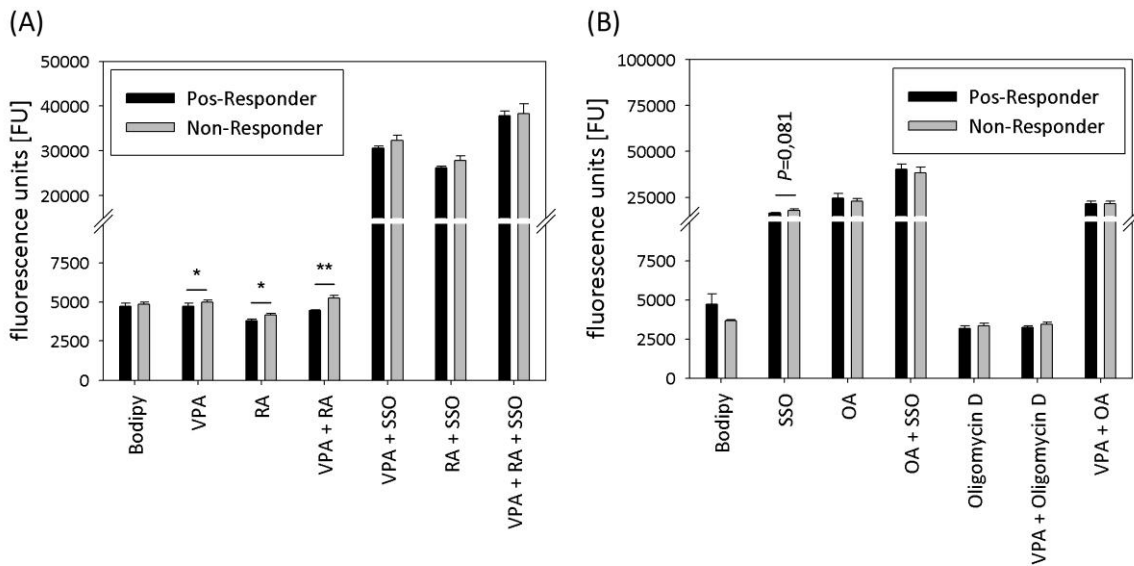
Figure 32 Determination of fatty acid uptake by fibroblasts using a BODIPY-labelled fatty acid analogue. (A) Impact of VPA, RA and SSO on fatty acid uptake. (B) Impact of SSO, OA and Oligomycin D on fatty acid uptake. Data are given as mean ± SEM of three Pos- and 3-Non-Responder fibroblast lines, each measured at least in duplicate (* = $P<0.05$; ** = $P<0.01$; *** = $P<0.001$)

To test whether addition of high amounts of a LCFA augments general fatty acid uptake by global up-regulation of fatty acid transporters, fibroblasts of Pos- and Non-Responders were treated with 1 mM oleic acid (OA). Analysis of imported BODIPY-FA amounts revealed that OA treatment triggers massive FA uptake. Combination of both OA and SSO resulted in a synergistic effect suggesting that OA leads to a general induction of fatty acid translocases as well as CD36. Treatment of fibroblasts with 10 $^{\mu g}/_{ml}$ Oligomycin D, an ATPase inhibitor (Lardy 1980), led not to the expected augmentation in fatty acid import. This implied that the coupling of ATP-generation and fatty acid uptake in fibroblasts is rather weak.

Since BODIPY-FA experiments suggested differences in fatty acid uptake between Pos- and Non-Responders, expression levels of several genes associated with fatty acid uptake and metabolism were determined by qRT-PCR in three Pos- and Non-Responders each. To rule out that any other known SCFA transporter may lead to differential VPA uptake, expression levels of MCT1, 2 and 4 were determined. Although most SCFA enter the cell via diffusion, it has been demonstrated for these MCTs that they accelerate butyrate uptake in the intestine (Thibault et al. 2010). Comparison of MCT expression among Pos- and Non-Responders did not show any gross differences (Figure 33A). Furthermore, VPA administration did not result in any notable alteration, suggesting that these MCTs are not regulated by VPA thus do not account for its transport.

Quantification of PPARγ levels, which is the upstream effector of CD36 (Zhou et al. 2008), revealed no obvious differences (Figure 33B), suggesting that it is not the cause of increased CD36 expression. However, determination of CPT1C levels (carnitine-palmitoyl-transferase 1C) led to an interesting observation. CPT1C is the rate-limiting enzyme in LCFA oxidation since it transfers activated LCFA-CoA onto carnitine, which allows shuttling into the mitochondria. Although controversially discussed, it has been suggested that CPT1C catalyzes Carnityl-VPA formation from VPA-CoA (Lheureux et al. 2005; Silva et al. 2008). Interestingly, CPT1C were twice as high in Non-Responders than in Pos-Responders irrespective of whether VPA was added or not (Figure 33B). This suggested that in Non-Responders the VPA-CoA to Carnityl-VPA reaction may be much faster, thus leading to an accelerated elimination of VPA from the cell. However, it still has to be proven whether this accounts for the non-responsiveness to VPA.
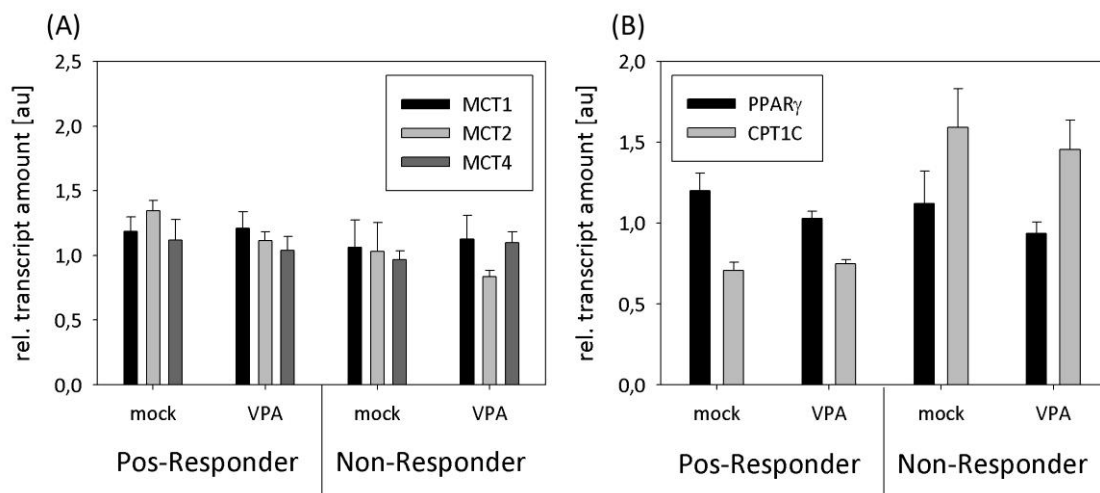
Figure 33   Expression analysis of genes associated with FA uptake and utilization by qRT-PCR. (A) Determination of MCT1, 2 and 4 expression, which functioning in butyrate uptake. (B) Expression analysis of PPARγ the downstream effector of CD36 and CPT1C, the rate-limiting enzyme in LCFA oxidation.

Since BODIY-FA measurements suggested that CD36 may function as a fatty acid transporter, a Non-Responder fibroblast line was treated with VPA and SSO in parallel (Figure 34A). This was done to test whether inhibition of CD36-mediated by SSO leads to an accumulation of VPA in the cell, thus induce *SMN2* expression. Although quantification of band intensity revealed that also single VPA treatment slightly increased SMN levels by 20%, the effect was more pronounced when SSO was added. However, SSO treatment in general reduced SMN levels compared to fibroblasts treated with either VPA or mock alone, suggesting the induction of either cellular stress or cytotoxic effects. Furthermore, the Pos-Responder ML16 was treated with VPA, SSO and RA (Figure 34B). RA was included in this round of experiments since its application induces CD36 expression in fibroblasts (Redfern

and Todd 1992). If CD36 functions as a VPA exporter, RA treatment should accordingly abolish VPA mediate up-regulation of SMN. However, this was not the case, although it was not tested whether CD36 indeed upregulatated. In addition, SSO treatment was included into the experiment. Even though it gave the impression that SSO surpressed the VPA effect, it has to taken in account that SSO treatment alone reduces SMN levels.

(A)   (B)

β-Actin   β-Actin

SMN   SMN

mock VPA SSO VPA+SSO   mock VPA VPA+SSO RA RA+VPA RA+VPA+SSO
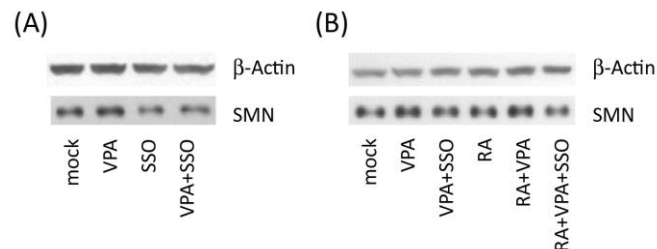
Figure 34   **Effect of SSO and RA on VPA treatment. (A) Non-Responder ML73 treated for 16 h with 500 μM VPA and 400 μM SSO either alone or in parallel. (B) Pos-Responder ML16 treated for 16 h with 500 μM VPA, 400 μM SSO and 1 μM RA either alone or in combination. β-Actin was used as loading control.**

Taken together, these results do not give a definite answer whether CD36 is functioning as VPA exporter or not. To clariy this issue, SSO treatment has to be optimized in such a way that no alterations in SMN levels are detected. Next steps would include a MTT-assay to determine whether the employed concentrations elicit any stress or cytotoxic responses. Furthermore, it has to be determined whether RA indeed induces CD36 expression or not. However, the finding that CPT1C is constitutively higher expressed in Non-Responders poses the question, whether the VPA-CoA to Carnityl-VPA reaction may be the crucial step in the Non-Responsiveness to VPA. Therefore it is needed to work out, whether CPT1C levels are possibly controlled by CD36. If it could be proven, that CD36 is furthermore controlled by RARβ levels, this would lead to an interesting causal chain making Carnityl-VPA formation as a tertiary effect of high RARβ expression in fibroblasts.

In summary, all experiments described so far give no definite clue to why some SMA patients respond positively to VPA whereas others do not. Transcriptome wide expression analysis led to the identification of four candidate genes differentially expressed between Pos- and Non-Responders. However, although knockdown and overexpression studies suggested functional links between theses genes, no definite mechanism could be established yet. The most overt candidate was CD36, a known LCFA transporter. Although HPLC-MS experiments did not indicated any differentially formed VPA metabolites, the observation that regulation of FA uptake by RA and VPA differs between Pos- and Non-Responders still points into this direction. Even though it is still speculative whether this has any functional impact, the finding that CPT1C is higher expressed in Non-Responders is of

great interest. Therefore, next steps should address the question whether there is any functional link between CD36, CPT1C and the response to VPA.

4.2 Identification and characterization of the putative SMA drug LBH589

LBH589, put on the market as Panobinostat, is a second generation hydroxamic acid-derived HDAC inhibitor originally developed by *Novartis* (Figure 35). LBH589 has been shown to inhibit all class I, II and IV HDAC enzymes at low nanomolar doses, suggesting a panHDAC activity. This has been further corroborated by the observation that IC_{50} values for all HDACs with the exception of HDAC4, HDAC7 and HDAC8 were around 13 nM (Atadja 2009). In line with this, LBH589 efficiently induces growth arrest and apoptosis in a wide variety of cancer cell lines derived from solid tumors and hematologic malignancies such as CTLC, acute myeloid leukemia and Hodgkin´s lymphoma. Compared to the well-established and FDA-approved HDACi SAHA (Vorinostat), the anti-proliferative effect of LBH589 on cancer cells was up to 100-fold stronger while normal cell lines remained spared (Shao et al. 2010). Furthermore, LBH589 inhibited growth of human myeloma cells resistant to standard chemotherapeutic agents such as doxorubicin and even potentiated the effects of drugs like bortezomib and dexamethasone (Maiso et al. 2006). Furthermore, the potential of LBH589 was underlined in several mouse studies. In CTLC mouse xenograft model, LBH589 led to 94% tumor regression compared to vehicle treated animals. Similar results were obtained in a colon cancer mouse model (Atadja 2009; Shao et al. 2010).

Initial phase I trials determined the terminal elimination half-life time ($T_{1/2}$) of LBH589. Depending on the individual study, values varying between 7 and 16 h were obtained (Ellis et al. 2008; Giles et al. 2006). Subsequent phase II trials in hematologic malignancies, in particular CTLC and Hodgkin´s Lymphoma produced good responses in most of the cases [reviewed in (Prince et al. 2009)]. Currently more than 80 clinical trials are ongoing employing LBH589 either in mono- or combined therapy for the treatment of diverse types of cancer (http://clinicaltrials.gov/search/intervention=lbh-589).

Based on these promising data, especially the high potency in HDAC inhibition, LBH589 was tested as a potential candidate for causal SMA therapy.
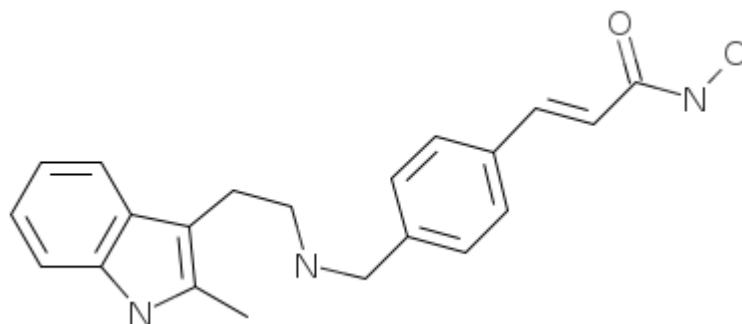
Figure 35   Chemical structure of LBH589 (Panobinostat)

4.2.1 Impact of LBH589 on SMN levels in SMA fibroblasts

In order to assess whether LBH589 is able to increase SMN protein in *SMN1*-deleted fibroblasts optimal dose and treatment time had to be initially determined. To identify the best combination out of both parameters, fibroblasts were treated in a kinetic experiment with LBH589 concentrations between 10 nM and 1 mM for time periods between 24 h and 96 h. It turned out that treatment for 64 h with concentrations between 100 nM and 1 mM LBH589 yielded the highest up-regulation of SMN protein compared to mock-treated cells. Therefore, all subsequent experiments were performed with a single dose of LBH589 for 64 h.

Next, three passages of different SMA fibroblasts (ML16, ML17 and ML5) were treated under the above mentioned conditions. Subsequently, SMN levels were analyzed by semi-quantitative western blotting using β-Actin as loading control (Figure 36). For both cell lines derived from SMA type I patients (ML16 and ML17) at concentrations between 400 and 750 nM LBH589 SMN elevated 6- to 8-fold. At lower concentrations between 100 and 300 nM LBH589, SMN levels were increased 3- to 5-fold. In the case of the fibroblast line ML5, derived from a SMA type II patient, SMN levels increased 3- to 4-fold at all concentrations higher than 200 nM. In all three cell lines a concentration of 1 µM of LBH589 did not further increase SMN amounts, suggesting that maximum *SMN2* induction already occurred at lower concentrations.
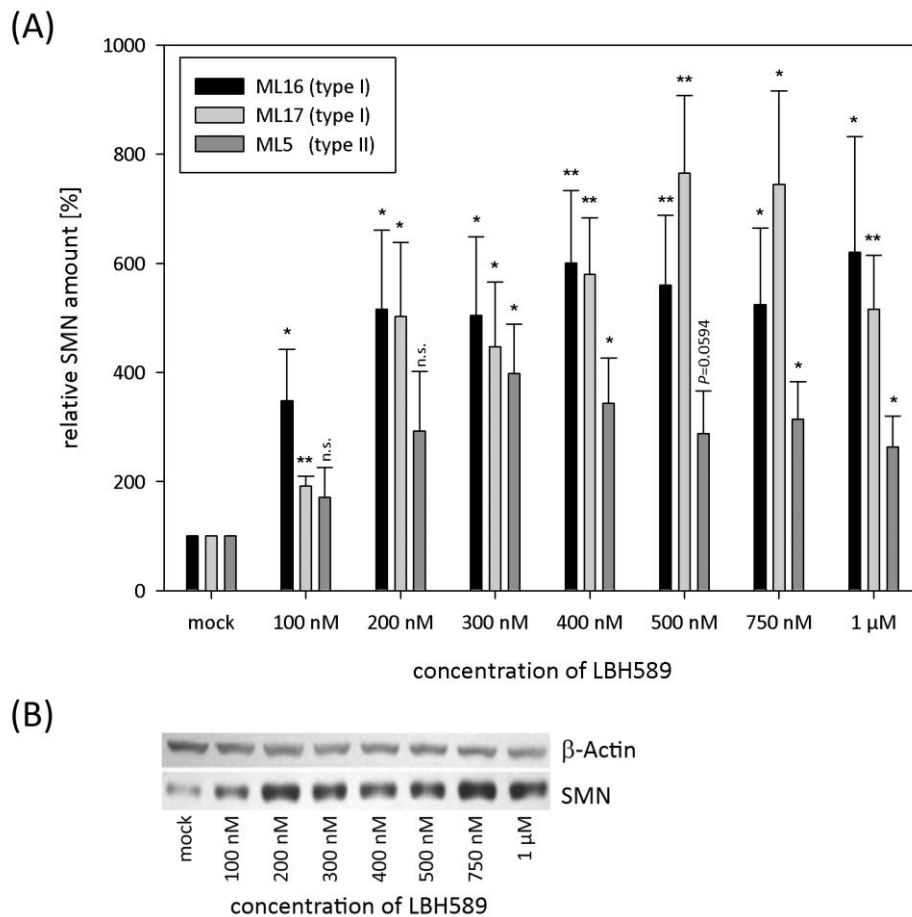
Figure 36   **Analysis of SMN amounts after LBH589 treatment (A) Diagrammatic representation of relative SMN amounts after treatment with the indicated concentrations of LBH589 for 64 h. Results are given as mean ± SEM. (B) Representative western blot stained with an anti-SMN antibody illustrating SMN protein amounts in ML5 after 64 h LBH589 treatment. β-Actin served as loading control. (* = *P*<0.05; ** = *P*<0.01; *** = *P*<0.001)**

4.2.2 Analysis of the impact of LBH589 on gems

Although LBH589 dramatically increased SMN protein amounts, the question remained open whether the additionally produced SMN is indeed functional thus fulfilling its normal cellular roles. Since studies showed that the number of nuclear SMN foci ("gems") correlates with the amount of SMN protein and inversely correlates with the SMA phenotype (Coovert et al. 1997), the elevated SMN protein amounts under LBH589 treatment should be reflected by an increased number of gems. To test whether this is indeed the case, fibroblasts were stained with a FITC-labelled SMN antibody and gems were counted in each 300 mock and LBH589 treated fibroblasts. DAPI was used to ensure nuclear localization of SMN foci (Appendix, Figure 63). In total three different fibroblast lines were investigated to exclude any cell line specific effects.

Comparison of both LBH589- and mock-treated cells revealed that in all three fibroblast lines the total number of cells containing gems increased equally approx. 7-fold (Figure 37) which matches the augmentation of SMN detected by western blotting. Noteworthy, not only the proportion of cells containing a single gem increased but also the number of cells containing two or more gems increased significantly. Taken together, these immuno-fluorescence stainings clearly corroborate the previous western blot data.
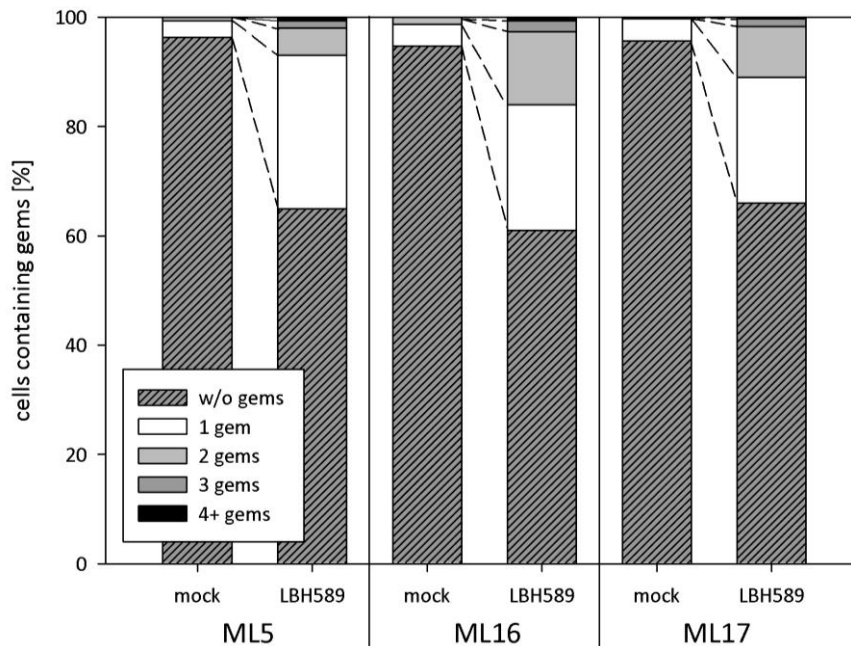
Figure 37   **Comparison of percentages of fibroblasts containing 0 to 4 or more gems. Fibroblasts were treated either for 64 h with solvent only or 400 nM LBH589. For each condition 300 cells were analysed.**

Based on the increased number of gems, it was investigated whether also other SMN complex components are upregulated by LBH589 or whether this is a SMN exclusive effect. Analyzing RNA from LBH589-treated *SMN1*-deleted fibroblasts (ML5) showed that Gemin2 transcript amounts were increased dose-dependently up to 3-fold whereas those of Gemin3 barely doubled for all tested concentrations (Figure 38A). In addition, Gemin expression was quantified in the fibroblast line ML6, derived from a healthy donor. This was done to elucidate whether Gemin2 and -3 are induced by SMN upregulation or whether they are generally induced by LBH589. Although SMN amounts in ML6 merely tripled both Gemin transcripts were up-regulated similarly to ML5, indicating that Gemin upregulation is most likely a general phenomenon of LBH589 treatment.

Furthermore, protein amounts of Gemin2 and Gemin3 were checked by quantitative western blot using β-Actin as loading control in ML5 (Figure 38B, C). It could be shown that both Gemins were increased 1.5- to 2-fold at 400 nM and 1 µM LBH589 although Gemin3 transcript amounts were not markedly increased. On the other hand post-translational

factors such as e.g. stabilization of Gemin3 by Gemin2 or SMN within the SMN complex cannot be excluded. In summary, these data show that not only SMN but also other components of the SMN complex are induced by LBH589.
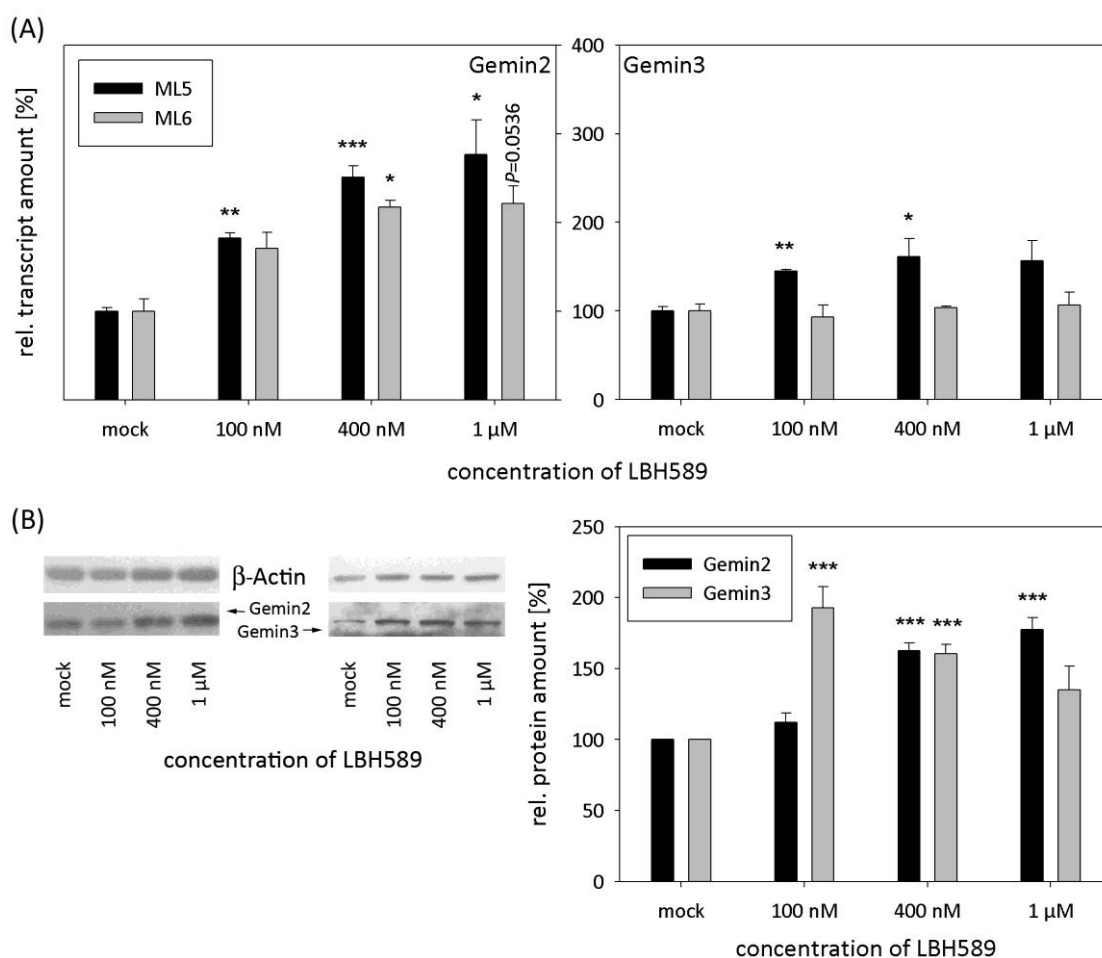
Figure 38 **Analysis of Gemin expression in LBH589-treated fibroblasts (A) Quantifcation of Gemin2 and -3 expression by qRT-PCR in ML5 (SMA type II) and ML6 (healthy donor) following 64 h LBH589 treatment. (B) Representative western blots illustrating the increase in Gemin expression under LBH589 treatment. β-Actin served as loading control. (C) Quantified Gemin2 and -3 protein amounts. (* = $P<0.05$; ** = $P<0.01$; *** = $P<0.001$)**

4.2.3 Comparison of the effects of VPA and LBH589

Nowadays, a number of putative SMA drugs have been investigated. However, only Phenylbutyrate (Mercuri et al. 2004) and VPA have yet been tested *in vivo* by clinical trials (Brichta et al. 2003; Swoboda et al. 2009). To compare the efficacy of LBH589 and VPA, fibroblasts were treated with either VPA or LBH589 in parallel. In total five different fibroblast lines were tested: two of them were VPA Pos-Responder (ML60 and ML67), two showed no change in SMN levels under VPA treatment (ML79 and ML82), whereas one fibroblast line (ML73) exhibited declined SMN amounts following exposure to VPA.

Quantification of SMN protein amounts following drug treatment showed that LBH589 clearly outscored the effect of VPA in all five tested fibroblast lines (Figure 39). In both cell lines reacting positively to VPA (ML60 and ML67), LBH589 increased SMN levels dose-dependently more than 4-fold and in the case of ML67 at 1 µM LBH589 even 10-fold higher SMN amounts were detected. In both VPA Non-Responder cell lines ML79 and ML82, LBH589 elevated SMN amounts 2- to 3-fold although the effect was not as strong as in ML67 and ML60. Most importantly, even in the fibroblast line ML73, which was derived from a VPA Non-Responder, LBH589 led to significantly 2- to 3-fold higher SMN amounts in a dose-dependent fashion. Taken together, LBH589 induces a much higher *SMN2* expression than VPA and is also effective in cell lines which do not positively respond to VPA. Still it has to be taken into account that the effect of LBH589 in fibroblast lines positively reacting to VPA is considerably stronger.
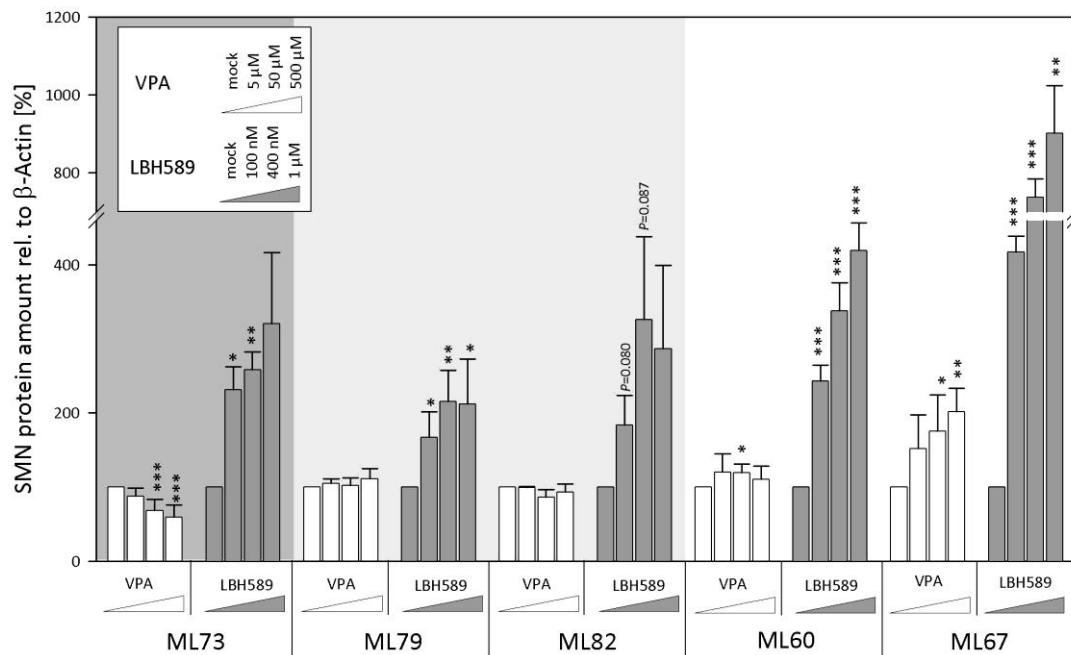
Figure 39   **Comparison of the effects of VPA or LBH589 treatment of different *SMN1*-deleted fibroblast lines. SMN levels were determined by quantitative western blotting using β-Actin as loading control. All results are given as mean ± SEM of three independent experiments. (* = *P*<0.05; ** = *P*<0.01; *** = *P*<0.001)**

4.2.4 Assessment of LBH589 cytotoxicity

Analysis of LBH589-treated *SMN1*-deleted fibroblasts gave outstanding results regarding the SMN protein levels. Nevertheless, these results are only remarkable if toxic side effects are minimal. To test whether LBH589 has any cytotoxic effects, cell viability of 96 h LBH589-treated fibroblasts was quantified by a MTT assay as described previously (Riessland et al. 2006). As shown in Figure 40, cell viability was not considerably reduced for LBH589

concentrations routinely employed. Starting at concentrations of 100 nM up to 10 µM, cell viability was reduced 5 to 15 % compared to mock-treated fibroblasts. However, this phenomenon is typically seen when treating cells with HDACi since they induce cell cycle arrest while the mock-treated cells still proliferate. Only at very high concentrations of >10 µM cell viability was notably reduced by more than 30%.
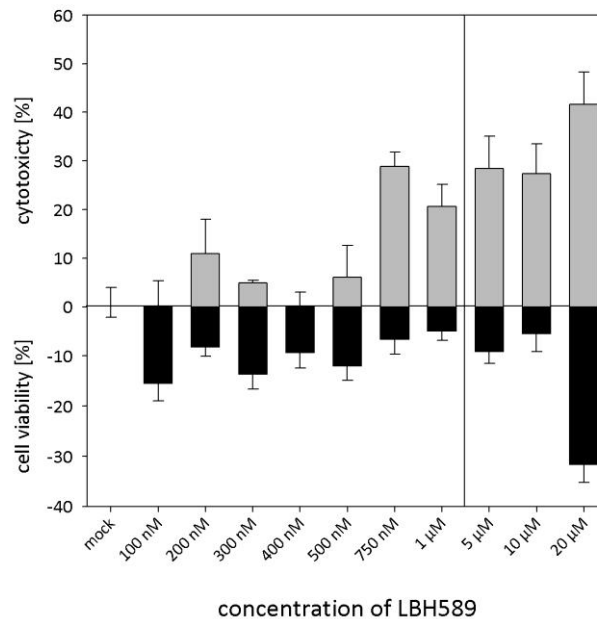
Figure 40   Diagrammatic representation of cell viability and cytotoxicty determined by a MTT and LDH assay. Fibroblasts were treated for 96 h with the indicated LBH589 concentrations. Vertical line indicates concentrations regularly used in this thesis.

To assure that reduced cell viability is indeed caused by cell cycle arrest and not due to cytotoxic side effects of LBH589, a LDH assay was performed (Figure 40). It turned out that notable cytotoxic effects (>30% dead cells) were detected at LBH589 concentrations starting from 750 nM, which become even more pronounced at higher concentrations. At lower concentrations up to 500 nM LBH589 cytotoxic effects were less than 5%.

Summarizing both assays, LBH589 does not severely interfere with cell survival at concentrations regularly used in this thesis. Most importantly, low concentrations of 400 nM, which already markedly induce *SMN2*, are well tolerated by fibroblasts.

4.2.5 Confirmation of LBH589 potential in other systems

So far it could be shown that LBH589 tremendously increases SMN protein amounts while showing low cytotoxicity in fibroblasts. However, the question remained whether the potential of LBH589 is restricted to human fibroblasts only or if similar effects can be observed in other systems which would be of fundamental importance for future clinical trials. Therefore, murine embryonic fibroblasts (MEFs) derived from SMA$_{Hung}$ mice (Hsieh-Li

et al. 2000)) were treated with the standard LBH589 regimen to test whether LBH589 is also able to induce *SMN2* expression in a murine context (Figure 41). Quantification of SMN protein amounts by western blotting showed that SMN levels were up to 12-fold increased at 400 nM LBH589. Furthermore, a 5- to 10-fold increase was detected already at concentrations between 100 and 300 nM LBH589. Similar to human fibroblasts 1 µM LBH589 did not further elevate SMN amounts.

(A)　　　　　　　　　　　　(B)
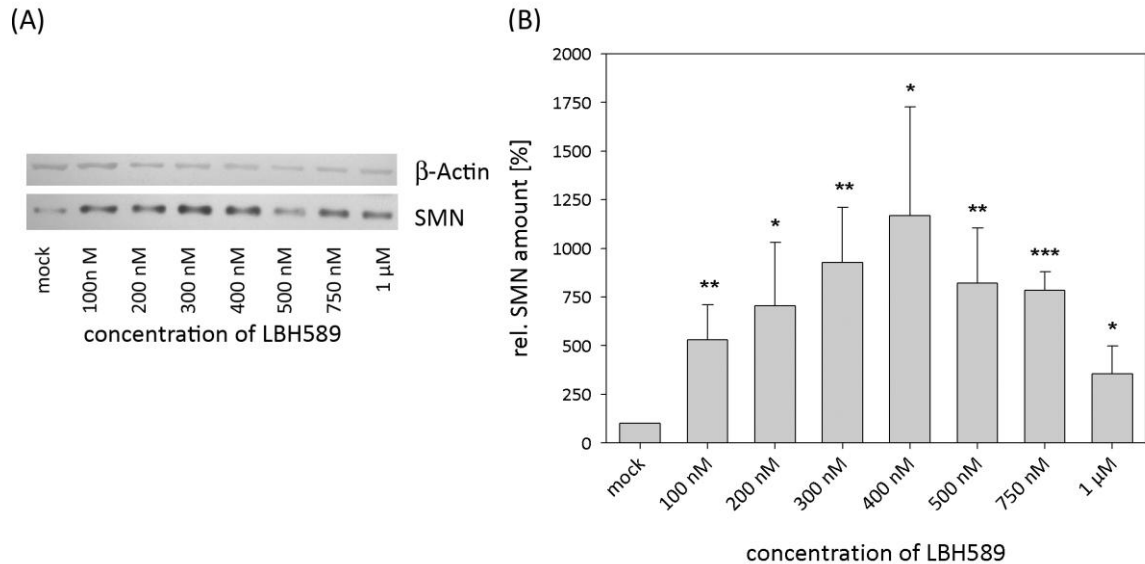
Figure 41　**(A) Representative western blot of MEFs from SMA$_{Hung}$ mice treated for 64 h with the indicated LBH589 concentrations. β-Actin was used as loading control. (B) Quantification of SMN levels following LBH589 treatment of MEFs. Data are given as mean ± SEM from three independent experiments. (* = *P*<0.05; ** = *P*<0.01; *** = *P*<0.001)**

Based on these convincing data, it was investigated next whether LBH589 is also capable to increase SMN amounts in neural tissue closer ressembling the actual SMA target tissue motor neurons. To do so, neural stem cells (NSCs) derived from two epilepsy patients who had undergone surgery were treated for 48 h with 200 and 400 nM LBH589 (Figure 42). In both cell lines (H23 and H30) SMN amounts were increased 2- to 5-fold while the stronger increase was present in H30 at 200 nM LBH589.
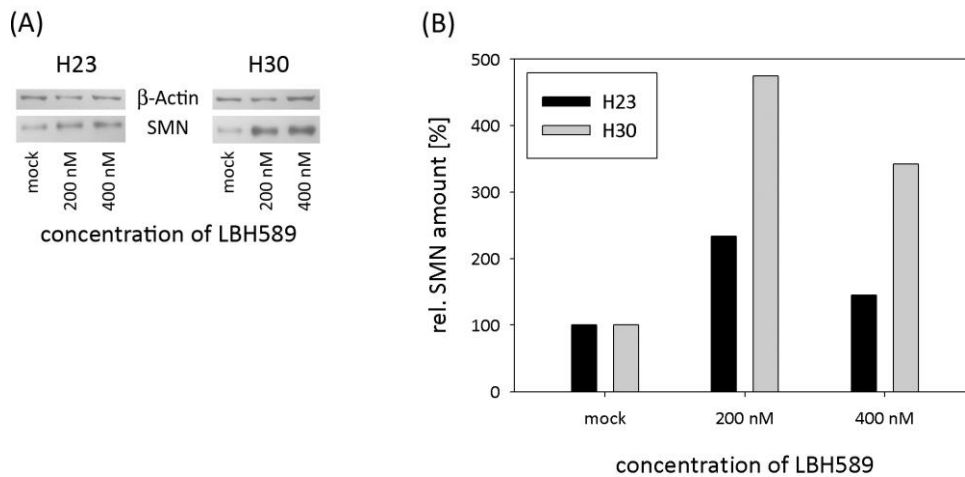
Figure 42   **(A) Representative western blot illustrating the increase of SMN following treatment of human NSCs. β-Actin served as loading control. (B) Quantified SMN protein amounts of LBH589-treated human NSCs.**

Taken together, both murine fibroblasts and human NSCs clearly showed that LBH589 is positively acting on SMN levels in various tissue systems. However, if LBH589 should be considered for use as a SMA drug it has to pre-clinically tested in SMA-like models. Therefore, as a first step towards an *in vivo* testing of LBH589, unaffected SMA carrier mice were subcuteanously injected with $40^{mg}/_{kg[bodyweight]}$ LBH589. This should address the question whether LBH589 is also able to increase *SMN2* expression *in vivo*. And if it does are SMN amounts also increased in the CNS implying that LBH589 crosses the blood-brain-barrier?

Determination of SMN protein amounts in different tissue extracts showed that following LBH589 treatment SMN protein increased by approx. 50% in the brain whereas no notable effect was observed in the liver (Figure 43A, D). This suggested that LBH589 is capable of crossing the blood-brain-barrier, which is a prerequisite for a prospective SMA therapy. To follow up this hypothesis, acetylation levels of histone H3 and H4 were determined in the CNS of LBH589-treated mice by ELISA (Figure 43B). In the spinal cord no noteworthy change was found in the amount of either acetylated histone H3 or H4. In contrast to that, acetylation of histone H3 increased 4 to 8 h after LBH589 injection in the brain by around 60%, indicating that LBH589 indeed induces histone hyperacetylation in the CNS. To corroborate these findings, *SMN2* expression was analyzed in spinal cords of LBH589-treated mice by qRT-PCR. It could be shown that already 2 h post injection SMN expression was increased 2- to 3-fold. This effect lasted for at least 24 h after LBH589 injection (Figure 43C). Taken together, these preliminary *in vivo* experiments with LBH589 underline its potential as prospective SMA drug and prove that LBH589 induces SMN expression not only *in vitro* but also *in vivo*.
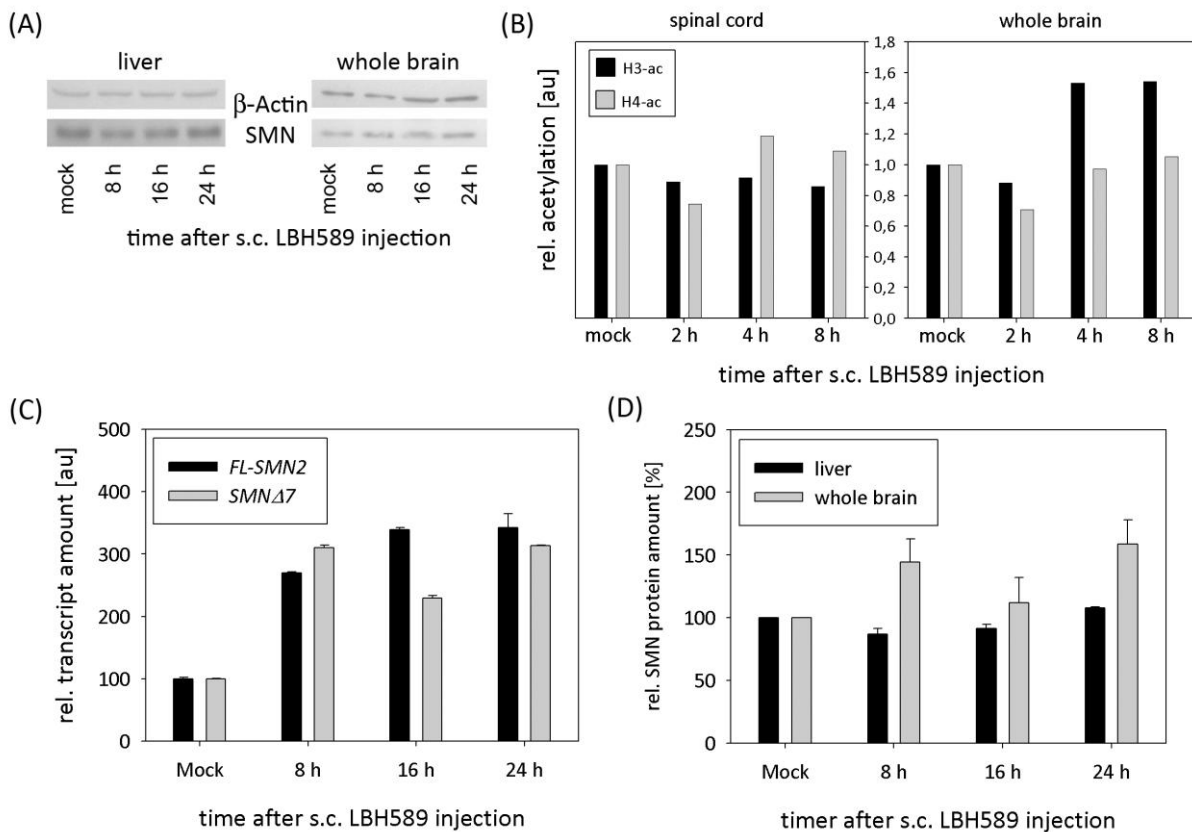
Figure 43   **Analysis of SMA carrier mice subcutaneously injected into the neck pucker with 40 $^{mg}/_{kg(bodyweight)}$ LBH589. (A) Western blot illustrating SMN protein amounts in liver and whole brain at different time points post injection. β-Actin served as loading control. (B) Acetylation leves of histone H3 and H4 of LBH589-injected mice determined by ELISA. (C) SMN2 expression in the spinal cord of treated mice. (D) Quantified SMN amounts in liver and whole brain extracts 8, 16 and 24 h after injection with LBH589 of mice. (s.c. = subcutaneously)**

4.2.6   Impact of LBH589 on *SMN2* mRNA levels and the *SMN2* promoter

4.2.6.1 Analysis of *SMN2* splicing

SMN2 produces two major transcripts, *FL-SMN2* and *SMN2Δ7*, of which the latter one is the predominant isoform accounting for 80 to 90% of all *SMN2* transcripts. To assess whether the increased SMN protein amounts following LBH589 treatment were due to transcriptional activation or *SMN2* splicing correction or a combination of both, *SMN2* transcript amounts in LBH589-treated fibroblasts were analyzed by qRT-PCR.

In total three fibroblast lines were tested and in all cases a significant increase in *FL-SMN2* amounts was detected whereas *SMN2Δ7* amounts stayed constant or even decreased slightly (Figure 44A). Almost 3-fold increased *FL-SMN2* levels were found in ML16 for 400 nM and 1 μM LBH589 while for both ML5 and ML17 a doubling of *FL-SMN2* was recorded at these concentrations. In contrast to that, *SMN2Δ7* amounts did not significantly decrease in

ML16 and 17, but were reduced for all tested concentrations in ML5. Taken together, in all three investigated fibroblast lines the *SMN2* splicing pattern was reversed towards *FL-SMN2* encoding for the fully functional and stable protein (Figure 44B).

Besides other possible explanations such as an altered promoter architecture or pre-mRNA processing, the detected shift in the *SMN2* splicing pattern could also be explained by an altered expression of proteins involved in *SMN* splicing. Since several splice factors are well known to bind *SMN* mRNA and to actively participate in *SMN* splicing (reviewed in (Wirth et al. 2006a)), these were checked for their expression in LBH589-treated cells. By performing semi-quantitative western blotting it could be shown that levels of hTRA2-β1, a splice factor known to promote *SMN2* exon 7 inclusion (Hofmann et al. 2000), were increased 2- to 3-fold at concentrations of 400 nM and 1 μM LBH589 (Figure 44C, E). Contrariwise, levels of SF2/ASF and SRp20 did not change in their expression on protein level.

On RNA level, transcript amounts for all tested splice factors were significantly decreased. Both *SRp20* and *SF2/ASF* mRNA levels were dose-dependently reduced to around 40% at 1 μM LBH589. This effect was not equally pronounced in the case of *hTRA2-β1*. Transcript levels settled down to approx. 60% at all three tested concentrations. These observations - reduced mRNA amounts while protein amounts increase – could most likely be explained by the auto-regulatory feedback circuits described for most of the SR-proteins (Ni et al. 2007) but needs of course further validation on protein level.
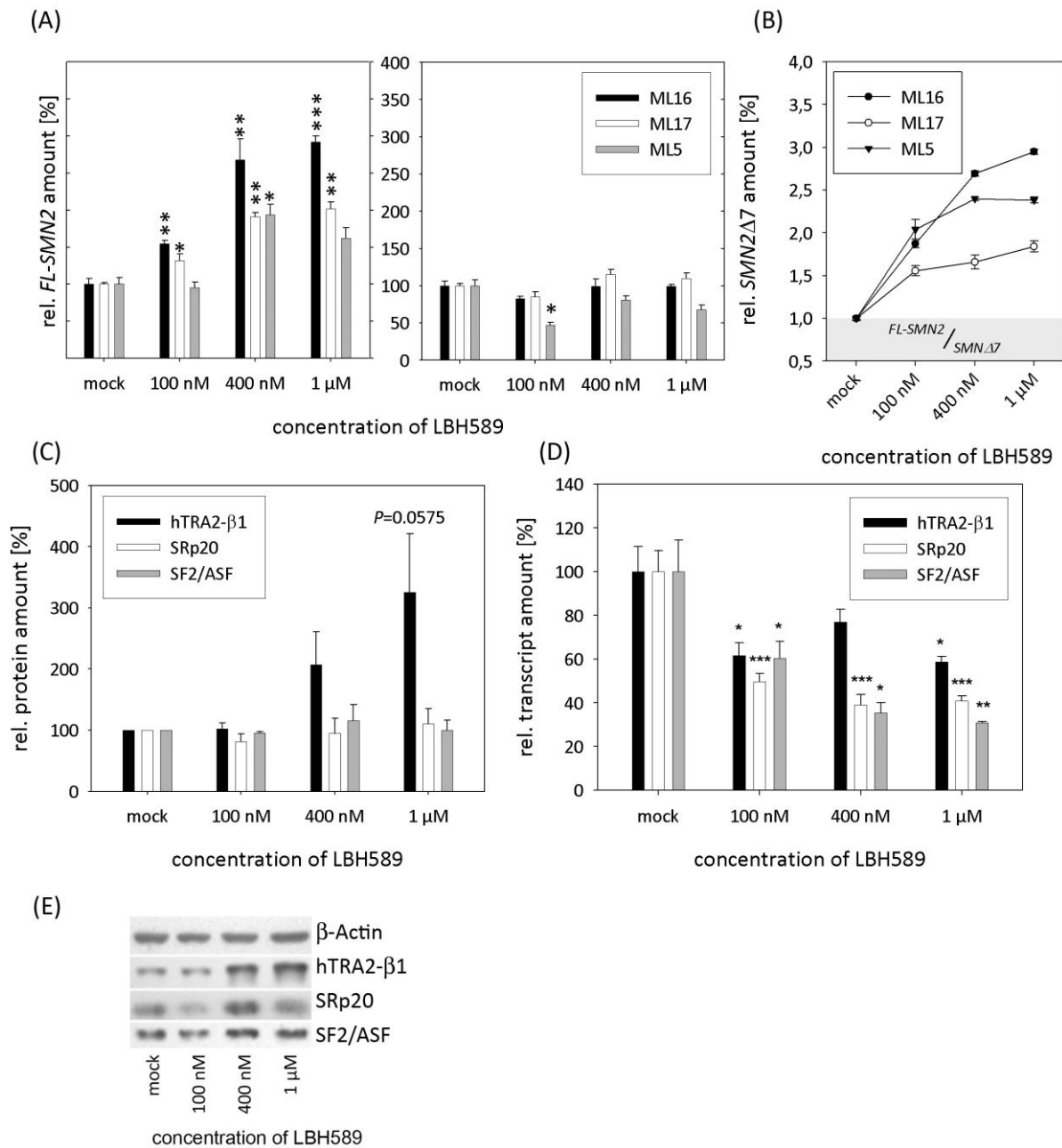
Figure 44   Analysis of SMN splicing under LBH589 treatment. (A) Diagrammatic representation of *FL-SMN2* **and** *SMN2Δ7* **amounts in three LBH589-treated fibroblast lines determined by qRT-PCR. (B) Calculated** *FL-SMN2/SMN2Δ7* **ratios.** *P***-values were below 0.001 for each data point. (C) Splice factor protein and RNA (D) amounts in LBH589 treated cells. (E) Representative western blot stained for splice factors involved in SMN splicing. β-Actin served as loading control. (* =** *P***<0.05; ** =** *P***<0.01; *** =** *P***<0.001)**

hTRA2-β1 was the only splice factor identified that was more abundant under LBH589 treatment. Based on this, the question came up whether hTRA2-β1 is of fundamental importance for the increase in SMN protein upon LBH589 treatment. To clarify this issue, hTRA2-β1 and SMN protein amounts were pursued in a time course experiment with 400 nM LBH589 treated ML5 up to 72 h (Figure 45A). Interestingly, both proteins increased

with a delay of 12 h after LBH589 addition. In the following, SMN amounts steadily increased and peaked at 48 h and 64 h at approx. 700%. hTRA2-β1 amounts showed the highest increase at 12 h with 250% and remained at around 200% for the following time points.

When looking at *SMN* transcripts a striking coincidence became obvious (Figure 45B). Within the first 12 h of LBH589 *SMN2Δ7* steadily increased up to 300% while *FL-SMN2* stayed constant. 12 h after LBH589 addition, the splicing pattern was suddenly reversed to *FL-SMN2* and persisted until the end of the experiment. This time point indeed matched the beginning of the steady SMN cumulation as well as the increase in hTRA2-β1 protein amounts. In conclusion, these data suggested that the up-regulation of *hTRA2-β1* is a prerequisite for the SMN protein increase in *SMN1*-deleted fibroblasts.
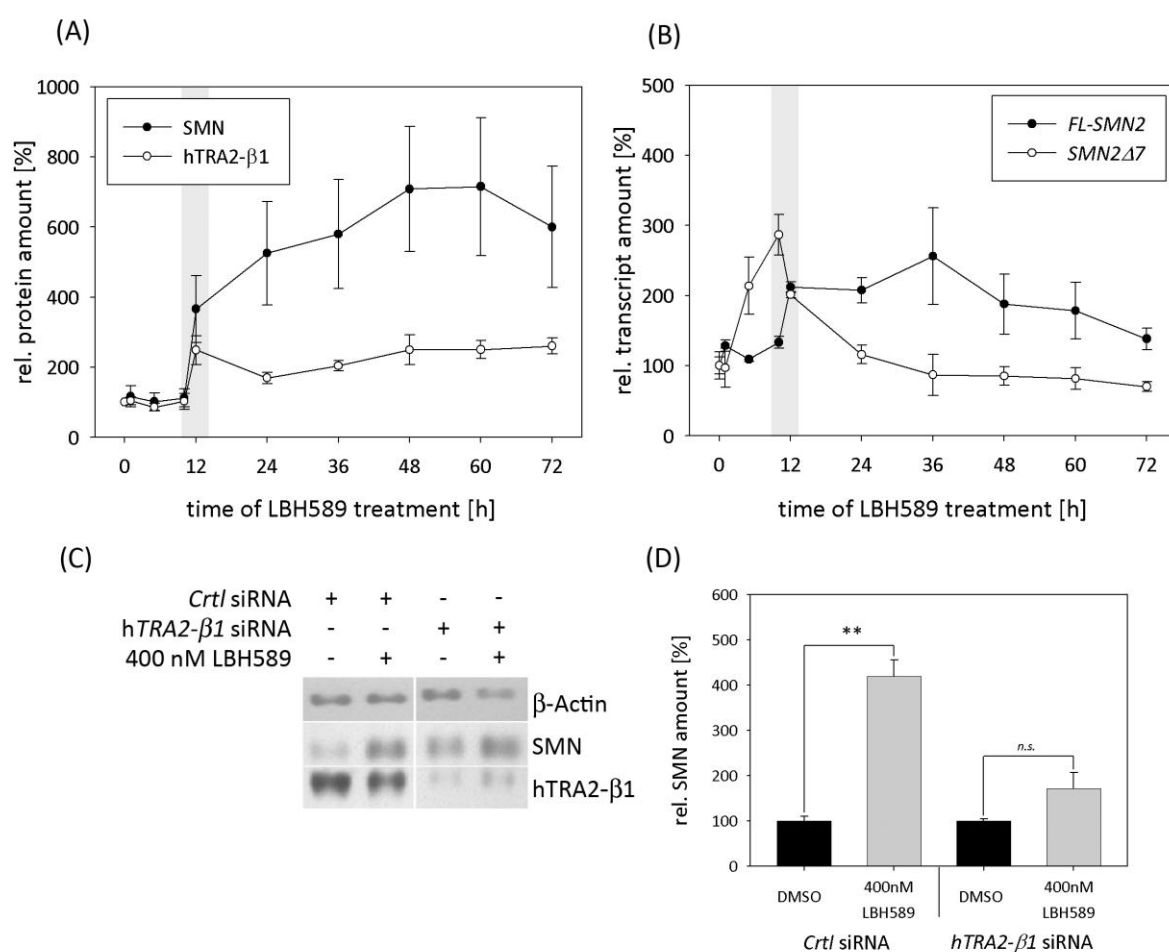
Figure 45   Time course analysis of LBH589 treatment. (A) Quantified protein amounts of hTRA2-β1 and SMN in 400 nM LBH589 treatment. Western blotting was performed using β-Actin as loading control. (B) *FL-SMN2* and *SMN2Δ7* amounts measured by qRT-PCR in up to 72 h LBH589 treated ML5. (C) Western blot illustrating the diminished response to LBH589 when hTRA2-β1 is knocked down. Quantified protein amounts are given in (D). (* = *P*<0.05; ** = *P*<0.01; *** = *P*<0.001).

To follow up this hypothesis, a knockdown of *hTRA2-β1* was performed to test whether its depletion hampers the induction of *SMN2* by LBH589 treatment (Figure 45C, D). Quantitative western blotting showed that LBH589 treatment of fibroblasts transfected with a non-targeting siRNA led to a significant up-regulation of SMN up to 450%. In contrast to that, LBH589 did not significantly increase SMN amounts in fibroblasts transfected with a siRNA targeting *hTRA2-β1*. Transfecting a siRNA targeting SRp20 did not reduce *SMN2* induction by LBH589 (data not shown). In summary, these data suggest that *hTRA2-β1* indeed is one of the first steps within the cascade leading to the tremendous increase in SMN protein under LBH589 treatment.

4.2.6.2 Analysis of the *SMN2* promoter

Previously it could be shown that LBH589 increases total *SMN2* transcription (Figure 44 and Figure 45). Thus, in a next step the *SMN2* promoter itself was investigated with regard to acetylation of lysine 9 of histone H3 (H3K9), which is a clear sign of active transcription (Roh et al. 2005). To this aim, ChIP was performed using an antibody directed against acetylated histone H3 with mock and 400 nM LBH589 treated fibroblasts.

Quantification of precipitated DNA-protein complexes by means of qRT-PCR showed that LBH589 elevated acetylation at all four previously described regions of the *SMN2* promoter (Figure 46) (Kernochan et al. 2005). The highest change (plus 250%) was detected at promoter region 2, which is located approx. 1000 bp upstream of the TSS. HuSP3 acetylation was increased by nearly 200% while HuSP1 and HuSP4 located directly at the TSS doubled in their H3K9 acetylation. To rule out any fibroblast line specific effects, these experiments were repeated in another fibroblast line but produced similar results (data not shown).
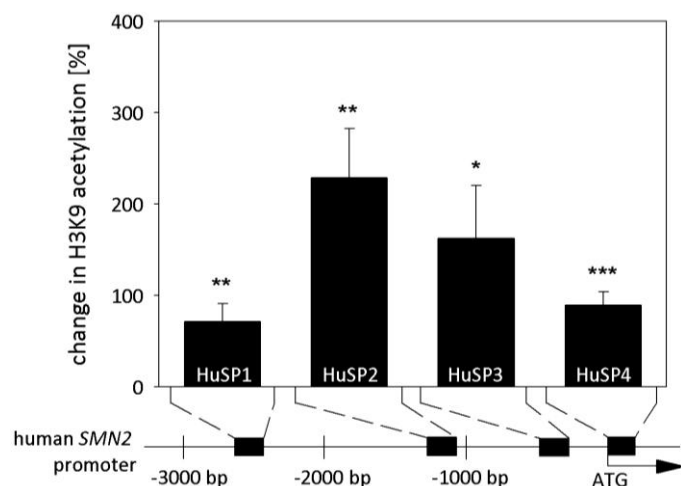
Figure 46   **Analysis of the H3K9 acetylation status of the *SMN2* promoter in LBH589-treated fibroblasts. Data are given as mean ± SEM of three independent experiments. (* = *P*<0.05; ** = *P*<0.01; *** = *P*<0.001)**

Based on the ChIP data it was tested whether the elevated H3K9 acetylation is accompanied by an increased *SMN2* promotor activity. Therefore, a NSC-34 reporter cell line stably transfected with the β-lactamase under the control of the human *SMN2* promoter was treated with LBH589. This cell line allows monitoring of *SMN2* promoter activity since the β-lactamase cleaves CCF2-AM (a dye which was added to cells in the course of this experiment) in a concentration-dependent manner (Jarecki et al. 2005). By treating this cell line with escalating LBH589 concentrations a dose-dependent augmentation in promoter activity was detected up to 2.5 au at 500 nM. This clearly shows that the increase in H3K9 acetylation is indeed accompanied by an activation of the *SMN2* promoter. Furthermore, already 200 nM LBH589 are sufficient to achieve nearly maximal *SMN2* induction. In contrast to that, 1 mM VPA increased *SMN2* promoter activity only slightly by 40%.

Calculations using these data by Dr. Christian Tränkle (*University of Bonn*) determined at EC_{50} of 108 nM for LBH589 which matches its HDAC IC_{50} (106 nM), suggesting that H3K9 acetylation and *SMN2* promoter activity go hand in hand and act in a 1:1 stoichiometry (Appendinx, Figure 64 and Figure 65).
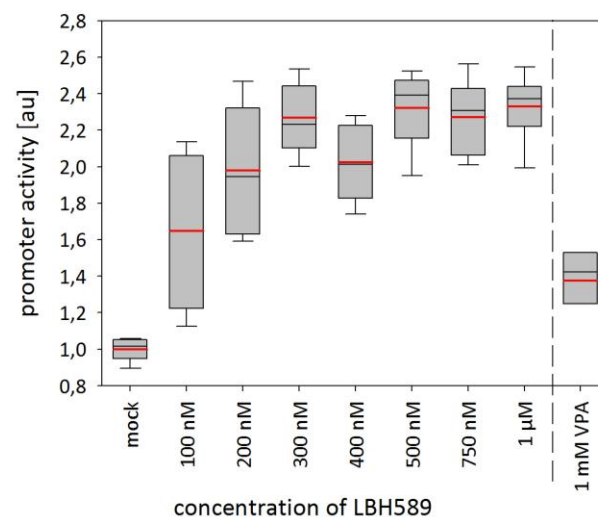
Figure 47   **Box plot illustrating the increased *SMN2* promotor activity in 64 h LBH589-treated NSC-34 reporter cell. *P*-values for all tested concentrations were below 0.001. Boxes represent 50% quartiles including median in black, mean in red whereas whiskers display 5 and 95% quartiles.**

4.2.7 Characterization of LBH589-induced SMN protein increase

So far it could be shown that LBH589 elevated SMN protein amounts up to 8-fold and in some cases even up to 10-fold. On the other side *SMN2* promoter activity merely tripled under LBH589 regimen. Hence, the question arose which mechanism may account for this tremendous discrepancy. Two different scenarios are conceivable: On the one hand LBH589 may enhance mRNA stability, thereby allowing more often the translation of one and the

same mRNA. On the other hand, LBH589 may increase SMN protein stability thus leading to an accumulation of SMN protein over time.

4.2.7.1 Analysis of *SMN* mRNA turnover in treated fibroblasts

To investigate whether LBH589 increases *SMN2* mRNA stability *de novo* mRNA synthesis was blocked with Actinomycin D for different time periods in fibroblasts either treated with 400 nM LBH589 or mock. RNA was extracted from the respective samples and qRT-PCR was performed to quantify individual remaining transcript amounts. Using the resulting values mRNA half-life periods ($T_{1/2}$) were calculated for both *FL-SMN2* and *SMN2Δ7* as well as three control transcripts (Figure 48). For none of the tested transcripts any notable difference in mRNA stability was detected. Therefore, a stabilizing effect of LBH589 on the *SMN2* mRNA could be excluded as a factor leading to the discrepancy between promoter activity and SMN protein amounts.
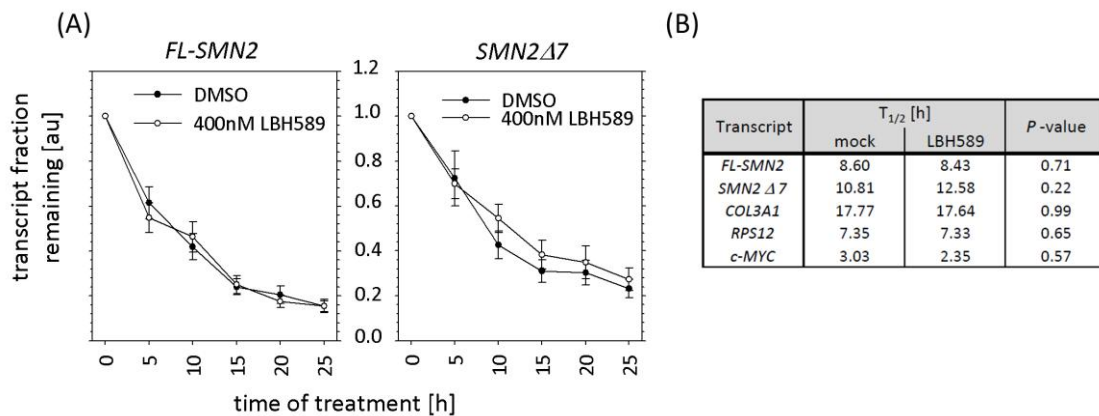
Figure 48   **Analysis of mRNA stability in LBH589-treated fibroblasts. (A) Diagrammatic comparison of *FL-SMN2* and *SMN2Δ7* fractions remaining after incubation for the indicated time periods with Actinomycin D. (B) Half life periods ($T_{1/2}$) of different transcripts calculated by approximated *e*-functions. Values are given as mean values from three independent experiments. Control transcripts *COL3A1*, *RPS12* and *c-MYC* served as control for long, medium or short half-life.**

4.2.7.2 Analysis of SMN protein turnover in treated fibroblasts

Since an increased SMN mRNA half-life could be excluded as the pivotal factor, it was investigated next whether rather SMN protein than mRNA turnover is affected by LBH589. SMN is degraded via the ubiquitin-proteasome-system (UPS) (Burnett et al. 2009; Chang et al. 2004). Hence, as a first step global proteasomal degradation was tested for alterations. Inhibition of the proteasome with the proteasome inhibitor MG-132 for 15 h resulted, as expected, in a doubling of SMN amounts since it is not longer degraded. However, adding MG132 to cells pre-treated for 48 h with LBH589 failed to further elevate SMN protein

levels, suggesting that LBH589 either directly inhibits the proteasome or that ubiquitinylation of SMN is reduced so that SMN is no longer targeted to the proteasome.

Similar results were obtained for p53, a protein which is known to be degraded by the proteasome. Combined treatment with MG132 and LBH589 failed to further increase protein amounts but rather led to a reduction of p53 induction by LBH589.
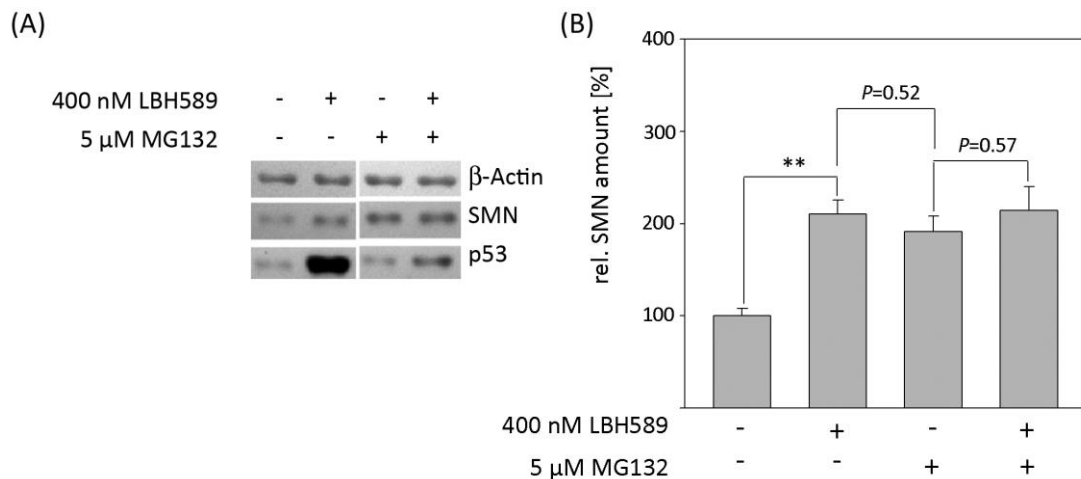
Figure 49   **Analysis of SMN turnover in LBH589 and MG132 treated cells. (A) Typical western blot showing combined and single treatment of LBH589 and MG132 of fibroblasts. (B) Analyzed SMN protein amounts of three independent experiments using β-actin as loading control.**

In total three different proteolytic activities differing by their target sequence have been identified within the proteasome (caspase-, trypsin- and chymotrypsin-like) (Kisselev et al. 1999). To address the question whether LBH589 directly inhibits the proteasome, a luciferin-coupled degradation assay was employed to determine catabolic rates for all three proteolytic activities in LBH589-treated fibroblasts (Figure 50). It turned out that for none of the LBH589 concentrations a significant inhibitory effect could be detected. In contrast to that, proteolytic activities were decreased by 50 to 80% by MG132. The lysosome inhibitor NH_4Cl had, as expected, only minimal effects on the proteasome. Interestingly, VPA slightly decreased trypsin- and chymotrypsin-like proteolytic rates but led to a notable increase of around 30% in caspase-like proteasomal degradation. Nevertheless, these data show that LBH589 has no inhibitory effect on the proteasome.
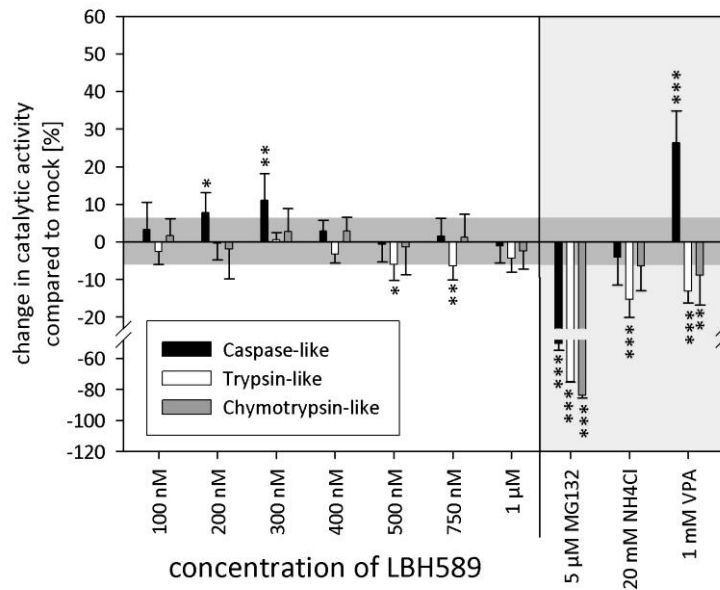
Figure 50   **Diagrammatic representation of the alteration in catalytic activities associated with the proteasome in LBH589-treated fibroblasts. MG132 served as positive control whereas NH₄Cl, a known inhibitor of the lysosome, acted as negative control. Dark gray area indicates natural activity fluctuation in mock-treated fibroblasts. (* = *P*<0.05; ** = *P*<0.01; *** = *P*<0.001)**

Degradation of proteins via the UPS is a two-step process: First ubiquitinylation of the protein and second degradation by the proteasome. Since no differences regarding their proteasomal activity in mock and LBH589-treated cells could be detected, focus was shifted on SMN ubiquitinylation. Therefore tri- and tetraubiquitinylated proteins were precipitated using agarose beads coupled to the ubiquitin-interaction-motif (UIM) of Rpn10/S5A. Total portion of ubiquitinylated SMN was determined by resolving equal amounts of non-ubiquitinylated SMN by western blot (Figure 51A). Quantification of protein amounts revealed that abundance of ubiquitinylated SMN was significantly reduced by 70% (Figure 51B). This suggested that besides promoter activation LBH589 also elevates SMN levels by reducing its turnover thereby leading to an accumulation over time.

Absence of non-ubiquitinylated proteins in the Rpn10/S5A precipitate was proven by staining against ODC (Ornithine decarboxylase), a protein which is known not to be ubiquitinylated (Figure 51C). Effective LBH589 treatment leading to increased SMN amounts was also proven by western blot (Figure 51E).
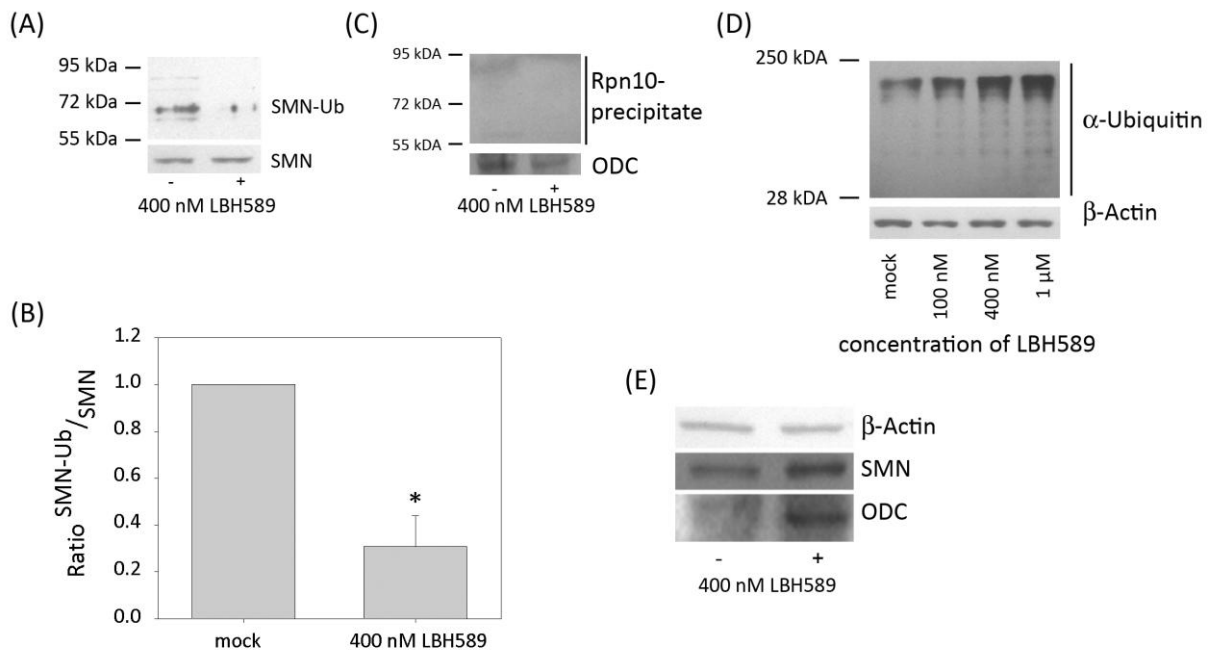
Figure 51 **Analysis of the UPS in LBH589-treated cells. (A) Representative western blot illustrating the decline in the amount of ubiquitinylated SMN precipitated by the Rpn10/S5A UIM. Equal amounts of non-ubiquitinylated SMN were loaded. (B) Mean decline of SMN ubiquitinylation in three independent experiments ± SEM. (C) Typical western blot illustrating the absence of non-ubiquitinylated proteins in the Rpn10/S5A precipitate by staining against ODC. (D) Western blot using whole cell lysates illustrating total ubiquitinylation in LBH589-treated cells. (E) Western blot indicating increase in SMN and ODC amounts under LBH589 treatment. (* = $P<0.05$)**

Although SMN ubiquitinylation declined, total protein ubiquitinylation was not reduced under LBH589 treatment (Figure 51D). This suggested that the decline in SMN ubiquitinylation is rather a secondary than a primary effect of LBH589. It has previously been shown that SMN stability is enhanced by the incorporation of SMN into the SMN complex (Burnett et al. 2009). Based on this, it was argued that the observed reduction of ubiquitin coupling to SMN is rather a consequence of enhanced SMN complex formation whereby SMN is kept out of the UPS pathway. This was further underlined by the detected increase in Gemin2 and Gemin3 protein amounts – both of them SMN complex partners (Figure 38).

Summarized, besides transcriptional activation and splicing correction, LBH589 also acts post-transcriptionally on SMN levels by reducing SMN ubiquitinylation most likely through enhanced SMN complex formation.

4.2.7.3 Analysis of PKA activity in LBH589-treated fibroblasts

It has previously been shown that integration of SMN into the SMN complex is favoured by activation of PKA. Therefore, PKA activity and expression were analyzed in LBH589-treated

fibroblasts (Figure 52). PKA activity decreased dose-dependently to a minimum of 70% at 1 µM LBH589. In contrast to that, expression of the catalytic subunit ε of PKA (termed PKA_{cat}) was increased to the same extent. Therefore, PKA activation as the initial trigger leading to an increased SMN complex formation could be excluded.

(A)

(B)
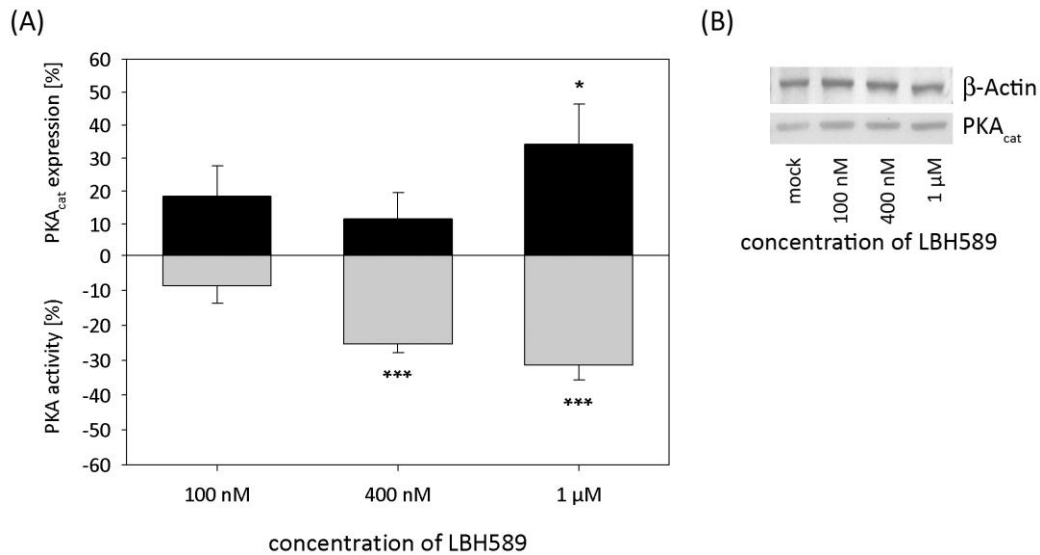
Figure 52   Analysis of PKA activity in LBH589-treated cells. (A) Diagrammatic summary of increased PKA_{cat} expression as well as reduced PKA activity following LBH589 treatment of fibroblasts. (B) Typical western blot illustrating PKA_{cat} levels at various LBH589 concentrations. (* = *P*<0.05; ** = *P*<0.01; *** = *P*<0.001)

In conclusion, these data clearly show that LBH589 is an outstanding candidate for a drug-based SMA therapy. Compared to other HDACis, the impact of LBH589 on SMN levels is the highest yet reported. Most importantly, LBH589 is able to induce *SMN2* expression in fibroblasts not responding to the classical HDACi VPA. Therefore, the next step towards a putative SMA therapy with LBH589 would be to evaluate its efficacy in a SMA-like mouse model like it has recently been reported for SAHA (Riessland et al. 2010).

4.3 Identification of Bortezomib (Velcade) as a putative SMA drug

Based on the finding that LBH589 was able to indirectly increase SMN amounts by reducing its ubiquitinylation, the therapeutic proteasome inhibitor Bortezomib (Velcade) was tested for its potential to increase SMN amounts. Bortezomib was originally developed by *Millenium Pharmaceuticals* as PS-341 (Adams 2002) as an anticancer drug. Clinical trials with diverse types of cancers such as solid tumors (Aghajanian et al. 2002; Papandreou et al. 2004) have subsequently proven Bortezomib´s efficacy and biocompatibility. Bortezomib became the first proteasome inhibitor clinically approved. Nowadays, it is routinely used for the monotherapy of progressive multiple myoloma.
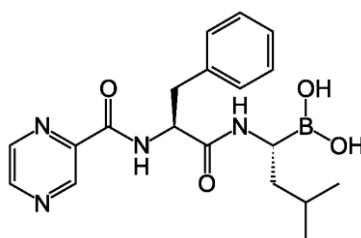
Figure 53   **Chemical structure of Bortezomib / PS-341 / Velcade**

To determine the concentration and treatment time Bortezomib was initially applied in a kinetic experiment to *SMN1*-deleted fibroblasts. Therefore, ML17 was treated for 8, 24 and 48 h with Bortezomib concentrations between 10 and 500 nM (Figure 54A). Summarized, 8 h of Bortezomib treatment modestly increased SMN amounts up to 170% maximum at 100 nM. Longer incubation times of either 24 or 48 h elevated SMN amounts up to approx. 250% for all concentrations higher than 50 nM. Based on these convincing data, a MTT assay was performed to test whether Bortezomib hampers cell viability at concentrations tested (Figure 54B). It turned out that concentrations higher than 20 nM Bortezomib dramatically decreased cell viability by more than 30%. At 200 nM Bortezomib, cell viability was already halved although SMN amounts were more than 2-fold increased. Hence, all subsequent experiments were performed with Bortezomib concentrations up to 20 nM maximum and an incubation time of 24 h.

In total four different fibroblast lines were treated with Bortezomib (Figure 54C, D). Three of them were derived from SMA patients (ML5, ML16 and ML17) whereas ML6 was derived from a healthy donor. Quantifying SMN levels by western blotting showed that in all three cell lines derived from SMA patients SMN was significantly increased 2- to 3-fold at 10 and 20 nM Bortezomib. At 1 nM Bortezomib, only tiny augmentations in SMN amounts were recorded. In the case of ML6 just 20 nM of Bortezomib led to a significant augmentation in SMN protein.
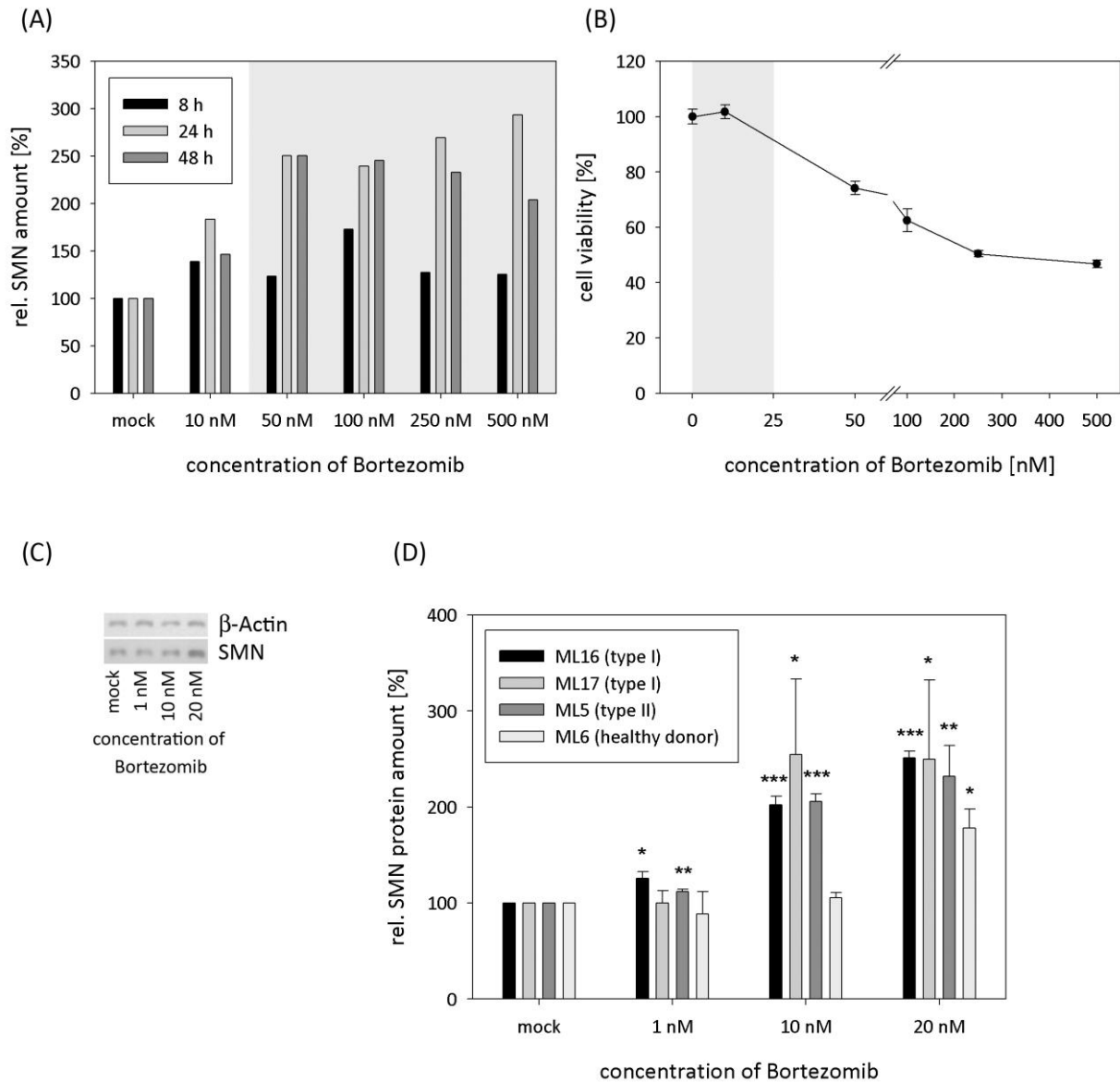
Figure 54   Analysis of Bortezomib´s impact on SMN levels. (A) Kinetic experiment with ML17 to determine optimal combination of drug concentration and treatment time. Toxic concentrations are marked in gray. (B) MTT assay with 96 h Bortezomib treated fibroblasts. Starting from 50 nM Bortezomib onwards *P*<0.0001. (C) Typical western blot with fibroblasts treated with the indicated Bortezomib concentrations. Quantified protein amounts are given in (D). (* = *P*<0.05; ** = *P*<0.01; *** = *P*<0.001)

Although these results were very promising, Bortezomib was not further investigated as a potential SMA drug since it does not pass the blood-brain-barrier (Hemeryck et al. 2007), which is a prerequisite for drug-based SMA therapy. However, it may be speculated whether combined therapy of an HDACi and Bortezomib may lead to synergistic effects (e.g. SAHA plus bortezomib in multiple myeloma therapy (McConkey 2010)) but these would fail to affect the α-motor neurons which are the target tissue of causal SMA therapy.

4.4 Identification of JnJ-26481585 as a potential SMA drug

Based on the promising LBH589 data, another auspicous second generation panHDACi, JnJ-26481585, was tested as a putative SMA drug. JnJ-26481585, originally developed by *Johnson and Johnson*, is a derivate of LBH589 sharing the same terminal indole-1-methyl-3-yl-methylamine and acrylamide residues while the central benzene is substituted by a 2(piperidine-1-yl)pyrimidine (Figure 55). *In vitro* studies using JnJ-26481585 showed a strong anti-proliferative activity in solid tumors at low nanomolar concentrations. This was further strengthened by the determination of the IC_{50} values for HDAC1 (0.11 nM), HDAC2 (0.33 nM) and HDAC3 (4.8 nM)(Arts et al. 2009). Moreover, *in vivo* studies with mice showed that combined treatment of bortezomib and JnJ-26481585 strongly reduced bone myeloma (Deleu et al. 2009b). Single treatment with JnJ-26481585 of 5T2 and 5T33 multiple myeloma mouse models led to a significant reduction in tumor load and angiogenesis (Deleu et al. 2009a).
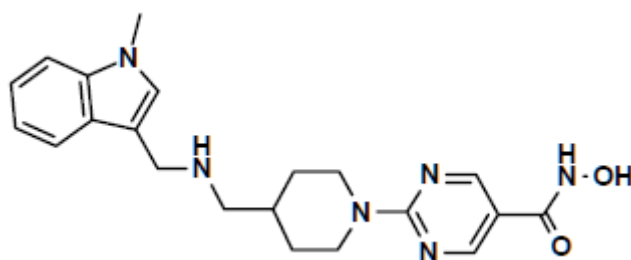
Figure 55 **Chemical structure of JnJ-26481585.**

To investigate whether JnJ-26481585 is capable of increasing SMN protein in *SMN1*-deleted fibroblasts at kinetic experiment was performed initially. Treatment for various time periods of up to 72 h with concentrations between 1 nM and 5 µM produced the highest augmentation at 64 h with concentrations around 400 nM JnJ-26481585 (data not shown). Therefore, all subsequent experiments were performed with this dose.

Treatment of ML16 with the above described conditions yielded a uniform 4-fold increase in SMN levels for concentrations between 100 nM and 1 µM JnJ-26481585 (Figure 56A, B). Applying either 10 nM or 5 µM resulted in a doubling of SMN amounts. Compared to the effect of LBH589, the impact of JnJ-26481585 on SMN was nearly the same. Similar to LBH589 a shift of the *SMN2* splicing pattern towards *FL-SMN2* was observed starting at concentrations of 100 nM JnJ-26481585 (Figure 56C). This effect steadily grew to 750 nM at which 250% *FL-SMN2* were recorded. Although not yet tested, probably *hTRA2-β1*, *SF2/ASF* and *SRp20* are also up-regulated by JnJ-26481585 since transcript amounts were dose-dependently decreased (Figure 56D). A similar decline in mRNA levels was detected for hTRA2-β1 under LBH589 treatment while protein amounts were doubled (Figure 44). Furthermore, JnJ-26481585 led to an up-regulation of the SMN-complex partners Gemin2 and Gemin3, suggesting a similar mode of action as discovered for LBH589 (Figure 51).

Based on these data, it was decided to routinely use JnJ-26481585 concentrations of 10 nM, 400 nM and 1 µM for further *in vitro* experiments. Quantification of SMN mRNA levels by qRT-PCR revealed that at 400 nM and 1 µM *SMN2∆7* was significantly declined. By contrast, *FL-SMN2* amounts were increased by 50% for both concentrations, thus confirming the previous data from single RNA experiments.
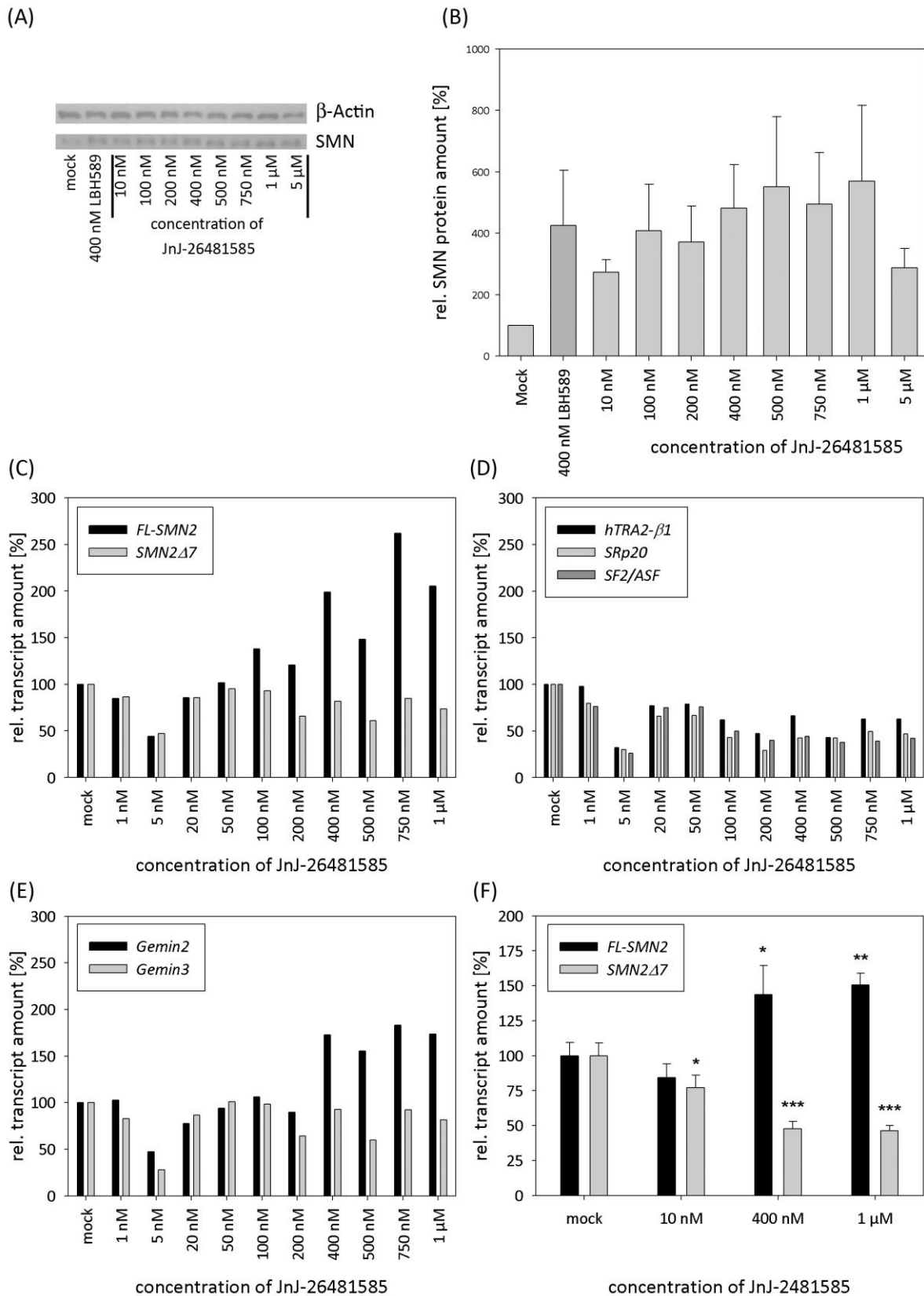
Figure 56   Analysis of the impact of JnJ-26481585 on *SMN1*-deleted fibroblasts. (A) Representative western blot illustrating the increase in SMN under JnJ-26481585 treatment. β-Actin was used as loading control. (B) gives mean protein amounts ± SEM from three independent experiments using ML16. (C) Quantification of *FL-SMN2* and *SMN2Δ7* transcript amounts at

the indicated JnJ-26481585 concentrations. (D) Expression of splice factors known to bind *SMN2* mRNA and SMN complex partners (E). (F) Mean SMN expression under JnJ-26481585 treatment of ML5 with the indicated concentrations. (* = *P*<0.05; ** = *P*<0.01; *** = *P*<0.001)

Furthermore, it was tested whether JnJ-26481585 has any toxic side effects. Using a MTT assay, cell viability was determined in fibroblasts treated for 96 h with JnJ-26481585. Starting from 100 nM onwards, cell viability was reduced by 30% for all concentrations. Although LBH589 was well tolerated in previous experiments (Figure 40A), a similar result was obtained for a concentration of 400 nM. This suggested that the used cell line ML103 is extremely sensitive to HDACi treatment.

As a first step towards an *in vivo* application, 20 $^{mg}/_{kg[bodweight]}$ JnJ-26481585 were subcutaneously injected into the neck pucker of unaffected SMA carrier mice. Both animals treated with JnJ-26481585 exhibited more than 2-fold increased SMN protein amounts in liver (Figure 57B, D). In contrast, no change in SMN levels could be observed in the brain. A second mock-treated animal was not analyzed since only extremely weak SMN signals could be obtained by western blotting. In addition, global histone H3 acetylation was analyzed by ELISA (Figure 57C). Although in the brain of JnJ-26481585-treated mice no increase in SMN levels was detected by western blot, histone H3 acetylation was markedly increased 6 h post injection.

(A)

(B)

(C)

(D)
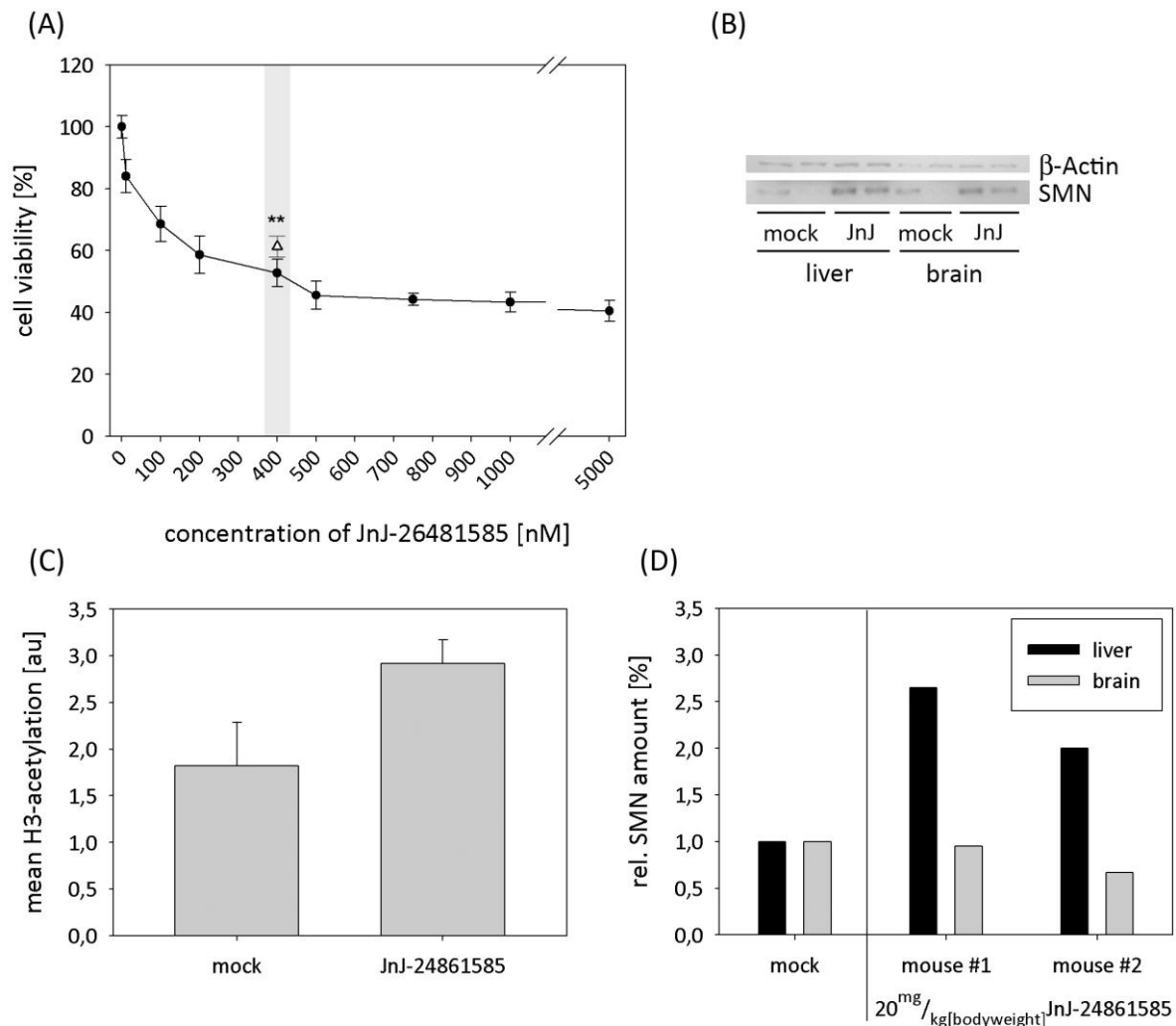
Figure 57   **Evaluation of JnJ-26481585´s cytotoxicity and *in vivo* potential. (A) MTT assay of fibroblasts treated for 96 h with the indicated concentrations. Open triangle indicates cell viability of cells treated for 96 h with 400 nM LBH589. (B) Representative western blot illustrating SMN amounts in different tissues 16 h after subcutaneous injection of 20 $^{mg}/_{kg[bodyweight]}$ JnJ-26481585. (C) Global histone H3 acetylation in the brain of JnJ-26481585-treated mice 6 h post injection. (D) Quantified protein from the western blot depicted in (B). (* = *P*<0.05; ** = *P*<0.01; *** = *P*<0.001)**

Summarized, these data suggest that JnJ-26481585 is indeed a promising candidate for a putative SMA therapy since it augmented SMN levels *in vivo* and *in vitro*. It may be argued that in the brain of JnJ-26481585-treated mice no increase in the SMN amounts could be detected, which would question the potential JnJ-26481585 as a SMA therapeutic. However, these experiments were performed without any dose optimization, implying that another treatment regimen may have led to a different outcome. Therefore, careful testing of different concentrations is needed as it has been reported e.g. for SAHA (Riessland et al. 2010). Once the optimal treatment conditions have been established, the potential of JnJ-26481585 as a SMA therapeutic can be investigated *in vivo*.

4.5   Characterization of an intermediate SMA-like mouse model

Several SMA-like mouse models have been generated of which some have already been employed for *in vivo* drug testing (Lorson et al. 2010). However, none of these animal strains exhibits an intermediate SMA-like phenotype, which would be desirable for the long-term evaluation of putative drugs. Therefore, it was tried to generate such a phenotype by crossbreeding two already established models. Similar to humans, the SMA phenotype in mice strongly correlates with the *SMN2* copy number. SMA$_{Hung}$ (*Smn*$^{-/-}$; *SMN2*$^{tgTW/tgTW}$) have four *SMN2* copies and exhibit no obvious phenotype apart from a necrotic tail. In contrast, SMA$_{Hung}$ animals having two *SMN2* copies (*Smn*$^{-/-}$; *SMN2*$^{tgTW/-}$) develop a severe SMA phenotype and usually die at an age of 10 days while SMA$_{Burghes}$ mice (*Smn*$^{-/-}$; *SMN2*$^{tgUS/tgUS}$) also possessing *SMN2* copies die prenatally. Based on these findings the following breeding was performed to generate SMA-like mice carrying three *SMN2* copies (marked in bold letters).

SMA$_{Hung}$ (*Smn*$^{-/-}$; *SMN2*$^{tgTW/tgTW}$)   x   SMA$_{Burghes}$ (*Smn*$^{+/-}$; *SMN2*$^{tgUS/tgUS}$)

$\downarrow$

Smn$^{+/-}$; *SMN2*$^{tgUS/tgTW}$ +   **Smn$^{-/-}$; SMN2$^{tgUS/tgTW}$**
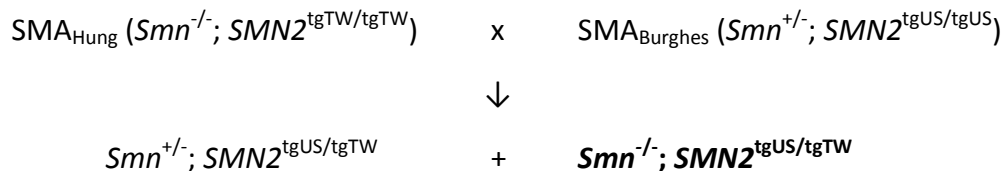
The respective breeding was set up and three litters were observed for a time period of more than 250 days. "SMA-like" animals could easily identified by their phenotypic appearance, which was also verified by genotyping (data not shown). Compared to their healthy litter mates possessing one copy of the murine *Smn* gene, these animals were lighter and also developed necrosis of the ears and tail, but no other noticeable differences were observed (Figure 58).
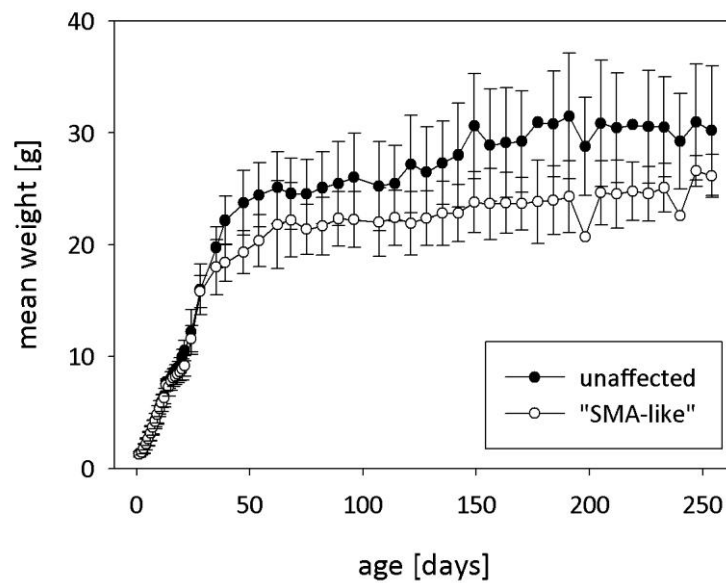
Figure 58 **Weightprogression of unaffected and SMA-like animals having three *SMN2* copies. Within the first 21 days of life mice were weighted daily. Afterwards weight was determined once a week.**

Since only 24 animals were analyzed of which six were used for protein preparation after 100 days no final statement about the medium survival could be drawn. Within a period of 250 days six out of nine unaffected animals died or had to be sacrificed because of open wounds due to continuous biting by their cage mates. Within the group of SMA-like animals two animals passed away after 150 or 180 days, respectively. Another male SMA-like mouse had to be sacrificed at an age of 217 days due to infection of the scrotum. Taken together, no obvious reduction in the survival of SMA-like mice could be observed. These findings were somehow unexpected because determination of SMN protein amounts in the liver and brain in both groups of mice clearly revealed that SMN was declined by 70% in the SMA-like animals (Figure 59).

Summarized, these data suggest that three *SMN2* copies seem to be sufficient to rescue the SMA phenotype in this experimental setup. A closer and more detailed evaluation would be necessary to identify subtle differences which may indicate a very mild SMA phenotype. However, this mouse model is not suitable for any drug testing since an increase in survival could not be applied as an outcome measurement.

(A)

(B)
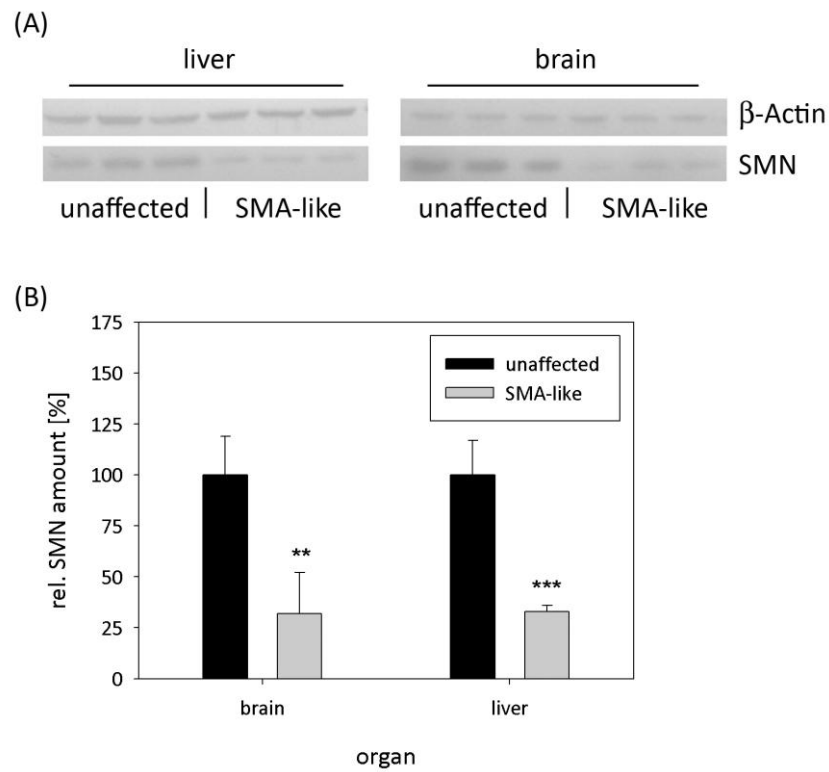
Figure 59   **Analysis of SMN protein levels in unaffected (*Smn*^{+/-}; *SMN2*^{tgUS/tgTW}) and SMA-like (*Smn*^{-/-};**
SMN2^{tgUS/tgTW}) animals. All assayed mice were females and 103 days of age. (A) Western blot
illustrating the reduced SMN amounts in SMA-like mice. Quantified amounts are given
in (B). β-Actin served as loading control. (* = _P_<0.05; ** = _P_<0.01; * = _P_<0.001)**

5. Discussion

Proximal spinal muscular atrophy (SMA) is a unique disorder in the field of human genetics. While the molecular cause of SMA is the functional absence of the *survival motor neuron gene 1* (*SMN1*), the disease severity is modified by a nearly identical copy gene, termed *SMN2* (Brahe 2000; Feldkotter et al. 2002; Lefebvre et al. 1995). In contrast to *SMN1,* which almost exclusively produces full-length transcripts, around 90% of *SMN2* transcripts are lacking exon 7 (Gennarelli et al. 1995; Lefebvre et al. 1995; Lorson et al. 1999). As a result, the SMNΔ7 protein is unable to fullfil its normal function, since it is less capable of oligomerizing and is rapidly degraded (Burnett et al. 2009; Lorson et al. 1998). The critical factor triggering alternative splicing is a translationally silent C to T transition at the beginning of exon 7 (Lorson et al. 1999), which leads to the disruption of an exonic splicing enhancer (ESE) and creates an exonic splicing silencer (ESS) instead (Kashima and Manley 2003; Lorson and Androphy 2000). Consequently, the splice factor SF2/ASF is displaced by hnRNP-A1, which negatively acts on exon 7 inclusion (Cartegni et al. 2006; Cartegni and Krainer 2002; Kashima et al. 2007a). Nevertheless, around 10% of *SMN2* transcripts are correctly spliced, thus giving rise to the fully functional full-length SMN protein (Gennarelli et al. 1995; Lefebvre et al. 1995; Lorson et al. 1999). Therefore, modulation and activation of *SMN2* has, self-evidently, become a major target for SMA therapy. Among the therapeutic strategies tested, activation of *SMN2* and correction of its splicing pattern *in vitro* and *in vivo* by means of HDAC inhibition has turned out to be effective (Brichta et al. 2003; Brichta et al. 2006; Garbes et al. 2009; Hahnen et al. 2006; Riessland et al. 2010; Riessland et al. 2006; Tsai et al. 2008). Especially, the HDAC inhibitor Valproic acid (VPA) has gained particular interest for several reasons: First, VPA is not an experimental drug. It has been used for more than 30 years in epilepsy therapy. Second, the favorable effects of VPA have been demonstrated *in vivo* in a SMA-like mouse model (Tsai et al. 2008). And most importantly, in a first pilot clinical trial with 20 SMA patients, VPA was able to up-regulate blood SMN transcript levels in around $^1/_3$ of tested subjects. In $^1/_3$ of the SMA patients, however, declined SMN levels were recorded, whereas in the remaining $^1/_3$ no change was observed (Brichta et al. 2006). Consequently, the question arose why a certain subset of SMA individuals is positively responding to VPA, whereas others do not. In the present work, the molecular differences between these SMA patients were investigated to reveal the underlying cause.

5.1 SMA-therapy with VPA

The primary aim of this thesis was the identification of the crucial factor(s), which account(s) for the differential response to VPA in SMA patients. Ideally, this factor should be of universal meaning, since e.g. a tissue specific one may help to understand the critical mechanisms, but would not be a feasible biomarker. The big advantage of such biomarker would be that patients could be screened before VPA treatment is started, to avoid futile or even harmfull treatment. At least in a few cancer types, some very first biomarkers for the

response to HDACi were identified. In a panel of 16 NSCLC (Non small cell lung cancer) cell lines, the cytotoxic effects of TSA and SAHA were correlated with the respective expression profiles. It could be demonstrated that the expression of three genes (*NQO1*, *SEC23A* and *PSME2*) indeed correlated with drug sensitivity (Miyanaga et al. 2008). In another study with 18 cancer lines of different origin, another four genes (*STAT1*, *ODC1*, *thymidylate synthetase* and *SKI*) were associated with the sensitivity to the HDACi belinostat (PXD101) (Dejligbjerg et al. 2008). However, within the field of cancer research debate is still ongoing, whether these genes could indeed be considered as general biomarkers for cancer HDACi sensitivity, since an *in vivo* proof is still missing (Stimson and La Thangue 2009). Nevertheless, the identification of such biomarker for SMA therapy with VPA would be a valuable tool to provide the optimal treatment possible to patients, while at the same time avoiding unnecessary side-effects. Furthermore, identification of markers for general VPA responsiveness would have vast implications for treatment strategies of other diseases in which VPA is indicated (e.g. epilepsy).

5.1.1 Fibroblasts and blood: Is the response to VPA the same?

During the first pilot clinical trial with VPA, blood samples from the VPA-treated individuals were taken to analyze the impact on *SMN* mRNA levels (Brichta et al. 2006). In some cases also blood-derived protein data could be collected. However, since appropriate handling and shipping of blood samples could not be guaranteed in all cases, *SMN2* mRNA levels were selected as the major read-out for VPA activity.

From virtually all patients and carriers included in the initial clinical trial fibroblast lines were established from standard skin biopsies. This was done for two reasons: First, for all subsequent experiments enough sample material was needed and this demand cannot be satisfied by blood samples. Second, the fibroblast lines allowed us to test whether the response to VPA treatment correlates between the two tissue systems fibroblasts and blood. In case of a positive result, one may speculate that a similar response may be elicited in the α-motor neurons, which are considered as the actual SMA target tissue.

To investigate whether the response between both tissue systems indeed correlates, all estabilished fibroblast lines were treated with VPA concentrations between 5 and 500 μM. Various doses of VPA were employed, since it could be demonstrated that primary fibroblast lines show striking concentration-dependent differences in their individual response to HDACi treatment (Brichta et al. 2003; Garbes et al. 2009). In conclusion, a likewise response to VPA in blood and fibroblasts could clearly be observed in nine out of 17 cases (Table 15; ML49, ML53, ML68, ML59, ML67, ML71, ML69, ML73 and ML82). In another three fibroblast lines, similar tendencies as in blood were obtained, but unfortunately these results lacked statistical significance (ML75, ML65 and ML60). In contrast to that, four fibroblast lines exhibited a clearly opposite response to VPA than expected from the blood data (ML63,

ML66, ML62 and ML71). Of note, the impact of VPA on SMN levels is rather low compared to other HDACi. While e.g. M344 elevated SMN levels up to 7-fold (Riessland et al. 2006) or LBH589 treatment resulted in 10-fold augmented SMN protein amounts (Garbes et al. 2009), VPA only led to a 2-fold increase maximum (ML67). Therefore, distinction between a positive response and a natural fluctuation was not unambiguous in single cases (e.g. ML60 and ML59). Nevertheless, without any major exceptions, the response to VPA was consistent within the individual cell lines, meaning that e.g. in the case a down-regulation was observed for 50 µM, similar results were obtained for the other two tested concentrations. In the following, additional fibroblast lines were established from SMA patients undergoing VPA therapy. In total, five additional fibroblast lines could be identified, which exhibited concordant results to the *in vivo* blood data (Table 16; ML79, ML86, ML94, ML95 and ML105), whereas in two fibroblast lines opposite results were obtained (ML89 and ML96). Since VPA therapy and sample collection is still ongoing, it could not be decided yet whether *in vivo* and *in vitro* data in another seven cell lines are similar. Nevertheless, once enough additional concordant fibroblast lines are identified, these will be used as a control group to verify data.

The question remained, why only in around 60% of the assayed fibroblasts a clear correlation could be observed. Although a study with SAHA, oxamflamtin and FK228 in cancer therapy suggested a strong correlation between the *in vitro* efficacy and the clinical outcome ($R > 0.75$) (Lindemann et al. 2007), the situation might be different in SMA therapy. It may be conjuctered that tissue-specific expression differences of HDACs (Lucio-Eterovic et al. 2008; Thomas 2009) between blood and fibroblasts may hamper a correlation, since VPA inhibits only class I and class IIA HDACs. Since no full concordance could be observed, it was reasoned that tissue-specific differences in HDAC composition may influence the extent of VPA-mediated *SMN2* induction, but not whether the fibroblasts respond or not. This is further corroborated by the finding that none of the HDACs was found to be differentially expressed between Pos- and Non-Responders by µ-array, implying that discrepant HDAC expression is not the cause for VPA non-responsiveness.

Although caution is needed when *in vitro* findings are extrapolated to *in vivo* data, the obtained concordance of nearly 60% is quite high. Since in several studies going from *in vitro* to a more complex *in vivo* system quite similar effects of VPA could be observed (Michaelis et al. 2004a; Michaelis et al. 2004b), our data coming from the reverse approach, going from the SMA patient to the more simplified fibroblast, is rather solid. Of course, the issue of inconsistent data within the remaining 40% of fibroblast lines needs to be addressed (e.g. ML71, ML62 and ML63). Possible explanations are that the impact of VPA on SMN levels in fibroblasts is much weaker than in blood. This may lead to the false negative identification of patients who exhibited only modestly increased SMN levels in blood as Non-Responders, if they are only evaluated on fibroblast level (e.g. ML60, ML82 and ML79). Such tissue-specific effects on the impact of VPA have been shown in rats. Treatment of these animals with VPA

results in up to 10-fold discrepant monoamine levels in different regions of the brain (Narita et al. 2002), implying that the difference between blood and fibroblasts may lead to such observations. Going into the same direction, it may happen that individual factors influeing the VPA effect on *SMN2* in blood are much more prominent in fibroblast, thus converting e.g. a blood Pos-Responder into a Non-Responder or *vice versa* (e.g. ML62 and ML96). This is of particular importance, since elevation of SMN protein due to HDAC inhibition by VPA is a multi-step process subjected to various regulatory mechanisms. Clear dose-response curves for VPA can be obtained *in vitro* using standardized rat liver lysates (Hahnen et al. 2006) or in blood by measuring glutathione reductase activity (Cotariu et al. 1992). But these measurements directly determine the effect of VPA on the respective enzymatic activity. Since not all tested fibroblast revealed clear dose-dependent effects (e.g. ML71, ML72, ML94 and ML105), additional factors, e.g. the co-repressor and co-activator complexes (Grozinger and Schreiber 2002), interfering with an absolute relation between VPA concentration and SMN protein, must play a role.

5.1.2 Candidate genes for non-responsiveness to VPA: Network or conincidence?

To identifiy the pivotal factor(s) accounting for the differential response to VPA, transcriptome-wide μ-array analysis of fibroblasts was performed. The comparison was designed in such a way that four Non-Responders (ML59, ML69, ML73 and ML82) were compared with five Pos-Responders (ML67, ML72, ML5, ML16 and ML17) in both mock and VPA treated state (Figure 12). This should address the question of which genes are differentially expressed in Pos-Responders versus Non-Responders under VPA treatment? And furthermore, is there an initial gene set-up which, most probably, would account for the observered differences after VPA application? Interestingly, μ-array analysis revealed that, even before the elimination of false-positive hits, the response to VPA treatment in Non-Responders was much lower than in Pos-Responders (Table 17, 977 transcripts vs. 1987 transcripts). After data correction, no single transcript was significantly altered by VPA treatment in Non-Responders, while in Pos-Responders 58 transcripts remained differentially expressed. Although several studies showed that HDACi treatment alters expression of up to 20% of all genes (Mariadason et al. 2000; Peart et al. 2005; Stimson and La Thangue 2009; Van Lint et al. 1996), the relatively small number of 58 transcripts was expected, since long-term VPA treatment of HEK293 merely changed expression of 200 transcripts (Milutinovic et al. 2007) There again, in this study using only one single cell line was used for all experiments. Comparision of several different cell lines or patients normally results in low numbers of differentially expressed genes due to the intraindividual differences. For example, in a study investigating the gene expression profile of six CTCL patients under LBH589 treatment, only 23 genes were identified to be commonly altered, while individual patients exhibited up 1,300 differentially expressed genes (Ellis et al. 2008). The perhaps most exciting finding of the μ-array analysis was that only nine genes were

differentially expressed between untreated Pos- and Non-Responders, which may be the initial set-up accounting for VPA non-responsiveness. Among these, the *RARβ* and three *HOX* genes (*HOXB3*, *HOXD10* and *HOXD11*) were found, suggesting a major developmental factor, which differs between Pos- and Non-Respoders.

To reduce the total number of transcripts to a feasible group, only those were selected for further analysis, which revealed a more than 2-fold expression difference. Subsequently, these were analyzed by qRT-PCR to verify the μ-array data (Figure 12, Appendix Table 25 and Table 26). Of the 18 tested genes, nine could clearly be confirmed, whereas nine gave conflicting results. However, this is a phenomenon typically seen when comparing μ-array and qRT-PCR data, since μ-array easily gives highly significant values when genes are expressed at a low levels (Etienne et al. 2004). For further experiments, a candidate gene approach was carried out by literature mining. Out of the remaining nine, the four candidate genes CD36, RARβ, IGFBP5 and TGFα were selected for further analysis (Figure 13).

Although for none of four the candidate genes any overt function directly linked to VPA has been reported so far, it is easily imaginable that RARβ, IGFBP5 and TGFα may account for the different response to VPA due to their involvement in the control of various biological processes. However, since the VPA Non-Responders also failed to respond to sodium butyrate, it stood to reason that functions related to fatty acids may account for our observation. Therefore, CD36, which is involved in lipid homeostasis as well as TSP1 signalling, was selected in addition. (A detailed description of all four candidate genes is given in 4.1.3.1 to 4.1.3.4 in the results part.)

Since the individual expression patterns of all four candidate genes could well be verified (Figure 14 to Figure 17), the next step was to ask why CD36 and RARβ are higher expressed in Non-Responders, while elevated levels of TGFα and IGFBP5 are present in Pos-Responders. Therefore, the coding regions as well as the 5`- and 3`-UTR of all four genes were sequenced. This was done, since e.g. several SNPs in the coding region or promoter of CD36 have been associated with obesity, insulin resistance (Bokor et al. 2010; Corpeleijn et al. 2006) or even CD36 defiency in Asian and African populations, the so-called Nak[a]-negative blood group (Fry et al. 2009; Yamamoto et al. 1990). Moreover, also for TGFα several haplotypes have been linked to cleft lip or teeth agenesis (Callahan et al. 2009; Vieira 2006). In addition, a SNP upstream of RARβ has been associated with *variant Creutzfeldt-Jakob-disease* (vCJD) (Mead et al. 2009), but it is not clear whether this SNP influences RARβ expression. Futhermore, the detection of SNP could have great impact for post-transcriptionally regulatory mechanism such as miRNAs. For example, it has been shown that IGFBP5 is regulated by the miRNAs miR-140 and miR27a in chondrocytes (Tardif et al. 2009). However, for none of the four genes an association between a certain SNP-type and the expression levels could be detected (Appendix, Figure 61 and Figure 62). Therefore, also an altered miRNA target site can be excluded. In summary, this implied that the differential

expression is caused either by a *cis*-acting element like a SNP located in the promoter or by a *trans*-acting element. While the former can easily be answered by promoter sequencing (which is currently in progress), the identification of *trans*-acting elements is rather complex and requires techniques like EMSA or newly developed methods such as *deconvulution of DNA interactions* (3D) (Nunez et al. 2008). As a first step towards the identifaction of any *cis*-acting elements, ChIP analysis of the promoters of four candidate genes was performed (Figure 22) since it is generally believed that promoter acetylation can serve as a surrogate marker for transcriptional activitiy (Allfrey et al. 1964; Grunstein 1997; Strahl and Allis 2000). Unfortunately, the observed differences were somehow unexpected. While in the Pos-Responders H3K9 acetylation increased after VPA treatment, the opposite happened in Non-Responders. There again, in line with these findings, we could demonstrate that VPA also did not induce *SMN2* promoter hyperacetylation in the Non-Responders or even led to hypoacetylation (Figure 9). Based on these ChIP data, the speculation is attractive, that VPA is not properly working as an HDACi in Non-Responders. This hypothesis corresponds nicely to the observation that no single transcript was differentially expressed in this group under VPA treatment, suggesting that either the Non-Responders are generally resistant to HDAC inhibition or that a VPA specific effect hampers its effects. However, the basal acetylation levels of the candidate promoters did not match with the observed expression pattern. While e.g. IGFBP5 is almost 5-fold higher expressed in Pos-Responders, the promoter seems to be more active in Non-Responders. Therefore, a more refined analysis of these promoters is needed to allow any final conclusion.

Since all four candidate genes are not located in the same chromosomal region (CD36 chr.7q11, RARβ chr.2q24, IGFBP5 chr.2q35, TGFα chr.2p13), the co-seggregation via a common haplotype can be excluded without much doubt. However, since a consistent expression pattern was found along all Non- and Pos-Responders, the question arose, whether one of the four candidate genes is epistatic to the other ones, thus leading to the observed pattern. Therefore, overexpression (Figure 24) and knockdown studies (Figure 23) were performed. This was done to test whether e.g. CD36 knockdown in a Non-Responder reduces RARβ levels and induces IGFBP5 and TGFα expression instead, thus creating the expression pattern of a Pos-Responder. In conclusion, none of the transfection experiments gave a definite hint, whether one of the selected four genes is the crucial factor, which controls expression of the other ones. Indeed, e.g. RARβ levels were doubled by CD36 knockdown (Figure 23) or decreased TGFα amounts had oppositional effects on RARβ expression, but it was not possible to create a gene regulatory network, which properly summarizes all observations. Nevertheless, since interference with one candidate gene altered expression of the others, it may be speculated that e.g. CD36 and RARβ or IGFBP5 and TGFα are not differentially expressed but rather differentially co-expressed. In order to verify this correlation, and to identify the causal determinant, like a common *trans*-regulatory element, a larger set of data is needed (de la Fuente 2010; Tsaparas et al. 2006).

However, RARβ is still the most interesting piece in this network puzzle, since it is typically not expressed in fibroblasts (Redfern and Todd 1992) and has been suggested to regulate CD36 expression (Wuttge et al. 2001). Nevertheless, so far the connecting pieces between the candidate genes could not be uncovered.

Since the candidate network may also include some secondary messengers, the cAMP levels in both Non- and Pos-Responders were determined (Figure 25). cAMP was chosen since it has been shown that VPA influences cellular cAMP levels (Chang et al. 2009; Gallagher et al. 2004; Montezinho et al. 2007). Further evidence came from the observation that IGFBP5 is regulated via a cAMP-responsive-element (Duan and Clemmons 1995) and that CD36 negatively controls the cAMP amounts via the *Src*-kinases (Roberts et al. 2010). Interestingly, addition of Forskolin and IBMX, both of them elevating cAMP by either adenylyl cyclase activation or phosphodiesterase inhibition, led to much higher cAMP levels in Non-Responders than in Pos-Responders. Since basal levels were comparable between both groups, these findings strongly suggested that the regulation of the second messenger cAMP is indeed altered. However, whether there is indeed an impact onto the candidate gene levels is not yet clear.

Moreover, the expression of the four candidate genes was quantified in the blood of VPA treated patients, because initially the expression of at least one of them was intended to be used as a biomarker. Unfortunately, for none of the four candidate genes a consistent picture could be obtained (Figure 19 to Figure 21). Merely a correlation for IGFBP5 between the blood and fibroblast data is suggestive, since all Non-Responders with the exception of ML69, which gives constantly excess values, exhibit lower levels than the Pos-Responders (Figure 20). Because CD36 is also functioning as a scavenger receptor in the innate immune system (Hoebe et al. 2005; Jimenez-Dalmaroni et al. 2009; Means et al. 2009), e.g. bacterial infection may dramatically influence the expression levels, thus explaining the observed CD36 data. TGFα was detected to be more or less equally expressed among all samples analyzed, leading to the speculation that its regulation in blood is different than in fibroblasts. Although RARβ was robustly expressed in fibroblasts of Non-Responders, in the respective blood samples RARβ transcripts could, going in line with the literature, not be detected (Szabova et al. 2003). Taken together, these results indicate that expression of none of the four candidate genes convincingly correlates between blood and fibroblasts. Since the intraindividual differences were too ambiguous, their expression levels cannot be used as a biomarker.

Finally, it was also tried to show the expression differences in CD36, IGFBP5 and RARβ on protein level. Unfortunately, all tested antibodies were of rather poor quality (Figure 18). CD36 was detected to be more or less equally expressed along all tested samples, thus not reflecting the RNA data. Typically, CD36 is heavily glycosylated, shifting its molecular weight from approx 51 kDA to an around 81 kDa heavy isoform (Hoosdally et al. 2009; Rac et al.

2007), which was not recognized by the employed antibody. Therefore, determination of CD36 levels after deglycosylation may lead to a different result. This is of particular importance since the translocation of CD36 to the plasma membrane is controlled by its glycosylation state (Hoosdally et al. 2009). Furthermore, RARβ was also found to be quite uniformly expressed in all tested fibroblast lines, although RNA results suggested up to 20-fold differences. However, since RARβ is barely expressed, qRT-PCR results may appear more drastic than they actually are. At least for IGFBP5 comparable protein and RNA data could be obtained. In fact, the achieved staining is very poor, but the observed band intensities indicate higher expression levels in the Pos-Responders. For TGFα no convincing staining could be obtained by either dot or western blot for all tested antibodies. However, since also for the neoplastic HeLa and HEK293 cells no TGFα signal could be obtained by immunoblotting, the results suggest an antibody problem.

In conclusion, the identified candidates sound quite attractive with regard to VPA Non-Responders. But an underlying network which, as a whole, controls responsiveness to VPA has not yet been identified. Nevertheless, the overexpression and knockdown studies clearly indicate a connection between these genes, although the results are rather cryptically. Sequencing of the candidate genes suggested that expression is most likely controlled by (a) *cis-* or *trans-*acting element(s), which still await identification. Among the tested candidate genes, IGFBP5 is yet the most convincing one, since its expression could be verified on protein level in fibroblasts as well as in the blood of VPA treated patients. However, using this data it cannot be yet explained why VPA Non-Responders exist. There again, the detailed characterization of VPA non-responsiveness may allow inference on the underlying factors. Basically, two possibilities are conceivable why VPA does not induce *SMN2* in Non-Responders: Either these patients or fibroblast lines, respectively, are generally resistant to HDACi treatment or our observation is specific to VPA, implicating a differential uptake or metabolism of VPA in Non-Responders. To address these issues, several experiments were performed, which are discussed in the following.

5.1.3   VPA treatment of Non-Responders: Resistent against HDACi?

VPA is an HDACi that induces also *SMN2* expression (Brichta et al. 2003; Gottlicher et al. 2001; Hahnen et al. 2006; Phiel et al. 2001). There again, several points refused that this is indeed the case in Non-Responders. First, on a transcriptome-wide scale, no single transcript was differentially expressed in Non-Responders. Second, ChIP analysis of the candidate gene promoters indicated that rather hypo- than hyperacetylation is triggered in this group. And most importantly, we demonstrated that in contrast to the Pos-Responders, VPA treatment did not increase H3K9 acetylation at all four previously described *SMN2* promoter regions (Figure 9) in the Non-Responders (Kernochan et al. 2005). Similar to the published data, the highest impact of VPA in Pos-Responders could be detected on HuSP2, while HuSP1 and HuSP3 were modestly affected. Interestingly, acetylation of HuSP4, which is located directly

at the ATG, was, like HuSP2, almost doubled by VPA treatment, suggesting a differential HDAC inhibition by VPA in fibroblasts and NSC-34 cells (Kernochan et al. 2005). In contrast, acetylation of the whole *SMN2* promoter was, with one single exception, reduced by 5 to 25% in the Non-Responders. In conclusion, these data clearly showed that VPA is not acting as an HDACi in Non-Responders. One may argue, that other genes typically induced by VPA, like *MMP2* or *GAD67*, were not directly assayed by qRT-PCR or ChIP (Gavin et al. 2009; Milutinovic et al. 2007), but this is refused by our μ-array analysis, which revealed that the expression of no single transcript was alterd by VPA treatment.

However, the lacking induction of *SMN2* expression in Non-Responders can easily be explained by the finding that VPA does not induce promoter hyperacetylation. At least two scenarios are conceivable why VPA does not induce *SMN2* promoter hyperacetylation. Either VPA is for any purpose not available as an HDACi in these cells, or the Non-Responders are generally inert to HDACi treatment. To test whether the latter hypothesis holds true, Non-Responders were treated with the well-known HDACi sodium butyrate, phenylbutyrate and LBH589 (Figure 10) (Andreassi et al. 2004; Andreassi et al. 2001; Garbes et al. 2009). Interestingly, it turned out that the Non-Responders are not generally resistant to HDACi treatment, but rather do not respond to a certain subset of HDACi. While the hydroxamic acid HDACi LBH589 and the aromatic fatty acid phenylbutyrate robustly increased SMN levels, the short-chain fatty acids VPA and Sodium butyrate failed to do so. Both VPA and sodium butyrate, which exhibited a comparably low HDAC inhibition potential (Bertrand 2010; Catalioto et al. 2009; Hahnen et al. 2006), have been suggested to enter the cell in a dual way by diffusion as well as active transport (Adkison and Shen 1996; Roy et al. 2006). Since both are short-chain fatty acids, it is conceivable that the uptake of the two is impaired or lowered to such extent in Non-Responders that they do not inhibit HDACs. To finally clarify whether being a VPA Non-Responder is specific to the lack of HDAC inhibition or whether general VPA effects are absent, another indicator of VPA´s activity was needed. Since it has been reported that VPA dose-dependently inhibits the cAMP-dependent protein kinase A (PKA) (Boeckeler et al. 2006; Chang et al. 2009), its catalytic rate was quantified in both Pos- and Non-Responders. Determination of PKA activity in Pos-Responders revealed, as expected, a dose-dependent decline in activity down to 65% minimum at 1 mM VPA (Figure 11). In contrast, the opposite result was detected in all three tested Non-Responders with even a 20% elevation in ML103. However, VPA does not directly inhibit the PKA, but rather influences the cellular cAMP content by activating the adenylyl cyclases (AC) and inhibiting the phosphodiesterases (PDI) (Chang et al. 2009; Gallagher et al. 2004; Montezinho et al. 2007). To test whether VPA influences PKA activity by alteration of cAMP homeostasis in Pos- and Non-Responder, cellular cAMP levels were determined by ELISA (Figure 25). Although not signifant, cAMP levels were lowered, as expected, by 20% in Pos-Responders. Contrariwise, cAMP amounts remained unchanged or slightly increased in Non-Responders, which matched to the PKA activity experiments. Taken together, this gives good

evidence why the PKA is not inhibited in Non-Responder. Since the two unrelated read-outs PKA and HDAC both indicated that VPA is not triggering its normal function, it may speculated that either VPA is not taken up by the cell or rapidly exported or completely metabolized into an inactive form. The hypothesis of a VPA or short-chain fatty acid HDACi specific effect is further strengthened by the finding that both LBH589 and phenylbutyrate resulted in the expected increase in SMN protein.

Similar to SMA, the phenomenon of VPA Non-Responders is also well-known in epilepsy therapy (Holland et al. 2010; Ollivier et al. 2009). But the underlying cause has not been identified yet. The experiments presented in this thesis, using VPA-treated SMA fibroblasts, give a first hint that perhaps a differential VPA metabolism (including uptake, conversion and disposal) may account for this observation. However, since so far neither differential uptake of HDACi or SCFA between individual fibroblasts lines has been reported, further experiments are needed to determine the responsible factor.

5.1.4 HPLC-MS/MS: Any differences in VPA uptake or metabolism?

Regardless, whether e.g. IGFBP5 controls CD36 expression or not, the question remained unanswered why Non-Responders do not react to VPA treatment. Since both ChIP analyses (Figure 9) as well as the PKA activity assay (Figure 11) indicated that VPA is not eliciting its normal inhibitory effect, the most obvious speculation was that VPA is simply not taken up by Non-Responders fibroblasts.

To investigate whether VPA is indeed differentially taken up into Non-Responder fibroblasts, a HPLC-MS/MS assay was set up to quantify the amount of VPA. The basic procedure, which includes a pre-column derivatization of VPA and its metabolites, was originally published for human blood plasma (Cheng et al. 2007), but adopted by us for primary fibroblasts. Although a couple more straight-forward methods have been published (e.g. (Deng et al. 2006; Matsuura et al. 2008)), the derivatization method was chosen, since it gave the highest sensitivity. First experiments using pure VPA and its hepatoxic metabolite 4-ene VPA (Cheng et al. 2007; Rettie et al. 1987; Silva et al. 2008) gave promising results corresponding well to the published data (Figure 28). Therefore, treated fibroblasts were analyzed in a kinetic experiment (Figure 29). While VPA could easily be quantified in the cell culture medium, barely any VPA signal was obtained for the corresponding cells. Moreover, 4-ene VPA could not be detected in any sample, since signal intensities were always below the signal for untreated cells, which was set as threshold. This suggested that the intracellular VPA concentrations are negligible. However, this conclusion is refused by the finding that VPA inhibits HDACs *in cellulo* (Eyal et al. 2005; Kernochan et al. 2005) with an IC_{50} between 1.5 and 7.9 mM (Eyal et al. 2005; Hahnen et al. 2006). Therefore, in a Pos-Responder at least VPA concentrations in the micromolar range should be detected. Hence,

the most likely explanation is that the cellular background coming from the derivatization of whole-cell-lysates is too high to allow efficient determination of VPA.

To test whether CD36 facilitates VPA import into the cell, HEK293 cells overexpressing CD36 were incubated with 10 µM or 1 mM VPA and the intracellular VPA content was measured (Figure 30). Based on the previous observations, VPA was quantified without derivatization, although this reduced sensitivity of the assay. In conclusion, for none of the analyzed samples a clear increase after VPA stimulus could be obtained, suggesting that CD36 is not participating in VPA transport. Further evidence came from the observation that MCT1, 2 and 4, which have been demonstrated to mediate butyrate transport (Roy et al. 2006), were not differentially expressed between Pos- and Non-Responders (Figure 33A). Taken together, these data implied that VPA rather slowly enters the fibroblasts via diffusion, although an active in- and export has been proposed at least for brain and choroid plexus (Adkison and Shen 1996; Gibbs et al. 2004; Naora et al. 1996). Furthermore, the metabolism of VPA was compared in Pos- and Non-Responder. Typically, 30-50% of a VPA dose appear in the urine as a glucoronide conjugate (Booth et al. 1996), while approx. 40% undergo mitochondrial β-oxidation. The remaining 15-20% are eliminated by other oxidative mechanisms (Silva et al. 2008). The vast majority of mitochondrial oxidation of VPA is facilitated by the P450 enzyme system, which catalyzes the formation of metabolites like 3-hydroxy-VPA, 3-oxo-VPA (Bjorge and Baillie 1991) or 4-ene VPA (Rettie et al. 1987). To determine whether differential formation of metabolites occurs between Pos- and Non-Responders, a shading assay was performed, which allows easy graphical identification of discrepancies (Figure 31) (Grundemann et al. 2005). Unfortunately, no obvious differences in VPA metabolism could be observed between VPA treated Pos- and Non-Responders in the mass-range up to 400 amu (atomic mass unit), which includes all oxidized VPA metabolites. The only overt discrepancy was found at 4.28 min and 192.2 amu. But since no additional peak could be detected for either the deuterized or undeuterized VPA, this signal could be excluded as a direct VPA metabolite. Moreover, addition to VPA to both Pos- and Non-Responders did not lead to the identification of any difference at all suggesting that no VPA has been taken up. Again it may be speculated about the underlying reasons. The most likely cause may be again the cellular threshold. Nevertheless, the only way to overcome this stumpling block would be to dramatically scale up the whole sample preparation to such extent that the signals clear excel the background. On the other side, it is also conceivable that the vast majority of internalized VPA is directly conjugated to Co-enzyme A (Aires et al. 2007) or carnitine (Silva et al. 2001). But these conjugates are out of the experimental detection range.

Taken together, the HPLC-MS/MS experiments did not lead to the identification of a differential VPA uptake or metabolism in Pos- and Non-Responders. Although identification of VPA and its metabolites has been published several times in urine or blood plasma, its quantification in fibroblasts turned out to be rather challenging.

5.1.5 VPA-therapy: Can a Non-Responder be turned into a Pos-Responder?

The most important question in terms of SMA therapy with VPA is whether it is possible to make a Non-Responder responding to VPA? And, is this achievable in such a way that could also be used in clinics? One popular example for such factor is the treatment of chronic hepatitis type C: While it is possible to treat patients in monotherapy with interferon-α, it has been shown that combined therapy of IFN-α and the virostatic ribavarin of INF-α Non-Responders results in sustained responses (Schalm et al. 1999).

To finally identify the determinant of VPA non-responsiveness, two different approaches were conducted. First, CD36, IGFBP5 and TGFα were knocked down and VPA was added to investigate whether any of the candidate genes impedes VPA mediate *SMN2* induction (Figure 26 and Figure 27). Interstingly, it turned out that knockdown of CD36, irrespective of whether VPA was added or not, completely deplets SMN from the cell by reducing *SMN* transcription. Since CD36 is a cell surface receptor (Hoosdally et al. 2009), a direct effect on *SMN* transcription is rather unlikely. However, TSP1 signalling is transmitted via CD36 and the *Src*-kinases. And at least in bone remodelling, a functional connection between SMN and *Src*-signalling has been proposed, which may explain the observed *SMN2* mRNA decline (Shanmugarajan et al. 2007). In contrast, knockdown of IGFBP5 post-transcriptionally increased SMN levels by more than 100% in the Pos-Responder ML73, whereas the effect was not so pronounced in ML82. Very recently, it has been shown that injection of a vector encoding IGF-1 increases life-span and weight of SMA-like animals, suggesting that IGF-1 modulation by IGFBP5 may cause the increase in SMN levels (Shababi et al. 2010a). Especially, since the effect of IGFBP5 knockdown was much more pronounced in ML82 when VPA was added, one may speculate that blocking of IGF-1 by IGFBP5 is indeed a possibility to convert a Non-Responder into a Pos-Responder.

The other trace followed was whether constitutive high CD36 levels have any impact on general fatty acid uptake. To this aim, LCFA uptake was quantified using a BODIPY-FA analogue (Figure 32). As expected from the CD36 expression data, Non-Responders tended to import more FA than Pos-Responders. This effect was even pronounced when VPA was added. However, addition of retinoic acid (RA) unexpectedly decreased FA uptake, although it has been published that it increases CD36 levels (Wuttge et al. 2001). Moreover, addition of SSO, a CD36-specific inhibitor (Coort et al. 2002), dramatically increased the amount of internalized BODIPY-FA. Both results from SSO and RA strongly suggested that CD36 is rather functioning as a FA exporter than importer in the tested fibroblasts. But to finally prove this hypothesis, up-regulation of other fatty acid handling proteins has to be excluded, and furthermore the fatty acid export itself has to be investigated in an appropriate experiment. Nevertheless, it was tested whether inhibition of CD36 via SSO *in vitro* turns a Non-Responder into a Pos-Responder (Figure 34). Although the western blot data are suggestive to state that this hypothesis is true, the negative effect of SSO itself on SMN levels has to be

taken in account. Furthermore, it has been suggested that SSO itself interferes with mitochondrial β-oxidation (Coort et al. 2002), which also may have implications for VPA metabolism. In addition, treatment of fibroblasts with Oligomycin D, an antibiotic, decoupling ATP-generation (Lardy 1980), had no boosting effect on FA internalization (Figure 32). This indicated that coupling between oxidative phosphorylation and FA uptake is very weak, thus FAs are no major source of energy in the assayed fibroblasts. In line with this, the expression levels of lipogenic protein PPARγ were not linked to elevated CD36 levels in all tested cell lines (Figure 33) (Zhou et al. 2008).

Interestingly, expression of CPT1C was found to be almost twice as high in Non-Responders as in Pos-Responder (Figure 33). CPT1C is of particular interest, since it has been speculated, but not yet proven, that CPT1C may catalyze the transfer of activated VPA-CoA to carnitine (Lheureux et al. 2005; Silva et al. 2008). This process is of fundamental importance for the β-oxidation of VPA, since formation of Carnityl-VPA at the outer mitochondrial membrane allows VPA to pass the inner mitochondrial membrane via the carnitine-acylcarnitine translocase (CACT). Once inside the the mitochondria, CPT2 catalyzes the reverse reaction from Carnityl-VPA to VPA-CoA (Silva et al. 2008). The detection of elevated CPT1C levels suggests that VPA may not elicit its inhibitory function in Non-Responders, since it is more rapidly transferred onto carnitine. However, this still needs to be proven.

5.1.6 Future aspects: Tackling VPA Non-Responder

The data discussed so far shed first light on the underlying cause of VPA non-responsiveness in SMA therapy. However, a bunch of fundamental questions remain. Perhaps the most important one is whether the identified candidate genes are indeed responsible for the occurance of VPA Non-Responder or whether they were just found by coincidence. Though, to answer this question a better understanding of the role of each candidate in VPA uptake and metabolism is needed.

Among the selected candidates, CD36 was the most overt one, since it is facilitating LCFA transport (Abumrad et al. 1993; Coburn et al. 2000; Endemann et al. 1993). Given that inhibition of CD36 mediated FA transport by SSO not convincingly turned a Non- into a Pos-Responder (Figure 34), it is still questionable whether the increased CD36 amounts found in Non-Responders indeed account for a differential VPA uptake or metabolism. On the other side, CPT1C, which catalyzes the formation of Carnityl-VPA (Lheureux et al. 2005; Silva et al. 2008), has been found to be higher expressed in Non-Responders than in Pos-Responders. Since ChIP as well as the PKA assay both indicated that VPA is not eliciting its typical inhibitory function, one may speculate about a more rapid formation of Carnityl-VPA in Non-Responders. This may sequester VPA, which is in Pos-Responders typically available for HDAC inhibition. To clarify this issue, several points have to be addressed: Perhaps the

easiest question to answer is whether the increased CPT1C expression indeed hampers *SMN2* induction by VPA? And if the answer is yes, are indeed higher Carnityl-VPA amounts present in Non-Responders? Furthermore, is there a link between CD36 or any other candidate gene and CPT1C?

Nonetheless, so far this work has been focused on the function of CD36 as a fatty acid transporter. Though, this is only part of the story since CD36 also functions as a receptor of thrombospondin-1 (TSP1). Since TSP1-signalling is mostly involved in angiogenesis, a direct connection from thrombospondin signalling to the response to VPA is rather vague. However, it has been shown that VPA treatment up-regulates TSP1 amounts *in vitro* (Cinatl et al. 2002), which then triggers via CD36 signalling proteins like p59[fyn], caspase 3 and the p38 MAPK cascade (Jimenez et al. 2000). Therefore, it is also needed to investigate whether increased TSP1-signalling in Non-Responders suppresses the response to VPA.

Another very interesting candidate is IGFBP5. Recently, it has been demonstrated that IGF-1, which is bound by IGFBP5, ameliorates the phenotype of SMA-like mice (Shababi et al. 2010a). Since knockdown of IGFBP5 increased SMN levels post-transcriptionally, it is conceivable that IGF-signalling may impact SMN levels. Although no differential expression of either IGF-1 or IGF-2 could be detected by μ-array analysis, up to 5-fold expression differences of IGFBP5 may alter the ratio of free to bound IGF. Therefore, it might be worth to also have a look on IGF protein, ternary complex formation (Ning et al. 2006) or downstream signaling molecules. Furthermore, one may test whether addition of IGF-1 or -2 or recombinant IGFBP5 alters SMN amounts in cell culture in Non- and Pos-Responders.

Moreover, the cause for the differential expression of all candidate genes is not yet known. Since it is not certain that promoter sequencing will lead to the identification of (a) SNP(s), which is associated with the response to VPA, one may also have a look for other *cis*-acting elements or test for the differential expression of miRNAs by qRT-PCR. Another still unclear issue is the question which of the four candidate genes is cause and which one is consequence. Although neither knockdown nor overexpression experiments gave a definite hint about the underlying mechanisms so far, one may still think about an epistatic regulator of the other three candidate genes. Therefore, the identifaction of a SNP, a *cis*- or *trans*-acting element may help to decipher the underlying network.

Although speculative yet, the finding of the determinant, which makes up the differences between a VPA Pos- and a Non-Responder would not only have an impact SMA therapy but would also have fundamental implications for e.g. epilepsy therapy. If the association between the determinant and the response could be verified in our control group, one may propose that it serves as a biomarker for VPA non-responsiveness in general. This biomarker could then be tested in epilepsy VPA Non-Responders to investigate whether the association holds true. Taken together, this would be a first step towards a tailor-made individualized VPA therapy, which eliminates the possibility of an unnecessary treatment. Moreover,

depending on nature of this factor, one may think about specific inhibitors or activators which can be given as a supplement to VPA therapy.

Nevertheless, even though there may be some compounds which *in vitro* can turn a VPA Non- into a Pos-Responder, *in vivo* confirmation will be needed. This may lead to a dilemma that the cause why somebody is not responding to VPA is known, but it is not possible to overcome this non-responsiveness. Therefore, the search for novel SMA drugs has to be continued. Since several HDACi like M344 or SAHA gave good read-outs *in vitro* as well as *in vivo*, it is self-evident to also test novel, far more potent HDACi second generation HDACi like e.g. LBH589.

5.2   Identification of LBH589 as a potential SMA drug

The experiments discussed so far emphasize the urgent need of potential SMA drugs. Since the analysis of HDACi as potential SMA therapeutics gave every single one promising results *in vitro* and *in vivo*, the second generation HDACi LBH589 was selected for further analysis for several reasons (Brichta et al. 2003; Brichta et al. 2006; Hahnen et al. 2006; Riessland et al. 2010; Riessland et al. 2006). First, *in vitro* studies as well as pre-clinical trials convincingly demonstrated its huge potency in inducing apoptosis in neoplastic enteties (Atadja 2009; Ellis et al. 2008; Prince et al. 2009; Shao et al. 2010). Second and most importantly, LBH589 already achieved orphan drug status for the treatment of CTCL by the FDA in 2007. Currently, more than 80 clinical trials are ongoing to expand the therapeutic spectrum from LBH589 onto additional types of cancer.

5.2.1   LBH589: A feasible drug to up-regulate SMN?

To test whether LBH589 is able to induce *SMN2*, initially a kinetic experiment was performed to establish the optimal treatment conditions. It turned out that treatment for 64 h at concentration between 100 nM and 1 µM gave the best results. Already concentrations of around 200 nM were sufficient to significantly increase SMN levels more than 5-fold (Figure 36). Moreover, SMN amounts were up to 10-fold increased at concentrations of 500 nM or 1 µM LBH589 in some cases. This of particular relevance, since compared to other HDACi the observed *in vitro* effect of LBH589 on SMN levels is the strongest reported so far (Avila et al. 2007; Brahe et al. 2005; Brichta et al. 2003; Hahnen et al. 2006; Riessland et al. 2006). While e.g. SAHA, another second generation HDACi, increases SMN levels in *SMN1*-deleted fibroblasts approx. 3-fold in the low micromolar range (Hahnen et al. 2006), 10-fold lower doses of LBH589 are required to induce a similar effect. Noteworthy, the HDACi M344 induced similar to LBH589 up to 7-fold elevated SMN amounts. However, high M344 concentrations of more than 50 µM turned out to be toxic (Riessland et al. 2006). In contrast, toxic side effects of LBH589 were only recorded for concentrations higher than 750 nM while 400 nM already fairly induced SMN production

6-fold (Figure 40). Of note, the observed up to 10-fold elevation of SMN protein is of such a high extent that almost theoretical levels of an unaffected carrier are reached.

One may speculate whether, as it has been shown previously for VPA, the effect of LBH589 is depending on the number of *SMN2* which are potentially activated (Brichta et al. 2003). Although suggestive, rather the opposite could be observed. While ML5, which is derived from a SMA type II patient having three *SMN2* copies, showed up to 4-fold increased SMN levels at maximum, both cell lines derived from type I patients exhibited more than 7-fold elevated SMN amounts irrespective of whether they carry two *SMN2* copies like ML17 or three *SMN2* copies like ML16 (Figure 36). There again, since all fibroblasts treated with VPA and LBH589 in parallel were, with the exception of ML82 (type IIIa), derived from SMA type II patients. This suggests that rather an individual factor than a correlation with the basal SMN levels is accounting for the observed differences in the response to LBH589.

Since previous results with VPA clearly demonstrated that within the group of SMA patients some are VPA Non- or Neg-Responder, the question arose whether the same phenomenon could be observed in LBH589 treatment. This is of particular importance, since the occurance of HDACi Non-Responder is not unique to VPA. Similar findings also have been obtained with MS-275 in several colon cancer models (Bracker et al. 2009). Though, it may be argued that the differences between the individual models are responsible for the discrepant therapeutic outcome. Nevertheless, also in LBH589 therapy of CTCL patients both Non- and Pos-Responders have been observed *in vivo* (Ellis et al. 2008). To follow up this issue, fibroblasts derived from VPA Pos-, Non- and Neg-Responder were treated with escalating LBH589 concentrations (Figure 39). It could be demonstrated that in all assayed fibroblast lines LBH589 increased SMN levels more than 2-fold. However, these data conjectured that the response to VPA may have an impact also on the effect of LBH589. While in Neg- and Non-Responder (ML73, ML79 and ML82) SMN was elevated modestly 2- to 4-fold, in both VPA Pos-Responder the effect was much more pronounced. Especially in ML67, which exhibited doubled SMN amounts under VPA treatment, LBH589 augmented SMN levels almost 10-fold. Since the underlying cause of VPA non-responsiveness is not known yet, it remains speculative which factor accounts for the observed discrepancy.

The data discussed so far were exclusively produced with *SMN1*-deleted fibroblasts. Even though the results were promising, it had to be proven that LBH589 also induces *SMN2* expression in other systems. Therefore, human neural stem cells (NSC) derived from epilepsy surgeries were treated with LBH589 (Figure 42) as well. It could demonstrated that both employed LBH589 concentrations increased SMN levels up to 4.5-fold. This verified that LBH589 is not only active in dermal fibroblasts, but also in neural tissue, which is the actual SMA target tissue. Moreover, treatment of murine embryonic fibroblasts derived from SMA-like mice (Hsieh-Li et al. 2000) resulted in up to 18-fold elevated SMN amounts indicating that LBH589 is also active in a murine context (Figure 41). To finally prove that LBH589 is a

promising candidate for SMA therapy, it was examined *in vivo* by sub-cutaneous injection of mice (Figure 41). Analysis revealed that both SMN protein and mRNA were elevated in the CNS of treated mice (Figure 43). Furthermore, histone acetylation was increased by 40% in the brain of LBH589 injected mice indicating that LBH589 is able to cross the blood-brain-barrier (Figure 43).

Taken together, these experiments addressed some very important aspects of a putative SMA drug. First, LBH589 is active *in vitro* in neural tissue. And second, LBH589 elicits its beneficial effects also *in vivo* for at least 24 h, although the half-life of LBH589 in mice is relatively short (IV $t_{1/2}$ = 1.37 hrs, oral $t_{1/2}$ = 2.90 hrs) (Atadja 2009; Otaegui et al. 2009). Since in humans a half-life of around 16 to 17 h for LBH589 was determined (Geng et al. 2006), *SMN2* activation in humans may be far more long-lasting. Furthermore, these data implicate that LBH589 crosses the murine blood-brain-barrier. Several clinical trials are ongoing evaluating the potency of LBH589 in the treatment of brain glioma, indicating that it is also able to cross the human blood-brain-barrier. In conclusion, LBH589 fullfills all prerequisites required for a more detailed evaluation in SMA-like mice. Moreover, compared to other small compounds tested for SMA therapy, the *in vitro* effect of LBH589 was tremendously stronger. Therefore, we investigated in detail the underlying cellular mechanism, which are altered by LBH589. The deeper understanding of these may help to develop therapeutic approaches targeting intermediate steps in the LBH589 cascade. First, *SMN2* mRNA under LBH589 treatment was investigated. And second, SMN protein under LBH589 treatment was tested.

5.2.2 *SMN2* mRNA: Promoter induction, splicing or both?

The tremendously increased SMN protein amounts under LBH589 may, among others, be explained by a strong induction of the *SMN2* promoter. To follow up this issue, ChIP analysis was performed to compare the effect of LBH589 to other well-known HDACi. Since ChIP analysis of the *SMN2* in LBH589-treated fibroblasts revealed results similar to those reported for VPA or SAHA in NSC-34 cells (Kernochan et al. 2005), promoter induction was excluded to account for the observed SMN protein levels. Nevertheless, since promoter acetylation was increased with the highest impact on HuSP2 (+220%) and HuSP3 (+170%), we also quantified promoter activity by using a *SMN2* promoter reporter cell line (Jarecki et al. 2005). By treating this cell line with escalating LBH589 concentrations, it could be demonstrated that already concentrations of around 200 nM LBH589 increased *SMN2* promoter activity 2-fold. At 300 nM maximal promoter activity of around 2.2 au was reached, which was not further elevated by higher LBH589 doses. Using these data an EC_{50} concentration of 108 nM was calculated. Surprisingly, this matched the IC_{50} of 106 nM concentration determined for LBH589, suggesting a 1:1 stoichiometry between HDAC inhibition and promoter activity at the *SMN2* promoter (Appendix, Figure 64 and Figure 65).

However, elevation of SMN protein amounts by HDACi treatment is not a sole consequence of *SMN2* promoter activation, but rather the result of various factors coming together. For example, it has been demonstrated for VPA and M344 that also hTRA2-β1 is increased, which consequently leads to a reversion of the *SMN2* splicing pattern (Brichta et al. 2003; Riessland et al. 2006). We analyzed *SMN2* expression and splicing under LBH589 regimen and could show that both *FL-SMN2* and *SMN2Δ7* give a common picture in various LBH589-treated fibroblasts. While *FL-SMN2* was elevated 2-fold, *SMN2Δ7* remained unchanged or even decreased. This resulted in a reversion of *SMN2* splicing pattern towards the beneficial *FL-SMN2* transcript. However, although this data indicated a shift in *SMN2* splicing, the conclusion that LBH589 fully restores correct *SMN* splicing is wrong. Since *SMN2* typically gives rise to around 10% *FL-SMN2* (Gennarelli et al. 1995; Lefebvre et al. 1995; Lorson et al. 1999) a doubling in its amounts implies 20% *FL-SMN2* from *SMN2* are generated, while 80% are still incorrectly spliced. Therefore, one would suppose that LBH589 ameliorates the SMA phenotype but not lead to a complete rescue. Nevertheless, to identify the splice factor accounting for this observation, several splice factors known to influence *SMN* splicing were tested (Singh 2007), but only hTRA2-β1 was found to be elevated. Based on this observation, we assayed the role of hTRA-β1 in LBH589 treatment by time-course experiments (Figure 45A, B) and knockdown studies (Figure 45C, D). In summary, it turned out that hTRA-β1 is indispensable for the efficient up-regulation of SMN protein by LBH589, since it facilitates the reversion of the *SMN2* splicing pattern. In contrast to the protein levels, mRNA amounts were significantly decreased for all assayed splice factors. Although this sounds contradictionary, these results were not unexpected. The observed discrepancy is most likely a result of the auto-regulatory feedback by which SR protein levels are controlled (Ni et al. 2007). For example, it has been demonstrated that high hTRA2-β1 amounts promote inclusion of an exon containing a premature stop codon into its own mRNA. This triggers *Nonsense-mediated mRNA decay* (NMD) of the transcript by which hTRA2-β1 protein amounts decline in the following (Mattox and Baker 1991; Stoilov et al. 2004). Based on this one may argue that the increased hTRA-β1 amounts led to the decrease mRNA amounts, whereas in the case of SF2/ASF and SRp20 the declined transcript levels already led to normalization of protein amounts.

Furthermore, the stability of the *SMN* mRNAs was assayed with Actinomycin D, since an enhanced mRNA half-life under LBH589 treatment would allow to more often translate one and the same mRNA (Figure 48). For example, the impact of HDACi on mRNA has been demonstrated using the examples TSA and Sodium butyrate, which decreased *claudin-1* mRNA stability whereby less protein was produced (Krishnan et al. 2009). However, no stabilizing or destabilizing effect on any of the tested mRNAs of LBH589 could be observed. Unlike previously reported data, which stated comparable half-lifes for *FL-SMN2* and *SMN2Δ7* of around 5 to 6 h in primary fibroblasts (Heier et al. 2007), in our experimental setup $T_{1/2}$ for *FL-SMN2* was approx. 8.5 h whereas *SMN2Δ7* had a half-life of around 11 h.

Though, most probably these differences were due to inter-individual differences between fibroblast lines used.

Taken together, the analysis of *SMN2* expression showed that LBH589 increases SMN levels by two ways: *SMN2* expression is induced via H3K9 hyperacetylation of the *SMN2* promoter plus a reversion of the *SMN2* splice pattern by increased hTRA2-β1 amounts. Furthermore, it could be demonstrated, that hTRA-β1 is the splice factor facilitating reversal of the *SMN2* splicing pattern and that *SMN2* mRNAs are similarly stable. In summary, the effect of LBH589 on *SMN2* mRNA is comparable to that of other HDACi reported. Therefore, the additional effect, which leads to 12-fold increased protein amounts, has to act on protein and not on RNA level.

5.2.3 SMN protein: More or less breakdown?

A common way to control protein abundance is to regulate its turnover. SMN is degraded via the ubiquitin-proteasome-system (UPS) (Burnett et al. 2009; Chang et al. 2004; Hsu et al. 2010). We initially tested whether inhibition of the proteasome by MG-132 in LBH589 treated cells leads to an additional elevation of SMN protein. While in mock treated cells MG-132 application increased SMN protein 2-fold, no such effect was detected when proteasomal SMN degradation was attenuated in fibroblasts under LBH589 treatment (Figure 49). This finding suggested that SMN protein turnover is indeed altered by LBH589. Hence, two possibilities arose how this is achieved. On the one hand LBH589 could, similar to MG-132, have an inhibitory effect on the proteasome. On the other hand, ubiquitinylation of SMN could be reduced. To test the former hypothesis, proteasomal degradation (Kisselev et al. 1999) in fibroblasts was quantified by a luciferase-coupled assay. In contrast to e.g. NVP-LAQ824, which reduced chymotrypsin-like proteasomal activity (Catley et al. 2003), no inhibitory effect of LBH589 on the proteasome could be detected (Figure 50). There again, clinical trials led to the observation that LBH589 boosts the effect of the protesome inhibitor bortezomib (e.g.(Ocio et al. 2010)). One popular line of explanation for this observation is that LBH589, similar to SAHA (Mitsiades et al. 2004), affects expression of proteasomal subunits, by which the cell becomes more prone for enhanced global protein degradation. In line with this, we observed an elevated global protein ubiquitinylation, but at least SMN seemed to remain spared. By precipitation of polyubiquitinylated proteins, we were able to prove that indeed SMN ubquitinylation was decreased by 70% (Figure 51). Purity of the precipitate was assured by staining against ODC, a protein which is known not to be ubiquitinylated (Zhang et al. 2003). Since ubiquitinylation of SMN is a prerequisite for its degradation, the detected reducing should consequently reduce its turnover, thus leading to a steady accumulation of SMN over time. This observation was somewhat surprising, since it is generally believed that HDACi treatment enhances protein degradation either directly by increasing non histone protein acetylation or indirectly by modulation of components of the ubiquitinylation machinery (Caron et al. 2005). For example, it has been

shown that both VPA and TSA enhance expression of the E2 ubiquitin conjugase Ubc8, by which ubiquitinylation of their substrates is enhanced (Kramer et al. 2003). Since the UCHL1, the enzyme fascilitating SMN ubiquitinylation (Hsu et al. 2010), was not identified at that time, it was argued that an enhanced SMN complexation may account for our observations. Several lines of evidence supported this hypothesis: First, it has been reported that incorporation of SMN into the SMN complex increases its half-life from around 4 to 15 h (Burnett et al. 2009); presumably by protecting SMN from UCHL1. Second, the time-course experiment clearly showed that *SMN2* expression remained the same, while SMN protein steadly increased, suggesting that SMN accumulates over time due to a decreased turnover. Although investigation of PKA activity, which is associated with SMN complexation (Burnett et al. 2009; Jablonka et al. 2007; Majumder et al. 2004), did not reveal an increase in PKA activity, SMN complexation may still be enhanced, since a third line of evidence came from fluorescent microscopy experiments. We counted gems in LBH589-treated fibroblasts and were able to show that, corresponding to the elevated expression of Gemin2 and -3 (Figure 38), the overall portion of fibroblasts containing gems increased as well as the number of cells containing multiple gems (Figure 37). Since the two Gemin2 and -3 directly bind to SMN inside the SMN complex (Pellizzoni 2007) and are furthermore both co-regulated with SMN (Feng et al. 2005), it was suggested that an enhanced SMN complex formation under LBH589 treatment keeps SMN out of the UPS by which SMN accumulates over time.

In conclusion, these data give a very detailed insight how the tremendously increased SMN amounts under LBH589 treatment come off. Besides transcriptional activation and splice pattern correction, LBH589 also stabilizes the SMN protein by increased complexation. Although these mechanical data were reported here for the first time, this mechanism must not exclusively apply to LBH589. Since it has been shown that TSA, SAHA and VPA, which all have been tested as SMA drugs (Avila et al. 2007; Brichta et al. 2003; Brichta et al. 2006; Hahnen et al. 2006; Riessland et al. 2010), interfere with proteasomal degradation (Kramer et al. 2003; Mitsiades et al. 2004) one may speculate that these HDACi may elicit a similar effect. However, this still needs to be proven.

5.2.4 Future aspects: LBH589, JnJ-26481585 or even Bortezomib?

In summary, a quite large number of small molecules have been identified within the past years, which positively influence the SMA phenotype. Among these, the six HDACi, VPA (Brichta et al. 2003; Brichta et al. 2006), sodium butyrate (Chang et al. 2001), phenylbutyrate (Brahe et al. 2005), SAHA (Hahnen et al. 2006; Riessland et al. 2010), TSA (Avila et al. 2007) and M344 (Riessland et al. 2006) have been successfully tested and have given promising results. Hence, why is a 7th HDACi like LBH589 needed? The answer is quite simple: *In vivo* studies with VPA in SMA patients only gave moderate effects and not all patients responded positively (Brichta et al. 2006; Swoboda et al. 2009; Weihl et al. 2006). A similar outcome was observed in phenylbutyrate treatment of SMA patients (Brahe et al. 2005; Mercuri et al.

2004). Even though, novel HDACi like SAHA (Riessland et al. 2010) and TSA (Avila et al. 2007) also proved their effectiveness in SMA-like mice, the questions remain whether the effect is the same in humans, and whether these drugs are also well-tolerated by young SMA children or even infants. The same problems need to be considered for LBH589. Therefore, and since no effective therapy for SMA is available yet, the search for novel, more potent SMA drugs has to be continued.

The *in vitro* studies described in this thesis characterize LBH589 as the most potent HDACi reported so far. None of the other small molecules, which already have been tested for SMA therapy, achieved an up to 10-fold elevation of SMN protein as LBH589 does. Besides an increase in SMN protein via *SMN2* promoter activation and splice pattern correction, a stabilizing effect on SMN via enhanced complex formation could be demonstrated. The next logical step in the process from an *in vitro* characterization towards a therapeutic SMA drug is an extended *in vivo* evaluation of LBH589 in SMA-like mice. Similar to what has been reported for SAHA (Riessland et al. 2010), the effect of LBH589 on survival, weight progression as well as motor neuron number, muscle histology, NMJ architecture or synaptic signaling has to be analyzed. Since recent publications showed that reduced SMN levels also interfere with normal heart development (Bevan et al. 2010; Shababi et al. 2010b), one may think about the investigation of the cardiac phenotype as well. Nevertheless, the most critical point of the *in vivo* characterization of LBH589 in mice is the selection of a proper animal model. Most of the studies testing therapeutic approaches employ mice which are severely affected (Hsieh-Li et al. 2000; Monani et al. 2000). Although these models easily give the answer whether the treatment regimens improve survival, the long-term surveillance of treated mice is not possible. To overcome this hitch, it was tried to generate an intermediate SMA-like mouse by the combination of two already published mouse models. Unfortunately, although the SMA-like mice were clearly lighter and exhibited typical signs of a murine SMA in mice like necrosis of the tail, these mice survived over 250 days, which is too long for an *in vivo* drug evaluation (Section 4.5).The crux of matter was that two *SMN2* copies in a *Smn* null background typically lead to early or even embryonic lethality (Hsieh-Li et al. 2000; Monani et al. 2000), while the three *SMN2* copies, like in our intermediate model, seem sufficient to guarantee survival. This suggested that the correlation between *SMN2* copies and the SMA phenotype in mice is similar to humans but the amount of SMN needed is less in mice. Similar observations came from a recent publication in which a mouse strain carrying a humanized *Smn* gene with the C to T transition was generated (Gladman et al. 2010). Although full-length transcripts were reduced by 60 to 80%, these mice the mean survival was not reduced. Taken together, for a contemporary *in vivo* evaluation of LBH589 one has to rely on the available mouse models. Even though these animals might not be the proper model for investigation of long-term effects, they allow comparison to the impact of other substances.

Based on the convincing data obtained with LBH589, its derivate JnJ-26481585 was also tested as a putative SMA drug. Although the *in vitro* characterization was rather limited compared to LBH589, the results were similar (Section 4.4). Concentrations between 400 nM and 1 µM JnJ-26481585 elevated SMN levels 6- to 8-fold. On RNA level a reversion of the *SMN2* splice pattern was observed, which was accompanied by an increased Gemin expression. Since also the cytotoxicity was comparable to what we found for LBH589, at least *in vitro* both HDACi are of equal value.

Moreover, based on the finding that LBH589 reduces SMN turnover, the proteasome inhibitor bortezomib was tested for its ability to increase SMN amounts. However, although the *in vitro* data were quite promising, further experiments were not conducted, because bortezomib does not pass the blood-brain-barrier (Hemeryck et al. 2007). Nevertheless, these results should not be underestimated since one may think of combined therapy of HDACi plus bortezomib as it is done in cancer therapy (Deleu et al. 2009b; Ocio et al. 2010).

In conclusion, these results highlight LBH589 and its derivate JnJ-26481585 as outstanding candidates for SMA therapy. Compared to all other small molecules tested so far, the *in vitro* results were superior. Based on the complete *in vitro* characterization of LBH589, it is self-evident to start now its *in vivo* evaluation. Since *in vitro* JNJ-26481585 gave likewise results, both compounds should be tested in comparison to decide which one gives the better outcome. Furthermore, one may treat animals in parallel with e.g. neurotrophic factors like IGF-1 or riluzole or combine HDACi treatment with ASO injection to test which combinations work best.

Novel therapeutic approaches like stem cell transplation or viral gene therapy are currently *in vogue*. They are inducing high hopes, while the possible side-effects and problems are typically underestimated. It remains elusive, whether these techniques will ever be a feasible approach for SMA therapy in humans and establishing them will take years of development. Marketing and authorization for these doubtless visionary approaches will take up yet more time and is likely to be associated with strict restrictions concerning indication and patient groups. Meanwhile, patients and their families are suffering from SMA and urgently need effective treatment for their disease.

A number of HDACi have already been approved by the authorities and are commercially available or are in the final stages of market approach. The side effects of these HDACi are in most of the cases well-known. For this reason, we propose to test LBH589 and JnJ-26481585 to be tested *in vivo* in SMA-like mice to take a further step towards SMA therapy.

6. Summary

Proximal spinal muscular atrophy (SMA) is the leading genetic cause of infant death in Western Europe. Its major characteristic is the progressive degeneration of the α-motor neurons in the anterior horns of the spinal cord. To date, no cure is available. SMA is caused by homozygous functional absence of the *survival motor neuron gene 1* (*SMN1*). Though, all SMA patients retain at least one copy of the nearly identical copy gene *SMN2.* In contrast to *SMN1*, which only produces full-length transcripts (*FL-SMN*), almost 90% of *SMN2* transcripts undergo alternative splicing and lack exon 7 (*SMN2Δ7*). Hence, *SMN2* gives predominantly rise to a truncated and unstable protein. But even though the amount of fully functional *SMN2* protein is not sufficient to compensate for the loss of *SMN1*, it has been shown that *SMN2* is the major disease modifying gene: The more *SMN2* a SMA patient has, the less severe is the phenotype. Self-evident, *SMN2* became the major target for potential SMA therapy. It has been demonstrated that epigenetic therapy by applying histone deacetylase inhibitors (HDACi) activates *SMN2* transcription and modulates *SMN2* splicing by inducing splice factor expression. In this way more *FL-SMN2* is produced, which gives rise to more full-length SMN protein. However, in a pilot clinical trial with the short-chain fatty acid HDACi *valproic acid* (VPA), the response to the treatment was quite diverse. Around $^1/_3$ of SMA patients exhibited increased *FL-SMN2* levels in blood (Pos-Responder). In contrast, in another $^1/_3$ no response was detected, while in the remaining $^1/_3$ SMN levels were even decreased (pooled as Non-Responder).

In the present work, the crucial factors determining VPA non-responsiveness were investigated. Fibroblast lines from all SMA patients included in the pilot clinical trial were established and treated with VPA. By western blot analysis, we were able to show that the response to VPA correlates between fibroblasts and blood in over 60%. To get a deeper insight into the reason why *SMN2* is not induced in Non-Responders, we performed *chromatin immunoprecipitation* (ChIP) analysis and could demonstrate that VPA does not trigger *SMN2* promoter hyperacetylation in Non-Responder fibroblast lines. Furthermore, we also showed that the *cAMP-dependent protein kinase A* (PKA) is not inhibited by VPA in Non-Responders. While HDACi of distinct chemical classes properly work in Non-Responder fibroblasts, the short chain fatty acid HDACi sodium butyrate led to results similar to VPA. Therefore, we speculated whether general mechanisms like fatty acid uptake and metabolism are causing the divergent response. To identify the crucial factors, fibroblasts of both Pos- and Non-Responders were compared by differential µ-array analysis. Data analysis revealed that in the Non-Responders no single gene was differentially expressed after VPA treatment, indicating that VPA is generally not acting as an HDACi. Furthermore, only nine genes were detected to be differentially expressed between untreated Pos- and Non-Responders, suggesting that these may be a predisposing set-up. After validation by qRT-PCR, the four candidates *cluster of differentiation* (*CD36*), *IGF-binding protein 5* (*IGFBP5*),

retinoic acid receptor β (*RARβ*) and *transforming growth factor α* (*TGFα*) were selected based on literature research. While *CD36* and *RARβ* showed a higher expression in Non-Responders, elevated levels of *IGFBP5* and *TGFα* were detected in Pos-Responders. In order to identify the cause of differential expression, all four genes were sequenced in both Pos- and Non-Responders and the respective promoters were analysed by ChIP. Since no SNP could be associated with the phenotype, knockdown and overexpression studies were conducted to investigate whether these four genes were identified by chance or are connected via a regulatory network. Although no obvious network could yet identified, data clearly indicated regulatory feedbacks between the candidate genes. Since CD36 is involved in LCFA transport, VPA uptake and metabolism were analyzed by HPLC-MS/MS. In summary, we could exclude that VPA is differentially metabolized between Pos- and Non-Responders. Futhermore, LCFA uptake in fibroblasts was measured using a fluorescent labeled fatty-acid analogue. Interestingly, these data suggest that in fibroblasts CD36 is rather functioning as a fatty acid exporter than an importer. While other known SCFA transporters were shown by qRT-PCR to be equally expressed, we detected increased *carnitine palmityl transferase 1 C* (CPT1C) levels in Non-Responders. Since this enzyme catalyzes formation of Carnityl-VPA, which is the initial step in the mitochondrial oxidation of VPA, it is the current focus of interest.

Futhermore, we identified the second generation HDACi LBH589 as well as its derivate JnJ-26481585 as compounds tremendously increasing SMN levels. At concentrations of 400 nM and 1 µM LBH589, up to 10-fold increased SMN amounts were recorded, which is the highest induction reported so far. Futhermore, we could demonstrate by fluorescence microscopy that also the number of small nuclear SMN foci termed gems increased in a similar fashion. Analysis of the *SMN2* promoter by ChIP as well measurement of the *SMN2* promoter activity using a reporter cell line revealed a 1:1 stoichiometry between HDAC inhibition and expression rate with an EC_{50} of approx. 108 nM. On RNA level, we could demonstrate that LBH589 increases SMN expression, but also reverses the *SMN2* splice pattern by up-regulation of hTRA2-β1, a splice factor promoting *SMN2* exon 7 inclusion. Subsequent knockdown and time-course experiments revealed that hTRA2-β1 is indeed an indispensable factor for LBH589-induced SMN amounts. Moreover, in order to identify the crucial factors for the vast SMN up-regulation under LBH589 treatment, we analyzed post-transcriptional factors like mRNA stability and proteasomal degradation. We were able to show that, most likely through enhanced complexation, ubiquitinylation of SMN is reduced, thus leading to a SMN accumulation over time. Moreover, by treating *murine embryonic fibroblasts* (MEF) and *neural stem cells* (NSC) from epilepsy surgeries we could prove that LBH589 is also active in both the neural and the murine context. In addition, as a first step towards an *in vivo* evalution, mice were sub-cutaneously injected with LBH589. Using tissue extracts, we could demonstrate that LBH589 increases both SMN protein and histone acetylation in central nervous system.

Based on these convincing results, LBH589 and JnJ-26481585 were proposed for extended *in vivo* testing in SMA-like mice to evaluate their therapeutic potential.

7. Zusammenfassung

Die proximal spinale Muskelatrophie (SMA) ist die häufigste genetische Kindestodesursache in West-Europa. Charakteristisch für eine SMA-Erkrankung ist eine fortschreitende Degeneration der α-Motoneuronen in the Vorderhörnern des Rückenmarks. Eine Therapie für SMA gibt es bis dato noch nicht. SMA wird durch den homozygoten funktionellen Verlust des *survival motor neuron Gens 1* (*SMN1*) verursacht. Allerdings konnte gezeigt werden, dass alle SMA-Patienten zumindest über eine Kopie des *SMN2*-Genes verfügen. *SMN2* ist beinahe identisch mit *SMN1*, unterscheidet sich jedoch drastisch in seinem Spleißmuster. Während *SMN1* ausschließlich Volllängen-Transkripte (*FL-SMN*) produziert, sind 90% aller *SMN2* Transkripte alternativ gespleißt. Ihnen fehlt das Exon 7 (*SMN2Δ7*), was zu einem verkürzten und instabilen Protein führt. Zwar reicht die Menge and *SMN2* Volllängenprotein nicht aus um für den Verlust von *SMN1* zu kompensieren, andererseits beeinflusst es jedoch den SMA Phänotyp: Über je mehr *SMN2* Kopien ein SMA Patient verfügt, desto milder ist der Krankheitsverlauf. Aufgrund dieser Beobachtungen ist *SMN2* natürlich ein erklärtes Ziel für eine SMA-Therapie. Es konnte gezeigt werden, dass die Verwendung von Histon Deacetylase Inhibitoren (HDACi) einerseits das *SMN2* Gen aktivieren und darüberhinaus auch sein Spleißmuster korrigieren. Zusammengefasst führt dies zu einer erhöhten *FL-SMN2* Menge, welche widerum zu einer erhöhten Menge an Volllängen-Protein führt. Eine Pilotstudie mit SMA-Patienten, die mit dem HDACi VPA behandelt wurden, ergab jedoch ein recht unterschiedliches Bild. In knapp einem Drittel der Patienten ist die Menge an *FL-SMN2* im Blut, wie erhofft, angestiegen (Pos-Responder). In einem weiteren Drittel jedoch konnte keine Änderung festgestellt werden, wohingegen im letzten Drittel die Menge an *FL-SMN2* durch VPA-Gabe sogar reduziert war (zusammengefasst als Non-Responder).

Die vorliegende Arbeit beschäftigt sich mit der Suche nach den Ursachen, aufgrund derer SMA-Patienten nicht positiv auf VPA reagieren. Von allen SMA-Patienten, die an der Pilot-Studie teilgenommen hatten, wurden Fibroblasten Linien aus Hautstanzen etabliert. Diese wurden dann mit VPA behandelt und die Menge an SMN-Protein mittels *Western blot* festgestellt. Es konnte gezeigt werden, dass in mehr als 60% der Fälle beide Gewebe, Blut wie Fibroblasten, gleichermaßen auf VPA ansprachen. Um zu verstehen, warum *SMN2* nicht durch VPA in Non-Respondern aktiviert wird, wurden Chromatin-Immunopräzipitationen (ChIP) durchgeführt. Es zeigte sich, dass das SMN Protein in Non-Respondern unter VPA-Behandlung nicht ansteigt, da VPA nicht zu einer *SMN2* Promotor Hyperacetylierung führt. Darüberhinaus konnte gezeigt werden, dass in mit VPA behandelten Non-Respondern die cAMP-abhängige Proteinkinase A (PKA) nicht inhibiert wird. Der HDACi Natriumbutyrate - ebenso wie VPA eine kurzkettige Fettsäure – löste ebenfalls keine *SMN2* Aktivierung in Non-Respondern aus wohingegen Sie eindeutig auf HDACi anderer Substanzklassen ansprachen. Daher lag es nahe zu vermuten, dass ein genereller Faktor, wie die Aufnahme von kurzkettigen Fettsäuren für unsere Beobachtungen verantwortlich ist. Um die Frage nach

den Gründen hierfür zu beantworten, wurde die Transkriptome von Pos- und Non-Responder Fibroblasten mittels Mikro-Array verglichen. Die Auswertung der Daten zeigte, dass in den Non-Respondern kein einziges Transkript differentiell unter VPA-Behandlung exprimiert wurde. Dies bedeutete, dass VPA generell nicht als HDACi in Non-Respondern wirkt. Interessanterweise wurden lediglich neun Gene gefunden, die signifikant unterschiedlich zwischen unbehandelten Pos- and Non-Respondern exprimiert wurden. Die einzelnen Transkripte wurden mittels qRT-PCR validiert und basierend auf publizierten Daten wurden die Gene *Cluster of Differentiation* (*CD36*), *IGF-binde Protein 5* (*IGFBP5*), *Retinoic Acid Receptor β* (*RARβ*) und *Transforming Growth Factor α* (*TGFα*) für weitere Experimente ausgewählt. *CD36* und *RARβ* sind beide in Non-Respondern höher exprimiert, wohingegen höherer Menge von *IGFBP5* und *TGFα* in Pos-Respondern gefunden wurden. Um die Ursache der differentiellen Expression zu bestimmen, wurden diese vier Gene in allen Fibroblasten-Linien durchsequenziert. Darüberhinaus wurden die Promotoren mittels ChIP verglichen. Da jedoch keine Assoziation zwischen einem SNP und dem VPA-Phänotyp gefunden werden konnte, wurden Überexpressions- und RNA-Interferenz-Versuche durchgeführt. Zwar konnte bis dato kein einheitliches regulatorisches Netzwerk gefunden werden, allerdings zeigte sich, dass es in der Tat verschiedene Mechanismen gibt, welche diese vier Kandidatengene regulatorisch koppeln. Da CD36 ein Fettsäuretransporter ist, wurden ebenfalls massenspektroskopische Versuche zur Aufnahme und Metabolisierung von VPA durchgeführt. Allerdings wurde kein unterschiedliches Metabolitenmuster detektiert, so dass eine differentielle Verstoffwechslung von VPA als Ursache für das Auftreten Non-Respondern ausgeschlossen werden kann. Ausgehend von diesen Daten wurde die generelle Fettsäureaufnahme von Fibroblasten verglichen. Interessanterweise lassen diese Daten vermuten, dass CD36 zumindest in Fibroblasten eher als Fettsäureexporter denn als -importer fungiert. Darüberhinaus konten wir zeigen, dass die *Carnintin Palmityl Transferase 1 C* (CPT1C) höher in Non-Responders exprimiert ist. Da CPT1C die Bildung von Carnityl-VPA katalysiert, konzentrieren sich unsere derzeitigen Experimente auf dieses Gen/Protein.

Ferner konnten wir den HDACi LBH589 und sein strukturell nah verwandtes Derivat JnJ-26481585 als potentielle SMA-Therapeutika identifizieren, die einem enormen Effekt auf die SMN-Protein Menge haben. So stieg die SMN Menge bis zu 10-fach bei LBH589 Konzentration von 400 nM beziehungsweise 1 µM an. Ein höherer Anstieg wurde bis dato noch nicht publiziert. Darüberhinaus konnten wir mittels Fluoreszenz-Mikroskopie zeigen, dass auch die Anzahl an *Gems*, nukleären SMN-Strukturen, gleichermaßen zunahm. ChIP-Analyse des *SMN2* Promoters, sowie die Messung der *SMN2* Promotoraktivität in einer Reporterzelllinie, zeigten, dass am *SMN2* Promoter HDAC-Inhibition und Promoter-Aktivität in einer 1:1 Stöichiometrie korrelieren. Es wurde eine EC_{50} von 108 nM LBH589 bestimmt. Auf RNA-Ebene konnten wir zeigen, dass LBH589 einerseits die SMN Expression steigert, aber auch das Spleißmuster durch Hoch-Regulation des Spleißfaktors hTRA2-β1, welcher den

Einbezug des *SMN2* Exons 7 fördert, revertiert. Anschließende RNA-Inteferenz-Experimente und Zeitreihen zeigten, dass hTRA2-β1 die Schlüsselfigur in der SMN-Steigerung durch LBH589 ist. Um die enorme Steigerung der Menge an SMN-Protein zu erklären, wurden des Weiteren post-transkriptionale Parameter wie mRNA-Stabilität und Proteinabbau untersucht. Mittels Präzipitations-Experimenten konnten wir zeigen, dass die Ubiquitinylierung von SMN stark reduziert ist. Ursächlich hierfür ist vermutlich eine verstärkte SMN-Komplex Bildung, die dann zu einer Anreicherung von SMN im Laufe der Zeit führt. Wir konnte ferner zeigen, dass LBH589 in humanen neuralen Stammzellen wie auch in murinen embryonalen Fibroblasten von SMA-Mäusen SMN Protein hochreguliert, was bedeutet dass es auch in neuralem oder murinem Zellen aktiv ist. Abschließend wurden LBH589 subkutan in Mäuse injiziert um zu untersuchen, ob sich eine *in vivo* Untersuchung von LBH589 anbietet. Die Analyse von Gewebeextrakten aus dem ZNS zeigte einerseits, dass die Menge an SMN Protein im Gehirn steigt und gleichermaßen auch die Histonacetylierung zunahm.

Basierend auf dieser überzeugenden Datenlage sollte LBH589, bzw. auch JnJ-26481585, in einer größer angelegten Studie im SMA-Tiermodell untersucht werden.

8. Pulication, lectures and scholarships

- Original publications

Riessland M, Ackermann B, Forster A, Jakubik M, Hauke J, **Garbes L**, Fritzsche I, Mende Y, Blumcke I, Hahnen E, Wirth B (2010) SAHA ameliorates the SMA phenotype in two mouse models for spinal muscular atrophy. Hum Mol Genet 19: 1492-506

Garbes L, Riessland M, Holker I, Heller R, Hauke J, Trankle C, Coras R, Blumcke I, Hahnen E, Wirth B (2009) LBH589 induces up to 10-fold SMN protein levels by several independent mechanisms and is effective even in cells from SMA patients non-responsive to valproate. Hum Mol Genet 18: 3645-58

Brichta L, **Garbes L**, Jedrzejowska M, Grellscheid SN, Holker I, Zimmermann K, Wirth B (2008) Nonsense-mediated messenger RNA decay of survival motor neuron 1 causes spinal muscular atrophy. Hum Genet 123: 141-53

- Lecture contributions

Garbes L, Heesen L, Bauer T, Hölker I, Thoenes M, Müller C, Dimos J, Heller R, Wirth B (2010) SMA-therapy with VPA: Why do we have Positive- and Non-Responders? *Abstract book* (14th Annual International SMA Research Group Meeting, Santa Clara, USA)

Lunke S, **Garbes L**, Hölker I, Heller R, Wirth B, El-Osta A (2010) A fine map of histone acetylation patterns in SMA patients *Abstract book* (14th Annual International SMA Research Group Meeting, Santa Clara, USA)

Riessland M, Ackermann B, Forster A, Jakubik M, Hauke J, **Garbes L**, Fritzsche I, Mende Y, Blumcke I, Hahnen E, Wirth B (2010) SAHA ameliorates the SMA phenotype in two mouse models for spinal muscular atrophy. *Abstract book* (European Society of Human Genetics Meeting, Gothenburg, Sweden)

Riessland M, Ackermann B, Forster A, Jakubik M, Hauke J, **Garbes L**, Fritzsche I, Mende Y, Blumcke I, Hahnen E, Wirth B (2010) SAHA ameliorates the SMA phenotype in two mouse models for spinal muscular atrophy. *Abstract book* (21th annual Meeting of the German Society of Human Genetics Meeting, Hamburg, Germany)

Wirth B, Riessland M, Holker I, Heller R, Hauke J, Trankle C, Coras R, Blumcke I, Hahnen E, **Garbes L** (2009) LBH589 induces up to 10-fold SMN protein levels by several independent mechanisms and is effective even in cells from SMA patients non-responsive to valproate. *Abstract book* (59th annual Meeting of the American Society of Human Genetics Meeting, Honolulu, USA)

Garbes L, Riessland M, Hölker I, Tränkle C, Hauke J, Hahnen E Heller R, Wirth B (2009) What did we learn from *in vivo* and *in vitro* treatment with HDACi in SMA? *Abstract book* (13th Annual International SMA Research Group Meeting, Cincinnati, USA)

- Poster contribution

Wirth B, Heesen L, Bauer T, Hölker I, Thoenes M, Müller C, Dimos J, Heller R, **Garbes L** (2010) SMA-therapy with VPA: Why do we have Positive- and Non-Responders? *Abstract book* (60th annual Meeting of the American Society of Human Genetics Meeting, Washington, USA)

Martinez FJ, Dinella JD, Stepaniants S, Grskovic M, **Garbes L**, Hölker I, Heller R, Wirth B, Strulovici B, Lum PY, Dimos J (2010) Discovery of disease gene expression signature in cells derived from Spinal Muscular Atrophy (SMA) patients. *Abstract book* (International society of stem cell research meeting, San Francisco, USA)

Riessland M, Ackermann B, Forster A, Jakubik M, Hauke J, **Garbes L**, Fritzsche I, Mende Y, Blumcke I, Hahnen E, Wirth B (2010) SAHA ameliorates the SMA phenotype in two mouse models for spinal muscular atrophy *Abstract book* (14th Annual International SMA Research Group Meeting, Santa Clara, USA)

Garbes L, Hölker I, Riessland M, Hauke J, Hahnen E, Wirth B (2008) The novel HDAC-inhibitor LBH589, a promising candidate for spinal muscular atrophy (SMA) drug therapy, significantly elevates SMN protein and RNA levels at nanomolar doses in vitro (21st course in "Medical Genetics",European School of Genetic Medicine, Bertinoro di Romagna, Italy)

Garbes L, Brichta L, Jedrzejowska M, Grellscheid SN, Holker I, Zimmermann K, Wirth B (2008) Nonsense-mediated messenger RNA decay of survival motor neuron 1 causes spinal muscular atrophy. (19th annual Meeting of the German Society of Human Genetics Meeting, Hannover, Germany)

Garbes L, Wirth B (2007) The c.495G>A silent mutation in exon 3 of the *SMN1* gene identified in patients with mild spinal muscular atrophy does not affect splicing and is therefore not pathogenic. (18th annual Meeting of the German Society of Human Genetics Meeting, Bonn, Germany)

- Scholarships

Anita McCauly Memorial Travel Scholarship 2009 of the "Families of SMA" to attend the 13th Annual International SMA Research Group Meeting in Cincinnati, USA

9. References

Abbott BD, Lin TM, Rasmussen NT, Albrecht RM, Schmid JE, Peterson RE (2003) Lack of expression of EGF and TGF-alpha in the fetal mouse alters formation of prostatic epithelial buds and influences the response to TCDD. Toxicol Sci 76: 427-36

Abumrad NA, el-Maghrabi MR, Amri EZ, Lopez E, Grimaldi PA (1993) Cloning of a rat adipocyte membrane protein implicated in binding or transport of long-chain fatty acids that is induced during preadipocyte differentiation. Homology with human CD36. J Biol Chem 268: 17665-8

ACTS (1996) A double-blind placebo-controlled clinical trial of subcutaneous recombinant human ciliary neurotrophic factor (rHCNTF) in amyotrophic lateral sclerosis. ALS CNTF Treatment Study Group. Neurology 46: 1244-9

Adams J (2002) Development of the proteasome inhibitor PS-341. Oncologist 7: 9-16

Adkison KD, Shen DD (1996) Uptake of valproic acid into rat brain is mediated by a medium-chain fatty acid transporter. J Pharmacol Exp Ther 276: 1189-200

Aghajanian C, Soignet S, Dizon DS, Pien CS, Adams J, Elliott PJ, Sabbatini P, Miller V, Hensley ML, Pezzulli S, Canales C, Daud A, Spriggs DR (2002) A phase I trial of the novel proteasome inhibitor PS341 in advanced solid tumor malignancies. Clin Cancer Res 8: 2505-11

Aires CC, Ruiter JP, Luis PB, ten Brink HJ, Ijlst L, de Almeida IT, Duran M, Wanders RJ, Silva MF (2007) Studies on the extra-mitochondrial CoA -ester formation of valproic and Delta4 -valproic acids. Biochim Biophys Acta 1771: 533-43

Allander SV, Larsson C, Ehrenborg E, Suwanichkul A, Weber G, Morris SL, Bajalica S, Kiefer MC, Luthman H, Powell DR (1994) Characterization of the chromosomal gene and promoter for human insulin-like growth factor binding protein-5. J Biol Chem 269: 10891-8

Allfrey VG, Faulkner R, Mirsky AE (1964) Acetylation and Methylation of Histones and Their Possible Role in the Regulation of Rna Synthesis. Proc Natl Acad Sci U S A 51: 786-94

Andreassi C, Angelozzi C, Tiziano FD, Vitali T, De Vincenzi E, Boninsegna A, Villanova M, Bertini E, Pini A, Neri G, Brahe C (2004) Phenylbutyrate increases SMN expression in vitro: relevance for treatment of spinal muscular atrophy. Eur J Hum Genet 12: 59-65

Andreassi C, Jarecki J, Zhou J, Coovert DD, Monani UR, Chen X, Whitney M, Pollok B, Zhang M, Androphy E, Burghes AH (2001) Aclarubicin treatment restores SMN levels to cells derived from type I spinal muscular atrophy patients. Hum Mol Genet 10: 2841-9

Andress DL (1995) Heparin modulates the binding of insulin-like growth factor (IGF) binding protein-5 to a membrane protein in osteoblastic cells. J Biol Chem 270: 28289-96

Andress DL, Birnbaum RS (1992) Human osteoblast-derived insulin-like growth factor (IGF) binding protein-5 stimulates osteoblast mitogenesis and potentiates IGF action. J Biol Chem 267: 22467-72

Angelozzi C, Borgo F, Tiziano FD, Martella A, Neri G, Brahe C (2008) Salbutamol increases SMN mRNA and protein levels in spinal muscular atrophy cells. J Med Genet 45: 29-31

Anhuf D, Eggermann T, Rudnik-Schoneborn S, Zerres K (2003) Determination of SMN1 and SMN2 copy number using TaqMan technology. Hum Mutat 22: 74-8

Arai T, Arai A, Busby WH, Jr., Clemmons DR (1994) Glycosaminoglycans inhibit degradation of insulin-like growth factor-binding protein-5. Endocrinology 135: 2358-63

Araujo Ade Q, Araujo M, Swoboda KJ (2009) Vascular perfusion abnormalities in infants with spinal muscular atrophy. J Pediatr 155: 292-4

Ardinger HH, Buetow KH, Bell GI, Bardach J, VanDemark DR, Murray JC (1989) Association of genetic variation of the transforming growth factor-alpha gene with cleft lip and palate. Am J Hum Genet 45: 348-53

Arts J, King P, Marien A, Floren W, Belien A, Janssen L, Pilatte I, Roux B, Decrane L, Gilissen R, Hickson I, Vreys V, Cox E, Bol K, Talloen W, Goris I, Andries L, Du Jardin M, Janicot M, Page M, van Emelen K, Angibaud P (2009) JNJ-26481585, a novel "second-generation" oral histone deacetylase inhibitor, shows broad-spectrum preclinical antitumoral activity. Clin Cancer Res 15: 6841-51

Atadja P (2009) Development of the pan-DAC inhibitor panobinostat (LBH589): successes and challenges. Cancer Lett 280: 233-41

Avila AM, Burnett BG, Taye AA, Gabanella F, Knight MA, Hartenstein P, Cizman Z, Di Prospero NA, Pellizzoni L, Fischbeck KH, Sumner CJ (2007) Trichostatin A increases SMN expression and survival in a mouse model of spinal muscular atrophy. J Clin Invest 117: 659-71

Avvakumov N, Cote J (2007) The MYST family of histone acetyltransferases and their intimate links to cancer. Oncogene 26: 5395-407

Balasubramanyam K, Varier RA, Altaf M, Swaminathan V, Siddappa NB, Ranga U, Kundu TK (2004) Curcumin, a novel p300/CREB-binding protein-specific inhibitor of acetyltransferase, represses the acetylation of histone/nonhistone proteins and histone acetyltransferase-dependent chromatin transcription. J Biol Chem 279: 51163-71

Bardoni B, Schenck A, Mandel JL (2001) The Fragile X mental retardation protein. Brain Res Bull 56: 375-82

Barnes PJ, Adcock IM, Ito K (2005) Histone acetylation and deacetylation: importance in inflammatory lung diseases. Eur Respir J 25: 552-63

Baron-Delage S, Abadie A, Echaniz-Laguna A, Melki J, Beretta L (2000) Interferons and IRF-1 induce expression of the survival motor neuron (SMN) genes. Mol Med 6: 957-68

Barrandon Y, Green H (1987) Cell migration is essential for sustained growth of keratinocyte colonies: the roles of transforming growth factor-alpha and epidermal growth factor. Cell 50: 1131-7

Battaglia G, Princivalle A, Forti F, Lizier C, Zeviani M (1997) Expression of the SMN gene, the spinal muscular atrophy determining gene, in the mammalian central nervous system. Hum Mol Genet 6: 1961-71

Baughan T, Shababi M, Coady TH, Dickson AM, Tullis GE, Lorson CL (2006) Stimulating full-length SMN2 expression by delivering bifunctional RNAs via a viral vector. Mol Ther 14: 54-62

Baughan TD, Dickson A, Osman EY, Lorson CL (2009) Delivery of bifunctional RNAs that target an intronic repressor and increase SMN levels in an animal model of spinal muscular atrophy. Hum Mol Genet 18: 1600-11

Baxter RC, Twigg SM (2009) Actions of IGF binding proteins and related proteins in adipose tissue. Trends Endocrinol Metab 20: 499-505

Bedard KM, Daijogo S, Semler BL (2007) A nucleo-cytoplasmic SR protein functions in viral IRES-mediated translation initiation. Embo J 26: 459-67

Berridge MV, Tan AS (1993) Characterization of the cellular reduction of 3-(4,5-dimethylthiazol-2-yl)-2,5-diphenyltetrazolium bromide (MTT): subcellular localization, substrate dependence, and involvement of mitochondrial electron transport in MTT reduction. Arch Biochem Biophys 303: 474-82

Bertini E, Burghes A, Bushby K, Estournet-Mathiaud B, Finkel RS, Hughes RA, Iannaccone ST, Melki J, Mercuri E, Muntoni F, Voit T, Reitter B, Swoboda KJ, Tiziano D, Tizzano E, Topaloglu H, Wirth B, Zerres K (2005) 134th ENMC International Workshop: Outcome Measures and Treatment of Spinal Muscular Atrophy, 11-13 February 2005, Naarden, The Netherlands. Neuromuscul Disord 15: 802-16

Bertrand P (2010) Inside HDAC with HDAC inhibitors. Eur J Med Chem 45: 2095-116

Bertrandy S, Burlet P, Clermont O, Huber C, Fondrat C, Thierry-Mieg D, Munnich A, Lefebvre S (1999) The RNA-binding properties of SMN: deletion analysis of the zebrafish orthologue defines domains conserved in evolution. Hum Mol Genet 8: 775-82

Bevan AK, Hutchinson KR, Foust KD, Braun L, McGovern VL, Schmelzer L, Ward JG, Petruska JC, Lucchesi PA, Burghes AH, Kaspar BK (2010) Early heart failure in the SMN{Delta}7 model of spinal muscular atrophy and correction by postnatal scAAV9-SMN delivery. Hum Mol Genet

Biondi O, Branchu J, Sanchez G, Lancelin C, Deforges S, Lopes P, Pariset C, Lecolle S, Cote J, Chanoine C, Charbonnier F (2010) In Vivo NMDA Receptor Activation Accelerates Motor Unit Maturation, Protects Spinal Motor Neurons, and Enhances SMN2 Gene Expression in Severe Spinal Muscular Atrophy Mice. J Neurosci 30: 11288-99

Bjorge SM, Baillie TA (1991) Studies on the beta-oxidation of valproic acid in rat liver mitochondrial preparations. Drug Metab Dispos 19: 823-9

Blum M (1998) A null mutation in TGF-alpha leads to a reduction in midbrain dopaminergic neurons in the substantia nigra. Nat Neurosci 1: 374-7

Blume-Jensen P, Hunter T (2001) Oncogenic kinase signalling. Nature 411: 355-65

Boeckeler K, Adley K, Xu X, Jenkins A, Jin T, Williams RS (2006) The neuroprotective agent, valproic acid, regulates the mitogen-activated protein kinase pathway through modulation of protein kinase A signalling in Dictyostelium discoideum. Eur J Cell Biol 85: 1047-57

Bokor S, Legry V, Meirhaeghe A, Ruiz JR, Mauro B, Widhalm K, Manios Y, Amouyel P, Moreno LA, Molnar D, Dallongeville J (2010) Single-nucleotide polymorphism of CD36 locus and obesity in European adolescents. Obesity (Silver Spring) 18: 1398-403

Boon KL, Xiao S, McWhorter ML, Donn T, Wolf-Saxon E, Bohnsack MT, Moens CB, Beattie CE (2009) Zebrafish survival motor neuron mutants exhibit presynaptic neuromuscular junction defects. Hum Mol Genet 18: 3615-25

Booth CL, Pollack GM, Brouwer KL (1996) Hepatobiliary disposition of valproic acid and valproate glucuronide: use of a pharmacokinetic model to examine the rate-limiting steps and potential sites of drug interactions. Hepatology 23: 771-80

Bork P (1993) The modular architecture of a new family of growth regulators related to connective tissue growth factor. FEBS Lett 327: 125-30

Bose JK, Wang IF, Hung L, Tarn WY, Shen CK (2008) TDP-43 overexpression enhances exon 7 inclusion during the survival of motor neuron pre-mRNA splicing. J Biol Chem 283: 28852-9

Bowerman M, Anderson CL, Beauvais A, Boyl PP, Witke W, Kothary R (2009) SMN, profilin IIa and plastin 3: a link between the deregulation of actin dynamics and SMA pathogenesis. Mol Cell Neurosci 42: 66-74

Bowerman M, Beauvais A, Anderson CL, Kothary R (2010) Rho-kinase inactivation prolongs survival of an intermediate SMA mouse model. Hum Mol Genet 19: 1468-78

Bowerman M, Shafey D, Kothary R (2007) Smn depletion alters profilin II expression and leads to upregulation of the RhoA/ROCK pathway and defects in neuronal integrity. J Mol Neurosci 32: 120-31

Brachmann R, Lindquist PB, Nagashima M, Kohr W, Lipari T, Napier M, Derynck R (1989) Transmembrane TGF-alpha precursors activate EGF/TGF-alpha receptors. Cell 56: 691-700

Bracker TU, Sommer A, Fichtner I, Faus H, Haendler B, Hess-Stumpp H (2009) Efficacy of MS-275, a selective inhibitor of class I histone deacetylases, in human colon cancer models. Int J Oncol 35: 909-20

Bradford MM (1976) A rapid and sensitive method for the quantitation of microgram quantities of protein utilizing the principle of protein-dye binding. Anal Biochem 72: 248-54

Brahe C (2000) Copies of the survival motor neuron gene in spinal muscular atrophy: the more, the better. Neuromuscul Disord 10: 274-5

Brahe C, Clermont O, Zappata S, Tiziano F, Melki J, Neri G (1996) Frameshift mutation in the survival motor neuron gene in a severe case of SMA type I. Hum Mol Genet 5: 1971-6

Brahe C, Vitali T, Tiziano FD, Angelozzi C, Pinto AM, Borgo F, Moscato U, Bertini E, Mercuri E, Neri G (2005) Phenylbutyrate increases SMN gene expression in spinal muscular atrophy patients. Eur J Hum Genet 13: 256-9

Braulke T (1999) Type-2 IGF receptor: a multi-ligand binding protein. Horm Metab Res 31: 242-6

Brichta L, Garbes L, Jedrzejowska M, Grellscheid SN, Holker I, Zimmermann K, Wirth B (2008) Nonsense-mediated messenger RNA decay of survival motor neuron 1 causes spinal muscular atrophy. Hum Genet 123: 141-53

Brichta L, Hofmann Y, Hahnen E, Siebzehnrubl FA, Raschke H, Blumcke I, Eyupoglu IY, Wirth B (2003) Valproic acid increases the SMN2 protein level: a well-known drug as a potential therapy for spinal muscular atrophy. Hum Mol Genet 12: 2481-9

Brichta L, Holker I, Haug K, Klockgether T, Wirth B (2006) In-vivo activation of SMN in SMA carriers and patients treated with valproate. Ann Neurol 59: DOI:10.1002/ana.20836

Briese M, Esmaeili B, Fraboulet S, Burt EC, Christodoulou S, Towers PR, Davies KE, Sattelle DB (2009) Deletion of smn-1, the Caenorhabditis elegans ortholog of the spinal muscular atrophy gene, results in locomotor dysfunction and reduced lifespan. Hum Mol Genet 18: 97-104

Bringman TS, Lindquist PB, Derynck R (1987) Different transforming growth factor-alpha species are derived from a glycosylated and palmitoylated transmembrane precursor. Cell 48: 429-40

Brunmeir R, Lagger S, Seiser C (2009) Histone deacetylase HDAC1/HDAC2-controlled embryonic development and cell differentiation. Int J Dev Biol 53: 275-89

Brzustowicz LM, Lehner T, Castilla LH, Penchaszadeh GK, Wilhelmsen KC, Daniels R, Davies KE, Leppert M, Ziter F, Wood D, et al. (1990) Genetic mapping of chronic childhood-onset spinal muscular atrophy to chromosome 5q11.2-13.3. Nature 344: 540-1

Buchan JR, Parker R (2009) Eukaryotic stress granules: the ins and outs of translation. Mol Cell 36: 932-41

Burghes AH, Beattie CE (2009) Spinal muscular atrophy: why do low levels of survival motor neuron protein make motor neurons sick? Nat Rev Neurosci 10: 597-609

Burglen L, Lefebvre S, Clermont O, Burlet P, Viollet L, Cruaud C, Munnich A, Melki J (1996) Structure and organization of the human survival motor neurone (SMN) gene. Genomics 32: 479-82

Burlet P, Huber C, Bertrandy S, Ludosky MA, Zwaenepoel I, Clermont O, Roume J, Delezoide AL, Cartaud J, Munnich A, Lefebvre S (1998) The distribution of SMN protein complex in human fetal tissues and its alteration in spinal muscular atrophy. Hum Mol Genet 7: 1927-33

Burlingame RW, Love WE, Wang BC, Hamlin R, Nguyen HX, Moudrianakis EN (1985) Crystallographic structure of the octameric histone core of the nucleosome at a resolution of 3.3 A. Science 228: 546-53

Burnett BG, Munoz E, Tandon A, Kwon DY, Sumner CJ, Fischbeck KH (2009) Regulation of SMN protein stability. Mol Cell Biol 29: 1107-15

Burt EC, Towers PR, Sattelle DB (2006) Caenorhabditis elegans in the study of SMN-interacting proteins: a role for SMI-1, an orthologue of human Gemin2 and the identification of novel components of the SMN complex. Invert Neurosci 6: 145-59

Busby WH, Jr., Nam TJ, Moralez A, Smith C, Jennings M, Clemmons DR (2000) The complement component C1s is the protease that accounts for cleavage of insulin-like growth factor-binding protein-5 in fibroblast medium. J Biol Chem 275: 37638-44

Callahan N, Modesto A, Deeley K, Meira R, Vieira AR (2009) Transforming growth factor-alfa gene (TGFA), human tooth agenesis, and evidence of segmental uniparental isodisomy. Eur J Oral Sci 117: 20-6

Calvo D, Dopazo J, Vega MA (1995) The CD36, CLA-1 (CD36L1), and LIMPII (CD36L2) gene family: cellular distribution, chromosomal location, and genetic evolution. Genomics 25: 100-6

Calvo D, Vega MA (1993) Identification, primary structure, and distribution of CLA-1, a novel member of the CD36/LIMPII gene family. J Biol Chem 268: 18929-35

Campbell L, Hunter KM, Mohaghegh P, Tinsley JM, Brasch MA, Davies KE (2000) Direct interaction of Smn with dp103, a putative RNA helicase: a role for Smn in transcription regulation? Hum Mol Genet 9: 1093-100

Carew JS, Giles FJ, Nawrocki ST (2008) Histone deacetylase inhibitors: mechanisms of cell death and promise in combination cancer therapy. Cancer Lett 269: 7-17

Carissimi C, Saieva L, Baccon J, Chiarella P, Maiolica A, Sawyer A, Rappsilber J, Pellizzoni L (2006a) Gemin8 is a novel component of the survival motor neuron complex and functions in small nuclear ribonucleoprotein assembly. J Biol Chem 281: 8126-34

Carissimi C, Saieva L, Gabanella F, Pellizzoni L (2006b) Gemin8 is required for the architecture and function of the survival motor neuron complex. J Biol Chem 281: 37009-16

Caron C, Boyault C, Khochbin S (2005) Regulatory cross-talk between lysine acetylation and ubiquitination: role in the control of protein stability. Bioessays 27: 408-15

Carrel TL, McWhorter ML, Workman E, Zhang H, Wolstencroft EC, Lorson C, Bassell GJ, Burghes AH, Beattie CE (2006) Survival motor neuron function in motor axons is independent of functions required for small nuclear ribonucleoprotein biogenesis. J Neurosci 26: 11014-22

Cartegni L, Hastings ML, Calarco JA, de Stanchina E, Krainer AR (2006) Determinants of exon 7 splicing in the spinal muscular atrophy genes, SMN1 and SMN2. Am J Hum Genet 78: 63-77

Cartegni L, Krainer AR (2002) Disruption of an SF2/ASF-dependent exonic splicing enhancer in SMN2 causes spinal muscular atrophy in the absence of SMN1. Nat Genet 30: 377-84

Carvalho T, Almeida F, Calapez A, Lafarga M, Berciano MT, Carmo-Fonseca M (1999) The spinal muscular atrophy disease gene product, SMN: A link between snRNP biogenesis and the Cajal (coiled) body. J Cell Biol 147: 715-28

Catalioto RM, Maggi CA, Giuliani S (2009) Chemically distinct HDAC inhibitors prevent adipose conversion of subcutaneous human white preadipocytes at an early stage of the differentiation program. Exp Cell Res 315: 3267-80

Catley L, Weisberg E, Tai YT, Atadja P, Remiszewski S, Hideshima T, Mitsiades N, Shringarpure R, LeBlanc R, Chauhan D, Munshi NC, Schlossman R, Richardson P, Griffin J, Anderson KC (2003) NVP-LAQ824 is a potent novel histone deacetylase inhibitor with significant activity against multiple myeloma. Blood 102: 2615-22

Chan YB, Miguel-Aliaga I, Franks C, Thomas N, Trulzsch B, Sattelle DB, Davies KE, van den Heuvel M (2003) Neuromuscular defects in a Drosophila survival motor neuron gene mutant. Hum Mol Genet 12: 1367-76

Chang HC, Dimlich DN, Yokokura T, Mukherjee A, Kankel MW, Sen A, Sridhar V, Fulga TA, Hart AC, Van Vactor D, Artavanis-Tsakonas S (2008) Modeling spinal muscular atrophy in Drosophila. PLoS One 3: e3209

Chang HC, Hung WC, Chuang YJ, Jong YJ (2004) Degradation of survival motor neuron (SMN) protein is mediated via the ubiquitin/proteasome pathway. Neurochem Int 45: 1107-12

Chang JG, Hsieh-Li HM, Jong YJ, Wang NM, Tsai CH, Li H (2001) Treatment of spinal muscular atrophy by sodium butyrate. Proc Natl Acad Sci U S A 98: 9808-13

Chang P, Chandler KE, Williams RS, Walker MC (2009) Inhibition of long-term potentiation by valproic acid through modulation of cyclic AMP. Epilepsia

Chari A, Golas MM, Klingenhager M, Neuenkirchen N, Sander B, Englbrecht C, Sickmann A, Stark H, Fischer U (2008) An assembly chaperone collaborates with the SMN complex to generate spliceosomal SnRNPs. Cell 135: 497-509

Chari A, Paknia E, Fischer U (2009) The role of RNP biogenesis in spinal muscular atrophy. Curr Opin Cell Biol 21: 387-93

Chen Q, Baird SD, Mahadevan M, Besner-Johnston A, Farahani R, Xuan J, Kang X, Lefebvre C, Ikeda JE, Korneluk RG, MacKenzie AE (1998) Sequence of a 131-kb region of 5q13.1 containing the spinal muscular atrophy candidate genes SMN and NAIP. Genomics 48: 121-7

Cheng H, Liu Z, Blum W, Byrd JC, Klisovic R, Grever MR, Marcucci G, Chan KK (2007) Quantification of valproic acid and its metabolite 2-propyl-4-pentenoic acid in human plasma using HPLC-MS/MS. J Chromatogr B Analyt Technol Biomed Life Sci 850: 206-12

Cho S, Dreyfuss G (2010) A degron created by SMN2 exon 7 skipping is a principal contributor to spinal muscular atrophy severity. Genes Dev 24: 438-42

Cifuentes-Diaz C, Frugier T, Tiziano FD, Lacene E, Roblot N, Joshi V, Moreau MH, Melki J (2001) Deletion of murine SMN exon 7 directed to skeletal muscle leads to severe muscular dystrophy. J Cell Biol 152: 1107-14

Cinatl J, Jr., Kotchetkov R, Blaheta R, Driever PH, Vogel JU, Cinatl J (2002) Induction of differentiation and suppression of malignant phenotype of human neuroblastoma BE(2)-C cells by valproic acid: enhancement by combination with interferon-alpha. Int J Oncol 20: 97-106

Clemetson KJ, Pfueller SL, Luscher EF, Jenkins CS (1977) Isolation of the membrane glycoproteins of human blood platelets by lectin affinity chromatography. Biochim Biophys Acta 464: 493-508

Coady TH, Lorson CL (2010) Trans-splicing-mediated improvement in a severe mouse model of spinal muscular atrophy. J Neurosci 30: 126-30

Coady TH, Shababi M, Tullis GE, Lorson CL (2007) Restoration of SMN function: delivery of a trans-splicing RNA re-directs SMN2 pre-mRNA splicing. Mol Ther 15: 1471-8

Cobben JM, Lemmink HH, Snoeck I, Barth PA, van der Lee JH, de Visser M (2008) Survival in SMA type I: a prospective analysis of 34 consecutive cases. Neuromuscul Disord 18: 541-4

Coburn CT, Hajri T, Ibrahimi A, Abumrad NA (2001) Role of CD36 in membrane transport and utilization of long-chain fatty acids by different tissues. J Mol Neurosci 16: 117-21; discussion 151-7

Coburn CT, Knapp FF, Jr., Febbraio M, Beets AL, Silverstein RL, Abumrad NA (2000) Defective uptake and utilization of long chain fatty acids in muscle and adipose tissues of CD36 knockout mice. J Biol Chem 275: 32523-9

Coffey RJ, Jr., Derynck R, Wilcox JN, Bringman TS, Goustin AS, Moses HL, Pittelkow MR (1987) Production and auto-induction of transforming growth factor-alpha in human keratinocytes. Nature 328: 817-20

Conover CA, Kiefer MC (1993) Regulation and biological effect of endogenous insulin-like growth factor binding protein-5 in human osteoblastic cells. J Clin Endocrinol Metab 76: 1153-9

Coort SL, Willems J, Coumans WA, van der Vusse GJ, Bonen A, Glatz JF, Luiken JJ (2002) Sulfo-N-succinimidyl esters of long chain fatty acids specifically inhibit fatty acid translocase (FAT/CD36)-mediated cellular fatty acid uptake. Mol Cell Biochem 239: 213-9

Coovert DD, Le TT, McAndrew PE, Strasswimmer J, Crawford TO, Mendell JR, Coulson SE, Androphy EJ, Prior TW, Burghes AH (1997) The survival motor neuron protein in spinal muscular atrophy. Hum Mol Genet 6: 1205-14

Corpeleijn E, van der Kallen CJ, Kruijshoop M, Magagnin MG, de Bruin TW, Feskens EJ, Saris WH, Blaak EE (2006) Direct association of a promoter polymorphism in the CD36/FAT fatty acid transporter gene with Type 2 diabetes mellitus and insulin resistance. Diabet Med 23: 907-11

Corti S, Nizzardo M, Nardini M, Donadoni C, Salani S, Ronchi D, Saladino F, Bordoni A, Fortunato F, Del Bo R, Papadimitriou D, Locatelli F, Menozzi G, Strazzer S, Bresolin N, Comi GP (2008) Neural stem cell transplantation can ameliorate the phenotype of a mouse model of spinal muscular atrophy. J Clin Invest 118: 3316-30

Corti S, Nizzardo M, Nardini M, Donadoni C, Salani S, Ronchi D, Simone C, Falcone M, Papadimitriou D, Locatelli F, Mezzina N, Gianni F, Bresolin N, Comi GP (2009) Embryonic stem cell-derived neural stem cells improve spinal muscular atrophy phenotype in mice. Brain 133: 465-81

Cotariu D, Evans S, Lahat E, Theitler J, Bistritzer T, Zaidman JL (1992) Inhibition of human red blood cell glutathione reductase by valproic acid. Biochem Pharmacol 43: 425-9

Coverley JA, Baxter RC (1997) Phosphorylation of insulin-like growth factor binding proteins. Mol Cell Endocrinol 128: 1-5

Daughaday WH, Rotwein P (1989) Insulin-like growth factors I and II. Peptide, messenger ribonucleic acid and gene structures, serum, and tissue concentrations. Endocr Rev 10: 68-91

de la Fuente A (2010) From 'differential expression' to 'differential networking' - identification of dysfunctional regulatory networks in diseases. Trends Genet 26: 326-33

de Larco JE, Todaro GJ (1978) Growth factors from murine sarcoma virus-transformed cells. Proc Natl Acad Sci U S A 75: 4001-5

De Sarro G, Ascioti C, di Paola ED, Vidal MJ, De Sarro A (1992) Effects of antiepileptic drugs, calcium channel blockers and other compounds on seizures induced by activation of voltage-dependent L calcium channel in DBA/2 mice. Gen Pharmacol 23: 1205-16

de The H, Vivanco-Ruiz MM, Tiollais P, Stunnenberg H, Dejean A (1990) Identification of a retinoic acid responsive element in the retinoic acid receptor beta gene. Nature 343: 177-80

Deimling von F, Scharf JM, Liehr T, Rothe M, Kelter AR, Albers P, Dietrich WF, Kunkel LM, Wernert N, Wirth B (1999) Human and mouse RAD17 genes: identification, localization, genomic structure and histological expression pattern in normal testis and seminoma. Hum Genet 105: 17-27

Dejligbjerg M, Grauslund M, Christensen IJ, Tjornelund J, Buhl Jensen P, Sehested M (2008) Identification of predictive biomarkers for the histone deacetylase inhibitor belinostat in a panel of human cancer cell lines. Cancer Biomark 4: 101-9

Dekker FJ, Haisma HJ (2009) Histone acetyl transferases as emerging drug targets. Drug Discov Today 14: 942-8

Deleu S, Lemaire M, Arts J, Menu E, Van Valckenborgh E, King P, Vande Broek I, De Raeve H, Van Camp B, Croucher P, Vanderkerken K (2009a) The effects of JNJ-26481585, a novel hydroxamate-based histone deacetylase inhibitor, on the development of multiple myeloma in the 5T2MM and 5T33MM murine models. Leukemia 23: 1894-903

Deleu S, Lemaire M, Arts J, Menu E, Van Valckenborgh E, Vande Broek I, De Raeve H, Coulton L, Van Camp B, Croucher P, Vanderkerken K (2009b) Bortezomib alone or in combination with the histone deacetylase inhibitor JNJ-26481585: effect on myeloma bone disease in the 5T2MM murine model of myeloma. Cancer Res 69: 5307-11

Deng C, Li N, Ji J, Yang B, Duan G, Zhang X (2006) Development of water-phase derivatization followed by solid-phase microextraction and gas chromatography/mass spectrometry for fast determination of valproic acid in human plasma. Rapid Commun Mass Spectrom 20: 1281-7

Depoix C, Delmotte MH, Formstecher P, Lefebvre P (2001) Control of retinoic acid receptor heterodimerization by ligand-induced structural transitions. A novel mechanism of action for retinoid antagonists. J Biol Chem 276: 9452-9

Devlin RD, Du Z, Buccilli V, Jorgetti V, Canalis E (2002) Transgenic mice overexpressing insulin-like growth factor binding protein-5 display transiently decreased osteoblastic function and osteopenia. Endocrinology 143: 3955-62

DiDonato CJ, Morgan K, Carpten JD, Fuerst P, Ingraham SE, Prescott G, McPherson JD, Wirth B, Zerres K, Hurko O, et al. (1994) Association between Ag1-CA alleles and severity of autosomal recessive proximal spinal muscular atrophy. Am J Hum Genet 55: 1218-29

Dilworth FJ, Chambon P (2001) Nuclear receptors coordinate the activities of chromatin remodeling complexes and coactivators to facilitate initiation of transcription. Oncogene 20: 3047-54

Dimos JT, Rodolfa KT, Niakan KK, Weisenthal LM, Mitsumoto H, Chung W, Croft GF, Saphier G, Leibel R, Goland R, Wichterle H, Henderson CE, Eggan K (2008) Induced pluripotent stem cells generated from patients with ALS can be differentiated into motor neurons. Science 321: 1218-21

Duan C, Clemmons DR (1995) Transcription factor AP-2 regulates human insulin-like growth factor binding protein-5 gene expression. J Biol Chem 270: 24844-51

Dupe V, Davenne M, Brocard J, Dolle P, Mark M, Dierich A, Chambon P, Rijli FM (1997) In vivo functional analysis of the Hoxa-1 3' retinoic acid response element (3'RARE). Development 124: 399-410

Durand B, Saunders M, Leroy P, Leid M, Chambon P (1992) All-trans and 9-cis retinoic acid induction of CRABPII transcription is mediated by RAR-RXR heterodimers bound to DR1 and DR2 repeated motifs. Cell 71: 73-85

Ebert AD, Yu J, Rose FF, Jr., Mattis VB, Lorson CL, Thomson JA, Svendsen CN (2009) Induced pluripotent stem cells from a spinal muscular atrophy patient. Nature 457: 277-80

El Khoury JB, Moore KJ, Means TK, Leung J, Terada K, Toft M, Freeman MW, Luster AD (2003) CD36 mediates the innate host response to beta-amyloid. J Exp Med 197: 1657-66

Ellis L, Pan Y, Smyth GK, George DJ, McCormack C, Williams-Truax R, Mita M, Beck J, Burris H, Ryan G, Atadja P, Butterfoss D, Dugan M, Culver K, Johnstone RW, Prince HM (2008) Histone deacetylase inhibitor panobinostat induces clinical responses with associated alterations in gene expression profiles in cutaneous T-cell lymphoma. Clin Cancer Res 14: 4500-10

Emery AE (1991) Population frequencies of inherited neuromuscular diseases--a world survey. Neuromuscul Disord 1: 19-29

Endemann G, Stanton LW, Madden KS, Bryant CM, White RT, Protter AA (1993) CD36 is a receptor for oxidized low density lipoprotein. J Biol Chem 268: 11811-6

Etienne W, Meyer MH, Peppers J, Meyer RA, Jr. (2004) Comparison of mRNA gene expression by RT-PCR and DNA microarray. Biotechniques 36: 618-20, 622, 624-6

Eyal S, Yagen B, Shimshoni J, Bialer M (2005) Histone deacetylases inhibition and tumor cells cytotoxicity by CNS-active VPA constitutional isomers and derivatives. Biochem Pharmacol 69: 1501-8

Falsaperla R, Romeo G, Di Giorgio A, Pavone P, Parano E, Connolly AM (2001) Long-term survival in a child with arthrogryposis multiplex congenita and spinal muscular atrophy. J Child Neurol 16: 934-6

Fan L, Simard LR (2002) Survival motor neuron (SMN) protein: role in neurite outgrowth and neuromuscular maturation during neuronal differentiation and development. Hum Mol Genet 11: 1605-14

Febbraio M, Hajjar DP, Silverstein RL (2001) CD36: a class B scavenger receptor involved in angiogenesis, atherosclerosis, inflammation, and lipid metabolism. J Clin Invest 108: 785-91

Feldkotter M, Schwarzer V, Wirth R, Wienker TF, Wirth B (2002) Quantitative analyses of SMN1 and SMN2 based on real-time lightCycler PCR: fast and highly reliable carrier testing and prediction of severity of spinal muscular atrophy. Am J Hum Genet 70: 358-68

Feng W, Gubitz AK, Wan L, Battle DJ, Dostie J, Golembe TJ, Dreyfuss G (2005) Gemins modulate the expression and activity of the SMN complex. Hum Mol Genet 14: 1605-11

Fidzianska A, Rafalowska J (2002) Motoneuron death in normal and spinal muscular atrophy-affected human fetuses. Acta Neuropathol 104: 363-8

Finnin MS, Donigian JR, Cohen A, Richon VM, Rifkind RA, Marks PA, Breslow R, Pavletich NP (1999) Structures of a histone deacetylase homologue bound to the TSA and SAHA inhibitors. Nature 401: 188-93

Finsterer J, Stollberger C (1999) Cardiac involvement in Werdnig-Hoffmann's spinal muscular atrophy. Cardiology 92: 178-82

Firth SM, Clemmons DR, Baxter RC (2001) Mutagenesis of basic amino acids in the carboxyl-terminal region of insulin-like growth factor binding protein-5 affects acid-labile subunit binding. Endocrinology 142: 2147

Foust KD, Wang X, McGovern VL, Braun L, Bevan AK, Haidet AM, Le TT, Morales PR, Rich MM, Burghes AH, Kaspar BK (2010) Rescue of the spinal muscular atrophy phenotype in a mouse model by early postnatal delivery of SMN. Nat Biotechnol 28: 271-4

Frugier T, Tiziano FD, Cifuentes-Diaz C, Miniou P, Roblot N, Dierich A, Le Meur M, Melki J (2000) Nuclear targeting defect of SMN lacking the C-terminus in a mouse model of spinal muscular atrophy. Hum Mol Genet 9: 849-58

Fry AE, Ghansa A, Small KS, Palma A, Auburn S, Diakite M, Green A, Campino S, Teo YY, Clark TG, Jeffreys AE, Wilson J, Jallow M, Sisay-Joof F, Pinder M, Griffiths MJ, Peshu N, Williams TN, Newton CR, Marsh K, Molyneux ME, Taylor TE, Koram KA, Oduro AR, Rogers WO, Rockett KA, Sabeti PC, Kwiatkowski DP (2009) Positive selection of a CD36 nonsense variant in sub-Saharan Africa, but no association with severe malaria phenotypes. Hum Mol Genet 18: 2683-92

Gabanella F, Butchbach ME, Saieva L, Carissimi C, Burghes AH, Pellizzoni L (2007) Ribonucleoprotein assembly defects correlate with spinal muscular atrophy severity and preferentially affect a subset of spliceosomal snRNPs. PLoS One 2: e921

Gallagher HC, Bacon CL, Odumeru OA, Gallagher KF, Fitzpatrick T, Regan CM (2004) Valproate activates phosphodiesterase-mediated cAMP degradation: relevance to C6 glioma G1 phase progression. Neurotoxicol Teratol 26: 73-81

Garbes L, Riessland M, Holker I, Heller R, Hauke J, Trankle C, Coras R, Blumcke I, Hahnen E, Wirth B (2009) LBH589 induces up to 10-fold SMN protein levels by several independent mechanisms and is effective even in cells from SMA patients non-responsive to valproate. Hum Mol Genet 18: 3645-58

Gavin DP, Kartan S, Chase K, Jayaraman S, Sharma RP (2009) Histone deacetylase inhibitors and candidate gene expression: An in vivo and in vitro approach to studying chromatin remodeling in a clinical population. J Psychiatr Res 43: 870-6

Gavrilina TO, McGovern VL, Workman E, Crawford TO, Gogliotti RG, DiDonato CJ, Monani UR, Morris GE, Burghes AH (2008) Neuronal SMN expression corrects spinal muscular atrophy in severe SMA mice while muscle-specific SMN expression has no phenotypic effect. Hum Mol Genet 17: 1063-75

Geib T, Hertel KJ (2009) Restoration of full-length SMN promoted by adenoviral vectors expressing RNA antisense oligonucleotides embedded in U7 snRNAs. PLoS One 4: e8204

Geng L, Cuneo KC, Fu A, Tu T, Atadja PW, Hallahan DE (2006) Histone deacetylase (HDAC) inhibitor LBH589 increases duration of gamma-H2AX foci and confines HDAC4 to the cytoplasm in irradiated non-small cell lung cancer. Cancer Res 66: 11298-304

Gennarelli M, Lucarelli M, Capon F, Pizzuti A, Merlini L, Angelini C, Novelli G, Dallapiccola B (1995) Survival motor neuron gene transcript analysis in muscles from spinal muscular atrophy patients. Biochem Biophys Res Commun 213: 342-8

Gentry LE, Twardzik DR, Lim GJ, Ranchalis JE, Lee DC (1987) Expression and characterization of transforming growth factor alpha precursor protein in transfected mammalian cells. Mol Cell Biol 7: 1585-91

Ghyselinck NB, Dupe V, Dierich A, Messaddeq N, Garnier JM, Rochette-Egly C, Chambon P, Mark M (1997) Role of the retinoic acid receptor beta (RARbeta) during mouse development. Int J Dev Biol 41: 425-47

Gibbs JP, Adeyeye MC, Yang Z, Shen DD (2004) Valproic acid uptake by bovine brain microvessel endothelial cells: role of active efflux transport. Epilepsy Res 58: 53-66

Gicquel C, Le Bouc Y (2006) Hormonal regulation of fetal growth. Horm Res 65 Suppl 3: 28-33

Giesemann T, Rathke-Hartlieb S, Rothkegel M, Bartsch JW, Buchmeier S, Jockusch BM, Jockusch H (1999) A role for polyproline motifs in the spinal muscular atrophy protein SMN. Profilins bind to and colocalize with smn in nuclear gems. J Biol Chem 274: 37908-14

Giles F, Fischer T, Cortes J, Garcia-Manero G, Beck J, Ravandi F, Masson E, Rae P, Laird G, Sharma S, Kantarjian H, Dugan M, Albitar M, Bhalla K (2006) A phase I study of intravenous LBH589, a novel cinnamic hydroxamic acid analogue histone deacetylase inhibitor, in patients with refractory hematologic malignancies. Clin Cancer Res 12: 4628-35

Gilliam TC, Brzustowicz LM, Castilla LH, Lehner T, Penchaszadeh GK, Daniels RJ, Byth BC, Knowles J, Hislop JE, Shapira Y, et al. (1990) Genetic homogeneity between acute and chronic forms of spinal muscular atrophy. Nature 345: 823-5

Gladman JT, Bebee TW, Edwards C, Wang X, Sahenk Z, Rich MM, Chandler DS (2010) A humanized Smn gene containing the SMN2 nucleotide alteration in exon 7 mimics SMN2 splicing and the SMA disease phenotype. Hum Mol Genet

Gladman JT, Chandler DS (2009) Intron 7 conserved sequence elements regulate the splicing of the SMN genes. Hum Genet

Glass CK, Rosenfeld MG (2000) The coregulator exchange in transcriptional functions of nuclear receptors. Genes Dev 14: 121-41

Glozak MA, Sengupta N, Zhang X, Seto E (2005) Acetylation and deacetylation of non-histone proteins. Gene 363: 15-23

Gottlicher M, Minucci S, Zhu P, Kramer OH, Schimpf A, Giavara S, Sleeman JP, Lo Coco F, Nervi C, Pelicci PG, Heinzel T (2001) Valproic acid defines a novel class of HDAC inhibitors inducing differentiation of transformed cells. Embo J 20: 6969-78

Goudriaan JR, Dahlmans VE, Teusink B, Ouwens DM, Febbraio M, Maassen JA, Romijn JA, Havekes LM, Voshol PJ (2003) CD36 deficiency increases insulin sensitivity in muscle, but induces insulin resistance in the liver in mice. J Lipid Res 44: 2270-7

Grozinger CM, Schreiber SL (2002) Deacetylase enzymes: biological functions and the use of small-molecule inhibitors. Chem Biol 9: 3-16

Grundemann D, Harlfinger S, Golz S, Geerts A, Lazar A, Berkels R, Jung N, Rubbert A, Schomig E (2005) Discovery of the ergothioneine transporter. Proc Natl Acad Sci U S A 102: 5256-61

Grunstein M (1997) Histone acetylation in chromatin structure and transcription. Nature 389: 349-52

Grzeschik SM, Ganta M, Prior TW, Heavlin WD, Wang CH (2005) Hydroxyurea enhances SMN2 gene expression in spinal muscular atrophy cells. Ann Neurol 58: 194-202

Guillot N, Cuisset JM, Cuvellier JC, Hurtevent JF, Joriot S, Vallee L (2008) Unusual clinical features in infantile Spinal Muscular Atrophies. Brain Dev 30: 169-78

Guler HP, Zapf J, Schmid C, Froesch ER (1989) Insulin-like growth factors I and II in healthy man. Estimations of half-lives and production rates. Acta Endocrinol (Copenh) 121: 753-8

Haddad H, Cifuentes-Diaz C, Miroglio A, Roblot N, Joshi V, Melki J (2003) Riluzole attenuates spinal muscular atrophy disease progression in a mouse model. Muscle Nerve 28: 432-7

Haggarty SJ, Koeller KM, Wong JC, Grozinger CM, Schreiber SL (2003) Domain-selective small-molecule inhibitor of histone deacetylase 6 (HDAC6)-mediated tubulin deacetylation. Proc Natl Acad Sci U S A 100: 4389-94

Hahnen E, Eyupoglu IY, Brichta L, Haastert K, Tränkle C, Siebzehnrübl FA, Riessland M, Hölker I, Claus P, Romstöck J, Buslei R, Wirth B, Blümcke I (2006) In vitro and ex vivo evaluation of second-generation histone deacetylase inhibitors for the treatment of spinal muscular atrophy. J Neurochem: 10.1111/j.1471-4159.2006.03868.x

Hahnen ET, Wirth B (1996) Frequent DNA variant in exon 2a of the survival motor neuron gene (SMN): a further possibility for distinguishing the two copies of the gene. Hum Genet 98: 122-3

Haigis MC, Guarente LP (2006) Mammalian sirtuins--emerging roles in physiology, aging, and calorie restriction. Genes Dev 20: 2913-21

Hart K, Wilcox M (1993) A Drosophila gene encoding an epithelial membrane protein with homology to CD36/LIMP II. J Mol Biol 234: 249-53

Hauke J, Riessland M, Lunke S, Eyupoglu IY, Blumcke I, El-Osta A, Wirth B, Hahnen E (2009) Survival motor neuron gene 2 silencing by DNA methylation correlates with spinal muscular atrophy disease severity and can be bypassed by histone deacetylase inhibition. Hum Mol Genet 18: 304-17

Heier CR, DiDonato CJ (2009) Translational readthrough by the aminoglycoside geneticin (G418) modulates SMN stability in vitro and improves motor function in SMA mice in vivo. Hum Mol Genet 18: 1310-22

Heier CR, Gogliotti RG, DiDonato CJ (2007) SMN transcript stability: could modulation of messenger RNA degradation provide a novel therapy for spinal muscular atrophy? J Child Neurol 22: 1013-8

Helmken C, Wirth B (2000) Exclusion of Htra2-beta1, an up-regulator of full-length SMN2 transcript, as a modifying gene for spinal muscular atrophy. Hum Genet 107: 554-8

Hemeryck A, Geerts R, Monbaliu J, Hassler S, Verhaeghe T, Diels L, Verluyten W, van Beijsterveldt L, Mamidi RN, Janssen C, De Coster R (2007) Tissue distribution and depletion kinetics of bortezomib and bortezomib-related radioactivity in male rats after single and repeated intravenous injection of 14 C-bortezomib. Cancer Chemother Pharmacol 60: 777-87

Heuckeroth RO, Birkenmeier EH, Levin MS, Gordon JI (1987) Analysis of the tissue-specific expression, developmental regulation, and linkage relationships of a rodent gene encoding heart fatty acid binding protein. J Biol Chem 262: 9709-17

Ho L, Crabtree GR (2010) Chromatin remodelling during development. Nature 463: 474-84

Hoebe K, Georgel P, Rutschmann S, Du X, Mudd S, Crozat K, Sovath S, Shamel L, Hartung T, Zahringer U, Beutler B (2005) CD36 is a sensor of diacylglycerides. Nature 433: 523-7

Hofmann Y, Lorson CL, Stamm S, Androphy EJ, Wirth B (2000) Htra2-beta 1 stimulates an exonic splicing enhancer and can restore full-length SMN expression to survival motor neuron 2 (SMN2). Proc Natl Acad Sci U S A 97: 9618-23

Hofmann Y, Wirth B (2002) hnRNP-G promotes exon 7 inclusion of survival motor neuron (SMN) via direct interaction with Htra2-beta1. Hum Mol Genet 11: 2037-49

Holland KD, Monahan S, Morita D, Vartzelis G, Glauser TA (2010) Valproate in children with newly diagnosed idiopathic generalized epilepsy. Acta Neurol Scand 121: 149-53

Hoosdally SJ, Andress EJ, Wooding C, Martin CA, Linton KJ (2009) The Human Scavenger Receptor CD36: glycosylation status and its role in trafficking and function. J Biol Chem 284: 16277-88

Hsieh-Li HM, Chang JG, Jong YJ, Wu MH, Wang NM, Tsai CH, Li H (2000) A mouse model for spinal muscular atrophy. Nat Genet 24: 66-70

Hsu SH, Lai MC, Er TK, Yang SN, Hung CH, Tsai HH, Lin YC, Chang JG, Lo YC, Jong YJ (2010) Ubiquitin carboxyl-terminal hydrolase L1 (UCHL1) regulates the level of SMN expression through ubiquitination in primary spinal muscular atrophy fibroblasts. Clin Chim Acta

Hua Y, Sahashi K, Hung G, Rigo F, Passini MA, Bennett CF, Krainer AR (2010) Antisense correction of SMN2 splicing in the CNS rescues necrosis in a type III SMA mouse model. Genes Dev 24: 1634-44

Hua Y, Vickers TA, Okunola HL, Bennett CF, Krainer AR (2008) Antisense masking of an hnRNP A1/A2 intronic splicing silencer corrects SMN2 splicing in transgenic mice. Am J Hum Genet 82: 834-48

Hua Y, Zhou J (2004a) Rpp20 interacts with SMN and is re-distributed into SMN granules in response to stress. Biochem Biophys Res Commun 314: 268-76

Hua Y, Zhou J (2004b) Survival motor neuron protein facilitates assembly of stress granules. FEBS Lett 572: 69-74

Hwa V, Oh Y, Rosenfeld RG (1999) The insulin-like growth factor-binding protein (IGFBP) superfamily. Endocr Rev 20: 761-87

Iannaccone ST (1998) Spinal muscular atrophy. Semin Neurol 18: 19-26

Ibrahimi A, Sfeir Z, Magharaie H, Amri EZ, Grimaldi P, Abumrad NA (1996) Expression of the CD36 homolog (FAT) in fibroblast cells: effects on fatty acid transport. Proc Natl Acad Sci U S A 93: 2646-51

Jablonka S, Beck M, Lechner BD, Mayer C, Sendtner M (2007) Defective Ca2+ channel clustering in axon terminals disturbs excitability in motoneurons in spinal muscular atrophy. J Cell Biol 179: 139-49

Jablonka S, Schrank B, Kralewski M, Rossoll W, Sendtner M (2000) Reduced survival motor neuron (Smn) gene dose in mice leads to motor neuron degeneration: an animal model for spinal muscular atrophy type III. Hum Mol Genet 9: 341-6

Jarecki J, Chen X, Bernardino A, Coovert DD, Whitney M, Burghes A, Stack J, Pollok BA (2005) Diverse small-molecule modulators of SMN expression found by high-throughput compound screening: early leads towards a therapeutic for spinal muscular atrophy. Hum Mol Genet 14: 2003-18

Jhappan C, Stahle C, Harkins RN, Fausto N, Smith GH, Merlino GT (1990) TGF alpha overexpression in transgenic mice induces liver neoplasia and abnormal development of the mammary gland and pancreas. Cell 61: 1137-46

Jimenez-Dalmaroni MJ, Xiao N, Corper AL, Verdino P, Ainge GD, Larsen DS, Painter GF, Rudd PM, Dwek RA, Hoebe K, Beutler B, Wilson IA (2009) Soluble CD36 ectodomain binds negatively charged diacylglycerol ligands and acts as a co-receptor for TLR2. PLoS One 4: e7411

Jimenez B, Volpert OV, Crawford SE, Febbraio M, Silverstein RL, Bouck N (2000) Signals leading to apoptosis-dependent inhibition of neovascularization by thrombospondin-1. Nat Med 6: 41-8

Kariya S, Park GH, Maeno-Hikichi Y, Leykekhman O, Lutz C, Arkovitz MS, Landmesser LT, Monani UR (2008) Reduced SMN protein impairs maturation of the neuromuscular junctions in mouse models of spinal muscular atrophy. Hum Mol Genet 17: 2552-69

Kashima T, Manley JL (2003) A negative element in SMN2 exon 7 inhibits splicing in spinal muscular atrophy. Nat Genet 34: 460-3

Kashima T, Rao N, David CJ, Manley JL (2007a) hnRNP A1 functions with specificity in repression of SMN2 exon 7 splicing. Hum Mol Genet 16: 3149-59

Kashima T, Rao N, Manley JL (2007b) An intronic element contributes to splicing repression in spinal muscular atrophy. Proc Natl Acad Sci U S A 104: 3426-31

Kastner P, Mark M, Ghyselinck N, Krezel W, Dupe V, Grondona JM, Chambon P (1997) Genetic evidence that the retinoid signal is transduced by heterodimeric RXR/RAR functional units during mouse development. Development 124: 313-26

Kawaguchi Y, Kovacs JJ, McLaurin A, Vance JM, Ito A, Yao TP (2003) The deacetylase HDAC6 regulates aggresome formation and cell viability in response to misfolded protein stress. Cell 115: 727-38

Kedersha NL, Gupta M, Li W, Miller I, Anderson P (1999) RNA-binding proteins TIA-1 and TIAR link the phosphorylation of eIF-2 alpha to the assembly of mammalian stress granules. J Cell Biol 147: 1431-42

Kelter AR, Herchenbach J, Wirth B (2000) The transcription factor-like nuclear regulator (TFNR) contains a novel 55-amino-acid motif repeated nine times and maps closely to SMN1. Genomics 70: 315-26

Kernochan LE, Russo ML, Woodling NS, Huynh TN, Avila AM, Fischbeck KH, Sumner CJ (2005) The role of histone acetylation in SMN gene expression. Hum Mol Genet

Khan SN, Khan AU (2010) Role of histone acetylation in cell physiology and diseases: An update. Clin Chim Acta 411: 1401-11

Kim AH, Puram SV, Bilimoria PM, Ikeuchi Y, Keough S, Wong M, Rowitch D, Bonni A (2009) A centrosomal Cdc20-APC pathway controls dendrite morphogenesis in postmitotic neurons. Cell 136: 322-36

Kim HS, Nagalla SR, Oh Y, Wilson E, Roberts CT, Jr., Rosenfeld RG (1997) Identification of a family of low-affinity insulin-like growth factor binding proteins (IGFBPs): characterization of connective tissue growth factor as a member of the IGFBP superfamily. Proc Natl Acad Sci U S A 94: 12981-6

Kisselev AF, Akopian TN, Castillo V, Goldberg AL (1999) Proteasome active sites allosterically regulate each other, suggesting a cyclical bite-chew mechanism for protein breakdown. Mol Cell 4: 395-402

Kong L, Wang X, Choe DW, Polley M, Burnett BG, Bosch-Marce M, Griffin JW, Rich MM, Sumner CJ (2009) Impaired synaptic vesicle release and immaturity of neuromuscular junctions in spinal muscular atrophy mice. J Neurosci 29: 842-51

Kramer OH, Zhu P, Ostendorff HP, Golebiewski M, Tiefenbach J, Peters MA, Brill B, Groner B, Bach I, Heinzel T, Gottlicher M (2003) The histone deacetylase inhibitor valproic acid selectively induces proteasomal degradation of HDAC2. Embo J 22: 3411-20

Krishnan M, Singh AB, Smith JJ, Sharma A, Chen X, Eschrich S, Yeatman TJ, Beauchamp RD, Dhawan P (2009) HDAC inhibitors regulate claudin-1 expression in colon cancer cells through modulation of mRNA stability. Oncogene 29: 305-12

Kroiss M, Schultz J, Wiesner J, Chari A, Sickmann A, Fischer U (2008) Evolution of an RNP assembly system: a minimal SMN complex facilitates formation of UsnRNPs in Drosophila melanogaster. Proc Natl Acad Sci U S A 105: 10045-50

Kugelberg E, Welander L (1956) Heredofamilial juvenile muscular atrophy simulating muscular dystrophy. AMA Arch Neurol Psychiatry 75: 500-9

Kunjathoor VV, Febbraio M, Podrez EA, Moore KJ, Andersson L, Koehn S, Rhee JS, Silverstein R, Hoff HF, Freeman MW (2002) Scavenger receptors class A-I/II and CD36 are the principal receptors responsible for the uptake of modified low density lipoprotein leading to lipid loading in macrophages. J Biol Chem 277: 49982-8

Laemmli UK (1970) Cleavage of structural proteins during the assembly of the head of bacteriophage T4. Nature 227: 680-5

Lai IL, Lin TP, Yao YL, Lin CY, Hsieh MJ, Yang WM (2010) Histone deacetylase 10 relieves repression on the melanogenic program by maintaining the deacetylation status of repressors. J Biol Chem 285: 7187-96

Lardy HA (1980) Antibiotic inhibitors of mitochondrial energy transfer. Pharmacol Ther 11: 649-60

Lau MM, Stewart CE, Liu Z, Bhatt H, Rotwein P, Stewart CL (1994) Loss of the imprinted IGF2/cation-independent mannose 6-phosphate receptor results in fetal overgrowth and perinatal lethality. Genes Dev 8: 2953-63

Le TT, Pham LT, Butchbach ME, Zhang HL, Monani UR, Coovert DD, Gavrilina TO, Xing L, Bassell GJ, Burghes AH (2005) SMNDelta7, the major product of the centromeric survival motor neuron (SMN2) gene, extends survival in mice with spinal muscular atrophy and associates with full-length SMN. Hum Mol Genet 14: 845-57

Lee DC, Rose TM, Webb NR, Todaro GJ (1985) Cloning and sequence analysis of a cDNA for rat transforming growth factor-alpha. Nature 313: 489-91

Lefebvre S, Burglen L, Reboullet S, Clermont O, Burlet P, Viollet L, Benichou B, Cruaud C, Millasseau P, Zeviani M, et al. (1995) Identification and characterization of a spinal muscular atrophy-determining gene. Cell 80: 155-65

Lefebvre S, Burlet P, Liu Q, Bertrandy S, Clermont O, Munnich A, Dreyfuss G, Melki J (1997) Correlation between severity and SMN protein level in spinal muscular atrophy. Nat Genet 16: 265-9

Leid M, Kastner P, Chambon P (1992a) Multiplicity generates diversity in the retinoic acid signalling pathways. Trends Biochem Sci 17: 427-33

Leid M, Kastner P, Lyons R, Nakshatri H, Saunders M, Zacharewski T, Chen JY, Staub A, Garnier JM, Mader S, et al. (1992b) Purification, cloning, and RXR identity of the HeLa cell factor with which RAR or TR heterodimerizes to bind target sequences efficiently. Cell 68: 377-95

Lheureux PE, Penaloza A, Zahir S, Gris M (2005) Science review: carnitine in the treatment of valproic acid-induced toxicity - what is the evidence? Crit Care 9: 431-40

Liang WC, Yuo CY, Chang JG, Chen YC, Chang YF, Wang HY, Ju YH, Chiou SS, Jong YJ (2008) The effect of hydroxyurea in spinal muscular atrophy cells and patients. J Neurol Sci 268: 87-94

Lim SR, Hertel KJ (2001) Modulation of survival motor neuron pre-mRNA splicing by inhibition of alternative 3' splice site pairing. J Biol Chem 276: 45476-83

Lindekens H, Smolders I, Khan GM, Bialer M, Ebinger G, Michotte Y (2000) In vivo study of the effect of valpromide and valnoctamide in the pilocarpine rat model of focal epilepsy. Pharm Res 17: 1408-13

Lindemann RK, Newbold A, Whitecross KF, Cluse LA, Frew AJ, Ellis L, Williams S, Wiegmans AP, Dear AE, Scott CL, Pellegrini M, Wei A, Richon VM, Marks PA, Lowe SW, Smyth MJ, Johnstone RW (2007) Analysis of the apoptotic and therapeutic activities of histone deacetylase inhibitors by using a mouse model of B cell lymphoma. Proc Natl Acad Sci U S A 104: 8071-6

Liu H, Hu Q, D'Ercole A J, Ye P (2009) Histone deacetylase 11 regulates oligodendrocyte-specific gene expression and cell development in OL-1 oligodendroglia cells. Glia 57: 1-12

Liu H, Shafey D, Moores JN, Kothary R (2010) Neurodevelopmental consequences of Smn depletion in a mouse model of spinal muscular atrophy. J Neurosci Res 88: 111-22

Liu Q, Dreyfuss G (1996) A novel nuclear structure containing the survival of motor neurons protein. Embo J 15: 3555-65

Liu Q, Fischer U, Wang F, Dreyfuss G (1997) The spinal muscular atrophy disease gene product, SMN, and its associated protein SIP1 are in a complex with spliceosomal snRNP proteins. Cell 90: 1013-21

Lohnes D, Mark M, Mendelsohn C, Dolle P, Dierich A, Gorry P, Gansmuller A, Chambon P (1994) Function of the retinoic acid receptors (RARs) during development (I). Craniofacial and skeletal abnormalities in RAR double mutants. Development 120: 2723-48

Lorson CL, Androphy EJ (2000) An exonic enhancer is required for inclusion of an essential exon in the SMA-determining gene SMN. Hum Mol Genet 9: 259-65

Lorson CL, Hahnen E, Androphy EJ, Wirth B (1999) A single nucleotide in the SMN gene regulates splicing and is responsible for spinal muscular atrophy. Proc Natl Acad Sci U S A 96: 6307-11

Lorson CL, Rindt H, Shababi M (2010) Spinal muscular atrophy: mechanisms and therapeutic strategies. Hum Mol Genet 19: R111-8

Lorson CL, Strasswimmer J, Yao JM, Baleja JD, Hahnen E, Wirth B, Le T, Burghes AH, Androphy EJ (1998) SMN oligomerization defect correlates with spinal muscular atrophy severity. Nat Genet 19: 63-6

Luch A (2010) Molecular, clinical and environmental toxicology. Volume 2: clinical toxicology. Preface. Exs 100: XI-XIII

Lucio-Eterovic AK, Cortez MA, Valera ET, Motta FJ, Queiroz RG, Machado HR, Carlotti CG, Jr., Neder L, Scrideli CA, Tone LG (2008) Differential expression of 12 histone deacetylase (HDAC) genes in astrocytomas and normal brain tissue: class II and IV are hypoexpressed in glioblastomas. BMC Cancer 8: 243

Ludwig T, Eggenschwiler J, Fisher P, D'Ercole AJ, Davenport ML, Efstratiadis A (1996) Mouse mutants lacking the type 2 IGF receptor (IGF2R) are rescued from perinatal lethality in Igf2 and Igf1r null backgrounds. Dev Biol 177: 517-35

Luger K, Richmond TJ (1998) The histone tails of the nucleosome. Curr Opin Genet Dev 8: 140-6

Lunn MR, Wang CH (2008) Spinal muscular atrophy. Lancet 371: 2120-33

Maeshima K, Eltsov M (2008) Packaging the genome: the structure of mitotic chromosomes. J Biochem 143: 145-53

Maiso P, Carvajal-Vergara X, Ocio EM, Lopez-Perez R, Mateo G, Gutierrez N, Atadja P, Pandiella A, San Miguel JF (2006) The histone deacetylase inhibitor LBH589 is a potent antimyeloma agent that overcomes drug resistance. Cancer Res 66: 5781-9

Majumder S, Varadharaj S, Ghoshal K, Monani U, Burghes AH, Jacob ST (2004) Identification of a novel cyclic AMP-response element (CRE-II) and the role of CREB-1 in the cAMP-induced expression of the survival motor neuron (SMN) gene. J Biol Chem 279: 14803-11

Mangelsdorf DJ, Evans RM (1995) The RXR heterodimers and orphan receptors. Cell 83: 841-50

Mann GB, Fowler KJ, Gabriel A, Nice EC, Williams RL, Dunn AR (1993) Mice with a null mutation of the TGF alpha gene have abnormal skin architecture, wavy hair, and curly whiskers and often develop corneal inflammation. Cell 73: 249-61

Mariadason JM, Corner GA, Augenlicht LH (2000) Genetic reprogramming in pathways of colonic cell maturation induced by short chain fatty acids: comparison with trichostatin A, sulindac, and curcumin and implications for chemoprevention of colon cancer. Cancer Res 60: 4561-72

Mark M, Ghyselinck NB, Kastner P, Dupe V, Wendling O, Krezel W, Mascrez B, Chambon P (1998) Mesectoderm is a major target of retinoic acid action. Eur J Oral Sci 106 Suppl 1: 24-31

Mark M, Lohnes D, Mendelsohn C, Dupe V, Vonesch JL, Kastner P, Rijli F, Bloch-Zupan A, Chambon P (1995) Roles of retinoic acid receptors and of Hox genes in the patterning of the teeth and of the jaw skeleton. Int J Dev Biol 39: 111-21

Markowitz JA, Tinkle MB, Fischbeck KH (2004) Spinal muscular atrophy in the neonate. J Obstet Gynecol Neonatal Nurs 33: 12-20

Marquardt H, Hunkapiller MW, Hood LE, Todaro GJ (1984) Rat transforming growth factor type 1: structure and relation to epidermal growth factor. Science 223: 1079-82

Marquis J, Meyer K, Angehrn L, Kampfer SS, Rothen-Rutishauser B, Schumperli D (2007) Spinal muscular atrophy: SMN2 pre-mRNA splicing corrected by a U7 snRNA derivative carrying a splicing enhancer sequence. Mol Ther 15: 1479-86

Massague J (1983) Epidermal growth factor-like transforming growth factor. I. Isolation, chemical characterization, and potentiation by other transforming factors from feline sarcoma virus-transformed rat cells. J Biol Chem 258: 13606-13

Matsui Y, Halter SA, Holt JT, Hogan BL, Coffey RJ (1990) Development of mammary hyperplasia and neoplasia in MMTV-TGF alpha transgenic mice. Cell 61: 1147-55

Matsuura K, Ohmori T, Nakamura M, Itoh Y, Hirano K (2008) A simple and rapid determination of valproic acid in human plasma using a non-porous silica column and liquid chromatography with tandem mass spectrometric detection. Biomed Chromatogr 22: 387-93

Mattis VB, Ebert AD, Fosso MY, Chang CW, Lorson CL (2009a) Delivery of a read-through inducing compound, TC007, lessens the severity of a spinal muscular atrophy animal model. Hum Mol Genet 18: 3906-13

Mattis VB, Fosso MY, Chang CW, Lorson CL (2009b) Subcutaneous administration of TC007 reduces disease severity in an animal model of SMA. BMC Neurosci 10: 142

Mattis VB, Rai R, Wang J, Chang CW, Coady T, Lorson CL (2006) Novel aminoglycosides increase SMN levels in spinal muscular atrophy fibroblasts. Hum Genet 120: 589-601

Mattox W, Baker BS (1991) Autoregulation of the splicing of transcripts from the transformer-2 gene of Drosophila. Genes Dev 5: 786-96

McAndrew PE, Parsons DW, Simard LR, Rochette C, Ray PN, Mendell JR, Prior TW, Burghes AH (1997) Identification of proximal spinal muscular atrophy carriers and patients by analysis of SMNT and SMNC gene copy number. Am J Hum Genet 60: 1411-22

McBryant SJ, Lu X, Hansen JC (2010) Multifunctionality of the linker histones: an emerging role for protein-protein interactions. Cell Res 20: 519-28

McConkey D (2010) Proteasome and HDAC: who's zooming who? Blood 116: 308-9

McGovern VL, Gavrilina TO, Beattie CE, Burghes AH (2008) Embryonic motor axon development in the severe SMA mouse. Hum Mol Genet 17: 2900-9

McLean MJ, Macdonald RL (1986) Sodium valproate, but not ethosuximide, produces use- and voltage-dependent limitation of high frequency repetitive firing of action potentials of mouse central neurons in cell culture. J Pharmacol Exp Ther 237: 1001-11

McWhorter ML, Boon KL, Horan ES, Burghes AH, Beattie CE (2008) The SMN binding protein Gemin2 is not involved in motor axon outgrowth. Dev Neurobiol 68: 182-94

McWhorter ML, Monani UR, Burghes AH, Beattie CE (2003) Knockdown of the survival motor neuron (Smn) protein in zebrafish causes defects in motor axon outgrowth and pathfinding. J Cell Biol 162: 919-31

Mead S, Poulter M, Uphill J, Beck J, Whitfield J, Webb TE, Campbell T, Adamson G, Deriziotis P, Tabrizi SJ, Hummerich H, Verzilli C, Alpers MP, Whittaker JC, Collinge J (2009) Genetic risk factors for variant Creutzfeldt-Jakob disease: a genome-wide association study. Lancet Neurol 8: 57-66

Means TK, Mylonakis E, Tampakakis E, Colvin RA, Seung E, Puckett L, Tai MF, Stewart CR, Pukkila-Worley R, Hickman SE, Moore KJ, Calderwood SB, Hacohen N, Luster AD, El Khoury J (2009) Evolutionarily conserved recognition and innate immunity to fungal pathogens by the scavenger receptors SCARF1 and CD36. J Exp Med 206: 637-53

Meister G, Fischer U (2002) Assisted RNP assembly: SMN and PRMT5 complexes cooperate in the formation of spliceosomal UsnRNPs. Embo J 21: 5853-63

Melki J, Abdelhak S, Sheth P, Bachelot MF, Burlet P, Marcadet A, Aicardi J, Barois A, Carriere JP, Fardeau M, et al. (1990) Gene for chronic proximal spinal muscular atrophies maps to chromosome 5q. Nature 344: 767-8

Melki J, Burlet P, Clermont O, Pascal F, Paul B, Abdelhak S, Sherrington R, Gurling H, Nakamura Y, Weissenbach J, et al. (1993) Refined linkage map of chromosome 5 in the region of the spinal muscular atrophy gene. Genomics 15: 521-4

Melki J, Lefebvre S, Burglen L, Burlet P, Clermont O, Millasseau P, Reboullet S, Benichou B, Zeviani M, Le Paslier D, et al. (1994) De novo and inherited deletions of the 5q13 region in spinal muscular atrophies. Science 264: 1474-7

Mendelsohn C, Lohnes D, Decimo D, Lufkin T, LeMeur M, Chambon P, Mark M (1994) Function of the retinoic acid receptors (RARs) during development (II). Multiple abnormalities at various stages of organogenesis in RAR double mutants. Development 120: 2749-71

Mercuri E, Bertini E, Messina S, Pelliccioni M, D'Amico A, Colitto F, Mirabella M, Tiziano FD, Vitali T, Angelozzi C, Kinali M, Main M, Brahe C (2004) Pilot trial of phenylbutyrate in spinal muscular atrophy. Neuromuscul Disord 14: 130-5

Mercuri E, Bertini E, Messina S, Solari A, D'Amico A, Angelozzi C, Battini R, Berardinelli A, Boffi P, Bruno C, Cini C, Colitto F, Kinali M, Minetti C, Mongini T, Morandi L, Neri G, Orcesi S, Pane M, Pelliccioni M, Pini A, Tiziano FD, Villanova M, Vita G, Brahe C (2007) Randomized, double-blind, placebo-controlled trial of phenylbutyrate in spinal muscular atrophy. Neurology 68: 51-5

Meunier H, Carraz G, Neunier Y, Eymard P, Aimard M (1963) [Pharmacodynamic properties of N-dipropylacetic acid.]. Therapie 18: 435-8

Michaelis M, Michaelis UR, Fleming I, Suhan T, Cinatl J, Blaheta RA, Hoffmann K, Kotchetkov R, Busse R, Nau H, Cinatl J, Jr. (2004a) Valproic acid inhibits angiogenesis in vitro and in vivo. Mol Pharmacol 65: 520-7

Michaelis M, Suhan T, Cinatl J, Driever PH, Cinatl J, Jr. (2004b) Valproic acid and interferon-alpha synergistically inhibit neuroblastoma cell growth in vitro and in vivo. Int J Oncol 25: 1795-9

Michaud M, Arnoux T, Bielli S, Durand E, Rotrou Y, Jablonka S, Robert F, Giraudon-Paoli M, Riessland M, Mattei MG, Andriambeloson E, Wirth B, Sendtner M, Gallego J, Pruss RM, Bordet T (2010) Neuromuscular defects and breathing disorders in a new mouse model of spinal muscular atrophy. Neurobiol Dis 38: 125-35

Miettinen PJ, Chin JR, Shum L, Slavkin HC, Shuler CF, Derynck R, Werb Z (1999) Epidermal growth factor receptor function is necessary for normal craniofacial development and palate closure. Nat Genet 22: 69-73

Miguel-Aliaga I, Culetto E, Walker DS, Baylis HA, Sattelle DB, Davies KE (1999) The Caenorhabditis elegans orthologue of the human gene responsible for spinal muscular atrophy is a maternal product critical for germline maturation and embryonic viability. Hum Mol Genet 8: 2133-43

Milutinovic S, D'Alessio AC, Detich N, Szyf M (2007) Valproate induces widespread epigenetic reprogramming which involves demethylation of specific genes. Carcinogenesis 28: 560-71

Mitsiades CS, Mitsiades NS, McMullan CJ, Poulaki V, Shringarpure R, Hideshima T, Akiyama M, Chauhan D, Munshi N, Gu X, Bailey C, Joseph M, Libermann TA, Richon VM, Marks PA, Anderson KC (2004) Transcriptional signature of histone deacetylase inhibition in multiple myeloma: biological and clinical implications. Proc Natl Acad Sci U S A 101: 540-5

Miyajima H, Miyaso H, Okumura M, Kurisu J, Imaizumi K (2002) Identification of a cis-acting element for the regulation of SMN exon 7 splicing. J Biol Chem 277: 23271-7

Miyanaga A, Gemma A, Noro R, Kataoka K, Matsuda K, Nara M, Okano T, Seike M, Yoshimura A, Kawakami A, Uesaka H, Nakae H, Kudoh S (2008) Antitumor activity of histone deacetylase inhibitors in non-small cell lung cancer cells: development of a molecular predictive model. Mol Cancer Ther 7: 1923-30

Miyaoka K, Kuwasako T, Hirano K, Nozaki S, Yamashita S, Matsuzawa Y (2001) CD36 deficiency associated with insulin resistance. Lancet 357: 686-7

Miyaso H, Okumura M, Kondo S, Higashide S, Miyajima H, Imaizumi K (2003) An intronic splicing enhancer element in survival motor neuron (SMN) pre-mRNA. J Biol Chem 278: 15825-31

Mohan S, Baylink DJ, Pettis JL (1996) Insulin-like growth factor (IGF)-binding proteins in serum--do they have additional roles besides modulating the endocrine IGF actions? J Clin Endocrinol Metab 81: 3817-20

Mohan S, Nakao Y, Honda Y, Landale E, Leser U, Dony C, Lang K, Baylink DJ (1995) Studies on the mechanisms by which insulin-like growth factor (IGF) binding protein-4 (IGFBP-4) and IGFBP-5 modulate IGF actions in bone cells. J Biol Chem 270: 20424-31

Monani UR, Lorson CL, Parsons DW, Prior TW, Androphy EJ, Burghes AH, McPherson JD (1999) A single nucleotide difference that alters splicing patterns distinguishes the SMA gene SMN1 from the copy gene SMN2. Hum Mol Genet 8: 1177-83

Monani UR, Pastore MT, Gavrilina TO, Jablonka S, Le TT, Andreassi C, DiCocco JM, Lorson C, Androphy EJ, Sendtner M, Podell M, Burghes AH (2003) A transgene carrying an A2G missense mutation in the SMN gene modulates phenotypic severity in mice with severe (type I) spinal muscular atrophy. J Cell Biol 160: 41-52

Monani UR, Sendtner M, Coovert DD, Parsons DW, Andreassi C, Le TT, Jablonka S, Schrank B, Rossoll W, Prior TW, Morris GE, Burghes AH (2000) The human centromeric survival motor neuron gene (SMN2) rescues embryonic lethality in Smn(-/-) mice and results in a mouse with spinal muscular atrophy. Hum Mol Genet 9: 333-9

Montezinho LP, Mork A, Duarte CB, Penschuck S, Geraldes CF, Castro MM (2007) Effects of mood stabilizers on the inhibition of adenylate cyclase via dopamine D(2)-like receptors. Bipolar Disord 9: 290-7

Moore KJ, El Khoury J, Medeiros LA, Terada K, Geula C, Luster AD, Freeman MW (2002) A CD36-initiated signaling cascade mediates inflammatory effects of beta-amyloid. J Biol Chem 277: 47373-9

Morris ME, Felmlee MA (2008) Overview of the proton-coupled MCT (SLC16A) family of transporters: characterization, function and role in the transport of the drug of abuse gamma-hydroxybutyric acid. AAPS J 10: 311-21

Muller WE, Thakur NL, Ushijima H, Thakur AN, Krasko A, Le Pennec G, Indap MM, Perovic-Ottstadt S, Schroder HC, Lang G, Bringmann G (2004) Matrix-mediated canal formation in primmorphs from the sponge Suberites domuncula involves the expression of a CD36 receptor-ligand system. J Cell Sci 117: 2579-90

Mullis K, Faloona F, Scharf S, Saiki R, Horn G, Erlich H (1992) Specific enzymatic amplification of DNA in vitro: the polymerase chain reaction. 1986. Biotechnology 24: 17-27

Munsat TL, Davies KE (1992) International SMA consortium meeting. (26-28 June 1992, Bonn, Germany). Neuromuscul Disord 2: 423-8

Murali SG, Liu X, Nelson DW, Hull AK, Grahn M, Clayton MK, Pintar JE, Ney DM (2007) Intestinotrophic effects of exogenous IGF-I are not diminished in IGF binding protein-5 knockout mice. Am J Physiol Regul Integr Comp Physiol 292: R2144-50

Nagy L, Kao HY, Chakravarti D, Lin RJ, Hassig CA, Ayer DE, Schreiber SL, Evans RM (1997) Nuclear receptor repression mediated by a complex containing SMRT, mSin3A, and histone deacetylase. Cell 89: 373-80

Naora K, Ichikawa N, Nishimura N, Hirano H, Shen DD, Iwamoto K (1996) Saturable transport of valproic acid in rat choroid plexus in vitro. J Pharm Sci 85: 423-6

Narita N, Kato M, Tazoe M, Miyazaki K, Narita M, Okado N (2002) Increased monoamine concentration in the brain and blood of fetal thalidomide- and valproic acid-exposed rat: putative animal models for autism. Pediatr Res 52: 576-9

Ni JZ, Grate L, Donohue JP, Preston C, Nobida N, O'Brien G, Shiue L, Clark TA, Blume JE, Ares M, Jr. (2007) Ultraconserved elements are associated with homeostatic control of splicing regulators by alternative splicing and nonsense-mediated decay. Genes Dev 21: 708-18

Ning Y, Schuller AG, Bradshaw S, Rotwein P, Ludwig T, Frystyk J, Pintar JE (2006) Diminished growth and enhanced glucose metabolism in triple knockout mice containing mutations of insulin-like growth factor binding protein-3, -4, and -5. Mol Endocrinol 20: 2173-86

Nishino TG, Miyazaki M, Hoshino H, Miwa Y, Horinouchi S, Yoshida M (2008) 14-3-3 regulates the nuclear import of class IIa histone deacetylases. Biochem Biophys Res Commun 377: 852-6

Normanno N, De Luca A, Bianco C, Strizzi L, Mancino M, Maiello MR, Carotenuto A, De Feo G, Caponigro F, Salomon DS (2006) Epidermal growth factor receptor (EGFR) signaling in cancer. Gene 366: 2-16

Nunez E, Kwon YS, Hutt KR, Hu Q, Cardamone MD, Ohgi KA, Garcia-Bassets I, Rose DW, Glass CK, Rosenfeld MG, Fu XD (2008) Nuclear receptor-enhanced transcription requires motor- and LSD1-dependent gene networking in interchromatin granules. Cell 132: 996-1010

Ocio EM, Vilanova D, Atadja P, Maiso P, Crusoe E, Fernandez-Lazaro D, Garayoa M, San-Segundo L, Hernandez-Iglesias T, de Alava E, Shao W, Yao YM, Pandiella A, San-Miguel JF (2010) In vitro and in vivo rationale for the triple combination of panobinostat (LBH589) and dexamethasone with either bortezomib or lenalidomide in multiple myeloma. Haematologica 95: 794-803

Oh Y, Nagalla SR, Yamanaka Y, Kim HS, Wilson E, Rosenfeld RG (1996) Synthesis and characterization of insulin-like growth factor-binding protein (IGFBP)-7. Recombinant human mac25 protein specifically binds IGF-I and -II. J Biol Chem 271: 30322-5

Ollivier ML, Dubois MF, Krajinovic M, Cossette P, Carmant L (2009) Risk factors for valproic acid resistance in childhood absence epilepsy. Seizure 18: 690-4

Oprea GE, Krober S, McWhorter ML, Rossoll W, Muller S, Krawczak M, Bassell GJ, Beattie CE, Wirth B (2008) Plastin 3 is a protective modifier of autosomal recessive spinal muscular atrophy. Science 320: 524-7

Otaegui D, Rodriguez-Gascon A, Zubia A, Cossio FP, Pedraz JL (2009) Pharmacokinetics and tissue distribution of Kendine 91, a novel histone deacetylase inhibitor, in mice. Cancer Chemother Pharmacol 64: 153-9

Owen N, Doe CL, Mellor J, Davies KE (2000) Characterization of the Schizosaccharomyces pombe orthologue of the human survival motor neuron (SMN) protein. Hum Mol Genet 9: 675-84

Papandreou CN, Daliani DD, Nix D, Yang H, Madden T, Wang X, Pien CS, Millikan RE, Tu SM, Pagliaro L, Kim J, Adams J, Elliott P, Esseltine D, Petrusich A, Dieringer P, Perez C, Logothetis CJ (2004) Phase I trial of the proteasome inhibitor bortezomib in patients with advanced solid tumors with observations in androgen-independent prostate cancer. J Clin Oncol 22: 2108-21

Parker A, Rees C, Clarke J, Busby WH, Jr., Clemmons DR (1998) Binding of insulin-like growth factor (IGF)-binding protein-5 to smooth-muscle cell extracellular matrix is a major determinant of the cellular response to IGF-I. Mol Biol Cell 9: 2383-92

Parsons DW, McAndrew PE, Iannaccone ST, Mendell JR, Burghes AH, Prior TW (1998) Intragenic telSMN mutations: frequency, distribution, evidence of a founder effect, and modification of the spinal muscular atrophy phenotype by cenSMN copy number. Am J Hum Genet 63: 1712-23

Passini MA, Bu J, Roskelley EM, Richards AM, Sardi SP, O'Riordan CR, Klinger KW, Shihabuddin LS, Cheng SH (2010) CNS-targeted gene therapy improves survival and motor function in a mouse model of spinal muscular atrophy. J Clin Invest 120: 1253-64

Paushkin S, Charroux B, Abel L, Perkinson RA, Pellizzoni L, Dreyfuss G (2000) The survival motor neuron protein of Schizosacharomyces pombe. Conservation of survival motor neuron interaction domains in divergent organisms. J Biol Chem 275: 23841-6

Pavan B, Biondi C, Dalpiaz A (2009) Adenylyl cyclases as innovative therapeutic goals. Drug Discov Today 14: 982-91

Pearn J (1978) Incidence, prevalence, and gene frequency studies of chronic childhood spinal muscular atrophy. J Med Genet 15: 409-13

Peart MJ, Smyth GK, van Laar RK, Bowtell DD, Richon VM, Marks PA, Holloway AJ, Johnstone RW (2005) Identification and functional significance of genes regulated by structurally different histone deacetylase inhibitors. Proc Natl Acad Sci U S A 102: 3697-702

Pedrotti S, Bielli P, Paronetto MP, Ciccosanti F, Fimia GM, Stamm S, Manley JL, Sette C (2010) The splicing regulator Sam68 binds to a novel exonic splicing silencer and functions in SMN2 alternative splicing in spinal muscular atrophy. Embo J 29: 1235-47

Pellizzoni L (2007) Chaperoning ribonucleoprotein biogenesis in health and disease. EMBO Rep 8: 340-5

Pellizzoni L, Baccon J, Rappsilber J, Mann M, Dreyfuss G (2001a) Purification of native SMN complexes and identification of Gemin6 as a novel component. J Biol Chem

Pellizzoni L, Charroux B, Dreyfuss G (1999) SMN mutants of spinal muscular atrophy patients are defective in binding to snRNP proteins. Proc Natl Acad Sci U S A 96: 11167-72

Pellizzoni L, Charroux B, Rappsilber J, Mann M, Dreyfuss G (2001b) A functional interaction between the survival motor neuron complex and RNA polymerase II. J Cell Biol 152: 75-85

Pellizzoni L, Yong J, Dreyfuss G (2002) Essential Role for the SMN Complex in the Specificity of snRNP Assembly. Science 298: 1775-9

Pfeffer S, Ullrich A (1985) Epidermal growth factor. Is the precursor a receptor? Nature 313: 184

Phiel CJ, Zhang F, Huang EY, Guenther MG, Lazar MA, Klein PS (2001) Histone deacetylase is a direct target of valproic acid, a potent anticonvulsant, mood stabilizer, and teratogen. J Biol Chem 276: 36734-41

Piazzon N, Rage F, Schlotter F, Moine H, Branlant C, Massenet S (2008) In vitro and in cellulo evidences for association of the survival of motor neuron complex with the fragile X mental retardation protein. J Biol Chem 283: 5598-610

Podrez EA, Febbraio M, Sheibani N, Schmitt D, Silverstein RL, Hajjar DP, Cohen PA, Frazier WA, Hoff HF, Hazen SL (2000) Macrophage scavenger receptor CD36 is the major receptor for LDL modified by monocyte-generated reactive nitrogen species. J Clin Invest 105: 1095-108

Poirier H, Degrace P, Niot I, Bernard A, Besnard P (1996) Localization and regulation of the putative membrane fatty-acid transporter (FAT) in the small intestine. Comparison with fatty acid-binding proteins (FABP). Eur J Biochem 238: 368-73

Prince HM, Bishton MJ, Johnstone RW (2009) Panobinostat (LBH589): a potent pan-deacetylase inhibitor with promising activity against hematologic and solid tumors. Future Oncol 5: 601-12

Prior TW, Krainer AR, Hua Y, Swoboda KJ, Snyder PC, Bridgeman SJ, Burghes AH, Kissel JT (2009) A positive modifier of spinal muscular atrophy in the SMN2 gene. Am J Hum Genet 85: 408-13

Qian JF, Lazar-Wesley E, Breugnot C, May E (1993) Human transforming growth factor alpha: sequence analysis of the 4.5-kb and 1.6-kb mRNA species. Gene 132: 291-6

Rac ME, Safranow K, Poncyljusz W (2007) Molecular basis of human CD36 gene mutations. Mol Med 13: 288-96

Rahaman SO, Lennon DJ, Febbraio M, Podrez EA, Hazen SL, Silverstein RL (2006) A CD36-dependent signaling cascade is necessary for macrophage foam cell formation. Cell Metab 4: 211-21

Rajaram S, Baylink DJ, Mohan S (1997) Insulin-like growth factor-binding proteins in serum and other biological fluids: regulation and functions. Endocr Rev 18: 801-31

Rajendra TK, Gonsalvez GB, Walker MP, Shpargel KB, Salz HK, Matera AG (2007) A Drosophila melanogaster model of spinal muscular atrophy reveals a function for SMN in striated muscle. J Cell Biol 176: 831-41

Rastinejad F, Wagner T, Zhao Q, Khorasanizadeh S (2000) Structure of the RXR-RAR DNA-binding complex on the retinoic acid response element DR1. Embo J 19: 1045-54

Redfern CP, Todd C (1992) Retinoic acid receptor expression in human skin keratinocytes and dermal fibroblasts in vitro. J Cell Sci 102 (Pt 1): 113-21

Ren J, Jin W, Chen H (2010) oxHDL decreases the expression of CD36 on human macrophages through PPARgamma and p38 MAP kinase dependent mechanisms. Mol Cell Biochem

Ren Y, Silverstein RL, Allen J, Savill J (1995) CD36 gene transfer confers capacity for phagocytosis of cells undergoing apoptosis. J Exp Med 181: 1857-62

Rettie AE, Rettenmeier AW, Howald WN, Baillie TA (1987) Cytochrome P-450--catalyzed formation of delta 4-VPA, a toxic metabolite of valproic acid. Science 235: 890-3

Riessland M, Ackermann B, Forster A, Jakubik M, Hauke J, Garbes L, Fritzsche I, Mende Y, Blumcke I, Hahnen E, Wirth B (2010) SAHA ameliorates the SMA phenotype in two mouse models for spinal muscular atrophy. Hum Mol Genet 19: 1492-506

Riessland M, Brichta L, Hahnen E, Wirth B (2006) The benzamide M344, a novel histone deacetylase inhibitor, significantly increases SMN2 RNA/protein levels in spinal muscular atrophy (SMA) cells. Medgen: 113 (abstract P293)

Rinderknecht E, Humbel RE (1978a) The amino acid sequence of human insulin-like growth factor I and its structural homology with proinsulin. J Biol Chem 253: 2769-76

Rinderknecht E, Humbel RE (1978b) Primary structure of human insulin-like growth factor II. FEBS Lett 89: 283-6

Robert E, Guibaud P (1982) Maternal valproic acid and congenital neural tube defects. Lancet 2: 937

Roberts W, Magwenzi S, Aburima A, Naseem KM (2010) Thrombinspondin-1 induces platelet activation through CD36-dependent inhibition of the cAMP/protein kinase A signaling cascade. Blood

Rochette-Egly C (2003) Nuclear receptors: integration of multiple signalling pathways through phosphorylation. Cell Signal 15: 355-66

Rochette-Egly C, Oulad-Abdelghani M, Staub A, Pfister V, Scheuer I, Chambon P, Gaub MP (1995) Phosphorylation of the retinoic acid receptor-alpha by protein kinase A. Mol Endocrinol 9: 860-71

Rochette CF, Gilbert N, Simard LR (2001) SMN gene duplication and the emergence of the SMN2 gene occurred in distinct hominids: SMN2 is unique to Homo sapiens. Hum Genet 108: 255-66

Roh TY, Cuddapah S, Zhao K (2005) Active chromatin domains are defined by acetylation islands revealed by genome-wide mapping. Genes Dev 19: 542-52

Rosenfeld MG, Lunyak VV, Glass CK (2006) Sensors and signals: a coactivator/corepressor/epigenetic code for integrating signal-dependent programs of transcriptional response. Genes Dev 20: 1405-28

Rosenthal A, Lindquist PB, Bringman TS, Goeddel DV, Derynck R (1986) Expression in rat fibroblasts of a human transforming growth factor-alpha cDNA results in transformation. Cell 46: 301-9

Ross J (1995) mRNA stability in mammalian cells. Microbiol Rev 59: 423-50

Ross SA, McCaffery PJ, Drager UC, De Luca LM (2000) Retinoids in embryonal development. Physiol Rev 80: 1021-54

Rossoll W, Jablonka S, Andreassi C, Kroning AK, Karle K, Monani UR, Sendtner M (2003) Smn, the spinal muscular atrophy-determining gene product, modulates axon growth and localization of beta-actin mRNA in growth cones of motoneurons. J Cell Biol 163: 801-12

Roy CC, Kien CL, Bouthillier L, Levy E (2006) Short-chain fatty acids: ready for prime time? Nutr Clin Pract 21: 351-66

Roy N, Mahadevan MS, McLean M, Shutler G, Yaraghi Z, Farahani R, Baird S, Besner-Johnston A, Lefebvre C, Kang X, et al. (1995a) The gene for neuronal apoptosis inhibitory protein is partially deleted in individuals with spinal muscular atrophy. Cell 80: 167-78

Roy N, McLean MD, Besner-Johnston A, Lefebvre C, Salih M, Carpten JD, Burghes AH, Yaraghi Z, Ikeda JE, Korneluk RG, et al. (1995b) Refined physical map of the spinal muscular atrophy gene (SMA) region at 5q13 based on YAC and cosmid contiguous arrays. Genomics 26: 451-60

Rudnik-Schoneborn S, Berg C, Zerres K, Betzler C, Grimm T, Eggermann T, Eggermann K, Wirth R, Wirth B, Heller R (2009) Genotype-phenotype studies in infantile spinal muscular atrophy (SMA) type I in Germany: implications for clinical trials and genetic counselling. Clin Genet 76: 168-78

Rudnik-Schöneborn S, Forkert R, Hahnen E, Wirth B, Zerres K (1996) Clinical spectrum and diagnostic criteria of infantile spinal muscular atrophy: further delineation on the basis of SMN gene deletion findings. Neuropediatrics 27: 8-15

Rudnik-Schoneborn S, Heller R, Berg C, Betzler C, Grimm T, Eggermann T, Eggermann K, Wirth R, Wirth B, Zerres K (2008) Congenital heart disease is a feature of severe infantile spinal muscular atrophy. J Med Genet 45: 635-8

Rudnik-Schoneborn S, Lutzenrath S, Borkowska J, Karwanska A, Hausmanowa-Petrusewicz I, Zerres K (1998) Analysis of creatine kinase activity in 504 patients with proximal spinal muscular atrophy types I-III from the point of view of progression and severity. Eur Neurol 39: 154-62

Rudnik-Schoneborn S, Rohrig D, Morgan G, Wirth B, Zerres K (1994) Autosomal recessive proximal spinal muscular atrophy in 101 sibs out of 48 families: clinical picture, influence of gender, and genetic implications. Am J Med Genet 51: 70-6

Rudnik-Schoneborn S, Vogelgesang S, Armbrust S, Graul-Neumann L, Fusch C, Zerres K (2010) Digital necroses and vascular thrombosis in severe spinal muscular atrophy. Muscle Nerve 42: 144-7

Russman BS, Buncher CR, White M, Samaha FJ, Iannaccone ST (1996) Function changes in spinal muscular atrophy II and III. The DCN/SMA Group. Neurology 47: 973-6

Russman BS, Iannaccone ST, Samaha FJ (2003) A phase 1 trial of riluzole in spinal muscular atrophy. Arch Neurol 60: 1601-3

Salih DA, Tripathi G, Holding C, Szestak TA, Gonzalez MI, Carter EJ, Cobb LJ, Eisemann JE, Pell JM (2004) Insulin-like growth factor-binding protein 5 (Igfbp5) compromises survival, growth, muscle development, and fertility in mice. Proc Natl Acad Sci U S A 101: 4314-9

Sandgren EP, Luetteke NC, Palmiter RD, Brinster RL, Lee DC (1990) Overexpression of TGF alpha in transgenic mice: induction of epithelial hyperplasia, pancreatic metaplasia, and carcinoma of the breast. Cell 61: 1121-35

Sanger F, Nicklen S, Coulson AR (1977) DNA sequencing with chain-terminating inhibitors. Proc Natl Acad Sci U S A 74: 5463-7

Schalm SW, Brouwer JT, Bekkering FC, van Rossum TG (1999) New treatment strategies in non-responder patients with chronic hepatitis C. J Hepatol 31 Suppl 1: 184-8

Schmutz J, Martin J, Terry A, Couronne O, Grimwood J, Lowry S, Gordon LA, Scott D, Xie G, Huang W, Hellsten U, Tran-Gyamfi M, She X, Prabhakar S, Aerts A, Altherr M, Bajorek E, Black S, Branscomb E, Caoile C, Challacombe JF, Chan YM, Denys M, Detter JC, Escobar J, Flowers D, Fotopulos D, Glavina T, Gomez M, Gonzales E, Goodstein D, Grigoriev I, Groza M, Hammon N, Hawkins T, Haydu L, Israni S, Jett J, Kadner K, Kimball H, Kobayashi A, Lopez F, Lou Y, Martinez D, Medina C, Morgan J, Nandkeshwar R, Noonan JP, Pitluck S, Pollard M, Predki P, Priest J, Ramirez L, Retterer J, Rodriguez A, Rogers S, Salamov A, Salazar A, Thayer N, Tice H, Tsai M, Ustaszewska A, Vo N, Wheeler J, Wu K, Yang J, Dickson M, Cheng JF, Eichler EE, Olsen A,

Pennacchio LA, Rokhsar DS, Richardson P, Lucas SM, Myers RM, Rubin EM (2004) The DNA sequence and comparative analysis of human chromosome 5. Nature 431: 268-74

Schneider MR, Wolf E, Hoeflich A, Lahm H (2002) IGF-binding protein-5: flexible player in the IGF system and effector on its own. J Endocrinol 172: 423-40

Schrank B, Gotz R, Gunnersen JM, Ure JM, Toyka KV, Smith AG, Sendtner M (1997) Inactivation of the survival motor neuron gene, a candidate gene for human spinal muscular atrophy, leads to massive cell death in early mouse embryos. Proc Natl Acad Sci U S A 94: 9920-5

Schreiber AB, Winkler ME, Derynck R (1986) Transforming growth factor-alpha: a more potent angiogenic mediator than epidermal growth factor. Science 232: 1250-3

Selenko P, Sprangers R, Stier G, Buhler D, Fischer U, Sattler M (2001) SMN tudor domain structure and its interaction with the Sm proteins. Nat Struct Biol 8: 27-31

Serpente P, Tumpel S, Ghyselinck NB, Niederreither K, Wiedemann LM, Dolle P, Chambon P, Krumlauf R, Gould AP (2005) Direct crossregulation between retinoic acid receptor {beta} and Hox genes during hindbrain segmentation. Development 132: 503-13

Setola V, Terao M, Locatelli D, Bassanini S, Garattini E, Battaglia G (2007) Axonal-SMN (a-SMN), a protein isoform of the survival motor neuron gene, is specifically involved in axonogenesis. Proc Natl Acad Sci U S A 104: 1959-64

Shababi M, Glascock J, Lorson C (2010a) Combination of SMN trans-splicing and a neurotrophic factor increases the life span and body mass in a severe model of spinal muscular atrophy. Hum Gene Ther

Shababi M, Habibi J, Yang HT, Vale SM, Sewell WA, Lorson CL (2010b) Cardiac defects contribute to the pathology of spinal muscular atrophy models. Hum Mol Genet

Shafey D, Cote PD, Kothary R (2005) Hypomorphic Smn knockdown C2C12 myoblasts reveal intrinsic defects in myoblast fusion and myotube morphology. Exp Cell Res 311: 49-61

Shaltiel G, Mark S, Kofman O, Belmaker RH, Agam G (2007) Effect of valproate derivatives on human brain myo-inositol-1-phosphate (MIP) synthase activity and amphetamine-induced rearing. Pharmacol Rep 59: 402-7

Shanmugarajan S, Swoboda KJ, Iannaccone ST, Ries WL, Maria BL, Reddy SV (2007) Congenital bone fractures in spinal muscular atrophy: functional role for SMN protein in bone remodeling. J Child Neurol 22: 967-73

Shao W, Growney JD, Feng Y, O'Connor G, Pu M, Zhu W, Yao YM, Kwon P, Fawell S, Atadja P (2010) Activity of deacetylase inhibitor panobinostat (LBH589) in cutaneous T-cell lymphoma models: Defining molecular mechanisms of resistance. Int J Cancer

Shimasaki S, Ling N (1991) Identification and molecular characterization of insulin-like growth factor binding proteins (IGFBP-1, -2, -3, -4, -5 and -6). Prog Growth Factor Res 3: 243-66

Silva MF, Aires CC, Luis PB, Ruiter JP, Ijlst L, Duran M, Wanders RJ, Tavares de Almeida I (2008) Valproic acid metabolism and its effects on mitochondrial fatty acid oxidation: A review. J Inherit Metab Dis

Silva MF, Selhorst J, Overmars H, van Gennip AH, Maya M, Wanders RJ, de Almeida IT, Duran M (2001) Characterization of plasma acylcarnitines in patients under valproate monotherapy using ESI-MS/MS. Clin Biochem 34: 635-8

Silverstein RL, Baird M, Lo SK, Yesner LM (1992) Sense and antisense cDNA transfection of CD36 (glycoprotein IV) in melanoma cells. Role of CD36 as a thrombospondin receptor. J Biol Chem 267: 16607-12

Simon CM, Jablonka S, Ruiz R, Tabares L, Sendtner M (2010) Ciliary neurotrophic factor-induced sprouting preserves motor function in a mouse model of mild spinal muscular atrophy. Hum Mol Genet 19: 973-86

Singh NK, Singh NN, Androphy EJ, Singh RN (2006) Splicing of a critical exon of human survival motor neuron is regulated by a unique silencer element located in the last intron. Mol Cell Biol 26: 1333-46

Singh NN, Androphy EJ, Singh RN (2004) An extended inhibitory context causes skipping of exon 7 of SMN2 in spinal muscular atrophy. Biochem Biophys Res Commun 315: 381-8

Singh RN (2007) Evolving concepts on human SMN pre-mRNA splicing. RNA Biol 4: 7-10

Skordis LA, Dunckley MG, Yue B, Eperon IC, Muntoni F (2003) Bifunctional antisense oligonucleotides provide a trans-acting splicing enhancer that stimulates SMN2 gene expression in patient fibroblasts. Proc Natl Acad Sci U S A 100: 4114-9

Smith J, Su X, El-Maghrabi R, Stahl PD, Abumrad NA (2008) Opposite regulation of CD36 ubiquitination by fatty acids and insulin: effects on fatty acid uptake. J Biol Chem 283: 13578-85

Soares VM, Brzustowicz LM, Kleyn PW, Knowles JA, Palmer DA, Asokan S, Penchaszadeh GK, Munsat TL, Gilliam TC (1993) Refinement of the spinal muscular atrophy locus to the interval between D5S435 and MAP1B. Genomics 15: 365-71

Sossi V, Giuli A, Vitali T, Tiziano F, Mirabella M, Antonelli A, Neri G, Brahe C (2001) Premature termination mutations in exon 3 of the SMN1 gene are associated with exon skipping and a relatively mild SMA phenotype. Eur J Hum Genet 9: 113-20

Standker L, Wobst P, Mark S, Forssmann WG (1998) Isolation and characterization of circulating 13-kDa C-terminal fragments of human insulin-like growth factor binding protein-5. FEBS Lett 441: 281-6

Sterner DE, Berger SL (2000) Acetylation of histones and transcription-related factors. Microbiol Mol Biol Rev 64: 435-59

Stimson L, La Thangue NB (2009) Biomarkers for predicting clinical responses to HDAC inhibitors. Cancer Lett 280: 177-83

Stoilov P, Daoud R, Nayler O, Stamm S (2004) Human tra2-beta1 autoregulates its protein concentration by influencing alternative splicing of its pre-mRNA. Hum Mol Genet 13: 509-24

Strahl BD, Allis CD (2000) The language of covalent histone modifications. Nature 403: 41-5

Sun Y, Grimmler M, Schwarzer V, Schoenen F, Fischer U, Wirth B (2005) Molecular and functional analysis of intragenic SMN1 mutations in patients with spinal muscular atrophy. Hum Mutat 25: 64-71

Swoboda KJ, Prior TW, Scott CB, McNaught TP, Wride MC, Reyna SP, Bromberg MB (2005) Natural history of denervation in SMA: relation to age, SMN2 copy number, and function. Ann Neurol 57: 704-12

Swoboda KJ, Scott CB, Crawford TO, Simard LR, Reyna SP, Krosschell KJ, Acsadi G, Elsheik B, Schroth MK, D'Anjou G, LaSalle B, Prior TW, Sorenson SL, Maczulski JA, Bromberg MB, Chan GM, Kissel JT (2010) SMA CARNI-VAL trial part I: double-blind, randomized, placebo-controlled trial of L-carnitine and valproic acid in spinal muscular atrophy. PLoS One 5

Swoboda KJ, Scott CB, Reyna SP, Prior TW, LaSalle B, Sorenson SL, Wood J, Acsadi G, Crawford TO, Kissel JT, Krosschell KJ, D'Anjou G, Bromberg MB, Schroth MK, Chan GM, Elsheikh B, Simard LR (2009) Phase II open label study of valproic acid in spinal muscular atrophy. PLoS One 4: e5268

Szabova L, Macejova D, Dvorcakova M, Mostbock S, Blazickova S, Zorad S, Walrand S, Cardinault N, Vasson MP, Rock E, Brtko J (2003) Expression of nuclear retinoic acid receptor in peripheral blood mononuclear cells (PBMC) of healthy subjects. Life Sci 72: 831-6

Takahashi K, Tanabe K, Ohnuki M, Narita M, Ichisaka T, Tomoda K, Yamanaka S (2007) Induction of pluripotent stem cells from adult human fibroblasts by defined factors. Cell 131: 861-72

Tan J, Cang S, Ma Y, Petrillo RL, Liu D (2010) Novel histone deacetylase inhibitors in clinical trials as anti-cancer agents. J Hematol Oncol 3: 5

Tardif G, Hum D, Pelletier JP, Duval N, Martel-Pelletier J (2009) Regulation of the IGFBP-5 and MMP-13 genes by the microRNAs miR-140 and miR-27a in human osteoarthritic chondrocytes. BMC Musculoskelet Disord 10: 148
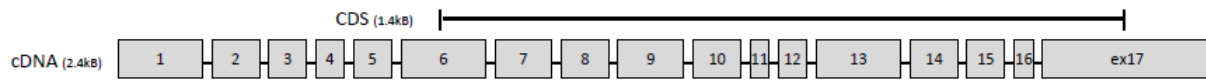
Terbach N, Williams RS (2009) Structure-function studies for the panacea, valproic acid. Biochem Soc Trans 37: 1126-32

Thibault R, Blachier F, Darcy-Vrillon B, de Coppet P, Bourreille A, Segain JP (2010) Butyrate utilization by the colonic mucosa in inflammatory bowel diseases: a transport deficiency. Inflamm Bowel Dis 16: 684-95

Thomas EA (2009) Focal nature of neurological disorders necessitates isotype-selective histone deacetylase (HDAC) inhibitors. Mol Neurobiol 40: 33-45

Thompson TG, Morrison KE, Kleyn P, Bengtsson U, Gilliam TC, Davies KE, Wasmuth JJ, McPherson JD (1993) High resolution physical map of the region surrounding the spinal muscular atrophy gene. Hum Mol Genet 2: 1169-76

Ting CH, Lin CW, Wen SL, Hsieh-Li HM, Li H (2007) Stat5 constitutive activation rescues defects in spinal muscular atrophy. Hum Mol Genet 16: 499-514

Todaro GJ, De Larco JE (1978) Growth factors produced by sarcoma virus-transformed cells. Cancer Res 38: 4147-54

Todaro GJ, Fryling C, De Larco JE (1980) Transforming growth factors produced by certain human tumor cells: polypeptides that interact with epidermal growth factor receptors. Proc Natl Acad Sci U S A 77: 5258-62

Todd AG, Morse R, Shaw DJ, McGinley S, Stebbings H, Young PJ (2010) SMN, Gemin2 and Gemin3 associate with beta-actin mRNA in the cytoplasm of neuronal cells in vitro. J Mol Biol 401: 681-9

Tomaszewicz K, Kang P, Wu BL (2005) Detection of homozygous and heterozygous SMN deletions of spinal muscular atrophy in a single assay with multiplex ligation-dependent probe amplification. Beijing Da Xue Xue Bao 37: 55-7

Tontonoz P, Nagy L, Alvarez JG, Thomazy VA, Evans RM (1998) PPARgamma promotes monocyte/macrophage differentiation and uptake of oxidized LDL. Cell 93: 241-52

Tripathi G, Salih DA, Drozd AC, Cosgrove RA, Cobb LJ, Pell JM (2009) IGF-independent effects of insulin-like growth factor binding protein-5 (Igfbp5) in vivo. Faseb J 23: 2616-26

Tsai LK, Tsai MS, Ting CH, Li H (2008) Multiple therapeutic effects of valproic acid in spinal muscular atrophy model mice. J Mol Med 86: 1243-54

Tsaparas P, Marino-Ramirez L, Bodenreider O, Koonin EV, Jordan IK (2006) Global similarity and local divergence in human and mouse gene co-expression networks. BMC Evol Biol 6: 70

Underhill MF, Birch JR, Smales CM, Naylor LH (2005) eIF2alpha phosphorylation, stress perception, and the shutdown of global protein synthesis in cultured CHO cells. Biotechnol Bioeng 89: 805-14

Valori CF, Ning K, Wyles M, Mead RJ, Grierson AJ, Shaw PJ, Azzouz M (2010) Systemic delivery of scAAV9 expressing SMN prolongs survival in a model of spinal muscular atrophy. Sci Transl Med 2: 35ra42

van Bergeijk J, Rydel-Konecke K, Grothe C, Claus P (2007) The spinal muscular atrophy gene product regulates neurite outgrowth: importance of the C terminus. Faseb J 21: 1492-502

Van Lint C, Emiliani S, Verdin E (1996) The expression of a small fraction of cellular genes is changed in response to histone hyperacetylation. Gene Expr 5: 245-53

Vassar R, Fuchs E (1991) Transgenic mice provide new insights into the role of TGF-alpha during epidermal development and differentiation. Genes Dev 5: 714-27

Vezain M, Saugier-Veber P, Goina E, Touraine R, Manel V, Toutain A, Fehrenbach S, Frebourg T, Pagani F, Tosi M, Martins A (2010) A rare SMN2 variant in a previously unrecognized composite splicing regulatory element induces exon 7 inclusion and reduces the clinical severity of spinal muscular atrophy. Hum Mutat 31: E1110-25

Vieira AR (2006) Association between the transforming growth factor alpha gene and nonsyndromic oral clefts: a HuGE review. Am J Epidemiol 163: 790-810

Villagra A, Cheng F, Wang HW, Suarez I, Glozak M, Maurin M, Nguyen D, Wright KL, Atadja PW, Bhalla K, Pinilla-Ibarz J, Seto E, Sotomayor EM (2009) The histone deacetylase HDAC11 regulates the expression of interleukin 10 and immune tolerance. Nat Immunol 10: 92-100

Vitte JM, Davoult B, Roblot N, Mayer M, Joshi V, Courageot S, Tronche F, Vadrot J, Moreau MH, Kemeny F, Melki J (2004) Deletion of murine Smn exon 7 directed to liver leads to severe defect of liver development associated with iron overload. Am J Pathol 165: 1731-41

Wahid F, Shehzad A, Khan T, Kim YY (2010) MicroRNAs: Synthesis, mechanism, function, and recent clinical trials. Biochim Biophys Acta

Walker MP, Rajendra TK, Saieva L, Fuentes JL, Pellizzoni L, Matera AG (2008) SMN complex localizes to the sarcomeric Z-disc and is a proteolytic target of calpain. Hum Mol Genet 17: 3399-410

Wang Z, Zang C, Cui K, Schones DE, Barski A, Peng W, Zhao K (2009) Genome-wide mapping of HATs and HDACs reveals distinct functions in active and inactive genes. Cell 138: 1019-31

Watanabe S, Lazar E, Sporn MB (1987) Transformation of normal rat kidney (NRK) cells by an infectious retrovirus carrying a synthetic rat type alpha transforming growth factor gene. Proc Natl Acad Sci U S A 84: 1258-62

Weihl CC, Connolly AM, Pestronk A (2006) Valproate may improve strength and function in patients with type III/IV spinal muscle atrophy. Neurology 67: 500-1

Werdnig G (1891) Two early infantile hereditary cases of progressive muscular atrophy simulating dystrophy, but on a neural basis. 1891. Arch Neurol 25: 276-8

Willis DE, van Niekerk EA, Sasaki Y, Mesngon M, Merianda TT, Williams GG, Kendall M, Smith DS, Bassell GJ, Twiss JL (2007) Extracellular stimuli specifically regulate localized levels of individual neuronal mRNAs. J Cell Biol 178: 965-80

Winkler C, Eggert C, Gradl D, Meister G, Giegerich M, Wedlich D, Laggerbauer B, Fischer U (2005) Reduced U snRNP assembly causes motor axon degeneration in an animal model for spinal muscular atrophy. Genes Dev 19: 2320-30

Wirth B (2000) An update of the mutation spectrum of the survival motor neuron gene (SMN1) in autosomal recessive spinal muscular atrophy (SMA). Hum Mutat 15: 228-37

Wirth B (2002) Spinal muscular atrophy: state-of-the-art and therapeutic perspectives. Amyotroph Lateral Scler Other Motor Neuron Disord 3: 87-95

Wirth B, Brichta L, Hahnen E (2006a) Spinal muscular atrophy and therapeutic prospects. Prog Mol Subcell Biol 44: 109-32

Wirth B, Brichta L, Schrank B, Lochmuller H, Blick S, Baasner A, Heller R (2006b) Mildly affected patients with spinal muscular atrophy are partially protected by an increased SMN2 copy number. Hum Genet 119: 422-8

Wirth B, el-Agwany A, Baasner A, Burghes A, Koch A, Dadze A, Piechaczeck-Wappenschmidt B, Rudnik-Schoneborn S, Zerres K, Schonling J (1995) Mapping of the spinal muscular atrophy (SMA) gene to a 750-kb interval flanked by two new microsatellites. Eur J Hum Genet 3: 56-60

Wirth B, Pick E, Leutner A, Dadze A, Voosen B, Knapp M, Piechaczek-Wappenschmidt B, Rudnik-Schoneborn S, Schonling J, Cox S, et al. (1994) Large linkage analysis in 100 families with autosomal recessive spinal muscular atrophy (SMA) and 11 CEPH families using 15 polymorphic loci in the region 5q11.2-q13.3. Genomics 20: 84-93

Wirth B, Schmidt T, Hahnen E, Rudnik-Schoneborn S, Krawczak M, Muller-Myhsok B, Schonling J, Zerres K (1997) De novo rearrangements found in 2% of index patients with spinal muscular atrophy: mutational mechanisms, parental origin, mutation rate, and implications for genetic counseling. Am J Hum Genet 61: 1102-11

Wolstencroft EC, Mattis V, Bajer AA, Young PJ, Lorson CL (2005) A non-sequence-specific requirement for SMN protein activity: the role of aminoglycosides in inducing elevated SMN protein levels. Hum Mol Genet 14: 1199-210

Workman E, Saieva L, Carrel TL, Crawford TO, Liu D, Lutz C, Beattie CE, Pellizzoni L, Burghes AH (2009) A SMN missense mutation complements SMN2 restoring snRNPs and rescuing SMA mice. Hum Mol Genet 18: 2215-29

Wurtz JM, Bourguet W, Renaud JP, Vivat V, Chambon P, Moras D, Gronemeyer H (1996) A canonical structure for the ligand-binding domain of nuclear receptors. Nat Struct Biol 3: 206

Wuttge DM, Romert A, Eriksson U, Torma H, Hansson GK, Sirsjo A (2001) Induction of CD36 by all-trans retinoic acid: retinoic acid receptor signaling in the pathogenesis of atherosclerosis. Faseb J 15: 1221-3

Yamamoto N, Ikeda H, Tandon NN, Herman J, Tomiyama Y, Mitani T, Sekiguchi S, Lipsky R, Kralisz U, Jamieson GA (1990) A platelet membrane glycoprotein (GP) deficiency in healthy blood donors: Naka- platelets lack detectable GPIV (CD36). Blood 76: 1698-703

Yamanaka Y, Wilson EM, Rosenfeld RG, Oh Y (1997) Inhibition of insulin receptor activation by insulin-like growth factor binding proteins. J Biol Chem 272: 30729-34

Yang XJ, Seto E (2008) The Rpd3/Hda1 family of lysine deacetylases: from bacteria and yeast to mice and men. Nat Rev Mol Cell Biol 9: 206-18

Ye P, D'Ercole J (1998) Insulin-like growth factor I (IGF-I) regulates IGF binding protein-5 gene expression in the brain. Endocrinology 139: 65-71

Yoo S, van Niekerk EA, Merianda TT, Twiss JL (2010) Dynamics of axonal mRNA transport and implications for peripheral nerve regeneration. Exp Neurol 223: 19-27

Yoshida M, Kijima M, Akita M, Beppu T (1990) Potent and specific inhibition of mammalian histone deacetylase both in vivo and in vitro by trichostatin A. J Biol Chem 265: 17174-9

Young PJ, DiDonato CJ, Hu D, Kothary R, Androphy EJ, Lorson CL (2002) SRp30c-dependent stimulation of survival motor neuron (SMN) exon 7 inclusion is facilitated by a direct interaction with hTra2 beta 1. Hum Mol Genet 11: 577-87

Young PJ, Le TT, Dunckley M, Nguyen TM, Burghes AH, Morris GE (2001) Nuclear gems and Cajal (coiled) bodies in fetal tissues: nucleolar distribution of the spinal muscular atrophy protein, SMN. Exp Cell Res 265: 252-61

Young PJ, Le TT, thi Man N, Burghes AH, Morris GE (2000) The relationship between SMN, the spinal muscular atrophy protein, and nuclear coiled bodies in differentiated tissues and cultured cells. Exp Cell Res 256: 365-74

Zechel C, Shen XQ, Chambon P, Gronemeyer H (1994a) Dimerization interfaces formed between the DNA binding domains determine the cooperative binding of RXR/RAR and RXR/TR heterodimers to DR5 and DR4 elements. Embo J 13: 1414-24

Zechel C, Shen XQ, Chen JY, Chen ZP, Chambon P, Gronemeyer H (1994b) The dimerization interfaces formed between the DNA binding domains of RXR, RAR and TR determine the binding specificity and polarity of the full-length receptors to direct repeats. Embo J 13: 1425-33

Zerres K, Davies KE (1999) 59th ENMC International Workshop: Spinal Muscular Atrophies: recent progress and revised diagnostic criteria 17-19 April 1998, Soestduinen, The Netherlands. Neuromuscul Disord 9: 272-8

Zerres K, Rudnik-Schoneborn S (1995) Natural history in proximal spinal muscular atrophy. Clinical analysis of 445 patients and suggestions for a modification of existing classifications. Arch Neurol 52: 518-23

Zerres K, Wirth B, Rudnik-Schoneborn S (1997) Spinal muscular atrophy--clinical and genetic correlations. Neuromuscul Disord 7: 202-7

Zhang H, Xing L, Rossoll W, Wichterle H, Singer RH, Bassell GJ (2006) Multiprotein complexes of the survival of motor neuron protein SMN with Gemins traffic to neuronal processes and growth cones of motor neurons. J Neurosci 26: 8622-32

Zhang M, Pickart CM, Coffino P (2003) Determinants of proteasome recognition of ornithine decarboxylase, a ubiquitin-independent substrate. Embo J 22: 1488-96

Zhang ML, Lorson CL, Androphy EJ, Zhou J (2001) An in vivo reporter system for measuring increased inclusion of exon 7 in SMN2 mRNA: potential therapy of SMA. Gene Ther 8: 1532-8

Zhang Z, Lotti F, Dittmar K, Younis I, Wan L, Kasim M, Dreyfuss G (2008) SMN deficiency causes tissue-specific perturbations in the repertoire of snRNAs and widespread defects in splicing. Cell 133: 585-600

Zhou J, Febbraio M, Wada T, Zhai Y, Kuruba R, He J, Lee JH, Khadem S, Ren S, Li S, Silverstein RL, Xie W (2008) Hepatic fatty acid transporter Cd36 is a common target of LXR, PXR, and PPARgamma in promoting steatosis. Gastroenterology 134: 556-67

Zhu J, Gianni M, Kopf E, Honore N, Chelbi-Alix M, Koken M, Quignon F, Rochette-Egly C, de The H (1999) Retinoic acid induces proteasome-dependent degradation of retinoic acid receptor alpha (RARalpha) and oncogenic RARalpha fusion proteins. Proc Natl Acad Sci U S A 96: 14807-12

Zou J, Barahmand-pour F, Blackburn ML, Matsui Y, Chansky HA, Yang L (2004) Survival motor neuron (SMN) protein interacts with transcription corepressor mSin3A. J Biol Chem 279: 14922-8

Zumbrunn J, Trueb B (1996) Primary structure of a putative serine protease specific for IGF-binding proteins. FEBS Lett 398: 187-92
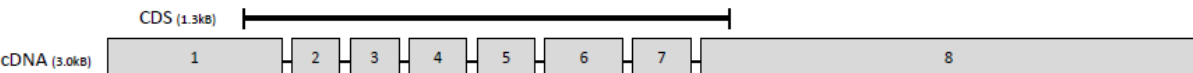
10. Appendix

CD 36 (ENSG00000135218)		
Amplicon	*Name*	*Sequence (5´ → 3´)*
Exon 1	CD36 ex1 fwd	aac gtg att tat ttg gaa cgt g
	CD36 ex1 rev	gca act caa ctg atg gta ttc g
Exon 2	CD36 ex2 fwd	tga tgg cag caa tgt gta gag
	CD36 ex2 rev	ctt gag ccc ggg agt tc
Exon 3	CD36 ex3 fwd	gga gtt caa atg act cct ctt tc
	CD36 ex3 rev	aga acc aca gtt gac ccc ac
Exon 4	CD36 ex4 fwd	cat ctg gaa tgg ctg taa tta
	CD36 ex4 rev	tgg gga cac aga gcc aaa g
Exon 5	CD36 ex5 fwd	tta gga caa gcc att cag gc
	CD36 ex5 rev	ctc cac cca aca caa cct tc
Exon 6	CD36 ex6 fwd	aga acg ggc aaa atg ata cg
	CD36 ex6 rev	gag ttg cag tgg ttc ata att acc
Exon 7	CD36 ex7 fwd	aag gct gca aac aat ctt cc
	CD36 ex7 rev	gac ttc tca gaa ata cat ggt caa g
Exon 8	CD36 ex8 fwd	ttg cta gag acc ctg gct g
	CD36 ex8 rev	aaa tga cca tgc ctc cat tc
Exon 9	CD36 ex9 fwd	tgc att ttg agt ttt ggc ag
	CD36 ex9 rev	tta gga tat atg tct cca gat cag c
Exon 10	CD36 ex10 fwd	tca ttt gag taa cca gtg att gag
	CD36 ex10 rev	agc aga aca gga gtt tcc ag
Exon 11	CD36 ex11 fwd	ggt aca ttg caa taa gat aaa agg ttc
	CD36 ex11 rev	tgt ggg aaa ggg agg tgg
Exon 12	CD36 ex12 fwd	cac tgg agg aga gat ttc tag g
	CD36 ex12 rev	att ttg tca cct ggg gtc tg
Exon 13	CD36 ex13 fwd	ttt agt atg tgt taa aat ttc cca atc
	CD36 ex13 rev	tgg ttg cat aag gat tat ggt aaa g
Exon 14	CD36 ex14 fwd	gac ata att ctt ccc cac cc
	CD36 ex14 rev	aag cca att aga atc act tca taa ac
Exon 15	CD36 ex15 fwd	tgc agt ttt aaa agt ttc aat tag tcc
	CD36 ex15 rev	cat aag cat tta ata tg att ggt gac
Exon 16	CD36 ex16 fwd	ccc cga gaa ttt att gaa agg
	CD36 ex16 rev	ttc aat tgg atc atc tca aat agg
Exon 17	CD36 ex17 fwd	gcc ttt ctt gac ttg caa aag
	CD36 ex17 rev	tct aca tgc agc aat cct gg

Table 18 **Primers for sequencing of CD36. Primers were designed by *Exon Primer* and were located between 100 and 200 bp within the adjacent intron. Furthermore a cartoon illustrating individual exon length is given.**

RARβ (ENSG00000077092)		
Amplicon	*Name*	*Sequence (5´ → 3´)*
Exon 1	RARB ex1_1 fwd	agg gtt cac cga aag ttc ac
	RARB ex1_1 rev	ttt ggc acg tag gct gtt g
	RARB ex 1_2 fwd	caa gcc tgg aaa atg gta aat g
	RARB ex1_2 rev	tgc tac caa tgc agt tta ttt cc
Exon 2	RARB ex2 fwd	ctg aat ttg ggg cag aag c
	RARB ex2 rev	tga tgt tac aca tcc agc cc
Exon 3	RARB ex3 fwd	tca cga gga ttt taa ggt tta tgt aag
	RARB ex3 rev	cca cat gac tgt gga agg tg
Exon 4	RARB ex4 fwd	ctc agg agc aca ggc cc
	RARB ex4 rev	cat gca cgt aca agg ttt cc
Exon 5	RARB ex5 fwd	ccc tcc tat aga gct tcc cg
	RARB ex5 rev	aat gtc tct tgg tcc cct cc
Exon 6	RARB ex6 fwd	tga ttg atg att tca gga cag g
	RARB ex6 rev	aac tcc aaa agg gga aat gag g
Exon 7	RARB ex7 fwd	aca agg aag agg gga aaa gg
	RARB ex7 rev	gca aca caa cct ggt aag gc
Exon 8	RARB ex8_1 fwd	tga aaa ttg gtc cct ggt tat c
	RARB ex8_1 rev	ttt ctg gtt gca tga aat gg
	RARB ex8_2 fwd	caa gaa gga cca aga agt ttt c
	RARB ex8_2 rev	gat gca gtt tga gag cat cag
	RARB ex8_3 fwd	gga aac agg act att gac agg ac
	RARB ex8_3 rev	tta att agc ccc ttg gca tc
	RARB ex8_4 fwd	ttg ttc aca agc cat tag gg
	RARB ex8_4 rev	aaa atg gaa ctg tgt tct ctg tc

Table 19   Primers for sequencing of RARβ. Primers were designed by *Exon Primer* and were located between 100 and 200 bp within the adjacent intron. Because of its length exon 8 was subdivided into four parts. Furthermore a cartoon illustrating individual exon length is given.

TGFα (ENSG00000163235)		
Amplicon	*Name*	*Sequence (5´ → 3´)*
Exon 1a	TGFa 1a fwd	ccc ccg gtc ccc gcc gag ttc
	TGFA 1a rev	gcc ctc ggc gga cac cga aac cac
Exon 1b	TGFa 1b fwd	cga cac cct gct tcc cc
	TGFa 1b rev	gga cac cga aac cac ttc tc
Exon 2	TGFa 2 fwd	cta ccg aac ctt tgc ctg tc
	TGFa 2 rev	cca ggg agg gag ctc ttg
Exon 3	TGFa 3 fwd	ttc ttg act ggt agg gtg gg
	TGFa 3 rev	ttg gat att gga ctg acc cc
Exon 4	TGFa 4 fwd	tcc ctg gag agc tag ggt aac
	TGFa 4 rev	tat act gcg gat gtc cct gg
Exon 5	TGFa 5 fwd	cct agg gca gat gct gta cc
	TGFa 5 rev	tgg aga agg tgg tcg ttt tc
Exon 6	TGFa 6-1 fwd	gct tat ttt ccc aac gtg gc
	TGFa 6-1 rev	tct taa agc tag ggt ctt cat gtg
	TGFa 6-2 fwd	aat tct gcc caa cac agg ag
	TGFa 6-2 rev	aca gag ggg aca gat ccc tg
	TGFa 6-3 fwd	aga aat ggt gcc att gaa gc
	TGFa 6-3 rev	ttg aag gga ccc act gtt tc
	TGFa 6-4 fwd	cct cca cta tgt ggg tct tcc
	TGFa 6-4 rev	gcc caa ggg atg taa act tg
	TGFa 6-5 fwd	tca gac aat tct atg acc cgt g
	TGFa 6-5 rev	ttt gca gct aac caa aga cta cc
	TGFa 6-6 fwd	aat gca agc ctg gtt gga c
	TGFa 6-6 rev	cat ccc tgg ctt ggt tcc
	TGFa 6-7 fwd	cct gac agg aaa tgt ttt ctt cta c
	TGFa 6-7 rev	aag cct ggt aaa tca atg gc
	TGFa 6-8 fwd	atg ccc aaa acc aag aac ac
	TGFa 6-8 rev	tgc aga gaa aag tct tca ttt cc

Table 20   **Primers for sequencing of TGFα. Primers were designed by *Exon Primer* and were located between 100 and 200 bp within the adjacent intron. Because of its length Exon 6 was subdivided into 8 parts. Furthermore a cartoon illustrating individual exon length is given.**
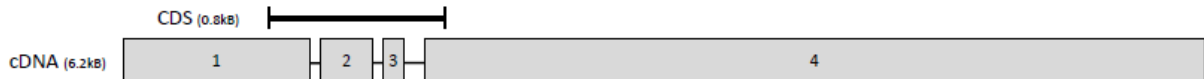
IGFBP5 (ENSG00000115461)		
Amplicon	*Name*	*Sequence (5′ → 3′)*
Exon 1	IGFBP5 1-1 fwd	ttg cag cta caa act ggc tg
	IGFBP5 1-1 rev	caa gca acc acc aaa ata atg
	IGFBP5 1-2 fwd	gct gag ggt tag aaa gcg g
	IGFBP5 1-2 rev	acc gcg gtg agc aac ac
	IGFBP5 1-3 fwd	gca cct gct cta cct gcc
	IGFBP5 1-3 rev	cga cta ctc ccg agc tgc
Exon 2	IGFBP5 2 fwd	ttt att act ccc ctc acc cc
	IGFBP5 2 rev	tga atg tcc att tag atg cag g
Exon 3	IGFBP5 3 fwd	cca ttc gtc agc gca gc
	IGFBP5 3 rev	caa ggt gga gtt tcc tgg c
Exon 4	IGFBP5 4-1 fwd	gta gac aag agg cag ggc ag
	IGFBP5 4-1 rev	ctg gtc tcg gtg cat gtc
	IGFBP5 4-2 fwd	gaa ggg aag gaa gtg ttt gtg
	IGFBP5 4-2 rev	tta aat gag ggc tga aac gg
	IGFBP5 4-3 fwd	tgc ata ttt cat tcc cca gg
	IGFBP5 4-3 rev	gtc cgg aga ctg tga ctt cc
	IGFBP5 4-4 fwd	att ccc cac gtg tgt tca tc
	IGFBP5 4-4 rev	agt ctt gtc cct tcc aaa gc
	IGFBP5 4-5 fwd	agg aaa gag agg aaa atg gg
	IGFBP5 4-5 rev	tcc agg ggc ata gga gat ag
	IGFBP5 4-6 fwd	cat gac aca gcg gag acc
	IGFBP5 4-6 rev	gag tct ggc gca ctt aca cc
	IGFBP5 4-7 fwd	tct tca cgg act gtg tct gg
	IGFBP5 4-7 rev	agt cgt ggg aaa gac aga gg
	IGFBP5 4-8 fwd	ctc cga atc taa gtg ctg cc
	IGFBP5 4-8 rev	atc ctc tct gac tct atg gg
	IGFBP5 4-9 fwd	gtt tag tga gac agg gct gc
	IGFBP5 4-9 rev	gag gag aga aca gag tta tgg tat g
	IGFBP5 4-10 fwd	acc tag ccc aca tgg ata g
	IGFBP5 4-10 rev	agg aga atc agg gac ttg cc

Table 21   **Primers for sequencing of IGFBP5 Primers were designed by *Exon Primer* and were located between 100 and 200 bp within the adjacent intron. Because of their length exons 1 and 4 were subdivided into three and 10 parts, respectively. Furthermore a cartoon illustrating individual exon length is given.**

Gene Symbol	Gene Description	logFC	AveExpr	PValue	adjPVal
ANKRD1	ankyrin repeat domain 1 (cardiac muscle)	1,006	8,985	1,5501E-06	0,0188219
MLLT11	"myeloid/lymphoid or mixed-lineage leukemia (trithorax homolog, Drosophila); translocated to, 11 "	0,784	8,758	2,5968E-06	0,0188219
ACTC1	actin, alpha, cardiac muscle 1	0,722	10,909	7,2896E-06	0,0352235
OLFML1	olfactomedin-like 1	0,908	7,32	1,15E-05	0,04162
IGFBP5	insulin-like growth factor binding protein 5	0,862	9,749	3,0958E-05	0,04162
SLC7A14	solute carrier family 7 (cationic amino acid transporter, y+ system), member 14	0,852	6,036	3,4781E-05	0,04162
GPR155	G protein-coupled receptor 155	0,85	6,239	3,1541E-05	0,04162
PRKAA2	protein kinase, AMP-activated, alpha 2 catalytic subunit	0,748	6,55	3,9E-05	0,04162
SLC38A4	solute carrier family 38, member 4	0,718	7,527	3,9259E-05	0,04162
KCND1	potassium voltage-gated channel, Shal-related subfamily, member 1	0,708	5,584	4,0422E-05	0,04162
KRT19	keratin 19	0,68	8,912	2,8872E-05	0,04162
SV2A	synaptic vesicle glycoprotein 2A	0,674	7,195	4,3067E-05	0,04162
INHBA	inhibin, beta A	0,644	8,854	0,00002659	0,04162
SLC16A4	solute carrier family 16, member 4 (monocarboxylic acid transporter 5)	0,578	7,719	4,1476E-05	0,04162
LANCL2	LanC lantibiotic synthetase component C-like 2 (bacterial)	-0,612	8,444	2,7797E-05	0,04162
LRCH2	leucine-rich repeats and calponin homology (CH) domain containing 2	0,92	7,484	8,3405E-05	0,0452257
FRRS1	ferric-chelate reductase 1	0,712	7,348	5,9164E-05	0,0452257
CXorf57	chromosome X open reading frame 57	0,676	6,064	6,3721E-05	0,0452257
MCAM	melanoma cell adhesion molecule	0,644	6,668	4,9931E-05	0,0452257
ITGA7	integrin, alpha 7	0,628	7,478	0,00010804	0,0452257
NAP1L3	nucleosome assembly protein 1-like 3	0,618	7,013	9,7739E-05	0,0452257
ACSS3	acyl-CoA synthetase short-chain family member 3	0,61	7,607	9,8556E-05	0,0452257
QPCT	glutaminyl-peptide cyclotransferase	0,594	8,321	7,6237E-05	0,0452257
CALCRL	calcitonin receptor-like	0,592	4,08	8,7176E-05	0,0452257
F3	coagulation factor III (thromboplastin, tissue factor)	0,578	9,539	8,6619E-05	0,0452257
SCN2A	sodium channel, voltage-gated, type II, alpha subunit	0,568	5,688	0,00010048	0,0452257
OSAP	ovary-specific acidic protein	0,536	8,404	0,00010726	0,0452257
COL11A1	collagen, type XI, alpha 1	0,532	7,192	8,3956E-05	0,0452257
AS3MT	arsenic (+3 oxidation state) methyltransferase	0,53	7,693	6,6562E-05	0,0452257
JAM2	junctional adhesion molecule 2	0,52	6,658	9,3268E-05	0,0452257
CRIP2	cysteine-rich protein 2	0,518	9,311	0,00010325	0,0452257
SPTLC3	serine palmitoyltransferase, long chain base subunit 3	0,508	6,264	0,00010213	0,0452257

Continued

Gene Symbol	Gene Description	logFC	AveExpr	PValue	adjPVal
KIAA1305	KIAA1305	0,508	7,662	0,0001092	0,0452257
---	---	-0,596	6,132	0,00010894	0,0452257
---	---	-0,706	4,633	9,0227E-05	0,0452257
RAB38	RAB38, member RAS oncogene family	0,698	5,951	0,00011558	0,046542
RFTN2	raftlin family member 2	0,762	6,847	0,00015506	0,0473376
CASP1	caspase 1, apoptosis-related cysteine peptidase (interleukin 1, beta, convertase)	0,656	6,39	0,00014332	0,0473376
PSG8	pregnancy specific beta-1-glycoprotein 8	0,634	3,823	0,0001362	0,0473376
GSTM5	glutathione S-transferase M5	0,61	6,761	0,00012587	0,0473376
RHOJ	ras homolog gene family, member J	0,514	6,835	0,00016001	0,0473376
RIMS2	regulating synaptic membrane exocytosis 2	0,508	5,74	0,00015813	0,0473376
PTPRF	protein tyrosine phosphatase, receptor type, F	0,486	7,875	0,00014813	0,0473376
TCEAL7	transcription elongation factor A (SII)-like 7	0,476	7,49	0,00015295	0,0473376
KIAA1199	KIAA1199	0,458	11,415	0,00015715	0,0473376
C2orf79	chromosome 2 open reading frame 79	-0,464	8,344	0,0001307	0,0473376
HP	haptoglobin	-0,466	3,087	0,00015865	0,0473376
SPRYD3	SPRY domain containing 3	-0,478	8,711	0,00013976	0,0473376
SCD	stearoyl-CoA desaturase (delta-9-desaturase)	-0,5	9,828	0,00012258	0,0473376
ABCA8	ATP-binding cassette, sub-family A (ABC1), member 8	0,764	5,68	0,00017098	0,0476628
KIAA0408	KIAA0408	0,73	5,803	0,00017028	0,0476628
HSPA2	heat shock 70kDa protein 2	0,456	8,662	0,00016587	0,0476628
GCA	grancalcin, EF-hand calcium binding protein	0,572	4,494	0,00017872	0,0482854
ELTD1	EGF, latrophilin and seven transmembrane domain containing 1	0,564	8,478	0,0001832	0,0482854
CCDC46	coiled-coil domain containing 46	0,452	6,292	0,00018181	0,0482854
BEX4	BEX family member 4	0,572	8,206	0,00019765	0,0493989
GPRASP1	G protein-coupled receptor associated sorting protein 1	0,506	6,013	0,00019714	0,0493989
LRRC49	leucine rich repeat containing 49	0,49	7,425	0,00019634	0,0493989

Table 22 **Transcripts differentially expressed between mock and VPA-treated Pos-Responders detected by µ-array. Negative prefix indicates higher expression in VPA-treated fibroblasts. (logFC = log-fold change; AveExpr = average expression; PValue = *P*-value; adjPVal = *P*-value after BH correction)**

Gene Symbol	Gene Description	logFC	AveExpr	PValue	adjPVal
LOC404266	hypothetical LOC404266	-1,738	6,93556	1,9006E-10	4,1448E-06
HOXB3	homeobox B3	-1,1495	7,05167	3,9218E-08	0,00042764
HOXD10	homeobox D10	2,8315	6,56	7,6585E-07	0,00334034
TGFA	transforming growth factor, alpha	1,444	5,53	7,5181E-07	0,00334034
GALNT12	UDP-N-acetyl-alpha-D-galactosamine:polypeptide N-acetylgalactosaminyltransferase 12 (GalNAc-T12)	-1,329	7,27722	7,3105E-07	0,00334034
HOXD11	homeobox D11	1,9425	6,92833	2,8645E-06	0,0104113
RARB	retinoic acid receptor, beta	-1,128	5,185	5,1102E-06	0,0159205
PITPNM3	PITPNM family member 3	1,381	6,57944	8,1593E-06	0,0222423
MAB21L1	mab-21-like 1 (C. elegans)	2,0165	6,88944	1,5636E-05	0,0253025
C11orf87	chromosome 11 open reading frame 87	1,411	7,605	1,3384E-05	0,0253025
OLFM1	olfactomedin 1	-0,8175	6,17889	1,3466E-05	0,0253025
DIO2	deiodinase, iodothyronine, type II	-1,0715	5,73833	1,4708E-05	0,0253025
EPHA4	EPH receptor A4	-1,3905	8,04778	1,3385E-05	0,0253025
KIAA1772	KIAA1772	-2,271	6,21833	1,6243E-05	0,0253025
TAS2R48	taste receptor, type 2, member 48	-0,69	3,89167	0,00002084	0,026734
TMTC2	transmembrane and tetratricopeptide repeat containing 2	-0,9985	6,37056	1,9996E-05	0,026734
CD36	CD36 molecule (thrombospondin receptor)	-2,2135	5,07333	1,9509E-05	0,026734
LYPD6	LY6/PLAUR domain containing 6	-1,0215	6,03278	2,4608E-05	0,0298133
AMIGO2	adhesion molecule with Ig-like domain 2	-0,9675	7,31389	2,7636E-05	0,0306525
LYPD6B	LY6/PLAUR domain containing 6B	-1,6675	7,03333	2,8111E-05	0,0306525
IGFBP5	insulin-like growth factor binding protein 5	2,4875	8,63722	4,4173E-05	0,0458727

Table 23   Transcripts differentially expressed between VPA-treated Pos- and Non-Responders detected by µ-array. Negative prefix indicates higher expression in VPA-treated Non-Responders. (logFC = log-fold change; AveExpr = average expression; PValue = *P*-value; adjPVal = *P*-value after BH correction)

Gene Symbol	Gene Description	logFC	AveExpr	PValue	adjPVal
LOC404266	hypothetical LOC404266	-1,5855	6,93556	8,4359E-10	1,8397E-05
HOXB3	homeobox B3	-1,324	7,05167	4,4899E-09	4,8957E-05
RARB	retinoic acid receptor, beta	-1,302	5,185	7,5694E-07	0,00550241
HOXD10	homeobox D10	2,654	6,56	1,8448E-06	0,0100577
GALNT12	UDP-N-acetyl-alpha-D-galactosamine:polypeptide N-acetylgalactosaminyltransferase 12 (GalNAc-T12)	-1,1965	7,27722	3,0067E-06	0,0131139
TMTC2	transmembrane and tetratricopeptide repeat containing 2	-1,1145	6,37056	5,1263E-06	0,0186323
HOXD11	homeobox D11	1,701	6,92833	1,5335E-05	0,0379679
---	---	0,6745	5,56833	1,5669E-05	0,0379679
DIO2	deiodinase, iodothyronine, type II	-1,081	5,73833	1,3207E-05	0,0379679

Table 24   Transcripts differentially expressed between mock treated Pos- and Non-Responders detected by μ-array. Negative prefix indicates higher expression in VPA-treated Non-Responders. (logFC = log-fold change; AveExpr = average expression; PValue = *P*-value; adjPVal = *P*-value after BH correction)

	fibroblast line	DIO2 µ-Array	DIO2 qPCR	GALNT12 µ-Array	GALNT12 qPCR	HOXB3 µ-Array	HOXB3 qPCR	HOXD10 µ-Array	HOXD10 qPCR	HOXD11 µ-Array	HOXD11 qPCR	LOC404266 µ-Array	LOC404266 qPCR	RAR β µ-Array	RAR β qPCR	TMTC2 µ-Array	TMTC2 qPCR
mock Pos-Responder	ML72	0,616	0,103	0,656	0,052	0,615	0,265	3,972	2,445	2,660	2,445	0,653	0,024	0,798	0,180	0,688	0,116
	ML67	0,825	1,076	0,526	0,443	0,747	0,665	1,214	3,508	1,103	3,508	0,671	0,408	0,719	0,336	0,692	0,642
	ML17	0,583	0,107	0,600	0,934	0,711	0,795	3,891	16,14	2,952	16,14	0,580	0,036	0,648	0,570	0,507	0,536
	ML16	0,921	1,136	0,733	0,619	0,800	0,658	1,434	4,484	1,406	4,484	0,553	0,261	0,572	0,302	0,574	0,392
	ML5	0,708	0,668	0,819	0,813	0,521	0,723	2,868	9,544	1,396	9,544	0,666	0,185	0,635	0,203	0,993	0,506
mock Non-Responder	ML82	1,507	2,524	1,200	1,560	1,473	1,551	0,392	0,073	0,616	0,073	1,796	14,81	2,420	11,49	1,205	0,975
	ML69	1,224	2,299	1,388	1,887	1,984	2,512	0,418	0,084	0,508	0,084	2,121	21,01	1,297	11,75	1,424	33,63
	ML59	1,604	4,024	1,870	2,987	1,916	2,229	0,448	0,429	0,599	0,429	1,924	19,98	1,711	19,49	1,728	1,536
	ML73	1,817	3,472	1,673	2,134	1,422	1,182	0,281	0,019	0,461	0,019	1,664	10,60	1,390	7,527	1,515	1,937
500 µM VPA Pos-Responder	ML72	0,583	2,582	0,718	2,248	0,721	0,992	3,249	0,028	2,624	0,028	0,635	10,43	0,844	1,203	0,737	1,188
	ML67	0,796	1,219	0,583	0,502	0,687	0,740	1,206	3,925	1,207	3,925	0,519	0,361	0,745	0,279	0,901	0,704
	ML17	0,537	0,101	0,765	1,136	0,668	0,950	4,257	14,53	2,624	14,53	0,502	0,032	0,618	0,430	0,615	0,829
	ML16	0,994	1,323	0,600	0,598	0,687	0,664	1,357	5,061	1,358	5,061	0,644	0,192	0,639	0,162	0,763	0,425
	ML5	0,759	0,749	0,854	0,905	0,716	0,697	2,676	8,649	1,426	8,649	0,601	0,181	0,705	0,107	0,901	0,842
500 µM VPA Non-Responder	ML82	1,446	1,721	1,183	1,243	1,432	1,657	0,418	0,083	0,634	0,083	1,458	12,60	1,439	3,363	1,310	0,954
	ML69	1,199	2,086	2,075	2,637	1,692	2,256	0,261	0,100	0,377	0,100	1,872	17,04	1,333	4,301	1,945	2,364
	ML59	1,684	3,007	2,004	2,759	1,623	1,733	0,379	0,438	0,385	0,438	2,593	18,84	2,181	4,797	1,569	1,884
	ML73	1,755	0,402	1,909	0,785	1,442	0,699	0,252	13,49	0,461	13,49	1,938	0,052	1,352	0,138	1,443	1,228

Table 25   Comparision of qRT-PCR and µ-array expression data. Depicted data of transcripts differentially expressed in untreated and treated fibroblasts. Transcripts verified by PCR are marked in gray. All values are scaled to fit for easier comparison. (qPCR = qRT-PCR)

fibroblast line		C11orf87		EPHA4		ANKRD1		CD36		KIAA1772		IGFBP5		LYPD6		PITPNM3		TGF α		MAP21L1	
		μ-Array	qPCR	μ-Array	qPCR	μ-Array	qPCR	μ-Array	qPCR	μ-Array	qPCR	μ-Array	qPCR	μ-Array	qPCR	μ-Array	qPCR	μ-Array	qPCR	μ-Array	qPCR
Pos-Responder	ML72	2,157	2,220	0,780	2,038	0,849	0,496	0,431	0,396	0,393	0,145	2,089	2,053	0,751	0,553	1,581	2,341	2,412	3,666	1,367	2,176
	ML67	2,280	3,336	0,526	1,419	3,349	3,848	0,618	0,519	0,775	0,808	3,278	3,562	0,971	1,003	2,001	6,172	1,064	1,539	1,141	3,356
	ML17	0,005	1,913	0,842	6,986	1,468	1,523	0,794	1,048	0,674	0,811	6,882	7,864	0,772	0,746	1,766	9,634	2,189	3,922	1,173	2,269
	ML16	1,049	1,532	0,380	0,000	2,836	1,446	0,602	0,464	0,467	0,435	2,644	1,720	0,822	0,640	1,880	2,631	2,144	2,911	0,859	1,502
	ML5	1,463	3,325	0,759	2,832	1,408	0,599	0,373	0,229	0,424	0,159	1,685	1,311	0,627	0,365	0,960	0,886	1,602	1,846	1,102	2,110
Non-Responder	ML82	0,870	0,342	1,294	3,015	1,722	0,898	2,745	3,064	1,377	1,104	0,884	0,575	1,281	1,384	0,813	0,454	0,678	0,333	0,966	0,419
	ML69	0,650	0,911	2,059	4,931	0,671	0,639	1,421	1,482	4,382	10,58	0,272	0,093	1,411	1,536	0,442	0,129	0,655	0,178	0,908	0,820
	ML59	0,450	0,119	1,935	2,798	0,923	0,402	4,713	3,946	1,792	2,042	0,413	0,234	1,451	1,610	0,651	0,230	0,674	0,315	0,987	0,482
	ML73	1,256	0,373	1,446	1,571	1,489	1,719	2,199	2,442	3,868	6,391	0,733	0,617	2,407	3,024	0,591	0,229	0,651	0,451	0,933	0,115

Table 26   Comparision of qRT-PCR and μ-array expression data. Depicted data of transcripts differentially expressed in treated fibroblasts. Transcripts verified by PCR are marked in gray. All values are scaled to fit for easier comparison. (qPCR = qRT-PCR)

Gene	Ensembl ID	Gene description	Function
DIO2	ENSG00000211448	deiodinase, iodothyronine, type II	Activation of thyroid hormone (Thyrosxine → 3,3,5-triiodothyronine)
GALNT12	ENSG00000119514	UDP-N-acetyl-alpha-D-galactosamine:polypeptide N-acetylgalactosaminyltransferase 12	Transfer of GalNAc from UDP-GalNAc to to hydroxygroup of peptide (O-linked glycosylation)
KIAA1772	ENSG00000141449	KIAA1772 (GREB1L)	estrogen dependent growth regulation in breast cancer
LYPD6	ENSG00000187123	LY6/PLAUR domain containing 6	not known (defined by LU domain)
MAP21L1	ENSG0000018066	mab-21-like 1	cell fate decision in *C.elegans*

Table 27 **Transcripts identified on the µ-array (adj.P<0.05; logFC>1), which were excluded from further analysis based on their function. KIAA1772 has recently been renamed as GREB1L. (GalNAc = UDP-N-acetyl-α-D-galactosamine)**

CD36	Patient/ fibro-blast line	before VPA treatment		under VPA treatment				
		Sample 1	Sample 2	Sample 1	Sample 2	Sample 3	Sample 4	Sample 5
Down-Regulation	P2/ML82	1,460	1,260	1,448	1,334	0,363	0,373	---
	P13/ML59	13,235	5,469	11,402	5,310	14,087	9,102	15,388
	P14/ML73	0,000	---	0,000	0,000	0,000	---	---
	P4/ML69	41,319	25,835	35,048	21,687	11,482	---	---
Up-Regulation	P5/ML60	13,235	5,469	11,402	5,310	14,087	9,102	15,388
	P8/ML67	2,154	2,101	6,591	7,641	3,485	---	---
	P7/ML72	3,935	3,039	12,564	6,839	4,591	---	---
No change	10197/ML86	0,213	---	0,444	0,745	1,677	---	---

IGFBP5	Patient/ fibro-blast line	before VPA treatment		under VPA treatment				
		Sample 1	Sample 2	Sample 1	Sample 2	Sample 3	Sample 4	Sample 5
Down-Regulation	P2/ML82	0,528	0,471	1,472	1,159	1,502	1,082	---
	P13/ML59	0,937	0,843	0,843	0,676	0,844	0,747	0,985
	P14/ML73	0,975	---	0,701	0,505	0,418	---	---
	P4/ML69	3,406	3,017	4,174	5,742	4,252	---	---
Up-Regulation	P5/ML60	1,304	2,679	1,701	5,098	3,895	1,901	3,253
	P8/ML67	0,921	2,812	0,790	1,983	0,559	---	---
	P7/ML72	0,890	1,611	1,763	0,731	1,267	---	---
No change	10197/ML86	0,570	---	1,202	0,714	1,623	---	---

TGFα	Patient/ fibro-blast line	before VPA treatment		under VPA treatment				
		Sample 1	Sample 2	Sample 1	Sample 2	Sample 3	Sample 4	Sample 5
Down-Regulation	P2/ML82	1,568	0,957	1,599	1,051	0,290	0,480	---
	P13/ML59	2,683	2,179	2,179	2,319	1,894	1,099	1,236
	P14/ML73	1,122	---	0,265	0,171	0,643	---	---
	P4/ML69	6,946	1,890	2,153	1,271	1,128	---	---
Up-Regulation	P5/ML60	0,769	0,742	0,436	0,365	0,411	0,406	1,017
	P8/ML67	1,321	0,982	0,699	2,019	0,879	---	---
	P7/ML72	0,888	0,355	0,768	0,904	0,584	---	---
No change	10197/ML86	0,034	---	0,285	0,068	0,136	---	---

Table 28   Expression analysis of CD36, IGFBP5 and TGFα in the blood of eight SMA-patients. RARβ is not expressed in blood. From each patient one or two samples were collected before VPA-treatment was started. Another three to five samples were collected under VPA-treatment. For each patient the SMN response to VPA-treatment in blood is given. With the exception of P5 the response was concordant between fibroblasts and blood. (Sample labeling: Identifier in Brichta et al. 2006 or patient ID / fibroblast line)
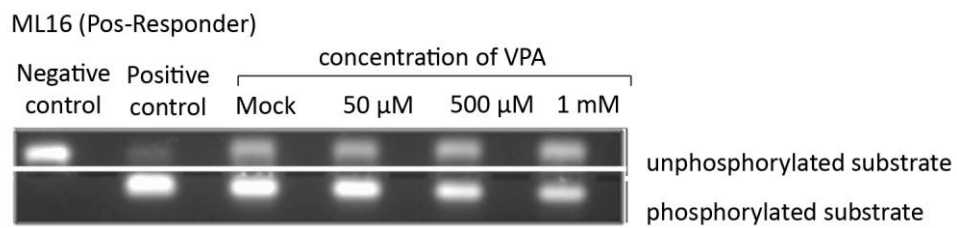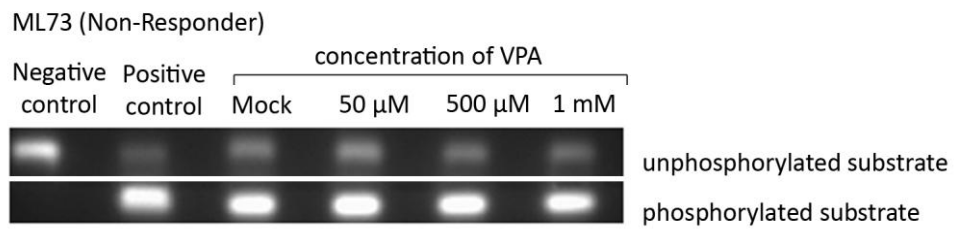
Figure 60   Agarose gels to separate phosphorylated and unphosphorylated PKA substrate. Subsequently bands were cut out, melted and quantified on a plate reader.
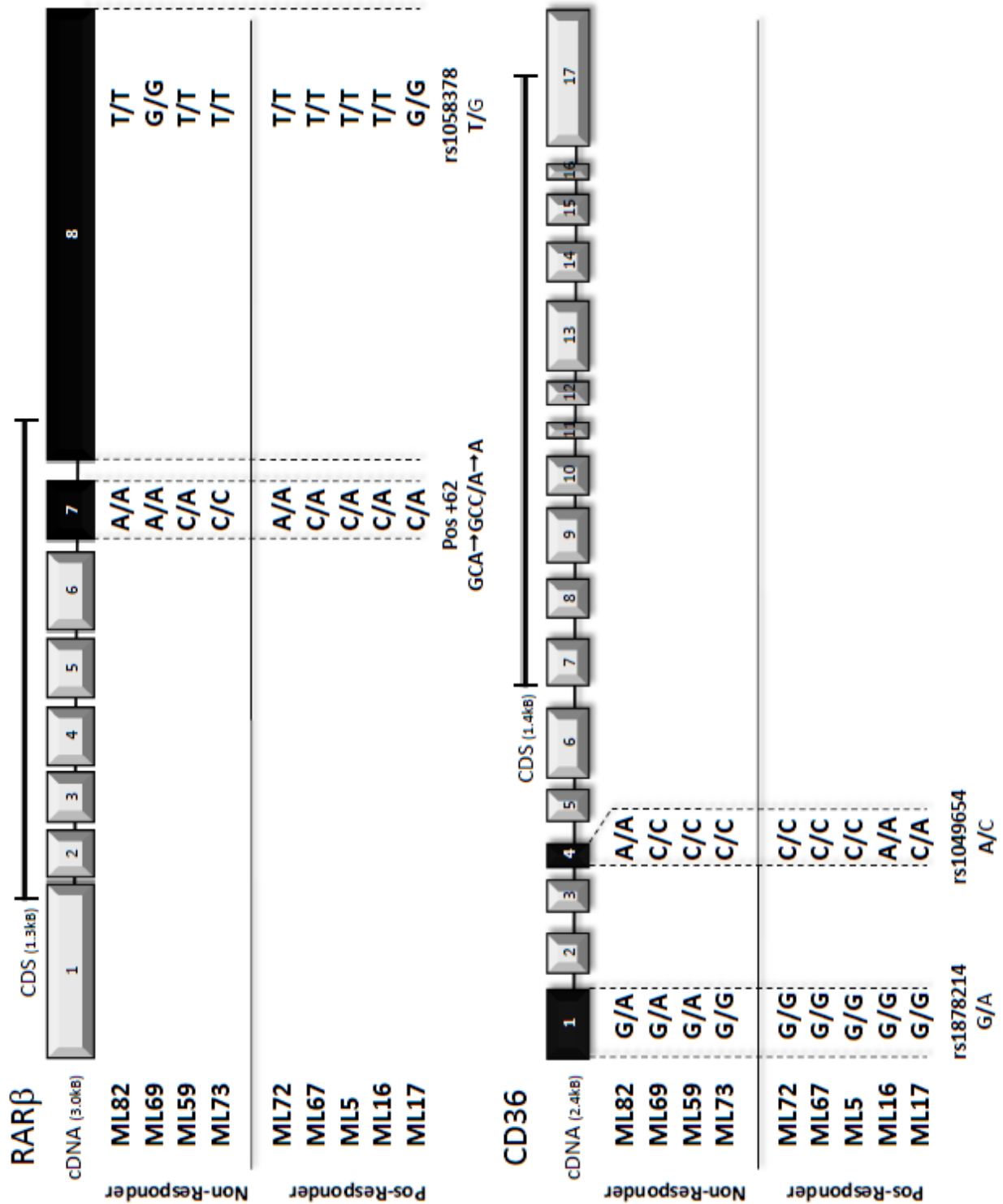
Figure 61 Summarized sequencing results for CD36 and RARβ – both found to be up-regulated in Non-Responders. For both genes exons are represented by gray rectangles. Exons in which differences have been found between cell lines are highlighted in black. In the legend, the major allele of found SNPs is written in bold letters. The detected SNP in CD36 exon 1 was excluded as the cause of higher CD36 expression by sequencing another five not yet confirmed Non-Responders. In exon 7 at Pos +62 of RARβ a previously not described silent A→C variation was found.

Figure 62 Summarized sequencing results for IGFBP5 and TGFα – both found to be up-regulated in Pos-Responders. For both genes exons are represented by gray rectangles. Exons in which differences have been found between cell lines are highlighted in black. In the legend, the major allele of found SNPs is written in bold letters. In the 3'UTR of TGFα encoded by the terminal exon 6 two previously not described variations were found. At Pos +1500 C→T and at Pos +1532 C→T.

Figure 63   Representitave picture of fibroblasts stained with a FITC-labelled SMN-antibody and DAPI. Gems are indicated by arrows.
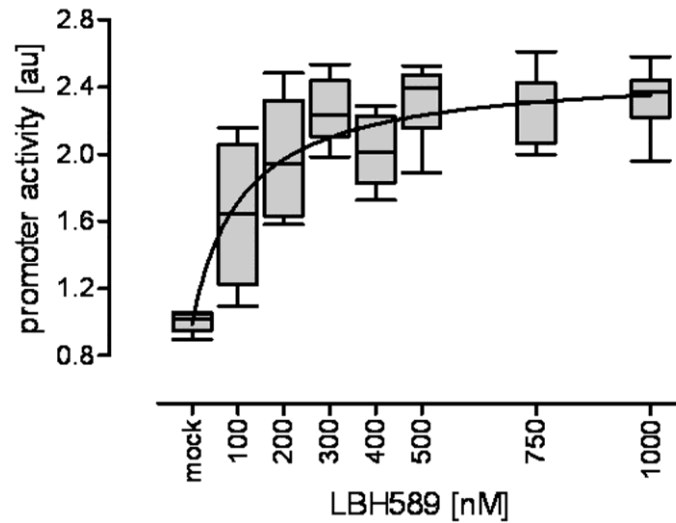
Figure 64   Analysis of *SMN2* promotor activity. Using a four paramter equotation top and bottom plateau as well as slope of the curve were determined. Based on these, an EC_{50} of 108 nM was calculated.
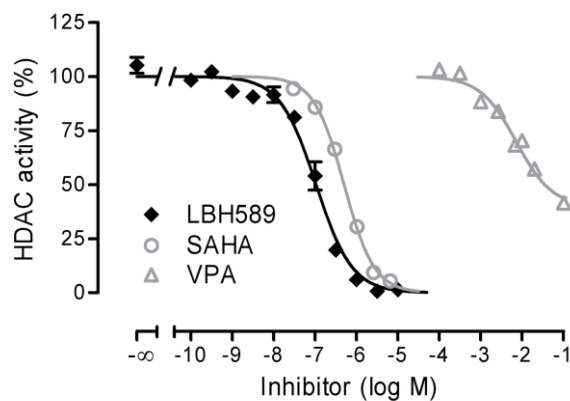
Figure 65   Determinition of HDAC inhibition by LBH589. Using rat liver lysastes, HDAC activity was determined and analysed nonlinearly for the indicated LBH589 concentrations. The depicted curve was used to determine the following values: IC_{10} = 12 nM, IC_{50} = 106 nM and IC_{90} = 953 nM. These data suggest tha LBH589 acts a panHDACi at concentrations regulary used in this thesis. LBH589 data is compared to those of SAHA and VPA

ATGGTGTTGCTCACCGCGGTCCTCCTGCTGCTGGCCGCCTATGCGGGGCCGGCCCAGAGCCTGGGCTCCT
TCGTGCACTGCGAGCCCTGCGACGAGAAAGCCCTCTCCATGTGCCCCCCCAGCCCCCTGGGCTGCGAGCT
GGTCAAGGAGCCGGGCTGCGGCTGCTGCATGACCTGCGCCCTGGCCGAGGGGCAGTCGTGCGGCGTCTAC
ACCGAGCGCTGCGCCCAGGGGCTGCGCTGCCTCCCCCGGCAGGACGAGGAGAAGCCGCTGCACGCCCTGC
TGCACGGCCGCGGGGTTTGCCTCAACGAAAAGAGCTACCGCGAGCAAGTCAAGATCGAGAGAGACTCCCG
TGAGCACGAGGAGCCCACCACCTCTGAGATGGCCGAGGAGACCTACTCCCCCAAGATCTTCCGGCCCAAA
CACACCCGCATCTCCGAGCTGAAGGCTGAAGCAGTGAAGAAGGACCGCAGAAAGAAGCTGACCCAGTCCA
AGTTTGTCGGGGGAGCCGAGAACACTGCCCACCCCCGGATCATCTCTGCACCTGAGATGAGACAGGAGTC
TGAGCAGGGCCCCTGCCGCAGACACATGGAGGCTTCCCTGCAGGAGCTCAAAGCCAGCCCACGCATGGTG
CCCCGTGCTGTGTACCTGCCCAATTGTGACCGCAAAGGATTCTACAAGAGAAAGCAGTGCAAACCTTCCC
GTGGCCGCAAGCGTGGCATCTGCTGGTGCGTGGACAAGTACGGGATGAAGCTGCCAGGCATGGAGTACGT
TGACGGGGACTTTCAGTGCCACACCTTCGACAGCAGCAACGTTGAG

Figure 66 **Schematic representation of the used IGFBP5-clone (GVO #528) which was purchased from** *Origene*. **The insert sequence was taken from the** *Origene* **homepage. More detailed information about the construct can be found under**

http://www.origene.com/orf_clone/search/retrieve_results.mspx?accn=NM_000599&sku=RC203797

ATGGGCTGTGACCGGAACTGTGGGCTCATCGCTGGGGCTGTCATTGGTGCTGTCCTGGCT
GTGTTTGGAGGTATTCTAATGCCAGTTGGAGACCTGCTTATCCAGAAGACAATTAAAAAG
CAAGTTGTCCTCGAAGAAGGTACAATTGCTTTTAAAAATTGGGTTAAAACAGGCACAGAA
GTTTACAGACAGTTTTGGATCTTTGATGTGCAAAATCCACAGGAAGTGATGATGAACAGC
AGCAACATTCAAGTTAAGCAAAGAGGTCCTTATACGTACAGAGTTCGTTTTCTAGCCAAG
GAAAATGTAACCCAGGACGCTGAGGACAACACAGTCTCTTTCCTGCAGCCCAATGGTGCC
ATCTTCGAACCTTCACTATCAGTTGGAACAGAGGCTGACAACTTCACAGTTCTCAATCTG
GCTGTGGCAGCTGCATCCCATATCTATCAAAATCAATTTGTTCAAATGATCCTCAATTCA
CTTATTAACAAGTCAAAATCTTCTATGTTCCAAGTCAGAACTTTGAGAGAACTGTTATGG
GGCTATAGGGATCCATTTTTGAGTTTGGTTCCGTACCCTGTTACTACCACAGTTGGTCTG
TTTTATCCTTACAACAATACTGCAGATGGAGTTTATAAAGTTTTCAATGGAAAAGATAAC
ATAAGTAAAGTTGCCATAATCGACACATATAAAGGTAAAAGGAATCTGTCCTATTGGGAA
AGTCACTGCGACATGATTAATGGTACAGATGCAGCCTCATTTCCACCTTTTGTTGAGAAA
AGCCAGGTATTGCAGTTCTTTTCTTCTGATATTTGCAGGTCAATCTATGCTGTATTTGAA
TCCGACGTTAATCTGAAAGGAATCCCTGTGTATAGATTTGTTCTTCCATCCAAGGCCTTT
GCCTCTCCAGTTGAAAACCCAGACAACTATTGTTTCTGCACAGAAAAAATTATCTCAAAA
AATTGTACATCATATGGTGTGCTAGACATCAGCAAATGCAAAGAAGGGAGACCTGTGTAC
ATTTCACTTCCTCATTTTCTGTATGCAAGTCCTGATGTTTCAGAACCTATTGATGGATTA
AACCCAAATGAAGAAGAACATAGGACATACTTGGATATTGAACCTATAACTGGATTCACT
TTACAATTTGCAAAACGGCTGCAGGTCAACCTATTGGTCAAGCCATCAGAAAAAATTCAA
GTATTAAAGAATCTGAAGAGGAACTATATTGTGCCTATTCTTTGGCTTAATGAGACTGGG
ACCATTGGTGATGAGAAGGCAAACATGTTCAGAAGTCAAGTAACTGGAAAAATAAACCTC
CTTGGCCTGATAGAAATGATCTTACTCAGTGTTGGTGTGGTGATGTTTGTTGCTTTTATG
ATTTCATATTGTGCATGCAGATCGAAAACAATAAAA

Figure 67   Schematic representation of CD36 cloned into pcDNA3.1/V5-His-TOPO (GVO #526) (*Invitrogen*). More detailed vector information can be found under

http://tools.invitrogen.com/content/sfs/vectors/pcdna3.1v5histopo_map.pdf

```
ATGGTCCCCTCGGCTGGACAGCTCGCCCTGTTCGCTCTGGGTATTGTGTTGGCTGCGTGC
CAGGCCTTGGAGAACAGCACGTCCCCGCTGAGTGCAGACCCGCCCGTGGCTGCAGCAGTG
GTGTCCCATTTTAATGACTGCCCAGATTCCCACACTCAGTTCTGCTTCCATGGAACCTGC
AGGTTTTTGGTGCAGGAGGACAAGCCAGCATGTGTCTGCCATTCTGGGTACGTTGGTGCA
CGCTGTGAGCATGCGGACCTCCTGGCCGTGGTGGCTGCCAGCCAGAAGAAGCAGGCCATC
ACCGCCTTGGTGGTGGTCTCCATCGTGGCCCTGGCTGTCCTTATCATCACATGTGTGCTG
ATACACTGCTGCCAGGTCCGAAAACACTGTGAGTGGTGCCGGGCCCTCATCTGCCGGCAC
GAGAAGCCCAGCGCCCTCCTGAAGGGAAGAACCGCTTGCTGCCACTCAGAAACAGTGGTC
```

Figure 68   Schematic representation of TGFα cloned into pcDNA3.1/V5-His-TOPO (GVO #527) (*Invitrogen*). For a higher resolution of the vector see Figure 67.

```
ATGTTTGACTGTATGGATGTTCTGTCAGTGAGTCCTGGGCAAATCCTGGATTTCTACACT
GCGAGTCCGTCTTCCTGCATGCTCCAGGAGAAAGCTCTCAAAGCATGCTTCAGTGGATTG
ACCCAAACCGAATGGCAGCATCGGCACACTGCTCAATCAATTGAAACACAGAGCACCAGC
TCTGAGGAACTCGTCCCAAGCCCCCCATCTCCACTTCCTCCCCCTCGAGTGTACAAACCC
TGCTTCGTCTGCCAGGACAAATCATCAGGGTACCACTATGGGGTCAGCGCCTGTGAGGGA
TGTAAGGGCTTTTTCCGCAGAAGTATTCAGAAGAATATGATTTACACTTGTCACCGAGAT
AAGAACTGTGTTATTAATAAAGTCACCAGGAATCGATGCCAATACTGTCGACTCCAGAAG
TGCTTTGAAGTGGGAATGTCCAAAGAATCTGTCAGGAATGACAGGAACAAGAAAAAGAAG
GAGACTTCGAAGCAAGAATGCACAGAGAGCTATGAAATGACAGCTGAGTTGGACGATCTC
ACAGAGAAGATCCGAAAAGCTCACCAGGAAACTTTCCCTTCACTCTGCCAGCTGGGTAAA
TACACCACGAATTCCAGTGCTGACCATCGAGTCCGACTGGACCTGGGCCTCTGGGACAAA
TTCAGTGAACTGGCCACCAAGTGCATTATTAAGATCGTGGAGTTTGCTAAACGTCTGCCT
GGTTTCACTGGCTTGACCATCGCAGACCAAATTACCCTGCTGAAGGCCGCCTGCCTGGAC
ATCCTGATTCTTAGAATTTGCACCAGGTATACCCCAGAACAAGACACCATGACTTTCTCA
GACGGCCTTACCCTAAATCGAACTCAGATGCACAATGCTGGATTTGGTCCTCTGACTGAC
CTTGTGTTCACCTTTGCCAACCAGCTCCTGCCTTTGGAAATGGATGACACAGAAACAGGC
CTTCTCAGTGCCATCTGCTTAATCTGTGGAGACCGCCAGGACCTTGAGGAACCGACAAAA
GTAGATAAGCTACAAGAACCATTGCTGGAAGCACTAAAAATTTATATCAGAAAAAGACGA
CCCAGCAAGCCTCACATGTTTCCAAAGATCTTAATGAAAATCACAGATCTCCGTAGCATC
AGTGCTAAAGGTGCAGAGCGTGTAATTACCTTGAAAATGGAAATTCCTGGATCAATGCCA
CCTCTCATTCAAGAAATGCTGGAGAATTCTGAAGGACATGAACCCTTGACCCCAAGTTCA
AGTGGGAACACAGCAGAGCACAGTCCTAGCATCTCACCCAGCTCAGTGGAAAACAGTGGG
GTCAGTCAGTCACCACTCGTGCAA
```
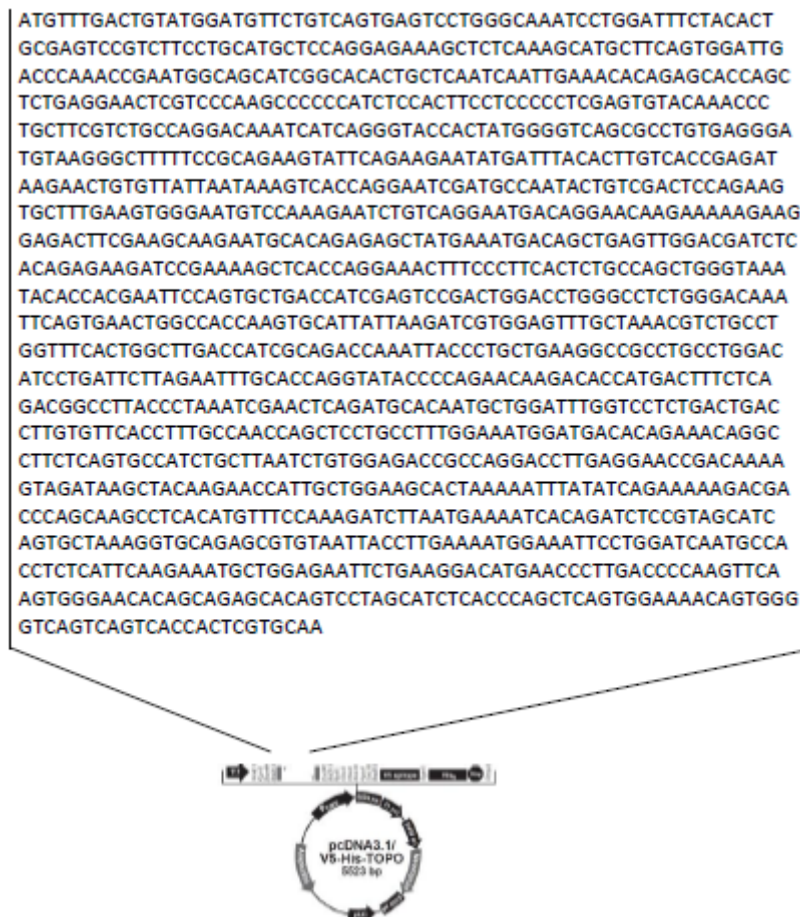
Figure 69   Schematic representation of RARβ cloned into pcDNA3.1/V5-His-TOPO (GVO #525) (*Invitrogen*). For a higher resolution of the vector see Figure 67.
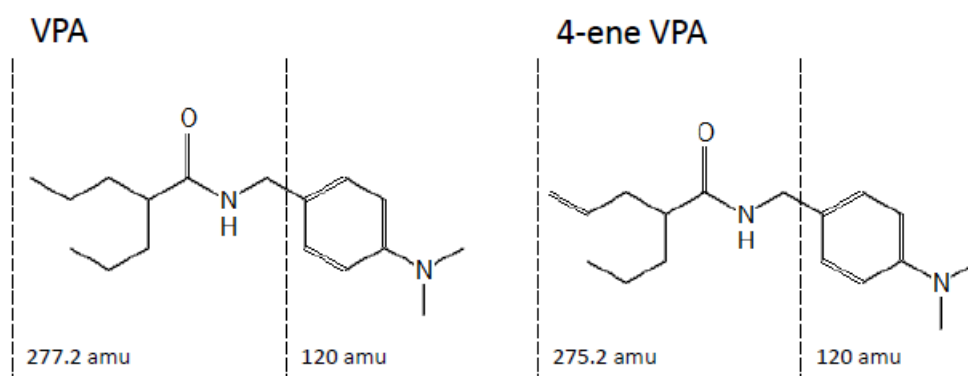
.

VPA

4-ene VPA

277.2 amu   120 amu

275.2 amu   120 amu

Figure 70   Precursor ion pairs for VPA and 4-ene VPA.

11. Erklärung

Ich versichere, dass ich die von mir vorgelegte Dissertation selbständig angefertigt, die benutzten Quellen und Hilfsmittel vollständig angeben und die Stellen der Arbeit - einschließlich Tabellen, Karten und Abbildungen -, die anderen Werken im Wortlaut oder dem Sinn nach entnommen sind, in jedem Einzelfall als Entlehnung kenntlich gemacht habe; dass diese Dissertation noch keiner anderen Fakultät oder Universität zur Prüfung vorgelegen hat; dass sie - abgesehen von unten angegebenen Teilpublikationen – noch nicht veröffentlicht worden ist sowie, dass ich eine solche Veröffentlichung vor Abschluss des Promotionsverfahrens nicht vornehmen werde. Die Bestimmungen der Promotionsordnung sind mir bekannt. Die von mir vorgelegte Dissertation ist von Prof. Dr. rer. nat. Brunhilde Wirth und Prof. Dr. rer. nat. Thomas Wiehe betreut und in der Arbeitsgruppe von Prof. Dr. rer. nat. Brunhilde Wirth durchgeführt worden.

Teilpublikationen sind in Kapitel 8 angegeben.

Köln, den 31.01.2011   Lutz Garbes